How merozoite surface antigen-specific antibodies inhibit *Plasmodium falciparum* growth *in vitro*

Lynne Mary Harris

A thesis submitted for the degree of Doctor of Philosophy

The University of Edinburgh

2013

Declaration

I declare that, except for where noted, all work contained in this thesis was performed and composed by myself. Where others have contributed to elements of the work, this is clearly stated in the text. No element of this work has been submitted for any other degree or professional qualification.

Lynne M. Harris

29/5/13

Abstract

In hyperendemic malarious regions adults develop protective immunity to *Plasmodium falciparum* infection. In order for this immunity to develop the host immune system must be able to recognise the parasite. One stage at which this occurs is prior to red blood cell invasion when the extracellular form of the parasite, the merozoite, presents the host immune system with a number of potential immunogens termed merozoite surface antigens. Antibodies to merozoite surface antigens are able to inhibit the growth and development of the parasite *in vitro*. This thesis explores the mechanisms by which merozoite surface antigen-specific antibodies exert this inhibition.

The affinity, fine specificity and Fc-mediated effects of antibodies may affect their functional activity. Immortalised B cell lines producing merozoite surface antigen-specific human monoclonal antibodies were generated in order to investigate the effect of these factors on their growth inhibitory activity *in vitro*. The preliminary characterisation of these mAbs is described in chapter 3. However, sufficient quantities of these mAbs could not be generated for their functional activity to be investigated *in vitro*.

Current dogma holds that the primary function of antibodies is to provide a molecular link between antigen recognition and pathogen destruction. However, all Abs have the ability to catalyse a reaction between singlet oxygen and water to generate hydrogen peroxide. This thesis explored the hypothesis that this antibody-catalysed water-oxidation pathway is responsible for the intraerythrocytic growth inhibition exerted by MSP-1-$_{19}$-specific Abs. An *in vitro* ACWO assay was developed to test this hypothesis and data suggest that ACWO may occur in infected RBCs associated with an anti- MSP-1-$_{19}$ monoclonal antibody.

Antibodies specific to an intrinsically unstructured region from the C-terminal half of merozoite surface protein 3.3, designated MSP3.3C, are highly effective at inhibiting

the *in vitro* growth of *P. falciparum*. This thesis explored the mechanisms responsible for this inhibition. This inhibition is caused by inhibition of the intraerythrocytic development of the parasite and not by inhibition of merozoite invasion. MSP3.3C specific Abs can access the intraerythrocytic parasite post invasion and completely arrest parasite development by inducing parasite death.

The findings presented in this thesis expand current knowledge of the mechanisms by which MSA-specific Abs inhibit the growth of *P. falciparum in vitro*. This may prove informative both in terms of our understanding of naturally acquired antibody mediated immunity to *P. falciparum* asexual stages and in furthering effective vaccine design against this deadly pathogen.

Acknowledgements

It has been a very long and bumpy journey from the day I was recruited as a PhD student to the day I write these words. I would like to take this opportunity to thank everyone who has contributed to that journey.

Going back to the beginning, I would like to thank Margarete Heck and all the organisers of the Wellcome Trust 4-year PhD programme in Edinburgh for providing me with the opportunity to take part in this excellent educational programme. Thanks must also go to the Wellcome Trust for fully funding me throughout my PhD adventure and for the inspiring meetings they provided at the Wellcome Trust in London.

Next, I would like to thank my PhD supervisor David Cavanagh for letting me loose in his lab for four years and the guidance he provided me with throughout that time. Thanks also go to my second supervisor Alex Rowe for advice and support throughout my PhD. I would like to thank Graeme Cowan and Alison Creasey for everything they taught me. Thanks go to Joanne Thompson for her help, guidance and support, particularly when things were not going well.

A big thank you to my beloved "Wellcome family": Hayden Selvadurai, Robert Ekiert, Elise Malavasi, my fellow Brit Tom Nowakowski and their partners Maire, Marta, Stefano and Ella for the amazing times we shared together in Edinburgh. Although we are now all scattered around the globe PostDocing I hope they'll be many reuninions in the years to come.

Thanks to my fellow Ashworthians Rebekah Easson, Harriet Stone and Johanna Nielsen for the many happy lunch hours we shared together. Thanks to Rachel Dakin for being a true friend.

Finally, a huge thank you to my father Robert and partner Tobias for their unconditional love and support over the years.

Table of abbreviations

Ab	Antibody
ACWO	Antibody-catalysed water oxidation
ACWOP	Antibody-catalysed water oxidation pathway
ADCI	Antibody-dependent cellular inhibition
ADRB	Antibody-dependent respiratory burst
AF	Alexa Fluor
AMA	Apical membrane antigen
bp	Base pair
BSA	Bovine serum albumin
DAPI	4',6'-diamidino-2-phenylindole
DCF	Dichlorofluorescein
DCFH	2',7'-dichlorodihydrofluorescein
DCFH-DA	Dichlorodihydrofluorescein diacetate
DHR	Dihydrorhodamine
DC	Digestive vacuole
EBV	Epstein-Barr virus
ELISA	Enzyme linked immunosorbent assay
ER	Endoplasmic reticulum
EXP	Exported protein
FcR	Fc receptor
FITC	Fluorescein isothiocyanate
FSC	Forward scatter
GIA	Growth inhibition assay
GPI	Glycosylphosphatidylinisotol
H	Hour
HRP	Horseradish peroxidase
HSP	Heat shock protein
IDC	Intra-erythrocytic developmental cycle

IFA	Immunofluorescence assay
Ig	Immunoglobulin
IMC	Inner membrane complex
IPTG	Isopropyl β-D-1-thiogalactopyranoside
iRBC	Infected red blood cell
kDa	Kilodalton
MFI	Median fluorescence intensity
Min	Minute
MSA	Merozoite surface antigen
MSP	Merozoite surface protein
NADPH	Nicotinamide adenine dinucleotide phosphate
OD	Optical density
ODN	Oligodeoxynucleotide
P. falciparum	*Plasmodium falciparum*
PBMC	Peripheral blood monocuclear cell
PCR	Polymerase chain reaction
PEXEL	*Plasmodium* export element
PHA	Phytohaemagglutinin
PM	Plasma membrane
PMA	Phorbol myristate acetate
PMN	Polymorphonuclear neutrophils
PTEX	*Plasmodium* translocon of exported proteins
PVM	Parasitophorous vacuole membrane
R 123	Rhodamine 123
RBC	Red blood cell
ROS	Reactive oxygen species
RT	Room temperature
S	Second
SEM	Standard error of the mean
SNP	Single nucleotide polymorphism
SSGIA	Stage-specific growth inhibition assay
TVN	Tubulovesicular network
uRBC	Uninfected RBC

Table of Contents

List of Figures and Tables

1 Introduction

1.1 General background

1.1.1 Malaria: the prevailing state of an ancient disease

Historical references, some greater than four thousand years old, describing the poor health, paroxysmal fevers and enlarged spleens of individuals residing in marshland areas, attest to the antiquity of coexistence between malaria parasites and their *Homo sapien* host. Over these millennia malaria has had a profound impact on our genomic evolution; genetic polymorphisms conferring resistance to the disease, particularly those affecting red blood cells (RBCs), have been selected for in high frequency in endemic populations (Flint et al., 1998). These genetic polymorphisms, which include the haemoglobinopathy haemoglobin S (Hill et al., 1991), the alpha and beta thalassaemias (Flint et al., 1986) and glucose-6-phosphate dehydrogenase deficiency (Ruwende et al., 1995), have left a large burden of genetic disease in human populations (Weatherall and Clegg, 2001).

Malaria continues to exert a significant burden on the human population; 216 million clinical cases and 1.2 million malaria deaths (mostly of children under 5 years of age) are estimated to have occurred in 2010 alone (Murray et al., 2012; World Malaria Report 2011, 2011). Although increased control activities in sub-Saharan Africa have resulted in a significant decrease in malaria deaths since 2004 (Murray et al., 2012), insecticide-resistant vectors and drug-resistant parasites remain a threat to the global eradication of malaria.

1.1.2 Malaria parasites and their vectors

In 1880, the French scientist Charles Louis Alphonse Laveran discovered that malaria was caused by a parasitic protozoan, which he named *Oscillaria malaria,* and not by the bacterium *Bacillus malariae,* the leading suspect of the time. We now

know that five species of protozoan apicomplexan parasites of the genus *Plasmodium* are able to infect humans; *Plasmodium falciparum* (*P. falciparum*), *Plasmodium knowlesi* (*P. knowlesi*), *Plasmodium malariae* (*P. malariae*), *Plasmodium ovale* (*P. ovale*) and *Plasmodium vivax* (*P. vivax*). *P. knowlesi* is thought to be primarily zoonotic in origin (Cox-Singh, 2012), whilst the other four species of parasite are spread from one human to another by the bite of the female *Anopheles* mosquito vector. Within this genus of 465 species, approximately 70 species are thought to act as human malaria vectors in the wild (Warrell and Gilles, 2003).

1.1.3 Clinical manifestations of the disease

The clinical presentations of malaria depend upon the species and strain of the infecting parasite, and the immunological status of the infected individual. Intense cyclical fevers are the hallmark of malarial infection and typically coincide with RBC lysis. Such fevers occur every 24 hours (h) in *P. knowlesi* infection, every 48 h in *P. falciparum, P. ovale and P. vivax* infection, and every 72 h in *P. malariae* infection. Accompanying symptoms include headache, nausea, and muscular aches, among others. Untreated cases of malaria are characterised by enlargement of the spleen. The most severe form of malaria is caused by complicated *P. falciparum* infection, during which life-threatening complications can arise, including renal failure, hepatic dysfunction, severe anaemia and cerebral malaria. In *P. vivax and P. ovale* malaria, relapse may occur years after initial infection due to reactivation of the dormant liver-stage form of the parasite (hypnozoites).

1.1.4 P. falciparum life cycle

Infection begins with inoculation of the infective stages, sporozoites, into the human host when the mosquito takes a blood meal. The majority of these sporozoites find a blood vessel, travel in the peripheral blood circulation, and reach the liver within 60 minutes of inoculation. Once there, sporozoites rapidly invade liver hepatocytes, where they undergo asexual multiplication (exoerythrocytic schizogony), which results in the production of many (> 10,000) uninucleate merozoites, a process which

takes ~ 6 days. These liver stage schizonts rupture from infected hepatocytes, releasing merozoites which invade RBCs. In erythrocytes, the parasite undergoes a second phase of asexual multiplication (schizogony) to produce 8-16 daughter merozoites per infected RBC. These infectious offspring are released when the RBC lyses and go on to invade other RBCs. This cycle of ~10-fold parasite multiplication continues and it is this stage of the infection that is responsible for malarial pathogenesis.

Some of the merozoites entering RBCs do not undergo schizogony but instead differentiate into male and female gametocytes that circulate in the peripheral blood until they are ingested by a female Anopheline mosquito. Within the mosquito, the male gametocyte divides into 8 flagellated microgametes, which escape the enveloping RBC and swim to the female macrogamete. Fertilisation occurs, resulting in the formation of a motile zygote (the ookinete) within the lumen of the mosquito gut. The ookinete moves between or through the cells of the stomach wall to become a conspicuous oocyst. Within the oocyst a third round of asexual multiplication occurs (sporogony), producing sporozoites that migrate to the salivary glands of the mosquito. When the mosquito next feeds, the transmission cycle is complete.

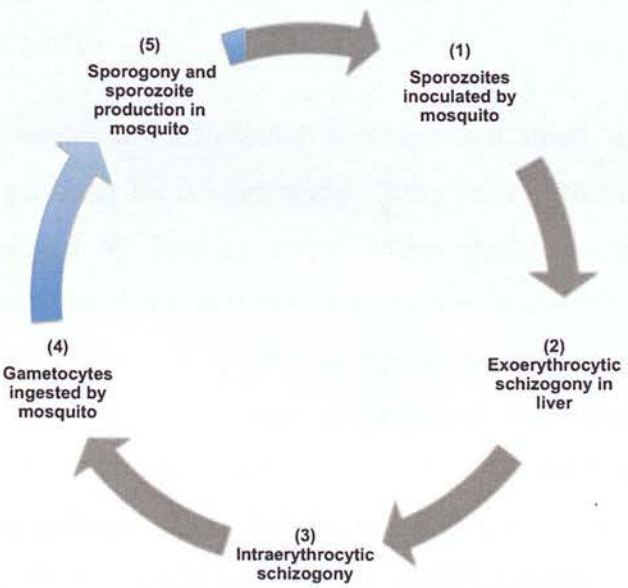

Figure 1 Schematic life cycle of *Plasmodium falciparum*

1.2 Merozoite invasion and developmental stages of the erythrocytic cycle

1.2.1 The intraerythrocytic developmental cycle of *P. falciparum*

Whilst the 48 hour long erythrocytic cycle of *P. falciparum* is a continuous, dynamic process, four distinct stages of parasite development can be distinguished based on morphological characteristics. The intraerythrocytic developmental cycle initiates with the invasion of a RBC by the extracellular merozoite and is followed by the formation of the parasitophorous vacuole during the ring stage. The parasite then embarks on a highly metabolic growth stage, the trophozoite stage. In the schizont stage, the parasite undergoes multiple rounds of replication in preparation for reinvasion of new RBCs. The different parasite stages were initially defined but based on light microscopic observation of morphological characteristics. More recently, large scale proteomics assays have confirmed that each of these developmental stages is distinguished by a unique protein content related to the specialised functionalities of that specific stage (Foth et al., 2011; Hall et al., 2005; Le Roch et al., 2004).

1.2.1 The merozoite

P. falciparum merozoites are ellipsoidal in shape and small in size, measuring approximately 1.3 μm long by 0.9 μm wide. They have a short flat-ended apical prominence, surrounded by 3 polar rings, within which a group of secretory organelles are housed; the dense granules, micronemes and rhoptries. An irregular and variably shaped nucleus is located in the posterior half of the merozoite. Projecting tufts of fine filaments form a structured coat overlying the entire merozoite surface, beneath which lies the trilaminar pellicle, consisting of the merozoite plasma membrane (PM) and beyond the apical pole region, the two membranes of the inner membrane complex (IMC) (Bannister et al., 2000b). Underneath the pellicle lie two or three microtubules (Bannister and Mitchell, 1995), a single elongated mitochondrion (Slomianny and Prensier, 1986) and an apicoplast

(Hopkins et al., 1999; Köhler et al., 1997). A single cytosomal ring is located on the side of the merozoite beneath the PM in a small gap in the IMC (Aikawa et al., 1966; Bannister et al., 2000b; Slomianny, 1990).

At least 11 merozoite surface proteins (MSPs) have been identified. A number of these, including MSP-1 and MSP-2, are attached to the PM though a C-terminal glycosylphosphatidylinositol (GPI)-lipid anchor, while others, such as MSP-3, MSP-6, and MSP-7, lack either a GPI anchor or transmembrane domain and are thought to associate with the surface through non-covalent interactions with other MSPs.

MSP-1, the most abundant protein on the merozoite surface, is initially synthesised during the trophozoite and schizont stages as a ~ 185 kilodalton (kDa) precursor protein (Holder and Freeman, 1982; Holder and Freeman, 1984), which exists in a complex with MSP-6 and MSP-7 (Pachebat et al., 2001; Trucco et al., 2001). MSP-1 undergoes a primary cleavage event during schizogany to yield four fragments of 83, 28, 38 and 42 kilodaltons (kDa) (Holder et al., 1985; Holder et al., 1987; Lyon et al., 1986a; Lyon et al., 1987; McBride and Heidrich, 1987). These fragments remain in a non-covalently linked complex on the merozoite surface until, during merozoite invasion, a secondary processing event occurs, cleaving the 42 kDa fragment into two fragments of 33 kDa and 19 kDa. The latter fragment is retained on the merozoite surface throughout invasion whilst all other fragments are thought to be shed either before or during the invasion process (Blackman et al., 1990). These primary and secondary cleavage events are carried out by the subtilisin-like serine proteases, PfSUB1 (Koussis et al., 2009) and PfSUB2 (Blackman and Holder, 1992; Harris et al., 2005), respectively.

P. falciparum MSP-3 is a somewhat diverse ~ 48 kDa protein that contains 12 copies of a heptad amino acid motif arranged in 3 contiguous blocks of four. These blocks are linked by short non-repetitive sequences and the hydrophobic amino acid alanine occupies the first and fourth positions within each heptad (McColl et al., 1994; Oeuvray et al., 1994). These regions may form coiled-coil α-helices and a synthetic peptide containing one of the blocks of four heptads was found to contain an α-helix

but did not form multimers of itself in solution (Mulhern et al., 1995). Three MSP-3 orthologues have been identified in *P. vivax* (MSP-3α, MSP-3β, and MSP-3γ), which contain alanine-rich heptad repeat sequences similar to those found in *P. falciparum* MSP-3 (Galinski et al., 1999; Galinski et al., 2001). MSP-6 contains significant sequence similarity to MSP-3 in its C-terminal half, and along with 7 other proteins forms the MSP-3 family of proteins with designations of MSP-3.1 through MSP-3.8 (Singh et al., 2009).

1.2.2 Merozoite invasion

Merozoite invasion is an efficient, highly orchestrated process in which the recognition, attachment and entry of an uninfected RBC by the extracellular merozoite occurs in ~ 90 seconds (Gilson and Crabb, 2009b). Prior to invasion merozoites must be released from the host cell that has housed them during their development. This involves disruption of both the parasite vacuolar and RBC membranes in a multistep process (Salmon et al., 2001; Wickham et al., 2003), which allows the non-motile merozoites to be ejected at high pressure into the circulating blood where they can encounter new RBCs.

The initially reversible, low affinity RBC-merozoite interaction occurs between elements of the merozoite's proteinaceous fibrillar projections and the RBC (Dvorak et al., 1975). MSPs are abundantly present all over the merozoite surface and have consequently been implicated as the molecular mediators of this interaction. Specifically, there is some evidence that MSP-1 and MSP-7 may mediate this initial merozoite-RBC interaction as disruption of their function, through specific antibody binding or gene knockout, respectively, impedes invasion (Blackman et al., 1990; Kadekoppala et al., 2008). Recently, synthetic MSP-11 peptides have been shown to both bind RBCs and inhibit merozoite invasion *in vitro*, suggesting that MSP-11 may also help mediate the RBC-merozoite interaction (Obando-Martinez et al., 2010). However, direct evidence for any such interactions are currently lacking.

Initial contact of the merozoite with a RBC elicits the emanation of rhythmic oscillations across the erythrocyte surface, disrupting the merozoite such that it becomes reoriented with the apical prominence facing the erythrocyte membrane. This results in the formation of a tight 4 nanometre (nm) membrane-to-membrane interaction (tight junction) between the parasite and the RBC, an essential and irreversible step which commits the parasite to host cell entry. This step is thought to be mediated by pairs of merozoite ligand-erythrocyte receptor interactions, each pair defining a redundant invasion pathway. Merozoite ligands identified include members of the erythrocyte-binding like (EBL) and reticulocyte binding like (*Pf*Rh) protein families and some of their binding partners on the RBC surface have been identified (Lobo et al., 2003; Sim et al., 1994; Tham et al., 2010).

The tight junction, whilst retaining its suberythrocytic electron density, moves posteriorly over the merozoite as the parasite moves into the RBC, powered by an internal actin-myosin motor (Baum et al., 2006; Keeley and Soldati, 2004) and shedding its surface coat as it does so. Succeeding moving junction formation, rhoptry organelles secrete proteins and lipids into the host cell that are incorporated into the parasitophorous vacuole membrane (PVM). Merozoite internalisation is estimated to be complete within 17 seconds (Gilson and Crabb, 2009b), at which time the merozoite inside the RBC is completely enclosed by the PVM.

Apical membrane antigen 1 (AMA-1) is synthesised in precursor form as an 83 kDa type I integral transmembrane protein (Narum and Thomas, 1994) and is targeted to micronemes (Bannister et al., 2003). Near the time of merozoite egress from the host RBC, AMA-1 is proteolytically processed to yield a 66 kDa protein that is translocated to and distributed over the entire merozoite surface (Healer et al., 2002). The mature form of AMA-1 contains a large extracellular domain, folding into three interacting domains with several protruding highly polymorphic loops. A hydrophobic trough in this ectodomain is the binding site for a complex of rhoptry neck proteins; RON2, RON4 and RON5 (Cao et al., 2009; Collins et al., 2009). The RON complex is thought to be translocated from the rhoptry neck into the erythrocyte membrane such that the parasite may be supplying both receptor and

ligand during host cell invasion (Gilson and Crabb, 2009a; Lamarque et al., 2011; Richard et al., 2010). Eventually, the vast majority of the AMA-1 ectodomain is shed from the merozoite surface via juxtamembrane cleavage by PfSUB2 and intramembrane cleavage mediated by an unknown factor (Harris et al., 2005; Howell et al., 2005; Howell et al., 2003), a process which may be essential for parasite survival (Olivieri et al., 2011).

1.2.3 The ring stage parasite

The ring stage begins shortly after invasion, with the parasite flattening into a biconcave discoidal shape with a diameter of 2 to 3.7 μm. The thick perimeter of the disk contains the majority of organelles, including a variably shaped nucleus and most of the ribosomes. The thinner centre contains the smooth membrane organelles. The exact shape of the disc varies, in some cases flat, but more often taking on a curved cuplike form (Bannister et al., 2004).

The developing parasite takes up and degrades large quantities of haemoglobin from the RBC cytosol, a costly process for the parasite, both in terms of the energy required and the toxic risk of free haem molecules. Haemoglobin degradation provides amino acids that are essential for parasite growth (Francis et al., 1997; Krugliak et al., 2002; McKerrow et al., 1993) and is thought to maintain the osmotic stability of the growing parasite (Lew et al., 2004; Lew et al., 2003).

The ring stage parasite endocytoses the haemoglobin-rich erythrocyte cytosol through a single active cytosome into small vesicles. Initially these food vacuoles are enclosed by two membranes, the inner and outer, derived from the PVM, and the parasite PM, respectively. As haemoglobin degradation proceeds, the inner membrane degrades, and small crystals of haemozoin, the product of haemoglobin degradation by the parasite, appear within single membrane vacuoles.

A distinctive class of double-membraned vesicles, which do not form part of the cytosomal system, appear at the parasite surface of rings, their outer membrane fused

with the parasite PM such that the inner vesicle gives the appearance of being exported into the PV space. It has been suggested that these vesicles may be involved in the export of membrane from the parasite surface into the PVM, which needs to expand in order to accommodate the growing parasite (Bannister et al., 2004).

The ring stage endures for a considerable proportion of the asexual cycle, with some pathogenesis occurring during this time due to the adherence of iRBCs to vessel walls (Cooke et al., 2001; Pouvelle et al., 2000). This stage ends as the parasite takes on a more spheroidal shape and becomes a trophozoite around 25 h into the cycle.

1.2.4 The trophozoite stage

The trophozoite stage is characterised by rapid parasite growth, adoption of a rounded shape and the appearance of haemozoin in a single food vacuole. As the parasite continues to grow it exports membranes — Maurer's clefts, the tubulovesicular network (TVN), small vesicles, and knobs — and other structures into the RBC it inhabits (Cooke et al., 2004; Haldar et al., 2001; Przyborski et al., 2003).

The TVN consists of spirals and loops of double membrane, often extending from the PVM to wrap around regions of host cytoplasm. The TVN shares antigenic similarity with the PVM, including the integral membrane proteins exported protein 1 (EXP-1) (Kara et al., 1988) and exported protein 2 (EXP-2) (Fischer et al., 1998), and some members of the early transcribed membrane protein family (ETRAMPS) (Spielmann et al., 2003).

Maurer's clefts are stacks of flattened lamellae of long slender membranes with an electronluscent lumen and an electron dense coat, mostly lysing near and parallel to the erythrocyte PM, to which they are attached by filamentous links (Kriek et al., 2003). Maurer's clefts can first be detected in early ring stages, where they are highly motile. Upon progression into the trophozoite stage their position becomes

fixed (Grüring et al., 2011). Several integral membrane proteins are resident in Maurer's clefts, including membrane-associated histidine-rich protein 1 (MAHRP1) (Spycher et al., 2003), skeletal binding protein 1 (SBP1) (Blisnick et al., 2000), ring exported protein 2 (REX2) (Spielmann et al., 2006) and Pf332 (Hinterberg et al., 1994).

Knobs are produced by the deposition of the Knob-associated histidine-rich protein (KAHRP) at the RBC cytoskeleton, which produces an angular prominence. Attached to knobs are members of the membrane embedded *P. falciparum* erythrocyte membrane protein 1 (PfEMP1) family of clonally variant proteins, surface exposed proteins that mediate, at least in part, the attachment of more mature stages of *P. falciparum* to the vascular endothelium of different organs, including the brain. This sequestration is one of the the main causes of *P. falciparum* malaria induced morbidity and mortality and the reason that only ring stages are seen in the blood of infected patients. Within the iRBC cytoplasm, there are many small (15 to 25 nm) vesicles, frequently associated with Maurer's clefts and the RBC PM.

During its development inside the mature human erythrocyte, which is a terminally differentiated cell lacking either intracellular organelles or endocytotic machinery (Chasis et al., 1989), the parasite establishes a *de novo* trafficking system. The parasite employs this system to export several hundred soluble and membrane-embedded proteins into the RBC compartment in order to foster its virulence, stabilise the host cell cytoskeleton and obtain nutrients from host plasma.

In order to access the RBC cytosol, parasite proteins must traverse both the parasite PM and the PVM. A hydrophobic signal sequence located either close to or up to 80 amino acids from the N-terminus facilitates insertion into the endoplasmic reticulum (ER) and is required to traffic proteins to the PV (Adisa et al., 2003; Cheresh et al., 2002; Waller et al., 2000; Wickham et al., 2001). Typically, in order for the protein to cross the PVM a second pentameric signal sequence known as the *Plasmodium* export element (PEXEL) is required (Hiller et al., 2004; Marti et al., 2004). This motif has the consensus R/KxLxE/Q/D, where x is any amino acid, and is located a

short distance downstream of the ER signal sequence. In the ER, the PEXEL motif is cleaved at the C-terminal side of the conserved Leucine residue by the aspartic protease plasmepsin V, to generate a new N-terminus which becomes acetylated (Boddey et al., 2010; Chang et al., 2008).

The *Plasmodium* translocon of exported proteins (PTEX) is the putative protein trafficking machinery responsible for the export of proteins across the PVM and into the RBC cytosol. Five proteins comprising PTEX have been identified; heat shock protein 101 (HSP101), thioredoxin 2 (TRX2), PTEX150, PTEX88 and EXP-2. HSP101, a AAA+ ATPase chaperone, hydrolyses ATP to putatively unfold cargo proteins prior to driving them across the PVM and EXP-2 is thought to homo-oligomerise in order to form the membrane spanning channel (Bullen et al., 2012; de Koning-Ward et al., 2009). However, definitive proof that PTEX acts as the protein translocon is so far lacking.

PEXEL-containing membrane proteins and parasite proteins that do not contain a PEXEL motif are exported across the PVM into the RBC. Given that only soluble proteins have been shown to associate with PTEX it remains to be determined whether separate trafficking pathways exist for these exported proteins. It has been suggested that parasite membrane proteins are loaded into nascent Maurer's clefts as they bud off from the PVM thus providing a route for export of these parasite proteins. However, the recent finding that Maurer's clefts are generated prior to the synthesis of most exported proteins argues against this (Grüring et al., 2011).

1.2.5 The Schizont stage

During the schizont stage the parasite beings to move away from trophic activities, including cytosomal feeding, and undergoes a series of mutliplications of its nucleus, mitochondrion, apicoplast and Golgi complex, while creating and assembling merozoite components in preparation for merozoite egress and invasion.

Schizont development can be divided into seven different stages based on ultrastructural changes (Margos et al., 2004) and these are outlined below. The parasite undergoes four rounds of endomitotic division, corresponding to stages 1 to 4, to generate sixteen daughter nuclei, although this number varies from 8 to 32 within a given schizont, thus suggesting that schizogony is an asynchronous process with relaxed regulation of final numbers (Margos et al., 2004). During the second stage, centres of merozoite assembly become visible near to the spindle pole bodies, comprising a Golgi-like cisterna and budding of a cluster of coated vesicles from the outer nuclear membrane (Bannister et al., 2000a). Merozoite apexes start to form; rhoptry precursors in the form of small spheroidal vesicles are present and the early stages of the pellicle and polar ring formation become visible.

Towards the end of stage 4 the final assembly of merozoites begins, as surface clefts, lined by the pellicle, begin to deepen around the foci of apical organelle formation. Nuclei now finish their division and migrate into each merozoite bud, accompanied by the mitochondrion and apicoplast which multiplied during earlier stages. Micronemes are formed in stage 5 (Bannister et al., 2003) and dense granules at stage 6. All the apical organelles are formed from the Golgi cisterna; rhoptries through the fusion of small Golgi-derived vesicles, where as micronemes and dense granules bud off directly from its cisterna. The mitochondria, apicoplast and micronemes are transported to their apical destination along the merozoite's subpellicular microtubules, now fully assembled along one side of the bud. By the sixth stage, the merozoites are nearly completely formed but remain attached to the residual parasite body by narrow stalks. The residual body consists of a mass of haemozoin crystals encased within the pigment vacuole membrane, surrounded by a parasite PM. By the final stage of schizont development the merozoites are fully mature and are fully detached from the residual body (Margos et al., 2004).

For merozoites to enter the bloodstream they must exit both the PVM encasing the developing merozoites and the RBC membrane. The molecular details of this process are still being worked out. It is thought that parasite-encoded proteases carry out a series of proteolytic events that result in merozoite exit from the RBC

following the rupture of the PVM and RBC membrane. The order in which these two membranes rupture is still a matter of debate (Salmon et al., 2001; Wickham et al., 2003).

1.3 Antibody mediated immunity to malaria

1.3.1 Immunity to malaria: an overview

P. falciparum infection in malaria naive individuals results in the onset of clinical symptoms associated with this disease. Yet in hyperendemic malarious regions malaria parasites are detected in the blood of asymptomatic individuals, indicating the presence of acquired protective immunity to *P. falciparum* infection in these populations. This immunity is thought to develop in three sequential stages - firstly, clinical immunity that reduces the risk of death from malaria; then anti-disease immunity that reduces the intensity of clinical symptoms; and after this, anti-parasite immunity which directly reduces the number of parasites within an infected individual (Schofield and Mueller, 2006).

The immune status of an individual is a product of the number and frequency of malaria inoculations experienced. Clinical immunity to severe attacks of malaria may be achieved after only one or two infections (Gupta et al., 1999). Consequently, young children less than 5 years of age are at high risk of severe malaria and death, as exemplified by this age-group accounting for the majority of deaths caused by malaria in Sub-Saharan Africa (Bryce et al., 2005). Clinical immunity to non-life threatening symptoms of malaria requires more and frequent inoculations of malaria, such that as children enter their primary school years, they will typically have low disease rates but retain significant parasitaemias. High parasite densities and prevalence often remain throughout childhood as clinical manifestations of the disease progressively decrease. Effective antiparasite immunity is only obtained after very many frequent inoculations and consequently is only obtained well into adulthood.

Due to the correlation between the age of an individual and the stage of malarial immunity attained, antimalarial immunity in endemic populations is often said to be "age-dependent." A more accurate description would be "duration of exposure" dependent, although there are age-dependent aspects to the attainment of malarial immunity. For example, extremely young children find it very difficult to acquire effective protective immunity to malaria, while older children and adults find it easier to do so (Baird, 1995; Baird et al., 1991).

Antimalarial immunity is non-sterilising, meaning that ongoing exposure to the pathogen is required in order to maintain immunity, and that parasites are present in blood of clinically immune individuals. Even relatively short periods of non-exposure, in the order of six months to a year, are enough for immunity to be lost. This is exemplified by immigrants from Sub-Saharan Africa living in Europe, who upon returning from a trip to their native endemic area during which they haven't taken prophylactic treatment, often present at hospital with malaria (Monge-Maillo and López-Vélez, 2012).

An individual living in a malaria endemic area is subject to a series of inoculations of malaria parasites that are both genetically and antigenically different from one another. Antimalarial immunity is strain-specific in the sense that protective immunity naturally acquired to one parasite strain, defined as parasites derived from a single natural inoculation, are better at protecting against re-infection with the homologous strain than with heterologous strains (Cavanagh et al., 2004; Conway et al., 2000; Eisen et al., 2002; Eisen et al., 1998; Jeffery, 1966).

The *P. falciparum* genome encodes several large hypervariable polymorphic gene families called the variant surface antigens (VSAs) (Baruch et al., 1995; Cheng et al., 1998; Kyes et al., 1999). An individual parasite expresses only one member of a VSA family at any given time (Chen et al., 1998; Scherf et al., 1998) but within a clonal parasite population there is switching between the expression of the individual genes of a VSA family (Kyes et al., 2001). This phenomenon is termed clonal antigenic variation and in order to regulate the infection the host must produce an

immune response to each antigenic variant as it arises. This variant specific immunity may explain how a single malaria infection can persist over many months or years. Antigenic polymorphism and variation are both thought to be immune evasion strategies utilised by the parasite and to contribute to the large number and frequency of inoculations required to achieve immunity in endemic populations (Mendis et al., 1991; Reeder and Brown, 1996).

1.3.2 Evidence for antibody mediated immunity to malaria

Several lines of evidence support a role for B cells and antibody in naturally acquired immunity to malaria. Firstly, the passive transfer of immunoglobulin G (IgG) purified from the serum of malaria immune individuals to children suffering from heavy *P. falciparum* infection results in a significant reduction in parasitaemia and the alleviation of clinical symptoms of the disease (COHEN et al., 1961; McGREGOR et al., 1963; Sabchareon et al., 1991). Secondly, during the first three months of life infants living in areas of high transmission intensity develop mild symptoms and low parasitaemias relative to the number of infective bites they receive (Snow et al., 1998). This has been attributed to the passive transfer of immune IgG from mother to infant as (i) levels of maternal and infant IgG match at birth (Logie et al., 1973), (ii) the length of time that this protection persists in infants approximately corresponds to the length of time that maternal IgG is predicted to be present for (Duah et al., 2010) and (iii) adult immune IgG blocks the cytoadherence of core blood iRBCs to microvascular endothelial cells more effectively than that of adult haemoglobin A-containing iRBCs (Amaratunga et al., 2011). However, direct evidence of an association between the level of maternal IgG and disease susceptibility in young infants is so far lacking. Thirdly, the presence and level of antibodies to defined malarial antigens has been associated with resistance to both symptomatic (Cavanagh et al., 2004; Egan et al., 1996; Mawili-Mboumba et al., 2003; Meraldi et al., 2004; Metzger et al., 2003; Polley et al., 2006) and asymptomatic malaria (Hogh et al., 1992; Riley et al., 1993) in endemic populations.

Data garnered from experimental models of malaria likewise suggest that antibodies are a crucial component of the protective immune response to malaria. The transfer of immune IgG or malarial antigen-specific mAbs to naive mice or monkeys can reduce or prevent infection in the recipient (Gysin et al., 1996; Narum et al., 2000; Spencer Valero et al., 1998) . Mice lacking B cells cannot clear parasites from *P. chabaudi chabaudi* AS infection and develop a chronic infection (Langhorne et al., 1998; Weid et al., 1996).

1.3.3 Characteristics of the antibody response

Seroepidemiological studies have shown that antibody responses that protect against clinical malaria are only acquired after repeat exposure, and once acquired, malaria-specific antibody levels, particularly in children, rapidly decline in the absence of ongoing exposure to the parasite (Akpogheneta et al., 2008; Cavanagh et al., 1998; Kinyanjui et al., 2007). This may go some way to explain why acquired immunity to malaria takes so long to develop, and why immunity is sometimes lost in the absence of continuous exposure. However, long-lived antibody responses do develop, particularly in older individuals (Drakeley et al., 2005; Taylor et al., 1996), and the cellular mechanisms underlying short-lived malaria specific antibody responses remain to be fully elucidated.

The distribution of immunoglobulin isotypes found in malaria immune individuals is skewed towards those of the cytophilic IgG1 and IgG3 subclasses. In contrast a prevalence of non-cytophilic immunoglobulin isotypes is found among unprotected individuals. This isotype imbalance has been proposed to explain the delayed acquisition of protective immunity seen in malaria endemic regions (Bouharoun-Tayoun and Druilhe, 1992).

1.3.4 Merozoite surface antigens as targets of antibody mediated immunity

From the 5268 proteins predicted to be encoded by the *P. falciparum* genome (Gardner et al., 2002), it has been possible to identify some of the antigenic targets of naturally acquired antibody mediated immunity (AMI) to *P. falciparum* infection. As MSAs are directly exposed to Abs in the bloodstream prior to invasion, it follows that they may be targets of naturally acquired AMI. Indeed there are a number of lines of evidence to suggest that this is the case.

If the prevalence or level of antibodies to a defined antigenic target correlates with resistance to or decreased frequency of clinical malaria, this can be taken as supportive evidence that this antigen in a target of protective immunity. Antibody responses to a number of MSAs have been correlated with resistance to clinical malaria, including the Block 2 region of MSP-1 (Cavanagh et al., 2004; Conway et al., 2000; Osier et al., 2008), MSP-1-19 (Egan et al., 1996), MSP-2 (Metzger et al., 2003; Osier et al., 2008; Polley et al., 2006) and MSP-3 (Osier et al., 2008; Roussilhon et al., 2007). Such studies have enabled the identification of antigenic targets of clinical immunity but in order to identify antigenic targets of anti-parasite immunity it is necessary to look for a correlation between the presence of antibodies and reduced risk of asymptomatic malaria infection. Such a correlation has been demonstrated for antibodies against MSP-1 (Chizzolini et al., 1988; Egan et al., 1996).

Population genetic analysis can be used to identify parasite antigens that are under strong selection by the host immune response. There is frequency-dependent selection on antigens, such that a pathogen with an allelic type at a low frequency in the population is more likely to escape an acquired immune response than a pathogen with a high frequency allelic type. As the advantage of the rare allelic form is soon lost if becomes more common, no single allele at that locus will reach fixation. In the case of polymorphic antigens encoded by single gene loci, this would result in selection maintaining different alleles within populations. Consequently, by

identifying which polymorphic loci are under strong balancing selection, one can identify which loci are targets of an allele-specific protective immune response. Such population genetic analyses have identified that a number of MSAs, including MSP-1 block 2, MSP-3.4, and MSP-7, as targets of acquired immunity (Conway et al., 2000; Tetteh et al., 2009).

Where successful protection from immunisation with malarial antigens in experimental models of malaria has been shown to correlate with, or be dependent upon, specific antibody responses, this has been taken as support for that antigen being a target of protective immunity. Numerous studies have provided such support for various regions of MSP-1 as targets of the protective immune response (Chang et al., 1996; Daly and Long, 1995; Ling et al., 1995; Siddiqui et al., 1987).

There are undoubtedly numerous antigenic targets of antibody mediated protective immunity yet to be identified, not least because novel blood stage specific *P. falciparum* antigens are still being described (Trieu et al., 2011). Although there are numerous lines of evidence that support the notion that MSAs are targets of antibody mediated protective immunity, a correlation between MSA-specific antibodies and protection does not explicitly prove causation. For this reason, researchers have tried to identify the causative mechanisms by which MSA-specific Abs bring about protective immunity.

1.3.5 Mechanisms of antibody mediated immunity to merozoite surface antigens

In vitro growth inhibition assays (GIAs) involve the addition of antimalarial antibodies to late trophozoite infected erythrocytes and the measurement of parasitaemia following the next invasion cycle. A lower parasitaemia relative to control cultures indicates that these antibodies inhibit the asexual growth of the parasite, either through disruption of merozoite invasion or interference with the subsequent intraerythrocytic development of the parasite. Antibodies to numerous MSAs have been shown to inhibit the *in vitro* growth of *P. falciparum* in GIAs,

including MSP-1 (Blackman et al., 1990), MSP-2 (Clark et al., 1989), MSP-6 and MSP-7(Kauth et al., 2006). This inhibition is mediated by binding of Ab alone, as no other effector cells of the immune system are present in these assays.

The binding of antibodies to the merozoite surface can prevent erythrocyte invasion through a number of different mechanisms. Antibodies to MSP-1 are able to agglutinate merozoites (Bergmann-Leitner et al., 2009; Lyon et al., 1997; Lyon et al., 1986b), thereby preventing their dispersal and ability to invade new erythrocytes. Antibodies are able to block the physical interaction between the merozoite antigens they bind to and their protein interaction partners. MSP-1 has been implicated in the attachment of the merozoite to the erythrocyte surface, and the binding of specific antibody has been shown to reverse this process (Perkins and Rocco, 1988). Antibodies specific to MSP-1_{42}, MSP-6, and MSP-7 are able to prevent secondary processing of MSP-1 by the subtilisin-like protease PfSUB1 (Bergmann-Leitner et al., 2006; Blackman et al., 1994; Guevara Patiño et al., 1997; Woehlbier et al., 2010), an essential prerequisite for merozoite invasion to occur (Child et al., 2010). Encouragingly, the same Ab function has been detected in the sera of individuals naturally exposed to malaria, although this was not correlated with growth inhibitory activity of that sera *in vitro* (Nwuba et al., 2002). Other MSP-1 specific Abs block the binding of these processing inhibitory anti-MSP-1 Abs and have accordingly been termed "blocking Abs" (Blackman et al., 1994; Guevara Patiño et al., 1997). Interestingly, some blocking Abs recognise epitopes that are spatially distinct in primary sequence to those recognised by the process inhibitory antibodies (Guevara Patiño et al., 1997).

Some MSP-1_{19}-specific antibodies do not interfere with the process of merozoite invasion, but adversely affect the development of the parasite inside the RBC post invasion (Arnot et al., 2008; Bergmann-Leitner et al., 2009; Moss et al., 2012; Woehlbier et al., 2006). The mechanism of this intraerythrocytic inhibition is unknown, although anti-MSP-1_{19} Abs have been shown to locate to the food vacuole post invasion (Dluzewski et al., 2008), which has lead some to speculate that these antibodies may interfere with food vacuole formation (Moss et al., 2012).

Some MSA-specific antibodies do not display growth inhibitory activity *in vitro* on their own but instead act in combination with effector cells of the immune system to inhibit the asexual growth of *P. falciparum*. This occurs during a process known as antibody-dependent cellular inhibition (ADCI), in which an interaction between monocytes and antibodies via their FcγRIIa and FcγRIIIa receptors results in the release of undefined soluble monocyte-derived factors, which mediate inhibition of parasitaemia (Bouharoun-Tayoun et al., 1990; Bouharoun-Tayoun et al., 1995; Jafarshad et al., 2007). ADCI activity requires antibody to bind its cognate antigen; targets of ADCI so far identified include MSP-1 block 2 (Galamo et al., 2009), MSP-3 (Oeuvray et al., 1994), and glutamate-rich protein (GLURP) (Theisen et al., 2000).

Opsonised merozoites have been shown to be phagocytosed by neutrophils *in vitro* (Kumaratilake et al., 1991; Kumaratilake et al., 1990), and neutrophil respiratory bursts are triggered by opsonised merozoites and enhanced by cytokines (Kumaratilake et al., 1997). Recently, a novel high throughput *in vitro* assay that measures the reactive oxygen species (ROS) generated by polymorphonuclear neutrophils (PMNs) in the presence of merozoites and immune IgG, termed antibody dependent respiratory burst (APRB), was found to correlate with naturally acquired clinical protection in endemic areas (Joos et al., 2010). Merozoites opsonised by MSP-2-specific Abs have been shown to be phagocytosed by monocytes *in vitro*, and this mechanism may explain some or all of the reduction in parasitaemia seen during ADCI (Stubbs et al., 2011).

As discussed earlier, there is an antibody subclass bias in response to *P. falciparum* infection, with cytophilic antibody subclass responses associated with protection to a higher degree than those of non-cytophilic subclasses. It is therefore interesting to note that the mechanisms of ADCI and APRB both rely on cytophilic antibody classes - this has lead some to suggest that these are important mechanisms in the *in vivo* response to *P. falciparum* infection.

1.4 Why this thesis?

The blood stage of *P. falciparum* infection is responsible for the symptomatic manifestations that result from this infection. It therefore follows that a reasonable strategy for therapeutic intervention would be to disrupt the growth of the parasite at this stage. Antibody mediated immunity is thought to compose a significant part of the protection developed against *P. falciparum* infection in endemic populations. Antigens expressed on the surface of the extracellular merozoite, being directly exposed to the human immune system, are deemed an obvious target for this antibody-mediated immunity. Indeed, there are multiple lines of evidence to support the notion that merozoite surface antigen specific antibodies play an important role in protective immunity to blood stage *P. falciparum* infection. This has lead to the development of numerous merozoite surface candidate vaccine antigens, which to date have proved at best partially effective in clinical trials (for recent reviews please see (Anders et al., 2010; Chauhan et al., 2010)). Some of the mechanisms by which antibodies to MSAs are able to inhibit *P. falciparum* growth have been identified. This thesis aims to delve deeper into these mechanisms, looking at antibodies specific to both well-characterised and novel merozoite surface vaccine candidate antigens. This is done with the view that gaining further insight into the mechanisms by which growth inhibitory antibodies act may increase our understanding of both parasite developmental processes and naturally acquired antibody mediated immunity, which may ultimately aid effective vaccine development.

1.5 Aims of this thesis

The general aim of this thesis was to investigate the mechanisms by which antibodies to merozoite surface antigens inhibit the growth of *P. falciparum in vitro*. My three results chapters address the following specific aims:

1. To generate human monoclonal antibodies to MSAs as useful reagents with which to investigate mechanisms of *in vitro* growth inhibition.

2. To investigate the hypothesis that the mechanism underpinning growth inhibition by anti-MSP-1_{19} antibodies is via an antibody-dependent water oxidationprocess, generating reactive oxygen species.

3. To elucidate how antibodies to a novel merozoite surface antigen target (MSP3.3) inhibit *P. falciparum* growth *in vitro*.

The order in which these results chapters are presented reflects the development of my ideas and hypotheses over the time of my PhD project.

2 Materials and Methods

This chapter describes materials and methods common to two or more results chapters of this thesis. Materials and methods specific to a single chapter can be found in the materials and methods section of that chapter.

2.1 Long term culture and manipulation of *P. falciparum*

2.1.1 Freezing of *P. falciparum*

Cultures with a high percentage of ring forms were selected for deep freezing. The culture was placed in a 15 mL falcon tube and centrifuged at 900 x G for 5 minutes. The supernatant was removed and deep freezing solution (28% glycerol, 3% D-sorbitol, 0.65% NaCl) was added drop by drop with mixing at a ratio of 1 volume of deep freezing solution to 1 volume of packed cells. RBCs were aliquoted into cryovials and stored at −70 °C overnight in a cryo 1 °C freezing container, then in liquid nitrogen for longer storage.

2.1.2 Thawing of *P. falciparum*

Parasites were maintained in liquid nitrogen for long-term storage, and removed when needed for culture. Cells were placed in a 37 °C incubator until fully thawed and then transferred to a 15 mL falcon tube. For a 1 mL packed cell volume (pcv), 200 µL of a 12% solution of NaCl in dH_20 was added drop by drop with constant mixing. RBCs were allowed to equilibrate for 3 mins at room temperature (RT) before the addition of 10 mL of a 1.8 % solution of NaCl in dH_20 drop by drop with constant mixing. This was followed by the addition of 10 mL of a 0.9% NaCl, 0.2% dextrose solution in dH_20 dropwise. RBCs were centrifuged (900 x G, 5 mins), the

supernatant removed and the cells resuspended in complete medium to a 5% haematocrit. Thereafter the culture was maintained under standard conditions.

2.1.3 Routine culturing of *P. falciparum*

Manipulations of live *P. falciparum* parasites were carried out in a class II microbiological safety cabinet located within a containment level 3 culture room. Parasites were cultured in RPMI 1640 medium (Invitrogen) supplemented with 2 mM glutamine, 25 mM glucose, 25 μg mL^{-1} gentamicin, 2 mM NaOH and 10 % pooled normal human serum (Scottish National Blood Transfusion Service), referred to as "complete medium" from this point. Parasite cultures were incubated at 37 °C, 5 % CO_2.

O+ human RBCs (Scottish National Blood Transfusion Service) were isolated from whole blood by passage through a leukocyte depletion filter. RBCs were washed 3 times with RPMI 1640 (900 x G, 5 mins), resuspended at 50% haematocrit in complete medium and stored at 4 °C.

Complete culture medium was changed daily by aspirating off the medium present in the culture flask and resuspending parasites in fresh complete medium at 5% haematocrit. Parasite cultures were diluted with uninfected RBCs as required to maintain a parasitaemia between 0.5% and 5%. During routine culturing parasitaemia growth was monitored using Giemsa-stained thin blood smears.

2.1.4 Giemsa staining

Approximately 10 μL of the parasite culture at 5% haematocrit was pipetted onto a microscope slide and spread thinly with a clean microscope slide. Thin blood smears were air-dried, fixed with 100% methanol for 30 secs and air-dried again. Slides were stained with Giemsa solution in phosphate buffered saline (PBS), pH 7.2. For routine monitoring of cultures staining was for 15 minutes with a 20% Giemsa solution. For morphological analysis of parasites staining was for 45 minutes with a

10% Giemsa solution. In both cases slides were then rinsed with water, air-dried again and a drop of immersion oil added in order to view the slide under a light microscope (100 x objective).

2.1.5 Laboratory isolates of *P. falciparum*

Laboratory strains used were single genotype clonal parasite populations, which had been adapted to long-term culture *in vitro*. The Wellcome strain, originating from Western Africa (del Portillo et al., 1987), was used.

2.1.6 Sorbitol synchronisation

Sorbitol synchronisation kills mature parasite stages via osmotic lysis; parasites less than 20 hours old are impermeable to sorbitol and therefore remain intact post sorbitol treatment, along with uninfected RBCs (Lambros and Vanderberg, 1979).

P. falciparum infected RBC cultures were pelleted by centrifugation (900 x G, 5 mins), the supernatant discarded and the cell pellet resuspended to its original volume in aqueous 5% D-sorbitol (Sigma) for 5 minutes at RT. An excess of RPMI 1640 was added and the cells were pelleted again (900 x G, 5 minutes), washed twice with RPMI 1640 and returned to standard culture conditions.

2.1.7 *Mycoplasma* contamination detection

As *Mycoplasma* are not visible on Giemsa-stained smears a polymerase chain reaction (PCR) detection kit (MycoSensor PCR assay kit, Stratagene) was employed to regularly check for mycoplasmal contamination. 100 µL aliquots of cell culture medium were heated at 95 °C for 5 minutes in a 1.5ml Eppendorf tube and then briefly centrifuged. 10 µL of StrataClean resin was added to each cell culture supernatant and the two components mixed together. The tube was spun briefly (1200 x G, 1 min) to pellet the resin and an aliquot of the supernatant taken for use as a template in the PCR reaction. The following were mixed in a clean PCR tube: 5 µL 10 x *Taq* reaction buffer, 0.4 µL 20 mM dNTP mix, 2 µL Mycoplasma primer

mix, 4 µL internal control template, 0.5 µL *Taq* DNA polymerase, 5 µL test supernatant and 33.1 µL sterile dH_20. PCR program: 10 min at 94 °C, 35 x (30 s at 94 °C, 60 s at 55 °C, 60s at 72 °C), followed by a 4 °C holding step. A positive control DNA sample and a negative control (dH_20) were included. PCR products were resolved on an agarose gel. The presence of a 500 base pair (bp) band indicated that the PCR reaction was successful whereas a band of 315 bp indicated that mycoplasmal contamination was present.

2.2 Antibody purification and labelling

2.2.1 Total IgG purification

Immunoglobulin G (IgG) was purified on a Akta Prime chromatography system using 1 mL or 5 mL HiTrap Protein G columns (GE Healthcare). Protein G is a cell surface protein of group G *Streptococci* that binds to the Fc region of IgG with high affinity. Samples from which IgG was to be purified (human B cell supernatants/mouse hybridoma supernatants/immunised rabbit sera) were diluted with or dialysed into PBS, passed through a 0.22 µM filter, followed by application to the column. The column was washed with 20 mM sodium phosphate, pH 7, to remove unbound proteins before elution of the IgG with 0.1 M glycine-HCl, pH 2.7, into tubes containing $1/5^{th}$ elution volume 1 M Tris-HCl, pH 9.0 neutralisation buffer. Eluted IgG fractions were dialysed extensively into PBS. The protein concentration of purified IgG was determined by measuring the absorbance at 280 nm on a Nanodrop spectrophotometer (Labtech). Where required, purified IgG was concentrated using Amicon Ultra centrifugal filter units (50-kDa cutoff; Millipore).

2.2.2 Antibody labelling

Purified antibodies were dialysed extensively into PBS and the concentration adjusted to 2 mg mL^{-1}. Sodium bicarbonate buffer was added to the antibody solution at a final concentration of 0.1M. The labelling dye (Alexa Fluor 488 or Alexa Fluor 633) was reconstituted in DMSO at a concentration of 10 mg mL^{-1}. 100 µL of this reactive dye solution was added per 10 mg of antibody solution. The

reaction was then incubated in the dark for 1 h at RT with continuous stirring. Dye-conjugated antibody was separated from unreacted labelling reagent by gel filtration on a HiPrep 26/10 desalting column (GE healthcare) pre-equilibriated with 5 column volumes of PBS. The reaction mixture was loaded onto the column by injection and dye-conjugated antibody collected in 5 mL fractions. The protein concentration of dye-conjugated IgG was determined by measuring the absorbance at 280 nm on a Nanodrop spectrophotometer (Labtech). Where required, dye-conjugated IgG was concentrated using Amicon Ultra centrifugal filter units (50-kDa cutoff; Millipore).

2.3 Flow cytometry

Samples were acquired using on a Becton Dickinson (BD) LSR II flow cytometer using BD FACS Diva software or on a BD FACScan flow cytometer using BD Cellquest software. Flow cytometry data were analysed with FlowJo version 9.4.11 software (Tree Star, Inc.). A list of the fluorophores used to stain parasites and the flow cytometer settings used to detect them are displayed in Table 2.1.

Fluorophore	Excitation (nm)	Emission (nm)	Excitation laser (nm)	Emission detector	Machine
Hoescht 33342	343	483	355	450/40	BD LSR II
DAPI	345	455	355	450/40	BD LSR II
Coriphosphine O	460	575	488	530/30 (green fluorescence) 630 LP (red fluorescence)	BD FACscan
DCF	495	529	488	525/50	BD LSR II
Alexa Fluor 488	499	519	488	525/50	BD LSR II
DHR	505	534	488	525/50	BD LSR II
JC-1 monomer form	514	529	488	525/50	BD LSR II
JC-1 J-aggregate form	585	590	488	610/20	BD LSR II
Alexa Fluor 633	632	648	633	660/20	BD LSR II

Table 2.1 Flow cytometry dyes and flow cytometer settings

2.4 Immunofluorescence assay

Immunofluorescence assay (IFA) is a technique used to visualise parasite antigens using an antigen-specific primary antibody followed by a secondary antibody conjugated to a fluorochrome. Serial dilutions of test samples were made in PBS containing 1% bovine serum albumin (BSA) and 0.01% sodium azide. A 25 µL volume of each dilution was added, in duplicate, to wells of a multispot slide containing acetone-fixed parasites and incubated at room temperature for 30 minutes. Antibody solutions were aspirated using a Pasteur pipette attached to a vacuum pump and slides washed three times with PBS. The slides were dried for 10 minutes at 50 °C, then each spot was incubated with 15 µL fluorescein isothiocyanate (FITC)-conjugated anti-mouse IgG or FITC-conjugated anti-human IgG for 30 minutes at room temperature. Slides were washed a further 3 times in PBS, stained with 0.5 µg mL^{-1} 4',6-diamidino-2-phenylindole (DAPI)/PBS and mounted in Citifluor (Citifluor Limited). Antibody-reactive parasites were viewed by FITC fluorescence and parasite nuclei by DAPI fluorescence with incident light of 390-440 nm and 450-490 nm respectively, using a fluorescence microscope with a 100 x objective.

3 The isolation and characterisation of merozoite surface antigen-specific human monoclonal antibodies

3.1 Introduction

MSP-1 is a ~ 195 kDa protein that ubiquitously covers the merozoite surface. Comparison of variant MSP-1 nucleotide sequences among different *P. falciparum* isolates has led to the demarcation of 17 distinct MSP-1 blocks characterised by their content of conserved, dimorphic or polymorphic sequences (Tanabe et al., 1987). Sequences of the highly polymorphic block 2 region of MSP-1 fall into one of three allelic types: K1, MAD20 and RO33, the first two of which vary greatly between isolates due to the extensive polymorphism of the tripeptide repeats present in each serotype (Cavanagh et al., 2004; Jiang et al., 2000; Miller et al., 1993). In contrast, the C-terminal MSP-1_{19} region is highly conserved among isolates. Cysteine-rich MSP-1_{19} is composed almost entirely of 2 tandemly repeated epidermal growth factor (EGF)-like domains (Blackman et al., 1991; Cooper, 1993). The structure of recombinant *P. falciparum* MSP-1-19 has demonstrated that these EGF domains are arranged side-by-side (Morgan et al., 1999; Pizarro et al., 2003), however no function has been ascribed to these domains to date.

MSP-2 is a highly polymorphic protein unique to *P. falciparum* that is GPI-anchored to the merozoite surface. In consists of a central variable region bounded by conserved N-terminal and C-terminal regions (Fenton et al., 1991; Smythe et al., 1990). The central variable region is composed of sequence repeats interspersed with non-repetitive dimorphic sequences, which enable classification of all MSP-2 sequences into one of the two allelic families, named after the *P.falciparum* isolates 3D7 and FC27.

MSP-1 Block 2, MSP-1_{19} and MSP-2 are thought to be targets of the protective immune response to blood stage *P. falciparum* infection. Several lines of evidence support this conclusion. Firstly, reduced risks of clinical malaria episodes are associated with serum IgG antibodies to MSP-1 Block 2 (Cavanagh et al., 2004; Conway et al., 2000; Polley et al., 2003), MSP-1_{19} (al-Yaman et al., 1996; Egan et al., 1996; Riley et al., 1992) and MSP-2 (al-Yaman et al., 1995; Metzger et al., 2003; Polley et al., 2006). Secondly, data from animal models are supportive of these MSAs playing a role in protective immunity. Vaccination with recombinant MSP-1_{19} (Ahlborg et al., 2002; Hirunpetcharat et al., 1997; Wipasa et al., 2002) or MSP-2 (Lougovskoi et al., 1999; Saul et al., 1992) antigens and passive transfer of MSP-1_{19} antibodies confer protection in mouse models of malaria (Daly and Long, 1995). *Aotus lemurinus griseimembra* are protected against virulent *P. falciparum* challenge following the generation of MSP 1 Block 2-specific or MSP-1_{19} -specific antibodies in response to MSP-1 Block 2 (Cavanagh *et al.*, manuscript in preparation) or MSP-1_{42} immunisation (Chang et al., 1996), respectively. A synthetic MSP-1 Block 2 construct containing all possible tripeptide repeat combinations seen within naturally occurring Block 2 sequences in addition to the semi-conserved Block 1 has been constructed. This novel polymorphic parasite antigen is immunogenic in experimental animals (Cowan et al., 2011). Thirdly, polymorphism in the genes encoding MSP-1 Block 2 and MSP-2 is actively maintained by balancing selection, indicating that an effective host immune response is generated against each allelic form of these two antigens (Conway, 1997; Conway et al., 2000).

MSP-1 and MSP-2 have received considerable attention as candidate vaccine antigens. However, to date no vaccine candidates based on these antigens have demonstrated high efficacy in human clinical trials, despite the strong aforementioned evidence that these antigens are targets of the protective immune response. Would identifying the critical epitopes targeted by these protective antibody responses, in addition to dissecting the functional mechanisms underpinning them, inform more effective vaccine design?

In vitro assays can be used to elucidate the mechanisms by which antibodies inhibit the growth of *P. falciparum*. Allele-specific growth inhibition by human anti-MSP-1 Block 2 antibodies has been demonstrated in an ADCI assay (Galamo et al., 2009), however antibodies alone are not inhibitory, with the exception of a report of inhibitory activity with one mouse monoclonal antibody (Locher et al., 1996). Antibodies to MSP-1_{19} are able to inhibit the growth of *P. falciparum in vitro* through a number of mechanisms, including agglutinating merozoites released from schizonts (Gilson et al., 2008), preventing PfSUB2 mediated secondary processing of MSP-1 (Blackman et al., 1994; Woehlbier et al., 2010) and interference with parasite growth post invasion (Bergmann-Leitner et al., 2009; Woehlbier et al., 2006). Human antibodies to MSP-2 are effective mediators of ADCI (Flueck et al., 2009; McCarthy et al., 2011).

Antibodies used to investigate anti-parasite effector mechanisms have primarily been mouse mAbs produced using hybridoma technology or whole IgG/antigen-specific IgG purified from the sera of immunised experimental animals or malaria-exposed humans. The advantage of using mouse mAbs is that the functional activity of an antibody can be mapped to the precise epitope it recognises. The following example illustrates the importance of identifying the fine specificity of antibody responses in order to understand the mechanisms by which anti-parasite effector mechanisms operate. Naturally acquired antibodies to MSP-1 include antibodies that inhibit the secondary processing of MSP-1, termed processing-inhibitory antibodies, in addition to non-inhibitory antibodies which disrupt this processing-inhibitory activity, referred to as blocking antibodies (Guevara Patiño et al., 1997; Nwuba et al., 2002). Therefore, eliciting Abs able to inhibit merozoite invasion through vaccination with MSP-1_{19} would be a wasted effort if blocking antibodies were simultaneously acquired. Furthermore, the fine specificity of MSP-1_{19} antibodies has been shown to be predictive of protection from *P. falciparum* infection and high density parasitaemia (Okech et al., 2004).

Identifying the fine specificity of an antibody response additionally allows examination of the binding affinity of the antibody, which may in turn affect its

functional phenotype. For example, in one study affinity-enhancing mutations in anti-AMA1 shark Ig new antigen receptors resulted in an increase in their functional GIA activity (Henderson et al., 2007). Well-characterised mAbs with GIA activity are against conformational epitopes, whereas many of the antigenic targets of ADCI are predicted to be intrinsically unstructured proteins (IUPs). Intriguingly, given that one might expect antibody interactions with IUPs to be of a fairly low affinity, it has been hypothesised that affinity may explain the difference in functional activity of these antibodies (Anders et al., 2010). More recently, a study in a malaria endemic region of Tanzania found that the affinity of antibodies to AMA1 and MSP-2 was associated with a lower risk of developing malaria during the follow-up period of the study, when subjects were parasite-positive at the beginning of the study (Reddy et al., 2012). The affinity of antibodies may also play a role in immune effector mechanisms to pregnancy-associated malaria. A recent study found that a higher proportion of high avidity anti-VAR2CSA antibodies were associated with a significantly lower risk of pregnant women developing placental malaria at the time of delivery (Tutterrow et al., 2012).

Some of the protective effects of MSA-specific antibodies are mediated trough the interaction of their Fc region with the Fc receptors (FcR) of immune effector cells and/or complement. There are important differences between the FcR systems of mice and humans, for example there are no known murine counterparts of human FcγRIIa, FcγRIIc and FcγRIIIb (Ravetch and Lanier, 2000). Naturally acquired antibodies from malaria immune individuals belong to the cytophilic IgG1 and IgG3 subclasses (Ferreira et al., 1998) and these antibody isotypes can elicit phagocytic signals through binding of FcγRIIa. The inability of mouse antibodies to activate signalling through binding human FcγRIIa precludes full analysis of potential Fc-mediated antiparasite effects using mouse mAbs. This is illustrated by the fact that ADCI requires synergistic activation of FcγRIIa and FcγRIIIa (Jafarshad et al., 2007).

The problems of investigating Fc-mediated effects using mouse mAbs or IgG purified from the serum of immunised experimental animals can be overcome by

using human antibodies purified from the sera of malaria-exposed individuals. However, it can be ethically and logistically difficult to obtain antibodies in sufficient quantities for use in IgG-hungry *in vitro* inhibition assays via this method. In addition, these antibodies are finite in their supply and polyclonal, thus not allowing for the investigation of the effects of antibody-epitope fine specificity.

Therefore full dissection of antibody functional activities is not possible using mouse mAbs and affinity-purified IgG from immunised animals or malaria-exposed humans due to the lack of information they provide about the fine specificity and Fc-mediated effects of the immune response. Human antibodies represent an ideal alternative with which to investigate anti-parasite effector mechanisms. Initial endeavours demonstrated that human mAbs could be generated by immortalising B cells with Epstein Barr-virus (EBV) (Kozbor and Roder, 1981; Steinitz et al., 1977; Steinitz et al., 1979) or by fusing B cells with a suitable partner to produce hybridomas (Karpas et al., 2001; Kozbor et al., 1982). However, until recently these methods had a very low efficiency.

An efficient method of human memory B cell immortalisation with Epstein-Barr virus (EBV) in the presence of irradiated mononuclear cells and a polyclonal memory B cell activator has been described (Traggiai et al., 2004). B cells producing antibodies of interest can be cloned from polyclonal B cell pools immortalised via this method and the desired mAbs isolated from the resultant supernatant. This method has been successfully employed to isolate VAR2CSA-specific human mAbs, which have proved useful in identifying functionally important epitopes within this CSA-binding molecule (Barfod et al., 2007; Barfod et al., 2010). This chapter describes efforts to isolate and characterise human mAbs specific to MSAs generated via this method.

3.2 Aims of this chapter

The research presented in this chapter aimed:

1. To isolate human MSA-specific mAbs from the EBV-transformed memory B cells of malaria exposed individuals.
2. To determine the IgG subclass of MSA-specific human mAbs.
3. To determine the light chain isotype of MSA-specific human mAbs.
4. To identify the epitopes recognised by these MSA-specific human mAbs.
5. To establish the affinity of these MSA-specific human mAbs.
6. To investigate the functional activities of these human mAbs in *in vitro* growth inhibition assays such as GIA and ADCI and how these might relate to characteristics of the mAbs established under aims 2-5.

3.3 Materials and methods

3.3.1 Media

The following media were used for culture and manipulation of peripheral blood mononuclear cells (PBMCs):

B cell medium: RPMI medium 1640 - L-Glutamine supplemented with 10% ultra low IgG fetal bovine serum (Invitrogen), 4 mM L-Glutamine (Invitrogen) and 1% penicillin-streptomycin (Invitrogen).

CPGT medium: RPMI medium 1640 - L-Glutamine supplemented with 10% ultra low IgG fetal bovine serum (Invitrogen), 4 mM L-Glutamine (Invitrogen), 1% penicillin streptomycin (Invitrogen), 323.83 nM CpG oligonucleotide (made to order, Oligo Factory) and 374 nM holotransferrin from human plasma (616424, Millipore).

3.3.2 CpG Oligonucleotide

A CpG phosphorothioate oligodeoxynucleotide (ODN) was synthesised by Oligo Factory. The sequence of the ODN is 5'TCG TCG TTT TGT CGT TTT GTC GTT3' (Hartmann and Krieg, 2000). The lyophilised ODN was reconstituted to 5 mg mL^{-1} in sterile dH_20, heated at 65 °C for 5 minutes and placed at 20 °C for long-term storage.

3.3.3 PBMC isolation from whole blood

40 mL of venous blood was collected in vacuettes (Greiner bio-one). Whole blood was diluted with 1 x PBS at a ratio 1:2 and aliquots of 20 mL of this mixture added to leucosep tubes (Greiner Bio-One) pre-filled with separation medium (Ficoll-Paque). Leucosep tubes were centrifuged at 800 x G for 15 minutes, which results in the separation of whole blood into different fractions. As much as possible of the top layer (consisting of plasma) was removed without disrupting the layer beneath it. The cell fraction below this, containing PBMCs, was harvested and transferred to a 50 mL falcon tube. The PBMC layer was resuspended in 20 mL of B cell medium and centrifuged at 300 x G for 10 minutes. The supernatant was taken off and the cells washed once more with 20 mL B cell medium (769 g for 10 minutes).

3.3.4 Irradiation of isolated PBMCs

Isolated PBMCs were resuspended in B cell medium at a concentration of 1 x 10^6 cells/mL and irradiated with 50 gray of gamma-radiation. Irradiated cells were spun down at 769 g for 5 minutes and washed twice with B cell medium. Following this, irradiated PBMCs were resuspended in CPGT medium at the required concentration.

3.3.5 EBV stock preparation

B95-8 is a marmoset EBV-transformed leukocyte cell line that produces infectious (transforming) EBV (Miller et al., 1972). Exponentially growing B95-8 cells were diluted to 0.5 x 10^6 cells mL^{-1} in B cell medium and incubated with 100 nM phorbol myristate acetate (PMA) for 2 hours at 37 °C. Cells were washed 3 times in Hanks' balanced salt solution (Invitrogen) then resuspended in B cell medium at a concentration of 1 x 10^6 cells mL^{-1}. The cells were incubated at 37 °C, 5% CO_2 for 48 hours. Following this, the B95-8 cells were centrifuged (500 x G, 8 minutes) and the EBV-containing supernatant harvested. Harvested supernatants were passed through a 0.22 μM membrane and then maintained at −80 °C for long term storage.

3.3.6 B cell immortalisation

PBMCs were maintained in liquid nitrogen for long-term storage before use. PBMCs were placed in a 37 °C incubator until fully thawed and then transferred to a 15 mL falcon tube. 5 mL of B cell medium was added drop-wise with mixing to the thawed PBMCs. The PBMCs were centrifuged at 500 x G for 8 minutes and then washed a further two times with B cell medium.

B cell purifications were carried out using Miltenyi Biotec CD22 microbeads and MS columns according to the manufacturer's instructions. A separation filter was used when applying PBMCs to the MS column in order to prevent cell clumping. Eluted cells were centrifuged at 769 x G for 8 minutes and resuspended at a concentration of 1 x 10^5 cells mL^{-1} in CPGT medium. An equal volume of EBV supernatant was added to this cell suspension and transfection allowed to occur over a 5 hour incubation at 37°C, 5% CO_2. Following this, B cells were diluted in CPGT medium to a concentration of 0.5 x 10^4 cells mL^{-1}. Then, 50 µL of this cell suspension was dispensed into the wells of a round-bottomed microtitre plate (Sigma-aldrich). An equal volume (50 µL) of irradiated PBMCs at a concentration of 1 x 10^6 cells mL^{-1} in CPGT medium were dispensed into each well. Plates were incubated at 37 °C, 5% CO_2.

3.3.7 Cloning of polyclonal immortalised B cell pools

Polyclonal B cell pools of interest were cloned by limiting dilution and/or single cell sorting.

3.3.7.1 Cloning by limiting dilution

PBMCs were isolated from venous blood and irradiated as described above. The number of live cells present was determined by trypan blue exclusion. Each polyclonal B cell line was diluted with CPGT medium to two different densities; 20 live cells mL^{-1} and 80 live cells mL^{-1}. 25 µL of the irradiated PBMC suspension was dispensed into the wells of a flat-bottomed 384-well microtitre plate, after which 25

μL of the 20 cells mL^{-1} suspension of B cells was added to each plate well. 25 μL of the irradiated PBMC suspension was dispensed in the wells of another flat-bottomed 384-well microtitre plate, to which 25 μL of the 80 cells mL^{-1} suspension of B cells was added to each plate well.

3.3.7.2 Cloning by single cell sorting sorting

PBMCs were isolated from venous blood and irradiated as described above. Irradiated PBMCs were resuspended in CPGT medium at a concentration of 0.5 x 10^6 cells mL^{-1}. 50 μL of the irradiated PBMC suspension was dispensed into the wells of a flat-bottomed 384-well microtitre plate. Polyclonal B cell lines were washed with RPMI 1640 and resuspended in ~ 3 mL RPMI at a density of 1 x 10^5 cells mL^{-1}. The B cells were then sorted on a FACSAria cell sorter such that one B cell was deposited into each well of the 384-well microtitre plate containing irradiated PBMCs.

3.3.7.3 Cloning by fluorescence-activated cell sorting

1 x 10^6 EBV-transformed B cells were centrifuged (500 x G, 8 minutes) and resuspended in 100 μL FACs buffer (1% BSA, 1 x PBS) containing 1.85 μg mL^{-1} of Alexa fluor 663-labeled recombinant MSP-1 Block 2 RO33 antigen. Cells were stained in the dark for 30 minutes and then washed extensively with FACs buffer prior to being resuspended in 300 μL FACs buffer. Stained B cells were run through a FACSAria cell sorter. Live B cells were gated on FSC and SSC. A second gate was applied to gated live B cells. This second gate was of Alexa fluor- MSP-1 Block 2 RO33 positive B cells and was defined based on Alexa Fluor 633-staining of MSP-1 Block 2 RO33-specific EBV-transformed B cells compared to Alexa Fluor 633-staining of a stained negative control, namely EBV-transformed B cells from a malaria naive individual which did not produce MSP-1 Block 2 RO33 -specific antibodies (confirmed by ELISA). B cells within this gate were then sorted such that one B cell was deposited into each well of the 384-well microtitre plate containing irradiated PBMCs (as described above).

3.3.7.4 Media supplementation

The plates were incubated at 37 °C, 5% CO_2. 7 and 14 days after cloning 15 µL of CPGT medium were added to plate wells. 21 days after cloning plates were examined by light microscopy for the presence of growing clones.

3.3.7.5 Other supporting media

For some cloning procedures immortalised B cells were cloned onto supportive media other than PBMCs. These were:

i) irradiated Jurkat cells, an IL-2 producing T lymphocyte cell line
ii) THP-1 cells that had been pre-incubated with 50 ng μL^{-1} PMA for 24 hours, prior to being washed and resuspended in CPGT medium
iii) THP-1 cells the had been pre-incubated with 5 µg/mL PHA for 24 hours, prior to being washed and resuspended in CPGT medium
iv) Jurkat cell supernatant
v) Mixed lymphocyte reaction supernatant
In all cases 50 µL of supporting medium (if containing cells these were at a concentration of 0.5×10^6 cells mL^{-1}) were placed into wells of a 384-well plate prior to the addition of B cells as described above. To all wells 2-Mercaptoethanol was added at a final concentration of 50 nM.

3.3.8 Routine culturing of immortalised B cells

Manipulations of immortalised B cells were carried out in a class II microbiological safety cabinet located within a containment level 2 culture room. Immortalised B cells were cultured in CPGT medium and incubated at 37 °C, 5% CO_2. CPGT medium was changed twice weekly (or more frequently if required) by pelleting cells by centrifugation, aspirating off the supernatant and resuspending the cells in fresh CPGT medium. Cells were maintained at a density between 1×10^5 and 1×10^6 cells mL^{-1} in T-25 or T-75 cell culture flasks or at a density of ~ 3×10^7 cells/mL when maintained in CELLine 1000 two-compartment bioreactors (Integra Biosciences).

3.3.9 Enzyme-linked immunosorbant assay (ELISA) protocols

The following buffers were used in the ELISA protocols detailed below:

Coating buffer: 15 mM Na_2CO_3, 35 mM $NaHCO_3$, pH 9.3
Washing buffer: PBS supplemented with 0.05% Tween-20
Blocking buffer: PBS supplemented with 0.05% w/v Tween-20 and 1% w/v skimmed milk powder
Development buffer: 0.04 mg mL^{-1} O-phenylenediamine, 0.012% H_20_2, 24.5mM citric acid monohydrate and 52 mM Na_2HPO_4, pH 5.0

3.3.9.1 B cell supernatant ELISA screening

All test B cell supernatants were added to duplicate wells on the same plate and on each plate a known positive and a known negative control were added in duplicate. 96-well microtitre plates (Greiner Bio One) were coated with 0.5 µg/mL recombinant antigen in coating buffer and incubated at 4 °C overnight. Plates were washed 3 times with washing buffer and then blocked for 5 hours at RT with 100 µL/well blocking buffer. Plates were washed 3 times with washing buffer prior to the addition of 100 µL B cell supernatant, which had previously been diluted 1/2 with blocking buffer. Plates were incubated overnight at 4 °C. Plates were washed 3 times with washing buffer before incubation with 100 µL/well horseradish peroxidase (HRP)-conjugated rabbit anti-human IgG (Dako Limited, UK) diluted 1/6000 in blocking buffer for 3 hours at RT. Plates were washed 3 times with washing buffer. The reaction was developed by the addition of 100µL/well substrate buffer. Plates were incubated in the dark for 10-15 minutes at RT. The reaction was stopped by the addition of 25 µL 2M H_2SO_4 per well. The optical density was read at 492 nm on a Labsystems Multiskan Ascent microtitre plate reader.

3.3.9.2 Serum ELISA screening

The ELISA method was the same as that described for B cell supernatant screening above, with the exception that the primary antibody source for the ELISA consisted of serum samples, diluted 1/500 in blocking buffer, not B cell supernatants.

3.3.9.3 Light chain isotype ELISA

The ELISA method used was the same as that employed for the screening of B cell supernatants, with the following modifications. Plates were coated with 0.5 μg mL^{-1} MSP-1 Block 2 GST fusion protein of the RO33 serotype. Secondary antibodies used were HRP-conjugated sheep anti-human kappa light chain (AP015, The Binding Site, UK) and HRP-conjugated sheep anti-human lambda light chain (AP017, The Binding Site, UK).

3.3.9.4 IgG subclass ELISA

The method used was the same as that employed for the screening of B cell supernatants, with the following modifications. Plates were coated with 0.5 μg mL^{-1} MSP-1 Block 2 GST fusion protein of the RO33 serotype. Secondary antibodies used were HRP-conjugated polyclonal sheep anti-human IgG1 (AP006, The Binding Site, UK) and HRP-conjugated polyclonal sheep anti-human IgG3 (AP008, The Binding Site, UK).

3.3.9.5 ELISA with biotinylated peptides

A set of 131 biotinylated 12-mer peptides spanning all possible linear epitopes located within the MSP-1 hybrid were synthesised by Mimotopes Proprietary Limited. Wells of ELISA plates (Immulon 4 HBX, Thermo Dynex) were coated with 100 μL 5 μg mL^{-1} streptavidin and incubated at 37 °C until dry. Plates were washed 3 times in washing buffer and then blocked for 3 hours at RT with 200 μL per well of 1% (w/v) ByCoA (Croda Healthcare) dissolved in PBS. Following this, plates were washed 3 times in washing buffer and 300 ng of each peptide dispensed in duplicate into plate wells. Plates were incubated at 4 °C overnight. Plates were washed 3 times with washing buffer and 100 μL B cell supernatants, diluted 1/2 in PBS supplemented with 1% (w/v) ByCoA, were dispensed in duplicate into plate wells. Plates were incubated overnight at 4 °C. Plates were washed 3 times with washing buffer and then incubated with 100 μL/well HRP-conjugated rabbit anti-human IgG (Dako Limited) diluted 1/6000 in PBS supplemented with 1% (w/v) ByCoA for 3 hours at RT. Plates were then washed 3 times with wash buffer and

100 µL development buffer added to each well. Plates were incubated for 10-15 minutes in the dark at RT, after which the reaction was stopped by the addition of 25 µL 2M H_2SO_4. The optical density was read at 492 nm on a Labsystems Multiskan Ascent microtitre plate reader.

3.3.10 Expression and purification of recombinant merozoite suface antigens

Plasmid pGEX constructs encoding GST, GST MSP-1 block 2 fusion proteins of the 3D7, Palo Alto, MAD20, Wellcome, and RO33 isolates, GST MSP-2 fusion proteins of the Dd2 and CH150/9 isolates and a GST MSP-1-19 fusion protein were provided by Dr. David Cavanagh (Cavanagh and McBride, 1997; Polley et al., 2006). 2 µL of each expression plasmid was transformed into chemically competent XL-1 *E. coli* (Stratagene) and plated onto LB agar plates containing 100 µg mL^{-1} ampicillin. Starter cultures of 10 mL LB broth containing 100 µg mL^{-1} ampicillin were inoculated with a single colony from a freshly streaked agar plate and incubated with shaking at 37 °C overnight. Conical flasks containing 1 L LB broth and 100 µg mL^{-1} ampicillin were inoculated with 10 mL starter culture and incubated at 37oC with shaking until the optical density had reached 0.6 AU cm^{-1}. At this point protein expression was induced by the addition of 1 mM isopropyl β-D-1-thiogalactopyranoside (IPTG). Cultures were incubated overnight at 30 °C with shaking, after which cells were centrifuged at 5000 x G and 4 °C for 10 minutes. The supernatant was poured off and cell pellets resuspended in 30 mL 50 mM Tris, 150 mM NaCl buffer, pH 8. The resuspended cells were then lysed by sonication and 1 U mL^{-1} DNAse I was added. The samples were centrifuged at 500 x G for 20 minutes and the lysates collected in a 50 mL falcon tube. Clarified lysates were passed through a 0.22 µM filter. GST or GST fusion proteins were purified on an Akta Prime chromatography system, using 1mL GSTrap HP columns (GE Healthcare). The GSTrap HP column was pre-equilibriated with 5 column volumes of PBS and the lysate applied to the column. The column was washed with 5 column volumes of PBS and column-bound GST or GST fusion proteins eluted with elution buffer (50 mM Tris pH8.0, 10mM reduced glutathione). Collected fractions were analysed by

BCA assay and SDS-PAGE for protein concentration and purity, respectively. Eluted proteins were dialysed extensively against PBS and then stored at −20 °C until further use.

3.4 Results

3.4.1 Screening and cloning of B cell immortalisations carried out at CMP

An efficient method of human memory B cell immortalisation via EBV transformation in the presence of irradiated mononuclear cells and a polyclonal memory B cell activator has been developed (Traggiai et al., 2004). Here, this method was employed to immortalise CD22+ memory B cells isolated from the peripheral blood of malaria-exposed individuals. Pools of human B cells immortalised via this method were screened for reactivity in ELISA with the following recombinant GST fusion proteins: MSP-1 Block 2 antigens of 5 different serotypes (3D7, Palo Alto, MAD20, Wellcome and RO33), MSP-2 antigens of 2 different serotypes (Dd2 and CH150/9) and MSP-1_{19}. Additionally, all immortalised B cell pools were screened against recombinant GST alone in order to control for any anti-GST responses. Positive pools reactive with recombinant MSPs but not GST alone were cloned by limiting dilution and/or FACS sorting. Any resultant B cell clones were tested for reactivity against the relevant recombinant MSP by ELISA.

Initially, two B cell immortalisation pools (DLB23 and DLB01) carried out by members of the human mAbs team at the Centre for Medical Parasitology (CMP), University of Copenhagen, were screened for reactivity with the aforementioned MSPs. Thirteen positive polyclonal pools from donor DLB23 were cloned by limiting dilution. Of these thirteen polyclonal lines, two lines generated clones with positive reactivity to MSPs. One of these clones, DLB23-5A7 remained positive and was expanded. Attempts to re-clone the other polyclonal pools originally identified as positive were not successful, as these pools were no longer positive by the time the results of the first attempts at cloning were known.

Initial screening of the second immortalisation (donor DLB01) identified 26 polyclonal wells with positive reactivity to the recombinant MSPs. Upon re-screening one week later, 7 polyclonal lines were still positive, of which 4 were successfully expanded, frozen down in liquid nitrogen and shipped to Edinburgh to be cloned. However, upon thawing and expansion in Edinburgh all 4 lines no longer gave positive reactions by ELISA. Table 3.1 summarises the main results of all B cell immortalisations carried out.

3.4.2 B cell immortalisations carried out in Edinburgh

The reagents and technology required to carry B cell immortalisations in Edinburgh were acquired. PBMC samples collected during a study in the Merehwa district of Zimbabwe were kindly provided by Dr. Francisca Mutapi. In the first instance, an immortalisation was carried out on CD22+ B cells isolated from the PBMCs of donor Zm_7054 whose serum had tested positive in ELISA against MSP-1-19, MSP-2 (Dd2) and MSP-2 (CH150/9). Although initial ELISA screening identified 11

Donor	Geographical origin of donor	Donor sex	Immortalisation successful	Number of polyclonal wells initially positive	Number of polyclonal lines cloned	Method of cloning	Number of polylconal lines with positive clones	Reactivity of positive clones
DLB23	Dodowa, Ghana	M	Yes	38	13	LD + Cell sorting	2	Block 2 R033
DLB01	Dodowa, Ghana	M	Yes	26	0	—	—	—
Zm_7054	Magaya, Zimbabwe	F	Yes	11	0	—	—	—
Dm	Cameroon	M	Yes	4	4	LD	0	—
Zm_684	Mutoko, Zimbabwe	M	Yes	56	4	Cell sorting	1	Block 2 RO33
Zm_627	Mutoko, Zimbabwe	M	Yes	0	—	—	—	—
Zm_1074	Mutoko, Zimbabwe	F	No	—	—	—	—	—
Ka	Ghana	M	Yes	8	3	LD + Cell sorting	0	0

Table 3.1 Summary of B cell immortalisations carried out.

Details of PBMC donors used in, and outcomes during the process of, B cell immortalisations. LD stands for limiting dilution.

polyclonal pools as positive against recombinant MSPs, none of these pools remained positive after lines were expanded and cloned.

Next, the serum of a visiting Ghanaian scientist who had recent exposure to malaria was tested by ELISA for reactivity with MSPs. This serum showed positive reactivity against MSP-2 (Dd2), MSP-2 (CH150/9) and MSP-1_{19} (Figure 3.1). Post immortalisation, 4 polyclonal B cell lines were identified as positive against recombinant MSPs in ELISA and cloned by FACs sorting. None of these lines generated positive clones.

3.4.3 Screening of PBMC samples from malaria exposed individuals

The serum of PBMC donors from the Murehwa district had previously been tested for reactivity against MSP-2 (Dd2), MSP-2 (CH150/9) and MSP-1_{19} by members of the Mutapi group (IIIR). Positive reactivities against these antigens were low, which made it difficult to select PBMC donors likely to yield MSP-specific mAb producing B cells when immortalised. In order to increase the chance of isolating B cell clones producing MSA-specific antibodies, a set of serum samples from malaria exposed PBMC donors living in the Mutoko district of Zimbabwe, an area of higher malaria endemicity than the Murehwa district, were obtained. In total 41 serum samples were screened for reactivity of IgG antibodies with GST and the following GST fusion proteins in ELISA: 3D7 Block 2, Palo Alto Block 2, MAD20 Block 2, Wellcome Block 2, RO33 Block 2, MSP-2 (Dd2), MSP-2 (CH150/9) and MSP-1_{19}. One or more serum samples showed positive reactivity against MSP-2 (Dd2), MSP-2 (CH150/9), MSP-1-19, Palo Alto Block 2, MAD20 Block 2 and RO33 Block 2 (Figure 3.2). Generally, higher reactivity was observed against MSP-1_{19} and MSP-2 than MSP-1 Block 2. Three donors whose serum displayed high reactivity to three or more antigens were prioritised for immortalisation; donors Zm_627, Zm_684 and Zm_1074, which correspond to serum samples 3, 12 and 41 in Figure 3.2, respectively.

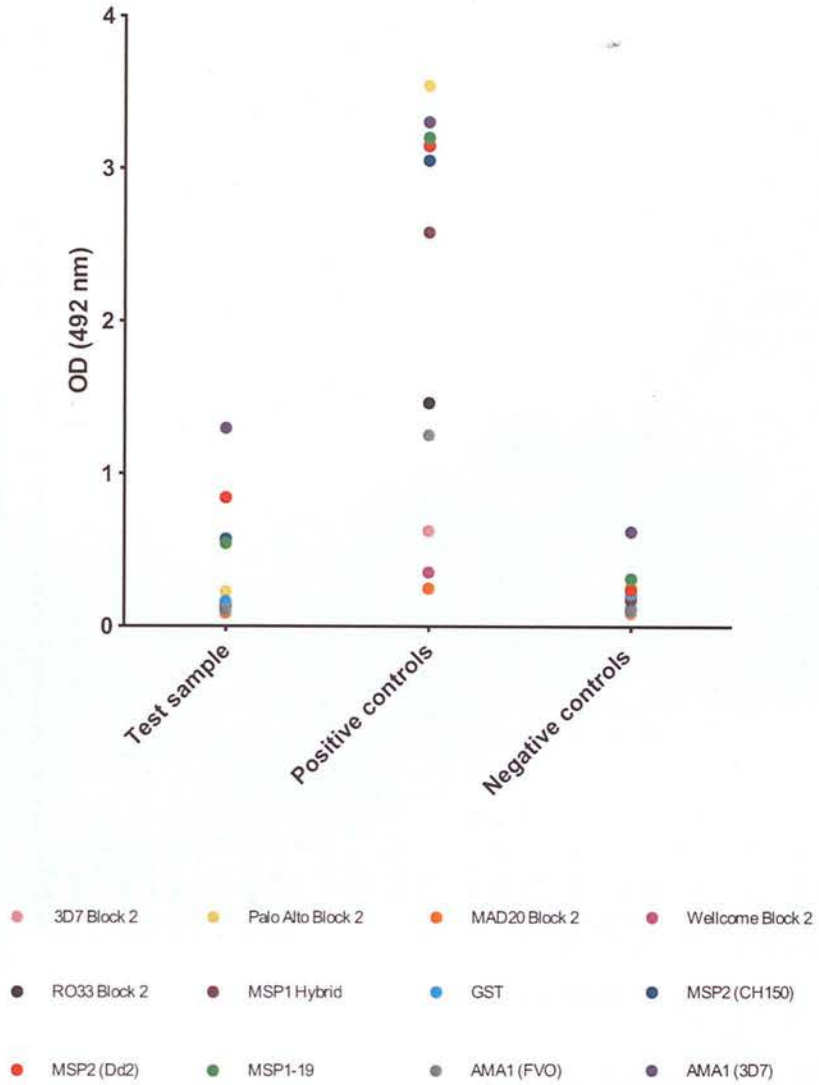

Figure 3.1 Screening of serum sample from donor Dm for IgG reactivity against recombinant MSP-1, MSP-2 and AMA-1 antigens.

The specific antigens used are denoted in the figure legend. Circles indicate the mean reactivity of two duplicate wells of a sample against a given antigen in OD units measured at 492 nm. As a positive and negative control, respectively, each recombinant antigen was reacted with human immune serum known to react positively and european serum known to react negatively, with that particular antigen.

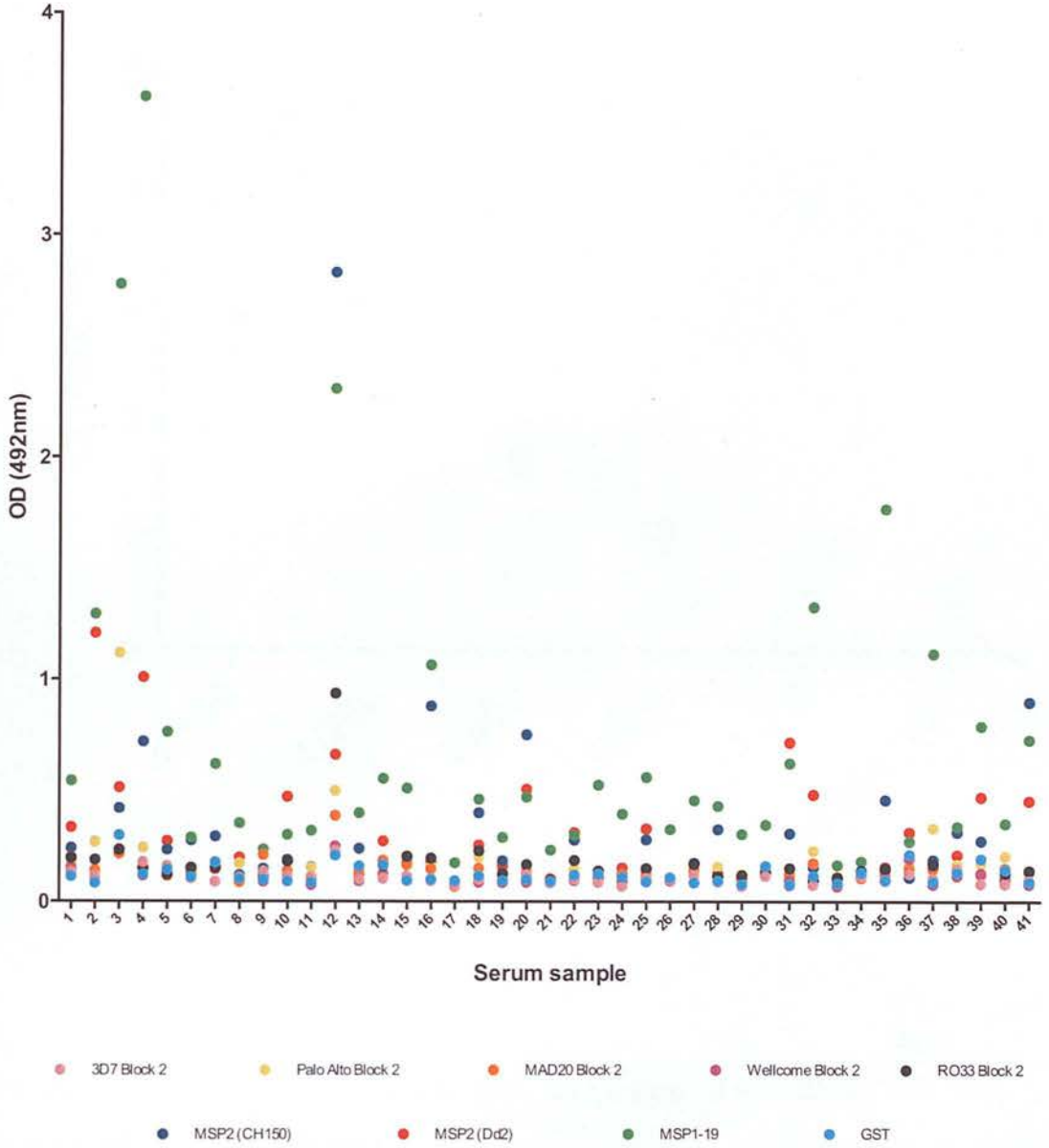

Figure 3.2 Reactivity of serum IgG antibodies from malaria exposed individuals with recombinant MSP-1 and MSP-2 antigens.

Circles indicate the reactivity of serum IgG antibodies from 41 malaria exposed individuals from the Mutoko region of Zimbabwe with the following recombinant GST fusion proteins; 3D7 Block 2 (pink), Palo Alto Block 2 (yellow), MAD20 Block 2 (orange), Wellcome Block 2 (purple), RO33 Block 2 (black), MSP-2 (CH150/9) (dark blue), MSP-2 (Dd2) (red), MSP-1-19 (green), in addition to GST alone (light blue). Each data point indicates the reactivity of serum IgG from a single individual against a single recombinant protein, shown as the mean of two duplicate wells in OD units measured at 492 nm.

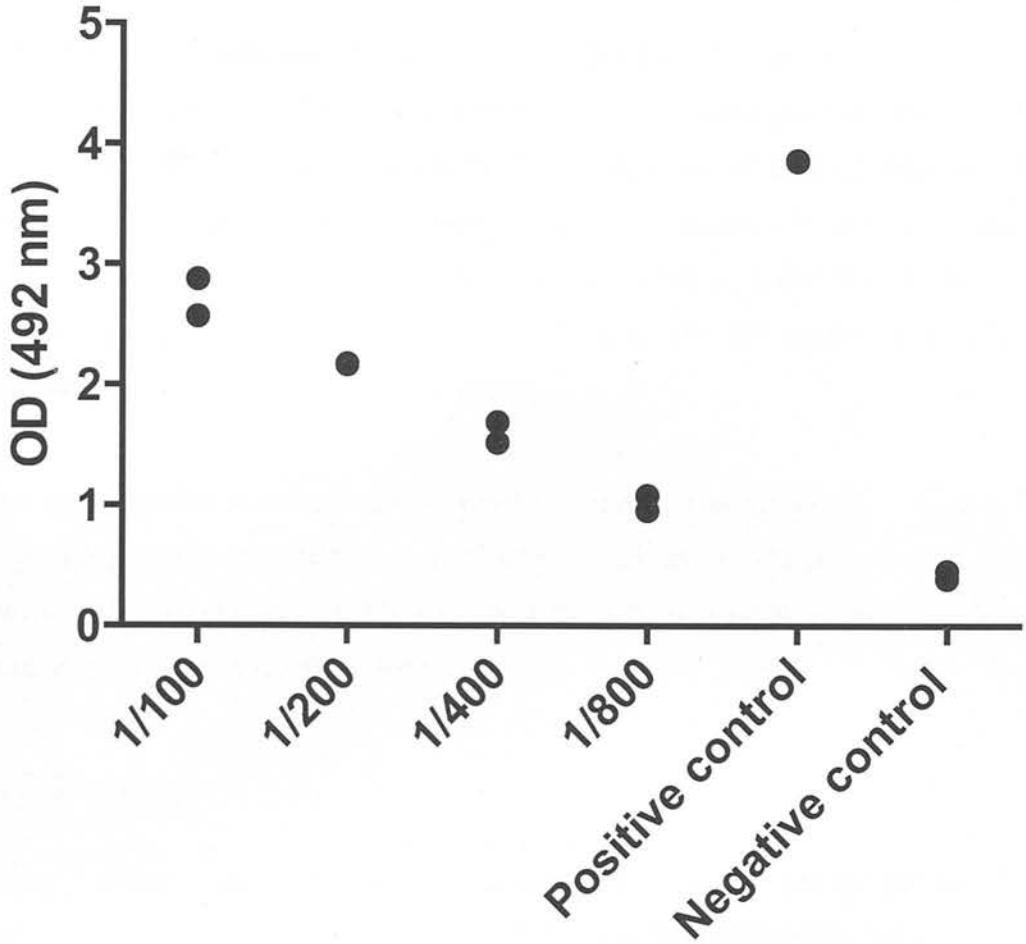

Figure 3.3 Reactivity of serum IgG antibodies from donor Ka with a recombinant antigen cocktail.

Serum from donor Ka was tested at the dilutions indicated on the x-axis for reactivity of IgG antibodies with a recombinant antigen cocktail. The antigen cocktail contained the following recombinant antigens in equal concentrations; 3D7 Block 2, Palo Alto Block 2, MAD20 Block 2, Wellcome Block 2, RO33 Block 2, MSP-2 (CH150/9), MSP-2 (Dd2), MSP-1-19 and MSP3.3. Positive and negative controls were a pool of hyperimmune sera and pooled European sera, respectively. For each sample, data points indicate duplicate ODs at 492 nm from individual wells.

3.4.5 Further B cell immortalisations

B cell immortalisations were carried out on isolated CD22+ memory B cells from Mutoko donors Zm_627, Zm_684 and Zm_1074. Proliferation of B cells was not observed after EBV transformation of B cells from donor Zm_1074, implying that the transformation process had not been successful. Memory B cells from donor Zm_627 were successfully transformed but no positive polyclonal wells were detected when screened by ELISA. Immortalisation Zm_684 yielded a polyclonal line from which generated positive clones.

Serum from another malaria-exposed visiting scientist was screened by ELISA for IgG antibodies with reactivity to a pool of recombinant MSPs (Figure 3.3). This serum was highly reactive in this ELISA, however, of 3 positive polyclonal lines cloned, none produced reactive clones.

3.4.5 Clones

At the end of this process, two of the polyclonal lines that had been cloned, one from donor DLB23 (DLB23-5A7) and one from donor Zm_684 (684-8B6), had resulted in a series of clones that were reactive with Block 2 RO33 in ELISA (Figure 3.4). Several clones from each original polyclonal line were expanded in culture. Whereas clones from 684-8B6 expanded rapidly, clones from DLB23-5A7 could not be expanded beyond 2 wells of a 96-well plate.

In total the polyclonal line DLB23-5A7 was cloned four times. The problem was not isolating clones of interest but getting them to grow once they had been single-cell sorted. Therefore, cloning onto a variety of different supportive media was trialled with the aim of encouraging growth of clones producing the antibody of interest. These support media were: irradiated PBMCs from a EBV negative donor, irradiated Jurkat cells, irradiated PMA-activated THP1 cells, irradiated PHA-activated THP1 cells, Jurkat cell supernatants and supernatants from human mixed lymphocyte reaction cultures. In addition 2-Mercaptoethanol was added to all FACs sorted B

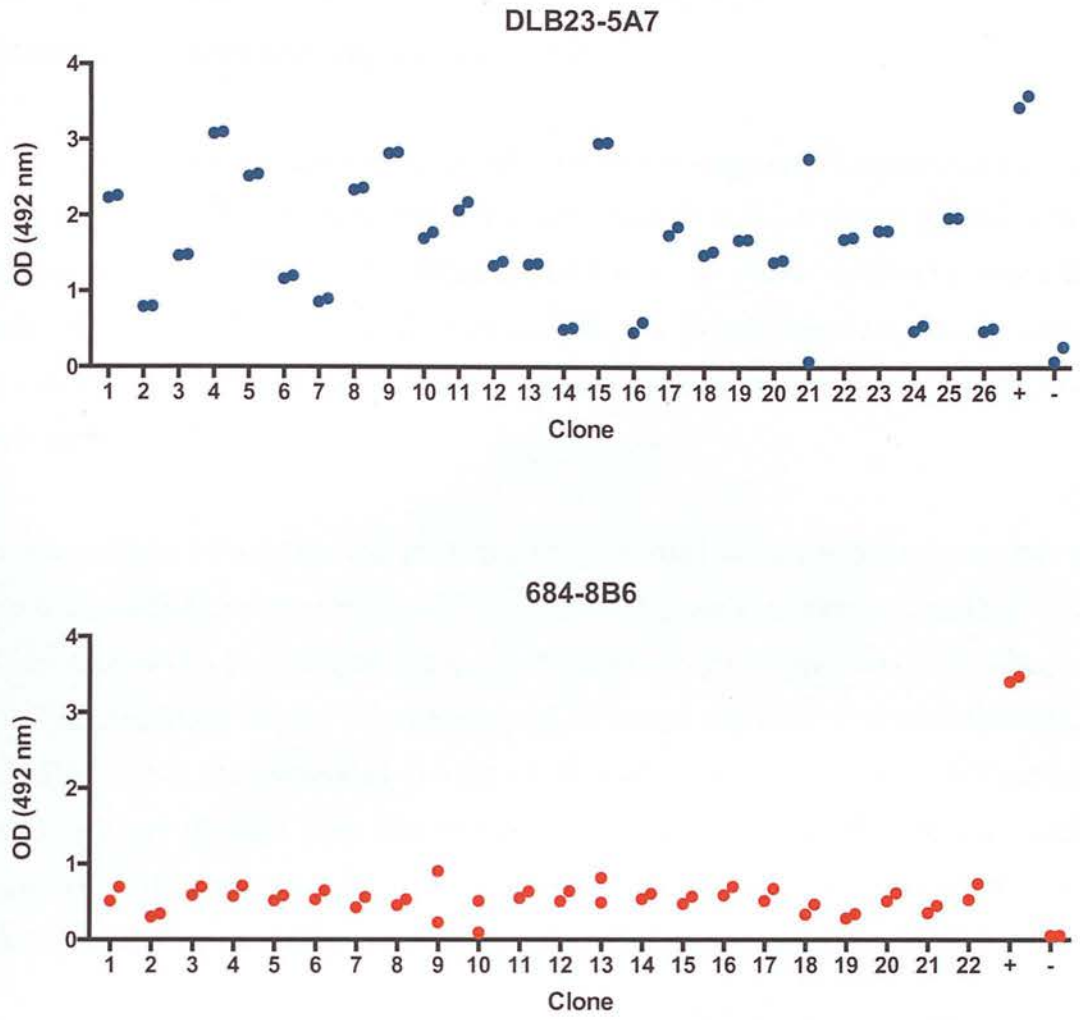

Figure 3.4 ELISA reactivity of IgG antibodies from B cell clone supernatants with MSP-1 Block 2 (RO33 serotype).

B cell supernatants from clones isolated from the polyclonal lines DLB23-5A7 and 684-8B6 were reacted with recombinant RO33 Block 2 in ELISA. Positive and negative control sera are indicated by the + and – signs, respectively. Data points represent duplicate optical densities from individual wells.

cells, as it has been reported that this helps single hybridoma cells grow to a self-sustaining population density (Lane et al., 1988).

In order to increase the probability of isolating and propagating clones producing the mAb of interest, B cells from the polyclonal pool DLB23-5A7 were stained with Alexa Fluor 633-labelled MSP-1 Block 2 RO33 and only Alexa Fluor 633-positive B cells were cloned (Figure 3.5). Despite this effort no B cell clonal populations grew to a density that allowed culture volumes beyond the volume of single wells of a 96-well plate.

In an attempt to circumvent this problem, the polyclonal line DLB23-5A7 was grown in a two-compartment bioreactor with the aim that if a large quantity of antibody-rich B cell supernatant be collected, the mAb of interest could be purified on an antigen-specific column by affinity chromatography. A clonal line generated from 684-8B6, 684-8B6-3, was also expanded and grown in another two-compartment bioreactor. Total IgG was purified from 684-8B6-3 supernatant. This IgG did not react with parasites in IFA and was only weakly reactive in ELISA. Only small amounts of total IgG were purified from polyclonal DLB23-5A7 supernatant.

3.4.6 IgG subclass

The antibody subclasses associated with protection to MSAs are IgG1 and IgG3 (Bouharoun-Tayoun and Druilhe, 1992; Cavanagh et al., 2004). Therefore, I tested whether MSP-reactive Abs from the DLB23-5A7 and 684-8B6 lines were of the IgG1 or IgG3 subclass by ELISA. B cell supernatants from each of three DLB23-5A7 and 684-8B6 lines were bound to immobilised recombinant Block 2 RO33 antigen on ELISA plates in duplicate. Anti-human total IgG, anti-human IgG1 and anti-human IgG3 secondary conjugated antibodies were reacted with antibodies from these B cell supernatants. For all three DLB23-5A7 clones, the anti-human IgG3 antibody gave significantly higher reactivity than anti-human IgG1. For all three 684-8B6 lines, the anti-human IgG1 antibody gave significantly higher reactivity than anti-human IgG3 (Figure 3.6).

A

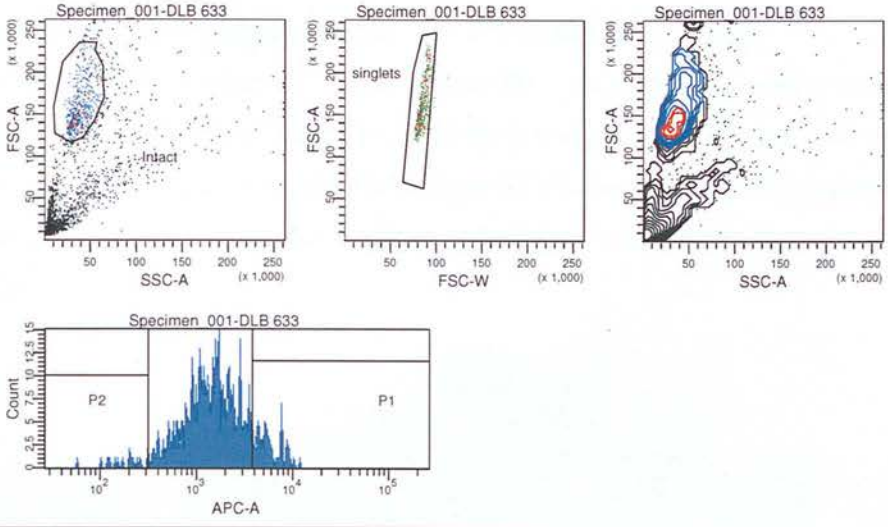

Tube: DLB 633

Population	#Events	%Parent	%Total
All Events	2,000		100.0
Intact	500	25.0	25.0
singlets	486	97.2	24.3
P1	65	13.4	3.2
P2	16	3.3	0.8

B

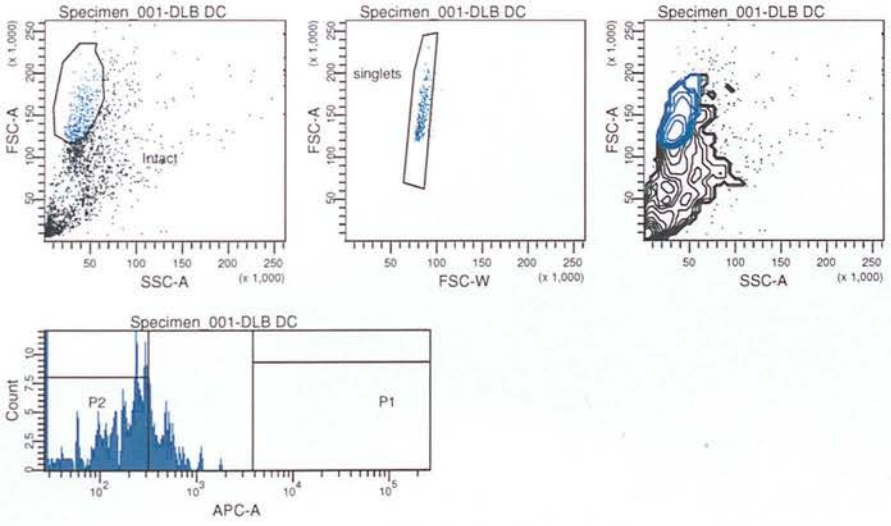

Tube: DLB DC

Population	#Events	%Parent	%Total
All Events	2,000		100.0
Intact	316	15.8	15.8
singlets	306	96.8	15.3
P1	0	0.0	0.0
P2	232	75.8	11.6

Figure 3.5 Fluorescence-activated cell sorting of polyclonal pool DLB23-5A7. EBV-transformed B cells from polyclonal pool DLB23-5A7 (panel A) and from a non-malaria exposed European donor were stained with Alexa Fluor 633-labelled recombinant MSP-1 Block 2 RO33 (panel B). First, healthy cells were gated on FSC-A and SSC-A (gate "intact"). Following this, a second gate, P1, was applied based on Alexa Fluor 633 (APC-A channel) Fluorescence. P1-gated cells from polyclonal pool DB23-5A7 were single cell sorted into a plate containing irradiated PBMCs.

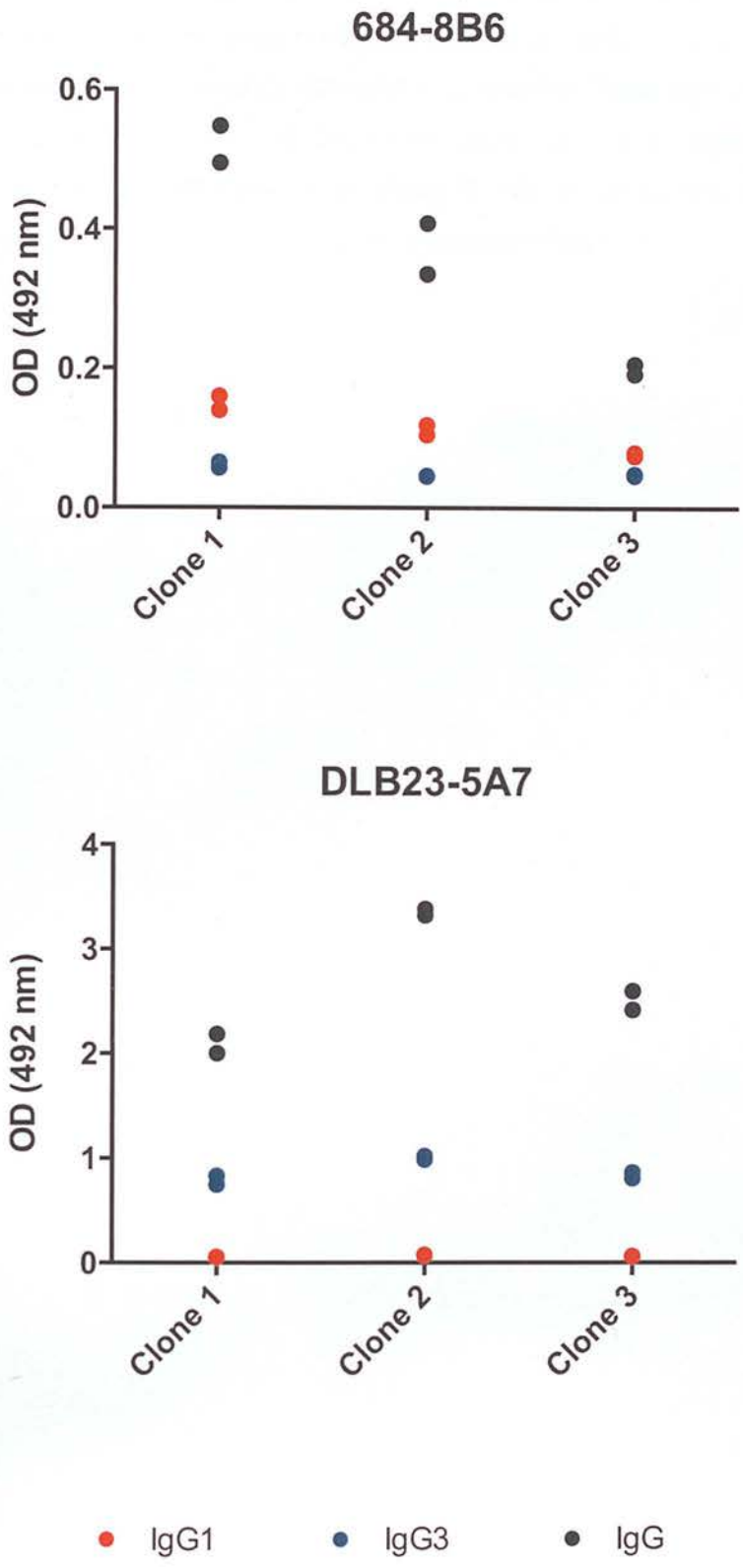
684-8B6
OD (492 nm)
0.6
0.4
0.2
0.0
Clone 1
Clone 2
Clone 3
DLB23-5A7
OD (492 nm)
4
3
2
1
0
Clone 1
Clone 2
Clone 3
IgG1
IgG3
IgG

Figure 3.6 Antibody subclass determination of mAbs DLB23-5A7 and 684-8B6. ELISA plates were coated with GST Block 2 RO33 antigen and B cell supernatants from each of 3 clonal DLB23-5A7 and 684-8B6 lines added. The reactivity of anti-human total IgG (black circles), anti-human IgG1 (red circles) and anti-human IgG3 (blue circles) antibodies with these B cell supernatants is shown. Data points indicate duplicate ODs at 492 nm from individual wells.

3.4.7 Light chain isotype

The light chain isotype of mAbs from DLB23-5A7 and 684-8B6 were determined by ELISA. B cell supernatants from an MSP-1 RO33 block 2 reactive line of DLB23-5A7 and a similarly reactive line from 684-8B6 were bound to immobilised recombinant Block 2 RO33 antigen on an ELISA plate in duplicate. Anti-human kappa light chain and anti-human lambda light chain antibodies were reacted with these B cell supernatants. For both DLB23-5A7 and 684-8B6 clones, the anti-human lambda light chain antibody gave significantly higher reactivity than anti-human kappa light chain antibody (Figure 3.7).

3.4.8 Epitope mapping

A peptide array consisting of 131 N-terminal biotinylated dodecapeptides with a 1-2 residue overlaps, covering all major linear epitopes in the Block 2 region of MSP-1, were used to fine-scale map the epitopes recognised by mAbs DLB23-5A7 and 684-8B6. The array contained all known repetitive sequences from the K1 and MAD20 serotypes, all non-repetitive regions from the K1, MAD20 and RO33 serotypes, and peptides spanning the junctions between the individual Block 2 serotypes. Given that MSP-1 Block 2 is an intrinsically unstructured protein and thus unfolded (nonglobular) in solution, one would predict its epitopes to be linear.

Consistent with the specificities of these mAbs determined by ELISA using recombinant Block 2 antigens, both mAbs reacted strongly with a set of peptides within the Block 2 RO33 serotype but did not react with peptides covering the K1 or MAD20 serotypes. These peptide reactivities were used to define a linear sequence containing all or the major components of the epitopes recognised by these mAbs. MAb 684-8B6 recognised the sequence KDGANTQV, located at the extreme N-terminus of Block 2 RO33, where as mAb DLB23-5A7 recognised the adjacent but non-overlapping sequence VAKPADAV (Figure 3.8).

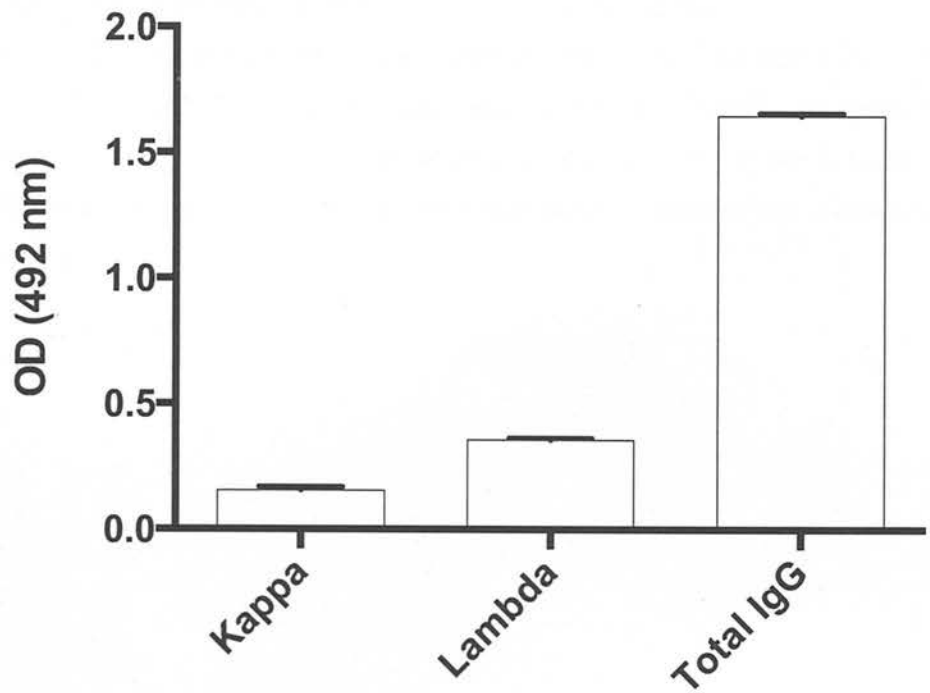
684-8B6
OD (492 nm)
2.0
1.5
1.0
0.5
0.0
Kappa
Lambda
Total IgG

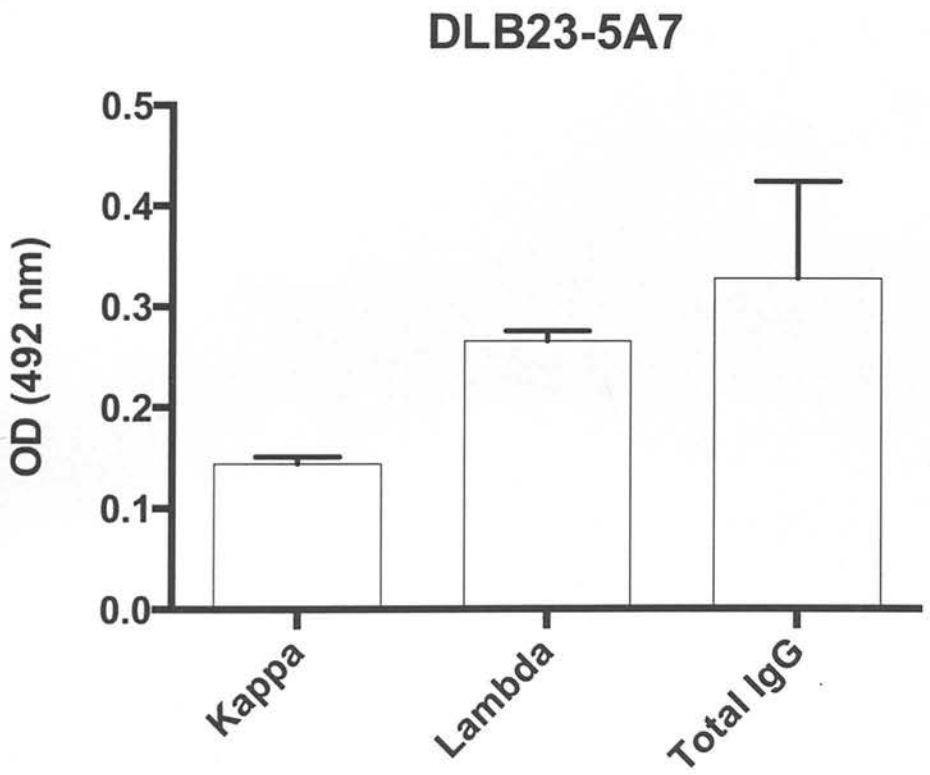
DLB23-5A7
OD (492 nm)
0.5
0.4
0.3
0.2
0.1
0.0
Kappa
Lambda
Total IgG

Figure 3.7 Antibody light chain isotype determination of mAbs DLB23-5A7 and 684-8B6.

ELISA plates were coated with GST Block 2 RO33 antigen and B cell supernatants from DLB23-5A7 or 684-8B6 added to duplicate wells. The reactivity of anti-human total IgG, anti-human kappa light chain and anti-human lambda light chain antibodies with these B cell supernatants is displayed. Each bar indicates the mean OD at 492 nm from duplicate wells with the standard error of the mean shown by the error bars.

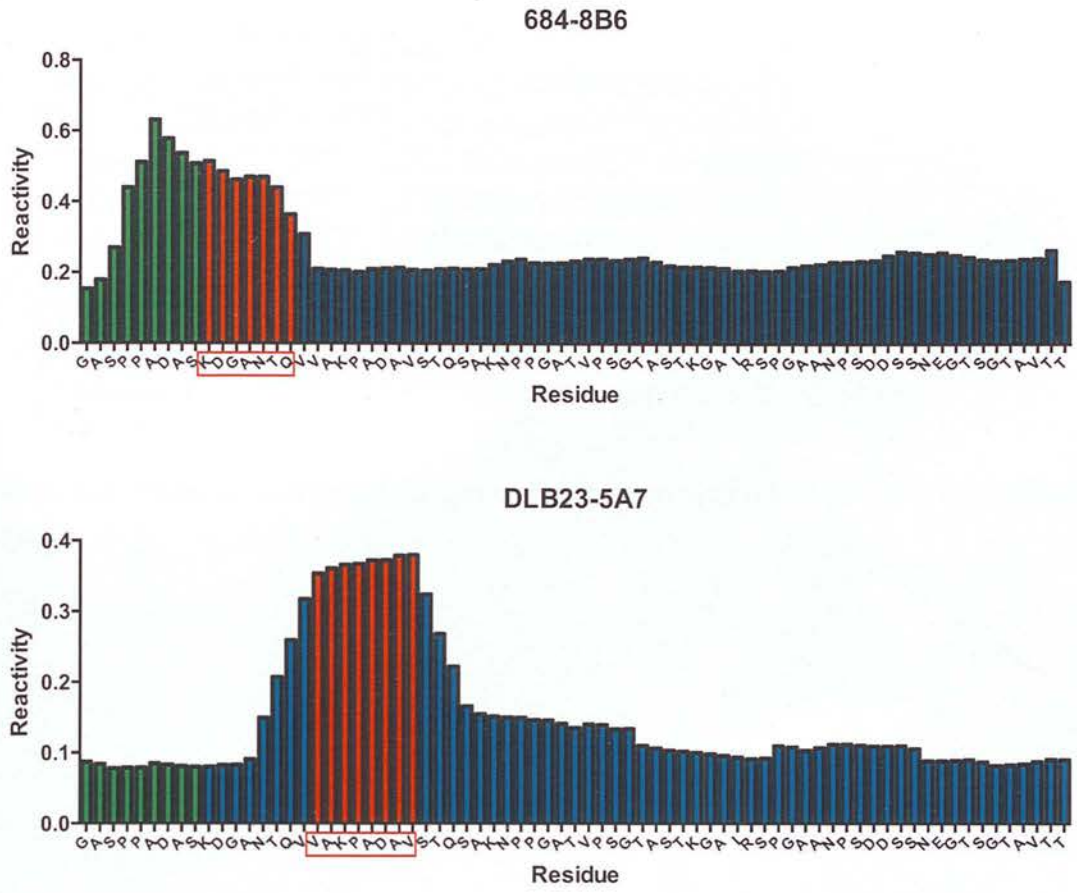

Figure 3.8 Recognition of peptide epitopes within MSP-1 Block 2 of the RO33 serotype by mAbs DLB23-5A7 and 684-8B6.

Each bar indicates the reactivity of the mAb indicated against that amino acid residue, calculated as the sum of the mean ODs of duplicate wells tested against peptides containing that reside/number of peptides containing that residue. Residues in green are from the K1/RO33 junction. All other resides are from the MSP-1 Block 2 RO33 sequence with minimal epitopes displayed in red.

Primer	Sequence
Heavy chain sense 1	5' CCATGGGACTGGACCTGGAGSDTC
Heavy chain sense 2	5' CCATGGAARCAYCTGTGGTTCTTY
Heavy chain sense 3	5' CCATGGGACAYACTTTGYTMCACR
Heavy chain sense 4	5' CCATGGGGGTCAACCGCCATCCTC
Heavy chain sense 5	5' CCATGGTCTGTCTCCTTCCTCATC
Heavy chain sense 6	5' CCATGGSARYYKKKVCTBHGCTGG
Heavy chain anti-sense	5' CTCGAGTCATTTACCCGGAGACAGGGA
Lambda sense	5' CATCATGTTTAAACAACATGRCCTGSDYYNYKCTNYKBCT
Lambda anti-sense	5' ATCGATTCASGARCATTCYGYAGGGGCMACTGTCTT

Table 3.2 Primers designed to generate human mAb heavy and light chain cDNA.

3.4.9 Cloning Ig chains

Obtaining the two MSP-1 reactive mAbs via affinity purification from Integra vessel supernatants had not been successful. An alternative method of generating these mAbs would be to clone the heavy- and light-chain-encoding genes into an expression vector, which could then be transfected into a mammalian cell culture and the mAbs purified from transfected cell supernatants. In order to achieve this, sets of primers designed to amplify any human IgG heavy chain-encoding gene and any IgG lambda light chain-encoding gene were designed. These primers are listed in Table 3.2. All primers were designed by aligning known human heavy and light chain IgG sequences (Robinson et al., 2012) with the exception of the sequence of the heavy chain IgG antisense primer which was obtained from a paper published by Mclean and colleagues (McLean et al., 2000). The primers were designed so that the IgG heavy- and light-chain-encoding genes could be cloned into the pTandem-1 vector.

3.5 Discussion

In 2004 research by Traggiai and colleagues demonstrated that the efficacy of B cell EBV transformation could be substantially improved by providing innate immune stimulation in the form of a toll-like receptor (TLR) 9 agonist (Traggiai et al., 2004). This technology has been utilised to define the structural and/or functional characteristics of human antibodies generated in response to a multitude of pathogens, a non-exhaustive list of which includes: *P. falciparum* (Barfod et al., 2007; Barfod et al., 2010), Norovirus G11.4 (Lindesmith et al., 2012), Human Immunodeficiency Virus 1 (HIV-1) (Corti et al., 2010), Cytomegalovirus (Macagno et al., 2010) and Severe Acute Respiratory Syndrome Coronavirus (SARS-CoV) (Traggiai et al., 2004). The aim of this chapter was to generate immortalised clonal B cell lines producing MSP-specific mAbs to investigate the functional activities of these antibodies in defence against *P. falciparum*.

I was able to partially characterise two MSP-1 specific mAbs from immortalised B cell lines. Consistent with previous findings that antibody responses generated to MSPs are of the cytophilic subclasses, one mAb was of the IgG1 subclass and the other of the IgG3 subclass. It has previously been reported that IgG subclass

responses to MSP-1 Block 2 are predominantly of the IgG3 subclass, where as the main IgG subclass seen in response to MSP-1_{19} is IgG1 (Cavanagh et al., 2001; Jouin et al., 2001). ADCI is mediated by antibodies of the IgG1 and IgG3 subclasses, with IgG3 being the more inhibitory of the two (Jafarshad et al., 2007; Tebo et al., 2001). The ADRB activity of polymorphonuclear neutrophils is also mediated by these cytophilic immunoglobulins, but in contrast to ADCI the IgG1 subclass may play the prevalent role in this process (Joos et al., 2010). This suggests that the mechanism of antibody-mediated anti-parasite activity may vary depending upon the isotype of the antibody in question. With the problems encountered in this project with the expansion of immortalised B cell clones, insufficient quantities of the mAbs DLB23-5A7 and 684-8B6 were obtained. These monoclonal human antibodies would have been useful tools with which to investigate ADCI and ADRB assays *in vitro* whilst controlling for antigenic specificity.

Both mAbs from the DLB23-5A7 and 684-8B6 B cell lines were of the lambda light chain isotype. A study of light chain isotype usage in anti-MSP-1 Block 2 antibodies found the kappa/lambda ratio to be highly skewed (Jouin et al., 2005). This study found that light chain usage of polyclonal serum antibodies specific to peptides from the central region of Block 2 RO33 were predominantly kappa, where as light chain usage of antibodies specific to a second C-terminal Block 2 RO33 peptide were mainly of the lambda isotype. The epitopes recognised by DLB23-5A7 and 684-8B6 were N-terminal to these peptides, with only a one residue overlap between the epitope recognised by DLB23-5A7 and the central Block 2 RO33 peptide used by Jouin and colleagues (Jouin et al., 2005). This may suggest that light chain isotype usage in Abs specific to epitopes within the N-terminal region of Block 2 RO33 are mainly of the lambda isotype.

By using N-biotinylated peptides with a 1 residue overlap inepitope mapping ELISA experiments, I was able to identify the minimal epitopes recognised by mAbs DLB23-5A7 and 684-8B6. However, due to the low amounts of antibody produced by small scale cultures of these B cell lines, it was not possible to use these mAbs in

any *in vitro* functional assays, to correlate the fine specificity of these antibodies with their functional activity (or lack thereof).

Unfortunately, sufficient quantities of MSP-specific human mAbs were not obtained during this project to allow investigation of their functional activity *in vitro*. This was due to a number of factors.

Firstly, four attempts were made to clone the immortalised polyclonal line DLB23-5A7. In all cases the process of cloning was successful, in that clones producing MSP-1 Block 2 RO33-specific mAb were obtained. However, none of these clones could be successfully expanded beyond two wells of a 96-well plate despite extensive efforts to provide the clones with a variety of conditions that were conducive to growth. It is possible that these clones did not grow because they were not stably transformed lines. B cells transformed with EBV are in the most part mortal and have low levels of telomerase activity (Counter et al., 1994; Sugimoto et al., 2004). This can result in progressive shortening of telomeres during each cell division, which leads to replicative senescence and results in permanent growth arrest (Shay and Wright, 2005; Stewart and Weinberg, 2006). Recently, in a study which aimed to obtain human mAbs specific to MSP-2 and a peptide from the gene *PFF0165c* of 16 EBV-immortalised B cell cultures from one donor only 3 were stably transformed and could be expanded to obtain mAbs of interest (Stubbs et al., 2011).

Recently, another improved method of establishing EBV-transformed B cells has been described (Hui-Yuen et al., 2011). In this method isolated PBMCs are transformed with EBV in the presence of the T cell immunosuppressant tacrolimus. This method allows prediction of successful EBV transformation through the identification of $CD23^{hi}CD58^{+}$ cells 3-4 days post transformation. I cloned polyclonal DBL23-5A7 onto irradiated PBMCs from an EBV seronegative individual in order to prevent T cell-mediated killing of EBV transformed B cells. However, growth of polyclonal pools with irradiated PBMCs from an EBV seronegative individual or a T cell immunosuppressive agent may have promoted

better growth of clones. In addition, the ability to identify successfully transformed cells via flow cytometry 3-4 days after EBV-transformation as opposed to 3 weeks after EBV-transformation via light microscopy would have enabled earlier down-selection of immortalised polyclonal wells, allowing efforts to be focused on those wells that might yield clones of interest.

Secondly, I experienced problems obtaining PBMC donor samples from areas of high malarial endemicity, as evidenced by the move to select donors from the Mutoko district instead of the Murehwa district, the former having a higher level of malarial endemicity than the latter. That said, the Mutoko district is a mesoendemic area for malaria (Mharakurwa et al., 2004) and access to PBMC samples from clinically immune individuals from a hyperendemic region may have proved more fruitful.

Thirdly, a B cell line single-cell sorted from the polyclonal line 684-8B6 was expanded into a two-compartment bioreactor and the supernatant harvested at regular intervals. When total IgG purified from this supernatant was tested for reactivity with parasites by IFA I was surprised to find that there was no reactivity. Whilst in culture, supernatants from this bioreactor had regularly been checked for reactivity with recombinant MSP-1 Block 2 RO33 by ELISA. However, upon re-examination of these ELISA results in light of the IFA results, the ODs, although positive were much lower than one would expect if all of the IgG present was specific for MSP-1 Block 2 RO33. This was puzzling given that the polyclonal line 684-8B6 was cloned by single cell sorting instead of limiting dilution precisely because it was assumed that this method gave a greater likelihood of single cell deposition. During single cell sorting a stringent gate can be applied, as was in this case, such that the chances of the deposition of a doublet into a given well is low. In cloning by limiting dilution, the frequency at which a given number of cells, *n*, is deposited into plate wells is modelled by a poisson distribution. Hence, although one might be using a dilution which increases the possibility of obtaining n=1 cells in a plate well, it is inevitable that on some occasions less than or greater than n=1 cells will be deposited in a well. In addition, cell aggregates can form during the process of cloning by

limiting dilution. It is unlikely, although possible that a cell doublet was deposited into the plate well during cloning of this line.

In any case, the most parsimonious explanation for the small amount of MSP-1 Block 2-specific mAb produced during growth of the what was the putatively clonal 684-8B6 line, is that it was not actually clonal. It is quite possible that the single cell sorted line was initially clonal and that a B cell of different specificity was introduced into that well via a microdroplet during culture manipulations. Manipulations of cloned B cells were carried out in 384-well plates, which are tecnically challenging to work with and the smaller distance between wells compared to a 96-well plate increases the likelihood of cross-contamination between wells. Indeed, incidents of accidential contamination of clonal cell lines are well known. For example, the *P. falciparum* isolate FCR-3 is thought to have contaminated 9 different isolates from disparate geographical regions, resulting in all 9 lines being identical to FCR-3 (Trager, 1993). If a B cell of another specificity was introduced by cross-contamination it may well have outcompeted the MSP-1 Block 2 RO33-specific B cells during culture in the bioreactor, particularly if the contaminating cell had switched off Ig-production. A recurrent phenomenon during the B cell work presented here was that many polyclonal or clonal pools that were initially positive in ELISA lost reactivity by the time they reached high enough densities to be frozen down or cloned. This might be explained by the B cells of interest being outcompeted by B cells of other specificities.

On reflection, there are two steps I could have taken to avoided this result. Firstly, I could have carried out several rounds of sub-cloning of this B cell line. Secondly, I could have tested B cell supernatant for parasite reactivity via IFA whilst the line was grown in the bioreactor. The IFA, being a less sensitive technique than ELISA would have alerted me to the fact that the line might not be clonal earlier.

MSP-specific human mAbs would be highly useful reagents with which to investigate mechanisms of antibody-mediated inhibition of *P. falciparum* growth. The efficacy of human hybridoma production has greatly improved in recent years

(Yu et al., 2008a; Yu et al., 2008b) and the generation of MSP-specific mAbs via these methods might be productive in future.

4: Is antibody-catalysed water oxidation responsible for intraerythrocytic growth inhibition by MSP-1_{19}-specific antibodies?

4.1 Introduction

The prevailing dogma holds that the primary function of antibodies is to provide a molecular link between pathogen recognition and pathogen destruction by the complement cascade or receptor-mediated phagocytosis. However, in the 1980's two research groups independently demonstrated that the antibody molecule is itself capable of complex chemical catalysis (Pollack et al., 1986; Tramontano et al., 1986): the antibody catalysis field was born. It has since become apparent that antibodies can be programmed to catalyse a multitude of chemical reactions (Janda et al., 1993; Jones et al., 2001; Li et al., 1994).

A catalytic ability intrinsic to all antibodies, irrespective of their antigenic specificity, is the capacity to catalyse a reaction between singlet oxygen ($^1O_2$) and water (H_2O) to generate hydrogen peroxide (H_2O_2): $x\,^1O_2+H_2O\rightarrow H_2O_2+(x-1)\,^3O_2$ (Wentworth et al., 2000; Wentworth et al., 2001). During this antibody-catalysed water-oxidation pathway (ACWOP) antibodies use H_20 as an electron source to facilitate its addition to $^1O_2$ to form H_20_3 as the first reaction product in a cascade of reactions that ultimately leads to the production of H_2O_2 (Wentworth et al., 2001). The reduction of $^1O_2$ is thought to be due to oxidation of a conserved tryptophan residue in a buried region of the antibody (Wentworth et al., 2000; Wentworth et al., 2001) and reaction intermediates are stabilised at the interface of antibody light and heavy chains (Datta et al., 2002). The $^1O_2$ substrate in this reaction can be generated *in vitro* by UV irradiation, irradiation by white light in the presence of a photosensitiser such as haematoporphyrin IX or by thermal decomposition of endoperoxides (Wentworth et al., 2000).

How does the potential of the antibody molecule to carry out antibody-catalysed water oxidation (ACWO) relate to antibody immune effector function *in vivo*? Activation of the ACWO pathway in the presence of $^1O_2$ produces holes in the cell wall of gram-negative bacteria, resulting in bacterial lysis and death (Wentworth et al., 2002). Production of H_2O_2 via the ACWO pathway was not sufficient for bacterial killing but a downstream species with the chemical signature of ozone (O_3) was (Wentworth et al., 2002). Does ACWO play any role in antibody-mediated immunity to blood stage *P. falciparum* infection?

P. falciparum is subject to considerable levels of oxidative stress during the intraerythrocytic developmental cycle (IDC) and the parasite has developed an extensive redox system in order to maintain adequate antioxidant defence throughout this period. This redox network comprises over twenty proteins, including antioxidant enzymes such as the glutathione- and thioredoxin-dependent proteins (Becker et al., 2003; Rahlfs et al., 2003) and superoxide dismutase, in addition to low molecular weight antioxidants, the most prominent of which is glutathione. However, *P. falciparum* is devoid of genes encoding either catalase or a classical glutathione peroxidase (Sztajer et al., 2001) and it has been suggested that the mechanisms *P. falciparum* employs for its antioxidant defence may only just be adequate (Becker et al., 2004). Hence, in theory, the generation of H_2O_2 and downstream reactive oxygen species (ROS) via the ACWOP if parasite-specific antibodies were to be presented with a biological source of $^1O_2$ could result in parasite death.

For the ACWOP to be active, Ig and singlet oxygen need to juxtapose. A potential source of $^1O_2$ during blood stage parasitaemia is that produced by the nicotinamide adenine dinucleotide phosphate (NADPH) oxidase pathway during the respiratory burst of activated phagocytes. It has been shown that antibodies utilise $^1O_2$ produced by the platelet NADPH oxidase pathway to produce H2O2 via the ACWO pathway during platelet destruction (Nardi et al., 2001).

O_3 is short-lived and catalase is ubiquitous in biological systems, therefore in order for activation of ACWOP to harm the parasite, catalytic Ig would need to be located in or close to the parasite. MSP-1_{19} specific antibodies bind to the extracellular merozoite and are carried into the RBC during merozoite invasion, where they persist until at least 35 hours after invasion (Moss et al., 2012). Parasites treated with anti- MSP-1_{19} antibodies *in vitro* display aberrant intraerythrocytic development (Arnot et al., 2008; Bergmann-Leitner et al., 2009). Could this antibody-mediated parasite damage be due to activation of the ACWOP by internalised MSP-1_{19} - specific antibodies?

This chapter aims to test the hypothesis that anti- MSP-1_{19} antibodies carried inside the RBC during merozoite invasion produce ROS via the ACWOP that are detrimental to the intraerythrocytic development of the parasite.

4.2 Materials and methods

4.2.1 Fluorescent dyes

The fluorescent dyes listed below were employed in the *in vitro* ACWO assay to detect parasite DNA, intracellular ROS or antibody. As a significant proportion of this chapter deals with the method development of this assay, the general methods attaining to these dyes are listed below, however, specific dye concentrations are indicated in the relevant results section.

4.2.1.1 Alexa Fluor 488 and Alexa Fluor 633

The antibodies used in the *in vitro* ACWO assay, 12.8 and anti-Ym1, were labelled with Alexa Fluor 488 or Alexa Fluor 633 so that the Abs could be detected by flow cytometry. Please see Chapter 2 for details of the labelling procedure. AF488 and AF633 are used in this Chapter as suffixes to denote an Ab that is labelled with Alexa Fluor 488 or Alexa Fluor 633, respectively.

4.2.1.2 DCFH-DA

A chemically reduced, acetylated form of fluorescein, 2',7'-dichlorodihydrofluorescein diacetate (DCFH-DA) was employed to detect intracellular ROS. This nonfluorescent lipid-soluble probe is relatively resistant to oxidation and diffuses across cell membranes where it is hydrolysed by intracellular esterases to 2',7'-dichlorodihydrofluorescein (DCFH). Upon oxidation by intracellular ROS, DCFH yields the highly fluorescent dichlorofluorescein (DCF). Lyophilised DCFH-DA (C2938, Invitrogen) was reconstituted in DMSO to give a 10 mM stock solution which was maintained at −20 °C in the dark for long-term storage.

DCFH-DA was applied either pre- or post-IgG treatment during *in vitro* ACWO assays. Where DCFH-DA loading was pre-IgG treatment, DCFH-DA was diluted to the required working concentration in 300 µL uninfected RBCs at 5% haematocrit in PBS. Post staining, DCFH-DA loaded uninfected RBCs were washed with PBS (500 x G, 5 minutes) and then used to dilute the parasite culture being used in the assay. Where DCFH-DA loading was post-IgG treatment DCFH-DA was diluted in 300 µL PBS to the required working concentration. Samples from experimental cultures were added to this solution and stained at 37 °C in the dark for 30 minutes. Post staining, cells were washed with PBS (500 x G, 5 minutes) and resuspended in 300 µL PBS prior to cell acquisition by flow cytometry.

4.2.1.3 Dihydrorhodamine 123

Dihydrorhodamine 123 (DHR 123) is an uncharged ROS indicator that diffuses across cell membranes. Upon oxidation by intracellular ROS DHR 123 is converted to cationic rhodamine 123 (R 123), which localises to mitochondria and displays green fluorescence.

A 5 mM stock solution of DHR 123 (D23806, Invitrogen) was diluted to the required concentration in 500 µL of uninfected RBCs at 5% haematocrit in RPMI 1640. Uninfected RBCs were stained for 20 minutes at 37 °C in the dark. Following this,

cells were washed with PBS (500g, 5 minutes) and resuspended in 300 µL PBS prior to *in vitro* ACWO assay setup.

4.2.1.4 DAPI

Samples from experimental or control cultures were added to 300 µL RPMI containing 1 µg mL^{-1} 4',6'-diamidino-2-phenylindole (DAPI). Cells were stained for 30 minutes at RT in the dark prior to acquisition on a flow cytometer.

4.2.1.5 Hoechst 33342

Please see the general materials and methods section.

4.2.2 Long-term culture and manipulation of murine hybridomas

4.2.2.1 Hybridomas

The following murine hybridomas were used: (i) 12.8, which produces an IgG2b/kappa antibody specific for an S-S dependent conformational epitope within the EGF-like domain 1 of $MSP\text{-}1_{19}$ (Conway et al., 1992; McBride and Heidrich, 1987; Wilson et al., 1987) and (ii) hybridoma line 4D10, which produces a mAb specific for murine Ym1, a chitinase-like protein. This hybridoma line was produced by Abnova Corporation, Taiwan and raised against the Ym1 peptide IPRLLLTSTGAGIID (Tara Sutherland, personal communication). The anti-Ym1 hybridoma line was gifted by Dr. Stephen Jenkins.

4.2.2.1 Media

The following media were used for culture and manipulation of murine hybridomas:

Hybridoma growth medium: RPMI medium 1640 - L-glutamine (Invitrogen) supplemented with 10% ultra low IgG FBS (Invitrogen), 4 mM L-Glutamine (Invitrogen) and 1% penicillin streptomycin (Invitrogen).

Hybridoma freezing medium: 40% v/v hybridoma growth medium, 10% v/v sterile DMSO and 50% v/v FBS.

Hybridoma thawing medium: RPMI medium 1640 - L-glutamine (Invitrogen) supplemented with 10% v/v ultra low IgG FBS (Invitrogen), 4 mM L-Glutamine (Invitrogen), 1% penicillin streptomycin (Invitrogen), 10% v/v BM Condimed (Roche) and 55 mM 2-mercaptoethanol.

Celline 1000 medium compartment medium: RPMI medium 1640 - L-glutamine (Invitrogen).

Celline 100 cell compartment medium: RPMI medium 1640 - L-glutamine (Invitrogen) supplemented with 10% v/v ultra low IgG FBS (Invitrogen).

4.2.2.2 Thawing of hybridoma cells

Hybridomas were maintained in liquid nitrogen for long-term storage. Hybridomas were thawed in a 37 °C water bath and then transferred to a 15 mL polypropylene centrifuge tube. 10 mL hybridoma growth medium was added dropwise with rotation. The tube was spun down for 5 minutes at 300 x G in a centrifuge. The supernatant was taken off and the cell pellet resuspended in 10 mL of thawing medium and the cells transferred to a T25 flask.

4.2.2.3 Routine culture and manipulation

Murine hybridomas were expanded in T75 flasks until 8 x 10^6 cells were obtained. These cells were spun down at 300 x G for 5 minutes, resuspended in 15 mL compartment medium and seeded into a Celline 1000 flask that had been pre-incubated at 37 °C, 5% CO_2 with 500 mL media compartment medium in the medium compartment.

Twice a week hybridoma cells were transferred to a 50 mL falcon tube, centrifuged at 300 x G for 5 minutes and the supernatant (containing the mAb of interest) harvested. Cells were resuspended in 15 mL fresh cell compartment medium, at a diluted density if required, and returned to the cell compartment. 500 mL of medium compartment medium was poured off from the medium compartment and replenished with an equal volume of fresh medium compartment medium.

4.2.2.4 Freezing

Hybridoma cells were frozen down when growth was in the exponential phase. Cells were resuspended, transferred to a 50 mL polypropylene tube and centrifuged at 300 x G for 5 minutes. The supernatant was removed and hybridoma cells resuspended in freezing medium at a concentration of 5 x 10^6 cells mL^{-1}. Hybridomas were aliquoted into cryovials and stored at −70 °C overnight in a cryo 1°C freezing container, then in liquid nitrogen for longer storage.

4.2.3 Antibody/protein irradiation and quantification of H_2O_2 production

H_2O_2 production by antibodies/proteins was measured using the Amplex Red hydrogen peroxide assay kit (A22188, Invitrogen). The Amplex Red reagent is a colourless substrate that reacts with H_2O_2 to produce the highly fluorescent product resorufin.

Aliquots of antibody/protein solution (100 µL, 6.7 µM protein in PBS, pH 7.4) were placed in glass vials, sealed and placed in the dark (treatment i) or irradiated with UV (treatment ii) or irradiated with UV in the presence of 40 µM haematoporphyrin IX (treatment iii). As controls 100 µL aliquots of aprotinin (6.7 µM protein in PBS, pH 7.4), PBS and 100 µM H_2O_2, and PBS alone were exposed to treatment (i). At 90 minutes after the application of treatments, 40 µM catalase (C9322, Sigma-Aldrich) was added to all samples.

At 0, 30, 60, 90 and 95 minutes after the application of treatments to samples, 10 µL was taken from each sample and added into a well of a 96-well microtiter plate containing 40 µL reaction buffer. 50 µL Amplex Red reagent solution (400 µM Amplex Red Reagent, 2 U mL^{-1} HRP in reaction buffer) was then added, and the plate was incubated in the dark for 30 mins. The optical density was read at 570 nm on a Labsystems Multiskan Ascent microtitre plate reader. The experiment was run in duplicate.

4.2.4 Titration of mAbs 12.8 and anti-Ym1 in the *in vitro* ACWO assay

P. falciparum parasites were synchronised by sorbitol treatment in order to yield a ~ 0-18 h post invasion culture. A second sorbitol treatment was performed 34 h later in order to obtain a 0-4 h post invasion culture. Synchrony of the 4 h cohort was maintained by sorbitol treatment every 48 hours until assay set up.

4 mg mL^{-1} solutions of anti-Ym1-AF488 and 12.8-AF633 in PBS were mixed in a 1:1 ratio to give a solution in which both of these mAbs were present at a concentration of 2 mg mL^{-1}. This antibody solution was serially diluted two-fold finishing at a 1:16384 dilution. Then, 50 µL of each dilution in PBS was dispensed in triplicate into the wells of a flat-bottomed microtitre plate (Costar, 3598). Following this, 50 µL of *P.falciparum* culture, consistently predominantly of late trophozoites and early schizonts, at 1% parasitaemia and 5% haematocrit, in twofold-concentration complete medium, was dispensed into each well. Therefore, at the outset of each assay parasites were present at 0.5% parasitaemia in complete culture medium at 2.5 % haematocrit. Plates were incubated at 37°C, 5% CO_2 for the duration of the assay.

Sampling time points were 21, 40 and 46 h after assay set up. At each time point 10 µL of resuspended parasites from each assay well were dispensed into 290 µL RPMI containing 1 µg mL^{-1} DAPI and stained for 30 mins at RT in the dark. Data from

these samples were then acquired on a BD LSR II flow cytometer. Data from 2000 iRBCs were acquired for each sample.

4.2.5 Comparison of the ability of Coriphosphine O, DAPI and Hoechst 33342 to stain early ring stage parasites

A highly synchronous early ring-stage culture at 5% haematocrit was set up. 20 µL of resuspendedparasites from this culture were added to 280 µL aliquots of RPMI containing DAPI (1, 0.5, 0.25, 0.125, 0.0625 or 0.03125 µg mL^{-1}), DAPI and 0.017% Triton X-100 (1, 0.5, 0.25, 0.125 µg mL^{-1}) Coriphosphine O (2, 1, 0.5, 0.25, 0.125 or 0.0625 µg mL^{-1}) or Hoechst 33342 (10, 5, 2.5, 1.25, 00625 or 0.03125 µg mL^{-1}). In addition, 20 µL of well-mixed 5% haematocrit uninfected RBCs were added to 280 µL RPMI containing 1 µg mL^{-1} DAPI, 1 µg mL^{-1} DAPI and 0.017% Triton X-100, 2 µg mL^{-1} Coriphosphine O or 10 µg mL^{-1} Hoechst 33342. Staining conditions were as follows: 60 minutes at 37°C in the dark, 30 minutes at RT in the dark and 15 minutes at RT in the dark, for Hoechst 33342-, DAPI- and Coriphosphine O-staining, respectively. Following this, cells were acquired on a BD LSR II flow cytometer.

4.2.6 *In vitro* ACWO assay

A number of variations of the *in vitro* ACWO assay are presented in this chapter, which reflects the evolution of the assay over time. As such, the assay outline is described below. For precise concentrations of materials used and assay sampling time points, please see the relevant results section.

Parasites were synchronised by sorbitol treatment in order to yield a ~ 0-18 h post invasion culture. Parasites were synchronised again 34 h later in order to obtain a 0-4 h post invasion culture. Synchrony of the 4 h culture was maintained by sorbitol treatment every 48 hours until assay setup. Where DCFH-DA loading was prior to assay treatments, uninfected RBCs pre-loaded with DCFH-DA were used to dilute this culture to 1 % parasitaemia, prior to addition to assay wells.

The experimental mAb treatment was 12.8-AF633 and the negative control mAb treatment was anti-Ym1-AF633. 50 µL of each mAb in PBS at the required concentration was dispensed in duplicate into the wells of a flat-bottomed microtitre plate (Costar, 3598). An equal volume (50 µL) of parasite culture at 0.5% parasitaemia and 5% haematocrit, consisting predominantly of schizonts in twofold-concentration complete medium, was dispensed into each well. Plates were incubated at 37°C, 5% CO_2.

At sampling time points post invasion, 10 µL of resuspended cells from each well were sampled. For wells where DCFH-DA measurement was post-treatment, parasites were stained with DCFH-DA. Parasites were stained with DAPI or Hoechst 33342 in order to detect parasite DNA. Data were acquired on a BD FACScan fluorescence-activated cell analyser or a BD LSRII flow cytometer.

4.3 Results

4.3.1 Development of the *in vitro* ACWO assay

4.3.1.1 Detection of intracellular ROS

We hypothesised that ACWOP is operational during *P. falciparum* intraerythrocytic growth inhibition by internalised MSP-1_{19} specific antibodies. Testing this hypothesis necessitated the development of a novel *in vitro* assay that could detect internalised anti- MSP-1_{19} antibodies and measure parasite oxidative stress in order to determine whether there was any correlation between the two.

The lipid soluble probe DCFH-DA was employed to detect intracellular ROS in the *in vitro* ACWO assay. Preliminary experiments were carried out to determine a working concentration of DCFH-DA that (i) did not cause blebbing/shrinking/lysis of cells and (ii) displayed a quantitative fluorescent shift upon encountering ROS intracellularly.

RBCs were loaded with DCFH-DA (0, 100, 200, 400 or 800 μM) and the DCF signal in the presence or absence of 200 μM H_2O_2 measured by flow cytometry. Figure 4.1 displays representative FACs plots of FSC versus SSC and FL-3 versus FL-1 fluorescence from this experiment. Loss of forward or side scatter can indicate shrinking or lysis of cells and at concentrations less than or equal to 200 μM DCFH-DA there was no indication that this had occurred. Within the DCFH-DA concentration range at which no cell lysis had occurred the greatest shift in DCF fluorescence (FL-1 channel) upon H_2O_2 treatment was observed at 100 μM DCFH-DA. Hence, the optimal DCFH-DA concentration for the *in vitro* ACWO assay was determined to be 100 μM, which is of the same order of magnitude as that used by other researchers using DCFH-DA to measure ROS in human erythrocytes (Amer et al., 2003; Mandal et al., 2005).

4.3.1.2 Stability of DCFH and DCF

If RBCs are loaded with DCFH-DA prior to antibody treatment the DCF fluorescence measured at later time points is the sum of DCF that has accumulated in that RBC since DCFH-DA loading minus any leakage of DCF from the RBC. On the other hand if RBCs are loaded with DCFH-DA at time points after IgG treatment then DCF fluorescence is a measure of the ROS level of the iRBC at that particular time point. If DCF fluorescence was only measured at time points after antibody treatment then one might miss some, if not all ROS, if they are transient. On the other hand, only measuring DCF fluoresence that had accumulated over time would not allow one to pinpoint when ROS were being produced intracellularly. We therefore decided to measure DCF fluorescence both pre- and post-antibody treatment during the *in vitro* ACWO assay.

A

100 μM DCFDA

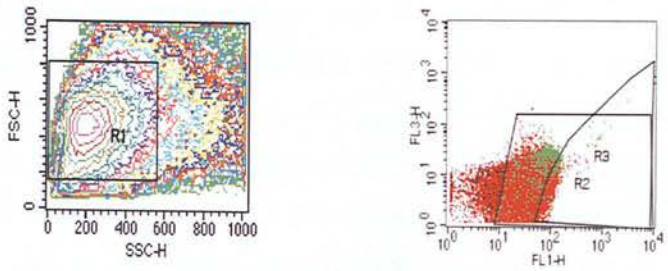

100 μM DCFDA + H_2O_2

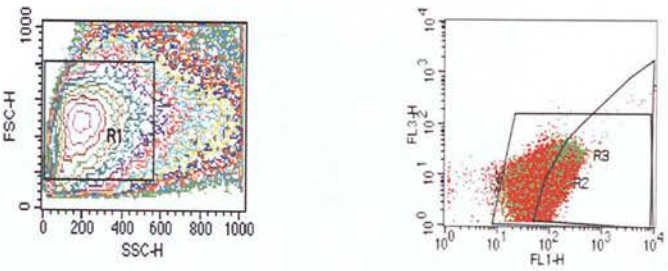

B

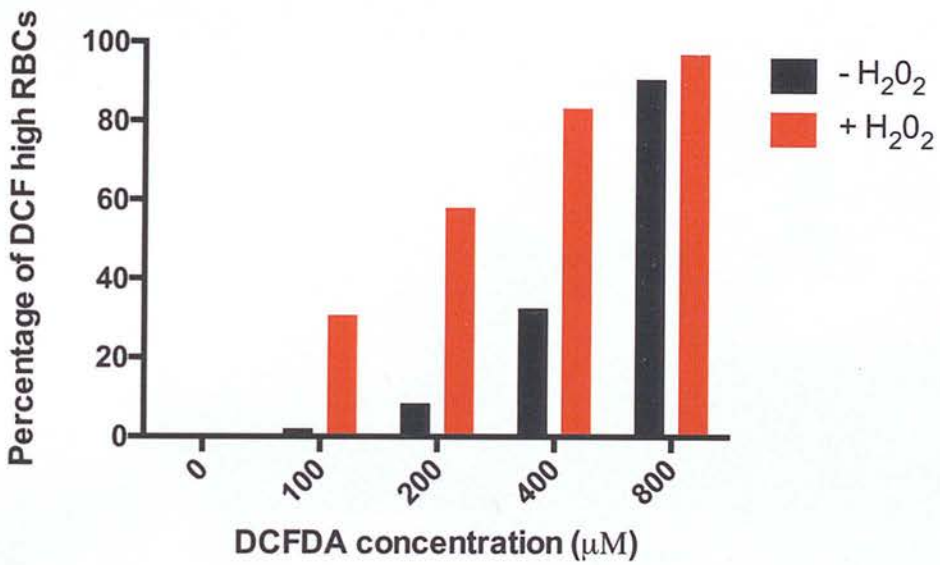

Figure 4.1 Titration of the intracellular ROS probe DCFH-DA.

(A) FSC versus SSC contour plots (left hand panels) and FL3 versus FL1 dot plots (right hand panels) of RBCs pre-loaded with 100 μM DCFH-DA in the absence (upper panels) or presence of 200 μM H202 (lower panels). Gate R1 defines healthy RBCs. Gates R2 and R3 define RBCs of low DCF fluorescence and high DC fluorescence, respectively. (B) Percentage of RBCs with high DCF fluorescence (gate R3) when pre-loaded with 0, 100, 200, 400 or 800 μM DCFH-DA in the presence (red bars) or absence (black bars) or 200 μM H202.

It was therefore important to identify (i) that RBCs preloaded with DCFH-DA remained responsive to DCF production and (ii) that once DCF had been formed inside the RBC it remained detectable over time. Figure 4.2 displays a typical time course experiment of DCFH responsivenes and DCF stability. To measure DCFH responsivenes, RBCs were pre-loaded with DHCF-DA at the start of the assay and at hourly intervals samples were taken and tested for the ability to exhibit DCF fluorescence when exposed to 200 μM H_2O_2. To measure DCF stability, RBCs were pre-loaded with DHCF-DA and exposed to 200 μM H_2O_2 at the start of the experiment. DCF fluorescence was then monitored at hourly intervals. No reduction in either DCFH responsiveness or DCF stability was detected (Figure 4.2).

4.3.1.3 Experimental and negative control antibodies

The *in vitro* ACWO assay required a source of MSP-1_{19} specific antibodies, which would serve as the experimental antibody and a non-*P. falciparum*-specific antibody, which would serve as a negative control. Given that this assay was being developed to test a hypothetical mechanism of antibody-mediated intraerythrocytic growth inhibition there was no positive control antibody available.

The mouse mAb 12.8, which recognises a conformational epitope within the EGF-like domain 1 of MSP-1_{19} was chosen as the experimental antibody. 12.8 is secreted from a mouse hybridoma cell line, thus providing a cheap, unvarying and unlimited supply of mAb of defined specificity. A hybridoma generated mAb specific to murine Ym1 was used the negative control antibody. These mAbs were labelled with Alexa Fluor 633 so that they could be detected directly without needing to employ the use of secondary antibodies.

Alexa Fluor 633-labelled 12.8 (12.8-AF633), Alexa Fluor 633-labelled anti-Ym1 (anti-Ym1-AF633), unlabelled 12.8 and unlabelled anti-Ym1 were tested for reactivity with intact parasites by IFA to confirm (i) that anti-Ym1 did not react with *P. falciparum* and (ii) that Alexa Fluor labelling of antibodies had not affected antibody specificity. 12.8 reacted strongly with parasites, displaying an endpoint titre of 2000 ng mL^{-1}, whereas anti-YM1 did not react with parasites at all in IFA,

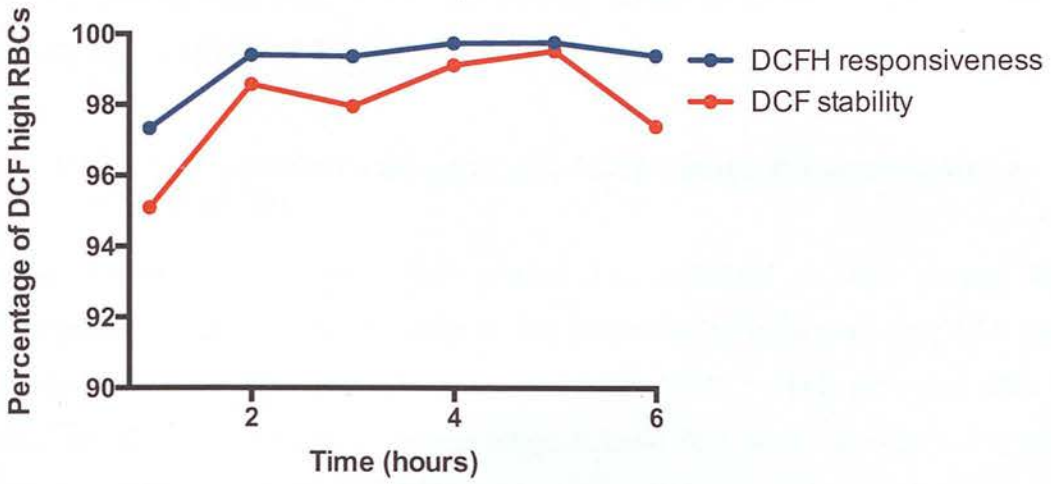

Figure 4.2. Measurement of DCFH responsiveness and DCF stability in RBCs over time.

To measure DCFH responsiveness (blue line), RBCs were pre-loaded with 100 μM DCFH-DA and incubated at 37oC, 5% CO2. At hourly intervals for the next 6 hours, samples were taken, exposed to 400 μM H202 and RBCs acquired by flow cytometry. To measure DCF stability (red line), RBCs were pre-loaded with DCFH-DA, exposed to 400 μM H202 and incubated at 37oC, 5% CO2. At hourly intervals for the next 6 hours, samples were taken and RBCs acquired by flow cytometry.

even at high concentrations. Antibody labelling did not affect the reactivity of either antibody in IFA (Figure 4.3).

4.3.1.4 12.8 and anti-Ym1 can carry out ACWO when presented with a source of $^1O_2$

Before determining whether 12.8 carried out catalytic ACWO during the intraerythrocytic developmental cycle it was important to determine that 12.8 and anti-Ym1 were capable of carrying out catalytic ACWO when provided with a source of $^1O_2$. Employing a method adapted from that used by Wentworth and colleagues (Wentworth et al., 2000), 12.8, 12.8-AF633, anti-Ym1 and anti-Ym1-AF633 were either not irradiated, or irradiated with UV light in the presence or absence of the photosensitiser haematoporphyrin IX, and hydrogen peroxide production measured using the Amplex Red reagent. Naive rabbit IgG and aprotinin served as positive and negative controls of ACWO activity, respectively (Wentworth et al., 2000). The time course of H_2O_2 production by these proteins is displayed in Figure 4.4. All mAbs produced H_2O_2 when irradiated with UV, with higher levels of H_2O_2 production in the presence of haematoporphyrin IX. Alexa Fluor 633-labelling of Abs reduced H_2O_2 production by a factor of approximately half. Antibodies incubated in the absence of UV treatment did not produce H_2O_2. The specificity of the Amplex Red reagent for H_2O_2 was confirmed by the addition of catalase resulting in H_2O_2 levels dropping down to pre-irradiation (baseline) levels. UV irradiation of buffer alone did not result in any H_2O_2 production.

4.3.2 Preliminary ACWO experiments

We wanted to test the hypothesis that anti-MSP-1_{19} antibodies internalised during merozoite invasion generated ROS via the ACWOP, which were detrimental to the intraerythrocytic development of the parasite. Given that abnormal forms of each intraerythrocytic parasite stage had been detected during intraerythrocytic growth inhibition by anti-MSP-1_{19} antibodies (Arnot et al., 2008), we reasoned that antibody-catalysed production of ROS might occur throughout the

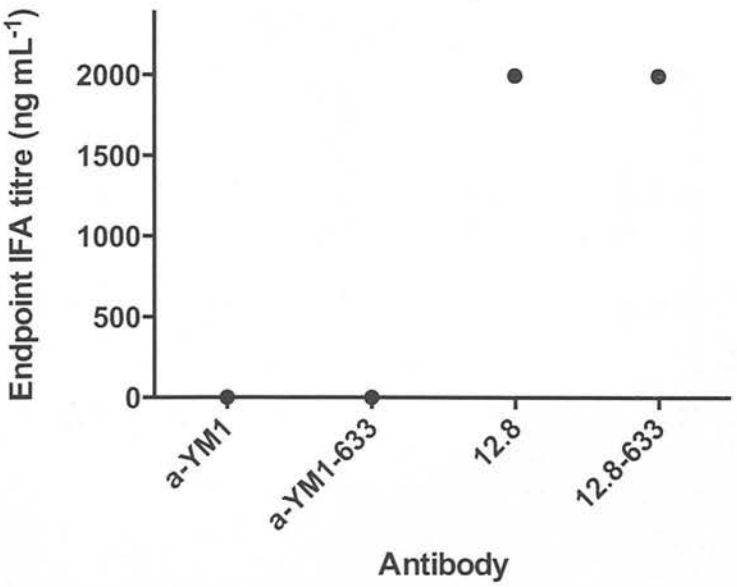

Figure 4.3 IFA reactivity of 12.8 and anti-Ym1.

IFA endpoint titres of unlabelled and Alexa Fluor 633-labelled mAbs 12.8 and Ym1 against *P. falciparum* mixed stage parasites of the wellcome strain.

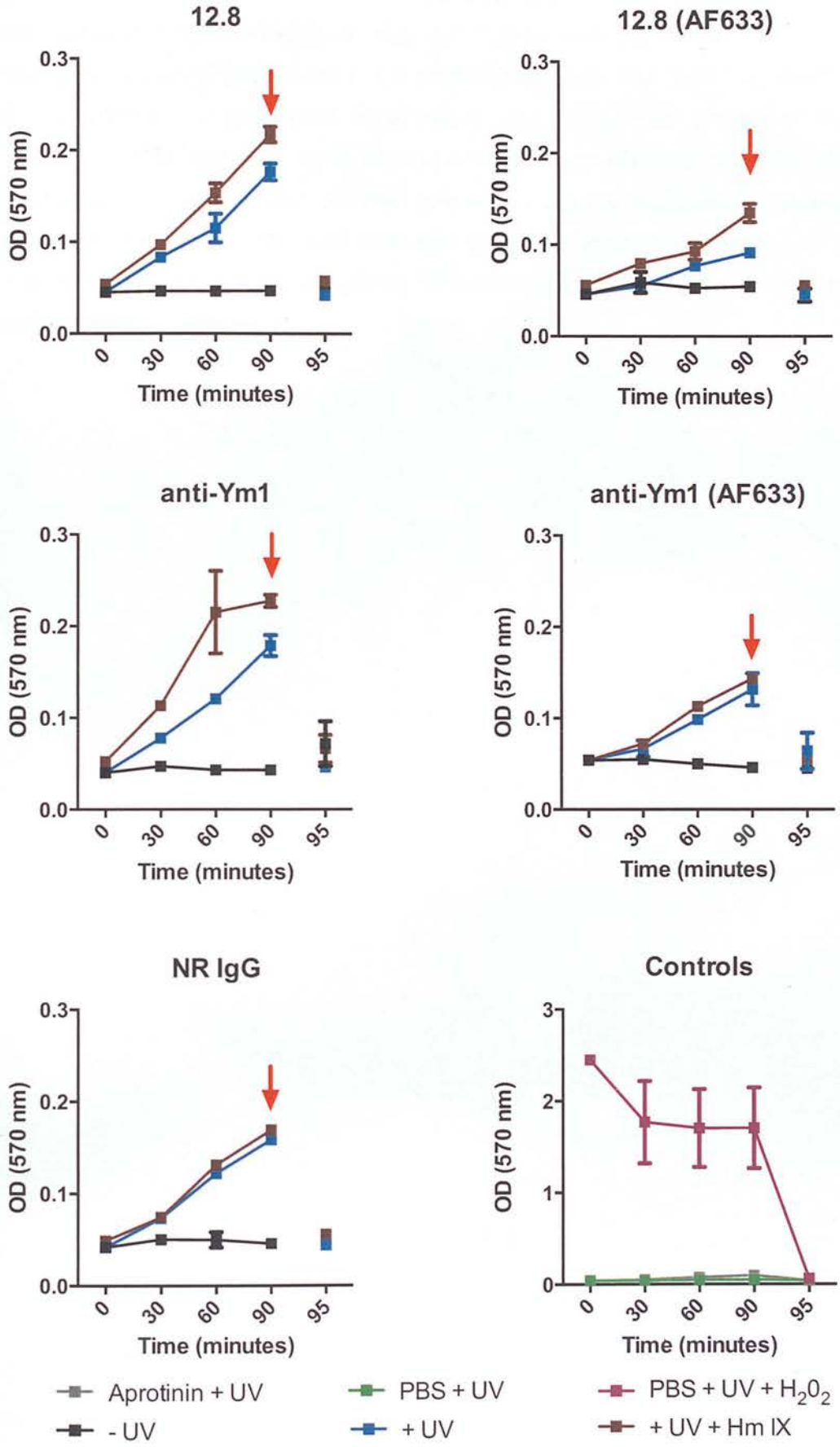
12.8
12.8 (AF633)
anti-Ym1
anti-Ym1 (AF633)
NR IgG
Controls
OD (570 nm)
Time (minutes)
0
30
60
90
95
0.0
0.1
0.2
0.3
1
2
3
Aprotinin + UV
- UV
PBS + UV
+ UV
PBS + UV + H_2O_2
+ UV + Hm IX

Figure 4.4 12.8 and anti-Ym1 mAbs produce H_2O_2 when irradiated with UV.
Time course of H202 production in PBS (pH 7.4) with UV (blue line), UV and HP (brown line) or no UV (black line) in the presence of 12.8, 12.8 (AF633), anti-Ym1, anti-Ym1 (AF633) or polyclonal naive rabbit IgG. The time course of H202 production in PBS (pH 7.4) alone or supplemented with aprotinin or H202, when irradiated with UV is also shown. Red arrows indicate the addition of catalase to protein samples. Each data point indicates hydrogen peroxide production, shown as the mean of two duplicate samples in OD units measured at 570 nm. Error bars indicate the standard error of the mean (SEM).

period the parasite was developing inside the RBC, or alternatively could occur early in the parasite's intraerythrocytic development, with parasitostatic or parasitocidal effects being evident throughout the parasite's intraerythrocytic development.

The rationale behind the design of the *in vitro* ACWO assay was that following invasion of RBCs in the presence of 12.8-AF633, a unique population of iRBCs with high Alexa633 fluorescence would be detected that would be absent from cultures that had undergone invasion in the presence of anti-Ym1-AF633. If this unique population of AF633 high iRBCs were identified, we wished to determine whether they were subject to a higher level of oxidative stress than iRBCs displaying low AF633 fluorescence.

Synchronous schizont iRBCs were allowed to undergo invasion into uninfected RBCs or uninfected RBCs pre-loaded with DCFH-DA in the presence of i) no antibody, ii) 1 mg mL^{-1} 12.8-AF633, or iii) 1 mg mL^{-1} anti-Ym1-AF633. Concomitantly, control uninfected RBCs or uninfected RBCs pre-loaded with DCFH-DA were incubated with 12.8-AF633 or anti-Ym1-AF633 in the absence of schizont iRBCs. Samples were taken at 17, 24, 39 and 44 hours post invasion. For treatment wells where uRBCs were not pre-loaded with DCFH-DA, samples were stained with DCFH-DA and then with DAPI prior to acquisition on a flow cytometer. For treatment wells where uRBCs were pre-loaded with DCFH-DA, samples were only stained with DAPI prior to being acquired on a flow cytometer.

Figure 4.5 displays representative dot plots of Alexa633 versus DAPI fluorescence for each of the 5 experimental treatments. A population of $DAPI^{high}$, $Alexa633^{high}$ parasites were identified in cultures that had undergone invasion in the presence of 12.8 -AF633. However, the same frequency of iRBCs were identified within this gate in cultures that had undergone invasion in the presence of anti-Ym1-AF633. Comparison of uRBCs that had been incubated in the presence or absence of antibody (i.e. comparing panel A with panels D and E) revealed Alexa633 staining of uRBCs in samples where uRBCs had been incubated in the presence of 12.8-AF633 or anti-Ym1-AF633. This implied that these mAbs were binding non-specifically to

RBCs and this might explain the equal frequencies of parasites observed in the $DAPI^{high}$ $Alexa633^{high}$ gate in cultures that had undergone invasion in the presence of 12.8-AF633 and anti-Yml-AF633.

Whilst carrying out preliminary ACWO experiments using DAPI as a parasite detection dye, several assays were carried out where parasites could not be detected post invasion by flow cytometry, although their presence could be detected on Giemsa-stained smears. We reasoned that this might be due to DAPI not being able to stain ring-stage parasites. To examine this hypothesis, the ability of DAPI, Coriphosphine-O and Hoechst 33342 to stain parasite DNA in a culture consisting predominantly of early ring stage parasites was assessed. In case the lack of DAPI staining was due to an inability of the dye to access parasite DNA, in parallel samples were also stained with DAPI containing the non-ionic detergent Triton X-100. Figure 4.7 displays the parasitaemia detected by flow cytometry using each of these dyes to detect parasite DNA. The three lowest concentrations of Hoechst 33342 gave parasitaemia in reasonable agreement with that measured by manual counting of Giemsa-stained smears (10.43%) (Figure 4.6 panel B). Coriphosphine O staining gave a similar, although slightly lower estimate of parasitaemia at the highest concentration of this dye tested (Figure 4.6 panel A). Across the range of concentrations tested, DAPI-stained samples gave parasitaemia estimates between 1.83 and 2.33% (Fig 4.6 panel C). The addition of Triton X-100 to DAPI stained cultures did not increase the parasitaemia detected by DAPI staining (Fig 4.6 panel D). Given, that DAPI staining resulting in vast underestimates of ring stage parasitaemia, Hoescht 33342 was used to detect parasite DNA in all subsequent experiments.

A: Infected RBCs

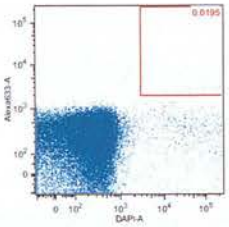

B: Infected RBCs + 12.8 (AF633)

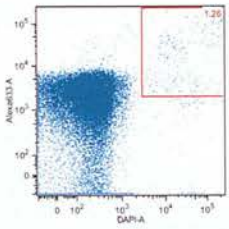

C: Infected RBCs + anti-Ym1 (AF633)

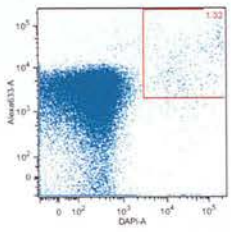

D: Uninfected RBCs + 12.8 (AF633)

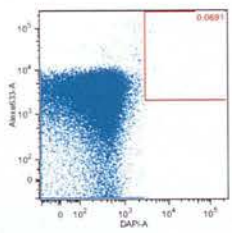

E: Uninfected RBCs + anti-Ym1 (AF633)

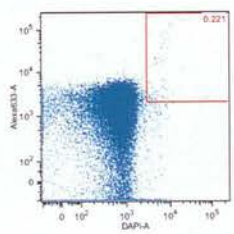

Figure 4.5 Representative plots of Alexa633 versus DAPI fluorescence from a preliminary *in vitro* ACWO experiment.

Representative Alexa633 versus DAPI dot plots of DCHF-DA loaded RBCs that had been incubated with schizont-infected RBCs that underwent invasion in the presence of no antibody (panel A), 12.8-AF633 (panel B), anti-Ym1-AF633 (panel C) or DCHF-DA-loaded RBCs incubated for the same time period with 12.8-AF633 (panel D) or anti-Ym1-AF633 (panel E). The gate displayed in red defines a region of high Alexa633 fluorescence and high DAPI fluorescence.

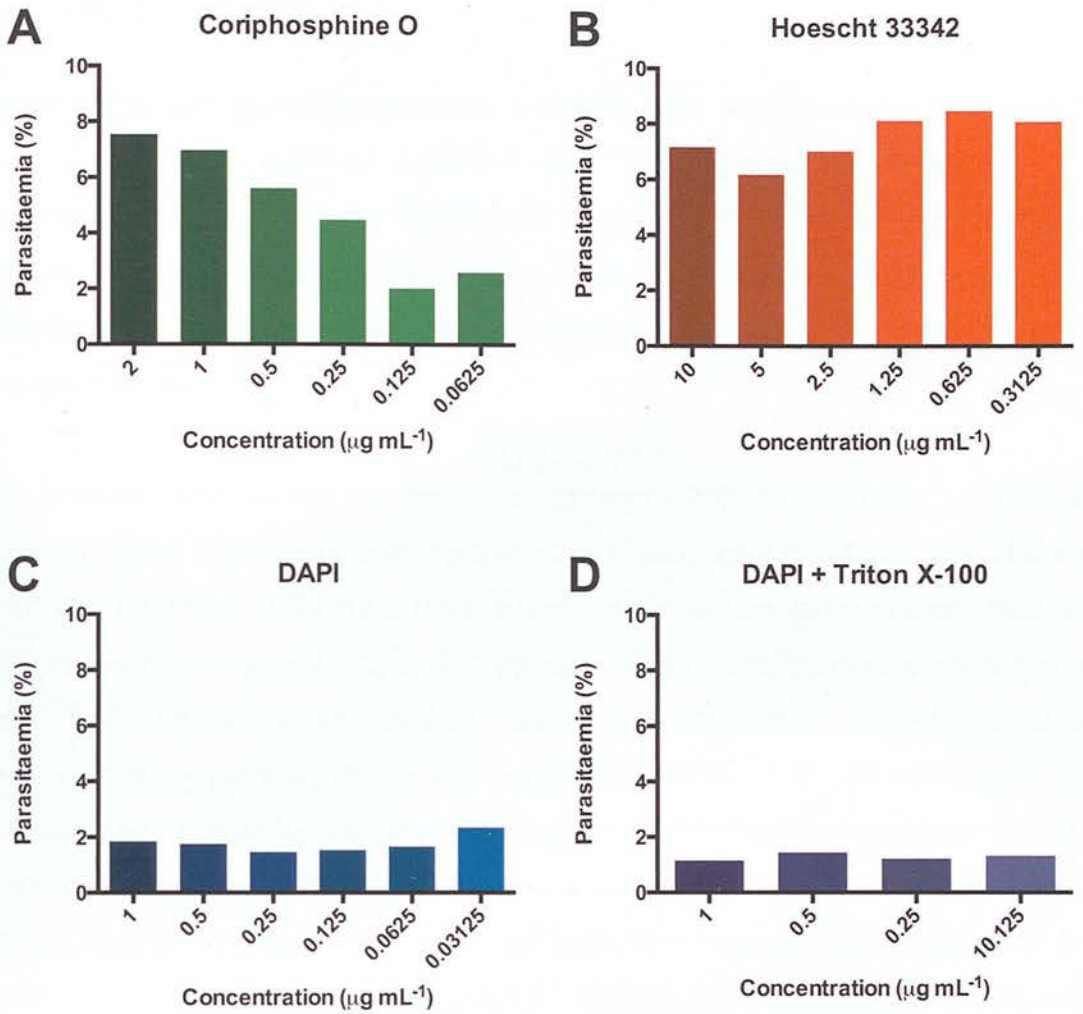

Figure 4.6 Comparasion of the ability of different DNA-binding dyes to estimate ring-stage parasitaemia.

Parasitaemia detected by flow cytometry when a highly synchronous early ring-stage culture was stained with (A) Coriphosphine O (2, 1, 0.5, 0.25, 0.125 or 0.0625 μg mL-1; green bars), (B) Hoechst 33342 (10, 5, 2.5, 1.25, 0.625, 0.3125 μg mL-1; orange bars), (C) DAPI (1, 0.5, 0.25, 0.125, 0.625, 0.03125 μg mL-1; blue bars) or (D) DAPI and 0.017% Triton X-100 (1, 0.5, 0.25, 0.125 μg mL-1; purple bars).

4.3.3 Antibody titration

In the preliminary ACWO experiments it had not been possible to gate 12.8-AF633 positive iRBCs as anti-Ym1-AF633 positive staining was also observed. As discussed above positive anti-Ym1-AF633 staining appeared to be due to a non-specific association of anti-Ym1-AF633 with the RBC surface. We reasoned that this could be due to the high antibody concentration used in these experiments, namely 1 mg mL^{-1}.

To determine whether this was the case, late stage iRBCs were allowed to undergo invasion in the presence of a mixture of 12.8-AF633 and Alexa Fluor 488-labelled anti-Ym1 (anti-Ym1-488) at equal concentrations, the concentration of each antibody ranging from 1000 μg mL^{-1} to 0.0625 μg mL^{-1}. If anti-Ym1 staining were due to a non-specific interaction with the RBC at high concentrations, one would expect to see this staining gradually lost as the concentration of anti-Ym1 lowers. Figure 4.7 displays flow cytometry histogram overlays of 12.8-AF633 and anti-Ym1-AF488 fluorescence of iRBCs 21, 40 and 46 h post invasion. As expected, at all time points AF488 fluorescence decreased as the anti-Ym1-AF488 concentration decreased. In contrast, as the concentration of 12.8-AF633 lowered, AF633 fluorescence splits into two distinct peaks leading to the formation of a valley in the histogram overlays. This valley demarcates the boundary between specific antibody binding and non-specific antibody binding. For uninfected RBCs AF633 fluorescence did not separate into two peaks and was indistinguishable from AF488 fluorescence (data not shown). Hence, a range of antibody concentrations at which 12.8-AF633, but not anti-Ym1-AF488 was specifically associated with the iRBC following invasion could be defined.

4.3.4 *In vitro* ACWO assay at lower antibody concentration

Given that a range of antibody concentration at which 12.8 but not anti-YM1 associated with iRBCs post invasion had now been defined, the *in vitro* ACWO assay was repeated using 3 concentrations of mAb from within this range, namely,

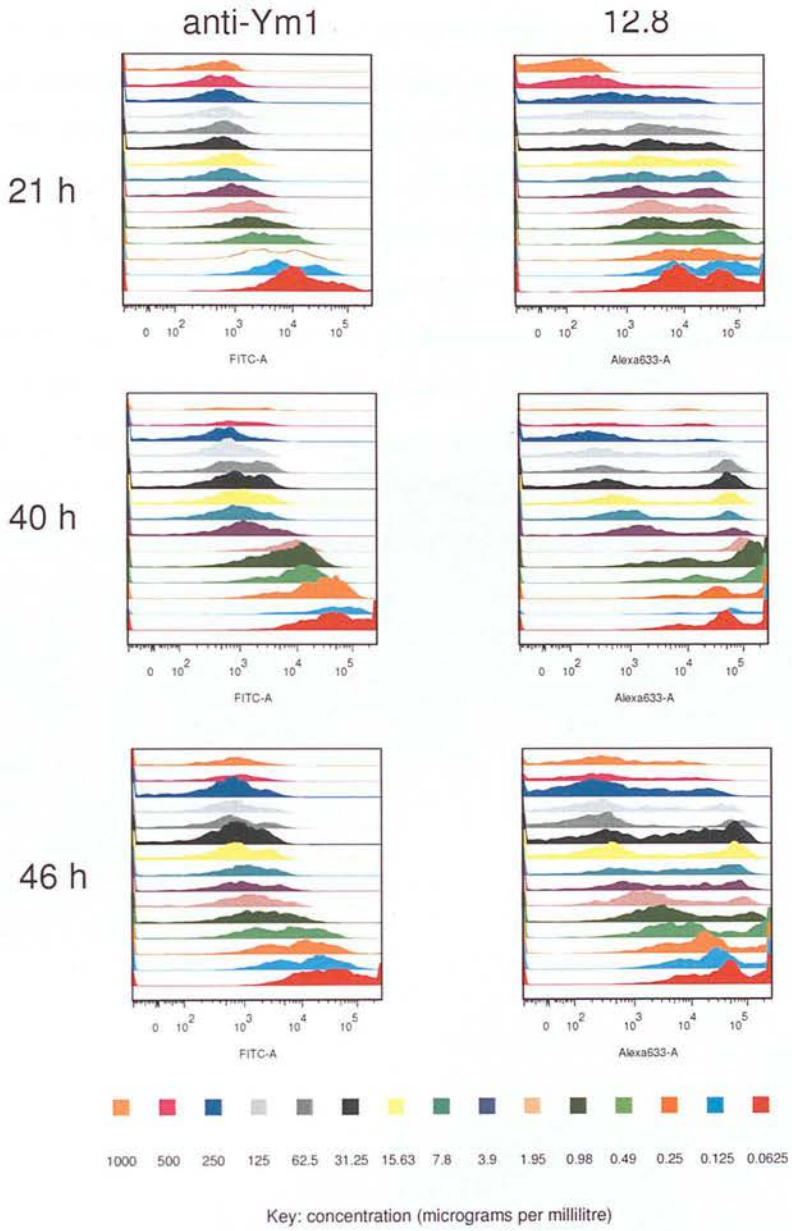
anti-Ym1
12.8
21 h
40 h
46 h
0 10^2 10^3 10^4 10^5
FITC-A
Alexa633-A
1000 500 250 125 62.5 31.25 15.63 7.8 3.9 1.95 0.98 0.49 0.25 0.125 0.0625
Key: concentration (micrograms per millilitre)

Figure 4.7 12.8 but not an irrelevant control antibody (anti-Ym1) is associated with newly infected RBCs following merozoite invasion.

Highly synchronous late-stage iRBCs were incubated with a mixed antibody solution containing 12.8 (AF633) and anti-Ym1 (AF488) at equal concentrations. Flow cytometry histograms of parasites sampled from assay wells at 21, 40 and 46 hours after assay set up. Anti-Ym1 fluorescence, detected in the FITC channel, is displayed in the left hand panels. 12.8 fluorescence, detected in the Alexa-633 channel, is displayed in the right hand panels. The concentration of 12.8 (AF633) and anti-Ym1 (AF488) was titrated two-fold from 1000 µg mL-1 to 0.0625 µg mL-1. Antibody concentration is indicated by histogram colour. Histograms are from individual assay wells and are representative of three triplicate assay wells.

125 μg mL-^{1}, 31.25 μg mL^{-1} and 3.9 μg mL^{-1}. DCFH-DA staining was carried out both pre and post treatment. Samples were acquired 13, 20, 37 and 44 hours after assay setup. A quadrant gate was applied to both infected and uninfected RBCs, which defined regions of high Alexa633 and low FITC fluorescence (gate Q1), high Alexa633 and high FITC fluorescence (gate Q2), low Alexa633 and high FITC fluorescence (gate Q3), and low Alexa633 and low FITC fluorescence (gate Q4). Representative plots illustrating this gating strategy for parasites that had undergone invasion into RBCs pre-loaded with DCFH-DA are shown in Figure 4.8 Panel A. In this experiment a unique population of Alexa633^{high}FITC^{high} parasites were identified in parasites that had undergone invasion in the presence of 12.8-AF633 but not in those that had undergone invasion in the presence of anti-Yml-AF63. This population was present across all three mAb concentrations at the 13 h and 20 h time points, however, at the 37 h and 44 h time points there was no significant difference between the percentage of events in Q2 in 12.8 -AF633 and anti-Yml-AF633 treated samples (Figure 4.8 panel B).

4.3.4.1 Re-titrating DCFH-DA

In the previous experiment there were a significantly higher number of Alexa633^{high}FITC^{high}-gated parasites in cultures that had undergone invasion in the presence of 12.8-AF633 than cultures that had undergone invasion in the presence of anti-Yml-AF633. However, the actual percentages of 12.8-AF633 treated parasites within this gate were still low and raised into question whether the effect being seen was a robust one. Given that these parasites displayed DCF fluorescence at the higher end of detection limits, we reasoned that lowering the concentration of DCFH-DA used in the experiment might increase our ability to detect parasites within this gate.

Synchronous schizont stage cultures were incubated with 31.25 μg mL^{-1} 12.8-AF633 or anti-Yml-AF633 and allowed to undergo invasion into RBCs pre-loaded with DCFH-DA at a concentration of 100 μM, 50 μM, 25 μM, 12.5 μM, 6.25 μM, 3.125 μM or 1.56 μM. 13 hours after assay set up, samples were stained with Hoechst 33342 and acquired on a flow cytometer. Infected RBCs were gated as described for

A

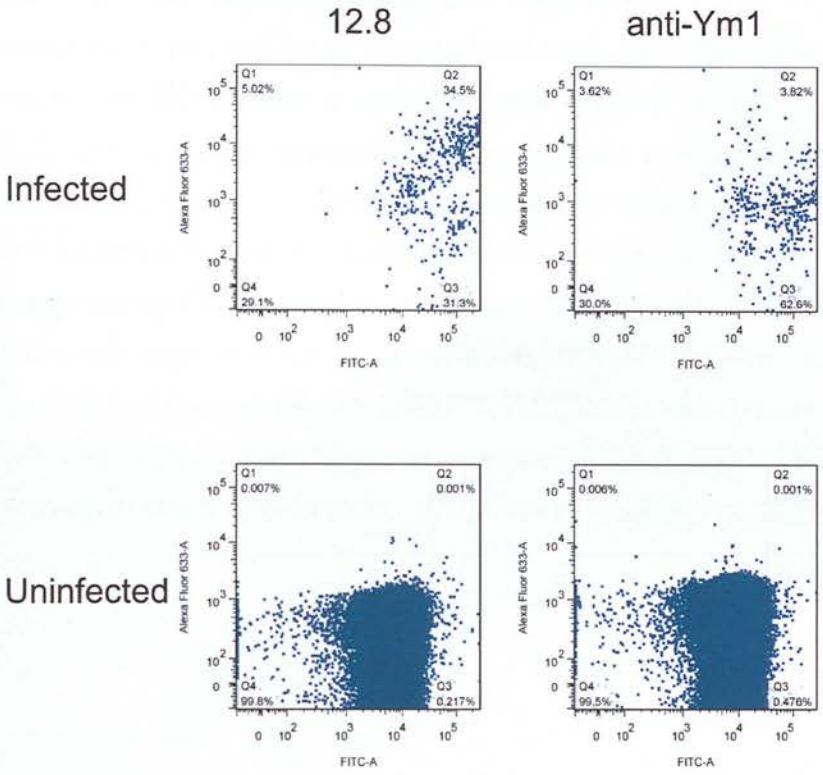
12.8
anti-Ym1
Infected
Uninfected
Q1
Q2
Q3
Q4
5.02%
34.5%
29.1%
31.3%
3.62%
3.82%
30.0%
62.6%
0.007%
0.001%
99.8%
0.217%
0.006%
0.001%
99.5%
0.476%
Alexa Fluor 633-A
FITC-A

B

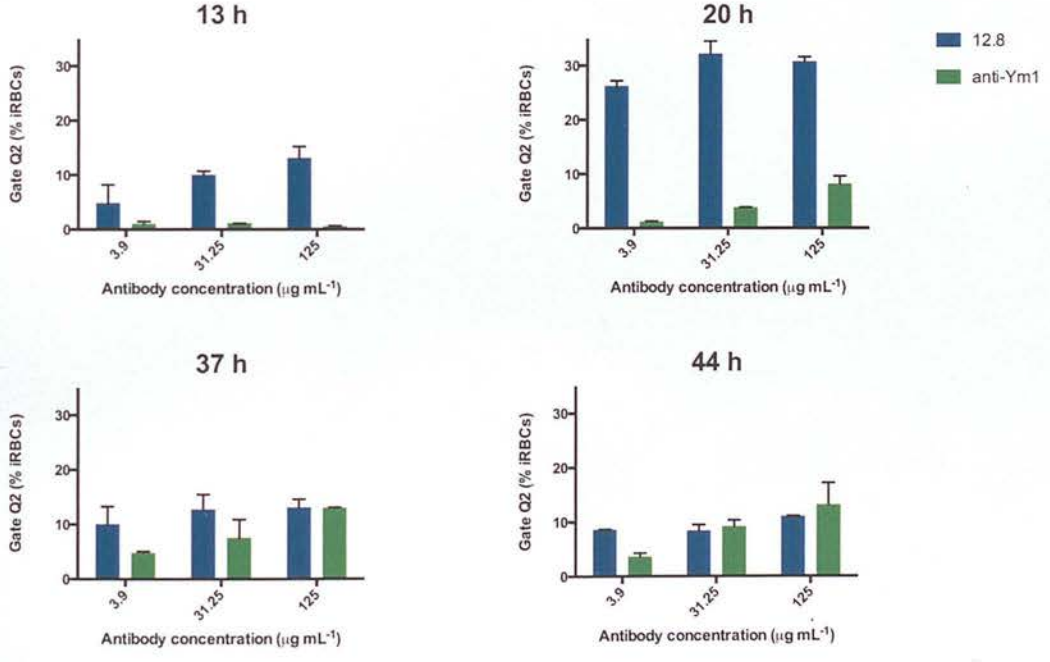
13 h
20 h
37 h
44 h
12.8
anti-Ym1
Gate Q2 (% iRBCs)
Antibody concentration (μg mL-1)
3.9
31.25
125

Figure 4.8 A unique population of antibody associated iRBCs displaying high DCF fluorescence is observed when *P. falciparum* undergoes invasion in the presence of the anti-MSP-1_{19}-specific mAb 12.8.

Synchronous schizont stage cultures were incubated with either 12.8-AF633 or anti-Ym1-AF633 and allowed to undergo invasion into DCFH-DA-loaded RBCs. At 13, 20, 37 and 44 hours after assay set-up, samples were acquired by flow cytometry. Samples were gated as infected or uninfected RBCs based on Hoechst staining. (A) A quadrant gate was applied to delineate four gates: Q1 (Alexa633^{high}FITC^{low}), Ab-associated iRBCs with low ROS level; Q2 (Alexa633^{high}FITC^{high}), Ab-associated iRBCs with high ROS level; Q3 (Alexa633^{low}FITC^{high}), Non Ab-associated iRBCs with high ROS level; Q4 (Alexa633^{low}FITC^{low}), Non Ab-associated iRBCs with low ROS level. (B) Graphs display the percentage of iRBCs in gate Q2 expressed as the mean of two duplicate wells. Error bars indicate the standard error of the mean.

the ACWO experiment (at lower antibody concentrations) described above. Figure 4.9 displays the percentage of parasites in gate Q2 for 12.8-AF633 and anti-Ym1-AF633 treated samples over the range of DCFH-DA concentrations used. At all concentrations of DCFH-DA there were more iRBCs in gate Q2 in 12.8-AF633 treated samples than anti-Ym1-AF633 treated samples. However, the percentage of iRBCs in gate Q2 was still low.

4.3.5 Dihydrorhodamine 123

Lowering the concentration of DCFH-DA had not resulted in an increase in the number of iRBCs in the $FITC^{high}633^{high}$ gate. We reasoned that the small percentage of iRBC events in gate Q2 might be due to DCFH not being prevalent in the subcellular compartment where 12.8 was located. Anti-$MSP\text{-}1_{19}$ antibodies internalised inside the RBC during invasion localise to the food vacuole (Dluzewski et al., 2008), an acidic compartment (pH 5.4-5.5) (Klonis et al., 2007). The main monoanion-dianion transition of DCF has a pKa of 5 (Leonhardt et al., 1971), hence DCF fluorescence will be affected by pH and in the case of the food vacuole would be expected to quench DCF fluorescence by a factor of ~2 (Fu et al., 2010). We therefore decided to use the ROS probe DHR 123 to investigate the potential catalytic ACWO activity of internalised 12.8. DHR 123 is a lipid soluble ROS indicator that is oxidised to cationic rhodamine 123 inside the cell. Given that the fluorescence spectrum of Rhodamine 123 is pH-independent from pH 4 to 10, one would not expect an acidic location of 12.8 to influence the ability of DHR 123 to detect ROS.

Synchronous schizont-stage cultures were incubated with no antibody, 12.8-AF633 or anti-Ym1-AF633 and allowed to undergo invasion into RBCs pre-loaded with DHR 123 at a range of concentrations. Figure 4.10 displays the median rhodamine 123 fluorescence intensity of iRBCs 23 hours after assay set up. The presence of 12.8 or anti-Ym1 antibody over this period did not appear to affect parasite ROS levels when compared to cultures incubated with no antibody.

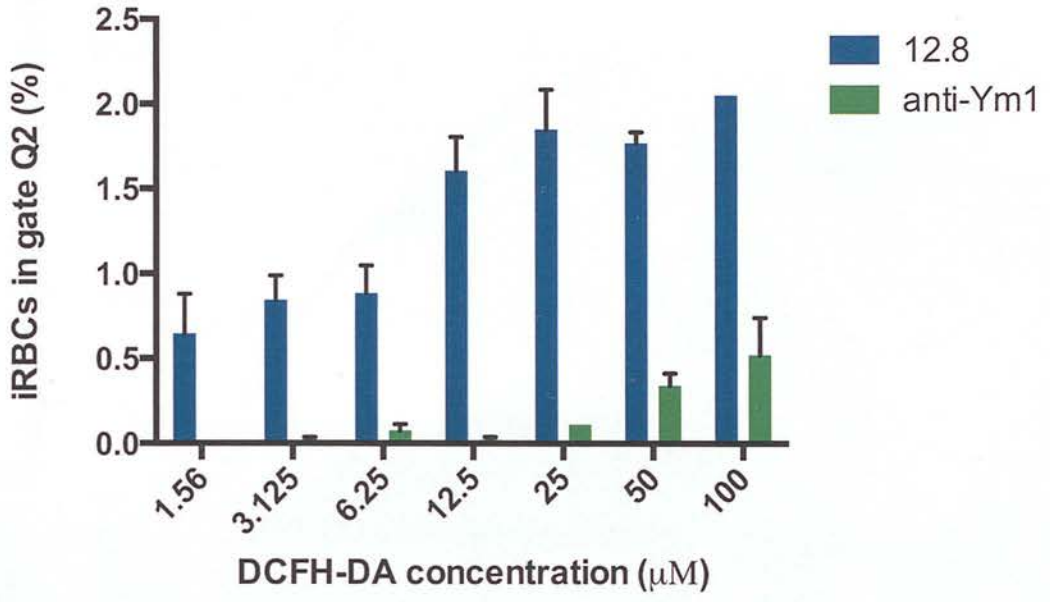

Figure 4.9 The proportion of iRBCs that are associated with the anti-MSP-1_{19} mAb 12.8 and display high DCF fluorescence remains low at lower concentrations of DCFH-DA.

Synchronous schizont stage cultures were incubated with either 12.8-AF633 or Ym1-AF633 and allowed to undergo invasion into RBCs pre-loaded with DCFH-DA at 1.56, 3.125, 6.25, 12.5, 25, 50 or 100 μM. At 13 hours after assay set up, samples were acquired by flow cytometry. Samples were gated as infected or uninfected RBCs based on Hoechst staining. A quadrant gate was applied to delineate four gates: Q1 (Alexa633^{high}FITC^{low}), Q2 (Alexa633^{high}FITC^{high}), Q3 (Alexa633^{low}FITC^{high}) and Q4 (Alexa633^{low}FITC^{low}). The graph display the percentage of iRBCs in gate Q2 expressed as the mean of two duplicate wells. Error bars indicate the standard error of the mean.

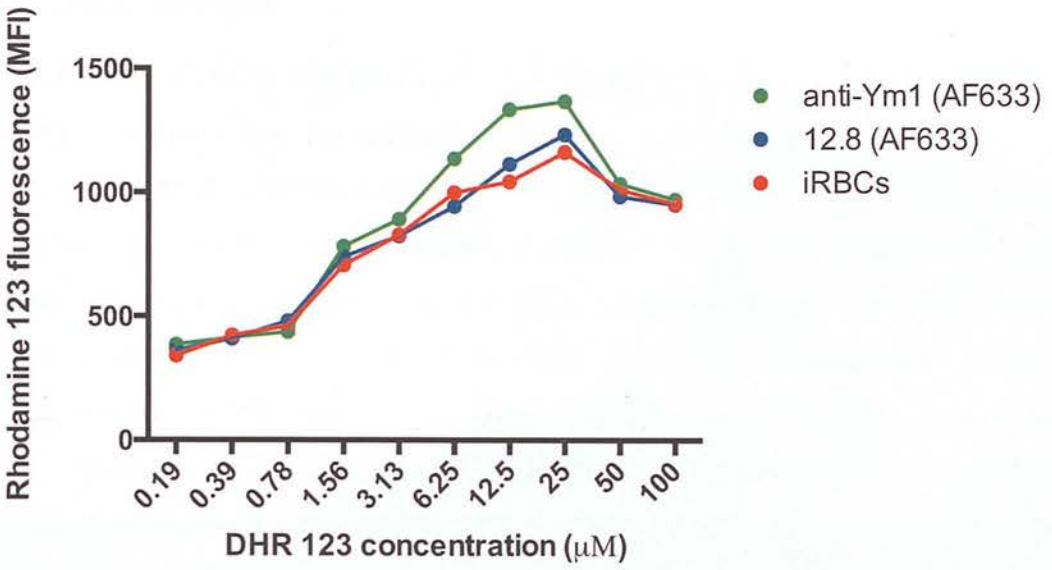

Figure 4.10 The intracellular ROS probe DHR 123 does not detect differences in the ROS level of iRBCs that have undergone invasion in the presence of no Ab, the anti-MSP-1_{19} mAb 12.8 or an anti-Ym1 mAb.

Synchronous schizont stage cultures were allowed to undergo invasion into RBCs pre-loaded with 0.19, 0.39, 0.78, 1.56, 3.13, 6.25, 12.5, 25, 50 or 100 μM DHR123 in the presence of anti-Ym1-AF633 (green line), 12.8-AF633 (blue) or no antibody (red line). The median rhodamine 123 fluorescence intensity of iRBCs 23 hours after assay set up is shown.

4.4 Discussion

This chapter set out to test the hypothesis that during merozoite invasion MSP-1_{19} specific antibodies are internalised inside the RBC and produce ROS via the ACWOP, which are detrimental to the intraerythrocytic development of the parasite. Production of ROS by the MSP-1_{19} specific mAb 12.8, following RBC internalisation during invasion, was not reliably detected despite extensive repeated efforts to optimise an assay to detect this effect. There was, however, some evidence in the *in vitro* ACWO experiments carried out at a lower Ab concentration that iRBCs specifically associated with 12.8 had a higher ROS level than iRBCs that had undergone invasion in the presence of the non-specific anti-Yml Ab. It is interesting to note that the effect seen was only discerable at time points that occurred early on in the IDC.

From the data presented here it is not possible to determine if the effect seen, namely increased iRBC ROS levels in the presence of specifically associated 12.8, is a real effect by which MSP-1_{19} specific Abs inhibit *P. falciparum in vitro* growth. The following possibilites exist (i) a more robust effect was not detected due to an inability to detect ACWO under the assay conditions used or (ii) ACWO by MSP-1_{19} specific antibodies is not the mechanism by which these antibodies inhibit the intraerythrocytic development of the parasite. Possibility (i) will be discussed first.

The aforementioned ACWO hypothesis was developed to attempt to explain the mechanism responsible for intraerythrocytic inhibition by MSP-1_{19} specific antibodies that had been observed both by our lab (Arnot et al., 2008) and other groups (Bergmann-Leitner et al., 2009; Moss et al., 2012). This inhibition had been observed using polyclonal anti-MSP-1_{19} antibodies purified from the serum of rabbits immunised with recombinant MSP-1_{19}. For the *in vitro* ACWO assay, the mAb 12.8 was chosen as the source of MSP-1_{19} specific antibody. The use of a mouse mAb over polyclonal antibodies was deemed advantageous as it provided a non-variable, continuous supply of antibody of defined specificity. Additionally, on a practical level there were not sufficient quantities of the polyclonal anti-MSP-1_{19}

IgG — that the intraerythrocytic growth inhibitiory effect had originally been detected with — left to carry out IgG hungry *in vitro* ACWO assays.

In hindsight 12.8 may not have been the most appropriate source of antibody to use. This is because the intraerythrocytic growth inhibition exerted by polyclonal anti-MSP-1_{19} antibodies is not replicated in GIAs carried out using 12.8. It therefore follows that the inability to convincingly detect ROS production by 12.8 in the *in vitro* ACWO assay may be because this antibody does not function via this mechanism. Given that anti-MSP-1_{19} specific Abs are known to inhibit *P. falciparum* growth through a number of different mechanisms *in vitro* (Blackman et al., 1994; Guevara Patiño et al., 1997), this does not preclude the possibility that other anti-MSP-119 specific Abs exert intraerythrocytic growth inhibition by activation of the ACWOP. It has in fact been reported that 12.8 inhibits merozoite invasion by preventing proteolytic processing of MSP-1_{42} by SUB2 (Blackman et al., 1990; Blackman et al., 1994; Guevara Patiño et al., 1997). However, this result has not been replicated when attempted by members of our lab or the GIA reference laboratory at the NIH (David Cavanagh, personal communication). Furthermore, in the experiments carried out with the Amplex red reagent, the level of H202 production was lower in Alexa Fluor-labelled Abs than in unlabelled Abs. This may have lowered the ability of the *in vitro* ACWO assay to detect an effect.

The most common *in vitro* assay used to measure *in vitro* growth inhibition by Abs is the GIA. The GIA is a crude measure of *in vitro* growth inhibition, requiring large quantities of Ab and lacking in the ability to distinguish inhibition of merozoite invasion from inhibition of the intraerythrocytic development of the parasite. It is unlikely that the GIA has the required sensitivity to detect an effect as specific as activation of the ACWOP. Here, we developed an assay with increased sensitivity relative to the GIA as we were looking for an effect that be quite transient and occur quite early on in the sequence of events that lead to intraerythrocytic growth inhibition. The detection of specific differences between treatment and control cultures in this assay required using low Ab concentrations at which one would not expect to see a growth inhibitory effect. In hindsight it is possible that this resulted

in the assay being carried out at a concentration of Ab that was too low to affect the oxidative stress levels of the parasite. A future avenue of research would be look for a correlation between intraerythrocytic growth inhibition by anti-MSP-1_{19} Abs and an increase in the level of oxidative stress experienced by the parasite. If such a correlation were detected one could then investigate whether increased ROS production was a cause or consequence of the intraerythrocytic inhibition observed

In order for antibodies to carry out ACWO they require a source of $^1O_2$. A potential biological source of this molecule is that generated by activated polymorphonuclear neutrophils (PMNs) and it has been hypothesised that PMN-bound antibodies use this $^1O_2$ to produce ozone via the ACWOP (Babior et al., 2003). It has recently been demonstrated that opsonised *P. falciparum* merozoites can trigger PMN respiratory bursts (Joos et al., 2010) and one can envisage several scenarios in which ACWO might facilitate or amplify this response: (i) merozoite bound antibody might activate PMNs and then intercept the $^1O_2$ produced during their respiratory burst to catalyse the production of H_20_2/O_3, (ii) neutrophil bound antibody could carry out the same function and (ii) ROS generated via mechanisms (i) or (ii) could be detrimental to nearby intraerythrocytic parasites, given that ROS metabolites are known to be distinctly toxic for intraerythrocytic parasites (Allison and Eugui, 1983; Clark and Hunt, 1983; Greve et al., 1999). Investigation of these possibilities would be particularly interesting given that antibody respiratory burst activity by PMN has been correlated with clinical protection to *P. falciparum* malaria *in vivo* (Joos et al., 2010). As with any *in vitro* model, the ACWO assay developed here is likely to be an oversimplification of what might occur *in vivo* and perhaps the inclusion of other cells types, for example PMN, is required for ACWO by MSA-specific antibodies to occur *in vitro*.

It is possible that internalised 12.8 did carry out ACWO but that the ROS probes we used failed to detect it. Given that MSP-1_{19} and anti- MSP-1_{19} antibodies locate to the developing digestive vacuole (DV) following merozoite invasion, it is reasonable to assume that internalised 12.8 may also localise there. The level of DCFH (the de-esterified form of DCFHA) that is present in the digestive vacuole will be a function

of the level and activity of intracellular esterases present in that subcellular compartment. Hypothetically, one would expect the DV to display the highest level of DCF fluorescence (ROS level) given that this is the site of haemoglobin digestion. However, Fu *et al.* (Fu et al., 2010) did not detect accumulation of DCF fluorescence in the DV, implying that there is not a sufficient quantity of DCFH present in this organelle or that there may be quenching of DCF fluorescence. The acidic pH of the DV could be responsible for quenching of DCF fluorescence but this would not explain our inability to detect rhodamine 123 fluorescence during the *in vitro* ACWO assay. The possibility exists that haematin in the DV could be responsible for quenching of both ROS indicators. The *in vitro* ACWO experiments presented in this chapter were carried out in complete medium that contained phenol red. It has subsequently come to my attention that the presence of phenol red greatly attenuates the DCF signal. Consequently, any future *in vitro* ACWO experiments should be carried out in phenol red-free medium. Use of a fluorogenic ROS probe that could be targeted to a particular subcellular compartment may prove useful is this regard. Additionally, it has been reported that DCFH-DA lacks specificity and can be auto-oxidised (Bonini et al., 2006; Pal et al., 2012). In future studies of *in vitro* ACWO activity fluorogenic probes which exhibit a greater degree of specificity, similar to those recently developed for detection of O_3 (Garner et al., 2009) or H_20_2 (Dickinson and Chang, 2008) may prove useful.

P. falciparum lacks catalase and a genuine glutathione peroxidase system and therefore might be considered vulnerable to ROS. Inded it is thought that the antimalarial actions of primaquine, chloroquine and artemisinin are mediated, at least in part, by increasing the oxidative stress level in the iRBC (Becker et al., 2004). However, it has emerged that *P. falciparum* imports a number of human proteins involved in antioxidant defence, including the antioxidant enzymes peroxiredoxin II (Koncarevic et al., 2009), superoxide dismutase and catalase (Foth et al., 2011). It therefore follows that *P. falciparum* may not be as vulnerable to ROS as previously thought. Indeed, Fu *et al.* (Fu et al., 2010) found that inactivation of RBC catalase did not result in a significant increase in the oxidative stress level experienced by *P.*

falciparum thus implying that glutathione peroxidase and other antioxidants may be sufficient to protect the parasite from oxidative stress.

The identification of ACWO in a seminal paper in 2000 by Wentworth and colleagues (Wentworth et al., 2000) spawned a flurry of research publications in this area. However, it remains to be determined how important this mechanism of antibody function is to immune defence *in vivo* and whether it plays any role in antibody mediated immunity to *P. falciparum* infection.

5 Investigation of the functional activity of MSP3.3-specific antibodies

5.1 Introduction

A novel gene, *PF10_0347*, was identified whilst searching the *P. falciparum* genome sequence for open reading frames containing homology to MSP3 (Pearce et al., 2005; Singh et al., 2009). The product of this gene, recently re-designated as MSP3.3, is one of six members of a family of proteins defined by the presence of a NLRNA/NLRNG signature motif. Additionally, all family members contain an N-terminal signature sequence and share a high degree of sequence conservation in their C-terminal halves (Singh et al., 2009). The MSP3.3 protein sequence, 424 amino acids in length, contains glycine-rich and leucine-zipper like motifs, in addition to two SUB1 processing sites (Figure 5.1).

MSP3.3 is unique to *P. falciparum* and displays a high degree of intraspecies amino acid sequence conservation; in one study, of 14 *P. falciparum* isolates sequenced, only four non-synonymous single nucleotide polymorphisms (SNPs) were identified, whilst another study located three non-synonymous SNPs in sequences encoding the C-terminal region of MSP3.3 from 36 *P. falciparum* isolates of disparate geographical origin (Singh et al., 2009; Tetteh et al., 2009). MSP3.3 is recognised by Abs elicited in response to *P. falciparum* infection in malaria endemic regions (Pearce et al., 2005) and is reported to be a target of ADCI (Singh et al., 2009).

In our lab, an intrinsically unstructured region from the C-terminal half of MSP3.3, designated MSP3.3C, has been expressed and purified as a recombinant antigen (K. Dhanasarnsombut, PhD thesis, University of Edinburgh; Dhanasarnsombut *et al.*, manuscript in preparation). Immunisation of rabbits with recombinant MSP3.3C elicited Abs specific to this antigen that were found to be remarkably effective at

inhibiting the *in vitro* growth of *P. falciparum* (Dhanasarnsombut). Light microscopic analysis of Giemsa-stained smears indicated that the intraerythrocytic development of *P. falciparum* might be compromised during these assays.

The mechanisms by which Abs to *P. falciparum* antigens inhibit the growth of the parasite are not fully understood, particularly when it comes to elucidating how these Abs may interfere with the biochemical and physiological development of the parasite inside the RBC. Dissecting these mechanisms would prove useful, both in terms of informing vaccine design to elicit functional immune responses and in developing an *in vitro* assay that can serve as a functional readout of an effective immune response, whether naturally acquired or vaccine induced. Thus this chapter aims to characterise the mechanism by which Abs to MSP3.3C inhibit the growth of *P. falciparum* parasites *in vitro*.

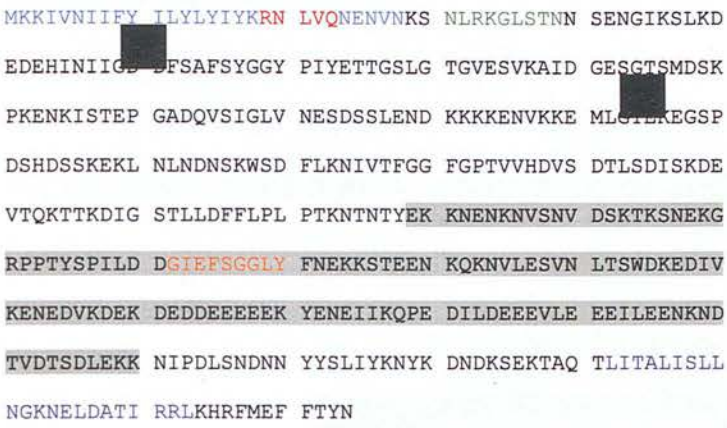

Figure 5.1 Amino acid sequence of MSP3.3

The N-terminal signal sequence (light blue residues), within which lies a PEXEL motif (red residues), in addition to the NLRNA/NLRNG signature motif (green residues), a glycline rich motif (orange residues) and a leucine-zipper like sequence (dark blue residues). The MSP3.3C region, comprised of residues 229 to 360, is marked with a shaded background. SUB1 processing sites are demarcated by downward arrows.

5.2 Materials and methods

Routine culturing of *P. falciparum* parasites is described in Chapter 2.

5.2.1 Rabbit immunisations and production of anti-MSP3.3C antibodies

As part of this earlier study in our lab, on the anti-parasite effects of antibodies to MSP3.3, two rabbits (coded 6066 and 6067) were immunised intramuscularly using 100 μg per dose of recombinant MSP3.3C antigen formulated with Freund's complete/incomplete adjuvant. Each animal was immunised on days 0, 7, 14, 28 and 42, with blood samples collected for serum on days 0, 8 and 49. Rabbits were housed and immunised at BioGenes GmbH (Berlin, Germany).

Total IgG from immunised rabbit sera was purified by affinity chromatography as detailed in Chapter 2. In order to obtain MSP3.3C-specific IgG, a MSP3.3C-coupled affinity column was prepared. 1 mL of a 7 mg mL^{-1} solution of recombinant MSP3.3 in coupling buffer (0.2 M $NaHCO_3$, 0.5 M NaCl, pH 8.3) was added to a 1 mL Hi-Trap N-hydroxy-succinimide (NHS)-activated Sepharose column (GE Healthcare) and the coupling reaction carried out according to the manufacturer's instructions (GE Healthcare). Purified total rabbit IgG was passed through this column. The column was washed extensively with PBS prior to eluting bound MSP3.3C-specific IgG with 0.1 M glycine-HCl pH 2.7 into tubes containing 1 M Tris pH 9.0 neutralisation buffer. Purification of MSP3.3C-specific IgG from total IgG was carried out by Kelwalin Dhanasarnsombut.

5.2.2 Growth inhibition assay with multiple time points

The GIA is used to test the ability of Abs against blood-stage *P. falciparum* antigens to inhibit parasite invasion and growth *in vitro*. The Ab treatments were anti-MSP3.3C IgG (total IgG from rabbit 6066), in addition to anti-AMA1 IgG and NR IgG, which served as positive and negative controls, respectively. Each Ab sample, at a stock concentration of 12 mg mL^{-1}, was serially diluted across four

concentrations; 6, 3, 1.5 and 0.75 mg mL^{-1}. 50 µL of each antibody dilution in RPMI 1640 (Invitrogen, 21870) was dispensed in duplicate into the wells of a flat-bottomed microtitre plate (Costar, 3598). An equal volume (50 µL) of parasite culture at 0.5% parasitaemia and 4% haematocrit, consisting predominantly of mid-stage schizonts in twofold-concentration complete medium, was dispensed into each well. Therefore, at the onset of the assay parasites were present at 0.5% parasitaemia in complete culture medium at 2% haematocrit. Plates were incubated at 37 °C, 5% CO_2. At three time points, 16 h, 27 h and 44 h after the start of the assay, (i.e. when negative control cultures were predominantly at ring, trophozoite and schizont stage, respectively), cells within each well were resuspended. Following this, 10 µL of cells from each well were dispensed into 290 µL of 3.47 µM Coriphospine O in RPMI 1640 and stained in the dark at RT for 15 mins. The data from these samples were acquired on a Becton Dickinson FACScan fluorescence-activated cell analyser. Data from 50, 000 cells were acquired for each sample.

5.2.3 Stage specific growth inhibition assay

A stage-specific growth inhibition assay (SSGIA) was developed from the standard GIA. In the SSGIA, immune IgG is added to highly synchronous cultures of mid-ring stage, mid-trophozoite stage or mid-schizont stage parasites, termed the SSGIA(R), SSGIA(T) or SSGIA(S), respectively. Unlike the standard GIA, where parasitaemia is measured 42 h after incubation with immune IgG, in the SSGIA parasites are sampled at 3 time points over one erythrocytic cycle, each time point corresponding to the next stage of parasite intraerythrocytic development. For example, in the SSGIA(R) immune IgG is added to parasites at mid-ring stage, then parasites are sampled at the subsequent life-cycle time points corresponding to trophozoite, schizont and (following re-invasion), ring stage. For clarity, assay set up and sampling time points for each assay are displayed in Table 5.1.

Parasites were synchronised by sorbitol treatment in order to yield a ~0-18 h post-invasion culture of ring stage parasites. A second sorbitol treatment was carried out 34 h later in order to obtain a 0-4 h post-invasion ring stage culture. Synchrony of this 0-4 h culture was maintained by sorbitol treatment every 48 hours until assay set

up. Ab added to cultures consisted of two separate anti-MSP3.3C IgG preparations, one being total IgG from rabbit 6066 and the other total IgG from rabbit 6067. In addition, anti-AMA1 IgG and NR IgG, served as positive and negative controls respectively. Each IgG was serially diluted across four concentrations; 12mg mL^{-1}, 6mg mL^{-1}, 3mg mL^{-1} and 1.5 mg mL^{-1}. Then, 50 µL of each antibody dilution in RPMI 1640 was dispensed in duplicate into the wells of a flat-bottomed microtitre plate (Costar, 3598). Following this, 50 µL of parasite culture at 0.8% parasitaemia and 4% haematocrit, in twofold-concentration complete medium, was dispensed into each well. Therefore, at the start of the assay parasites were present at 0.8% parasitaemia in complete culture medium at 2% haematocrit. Plates were incubated at 37 °C, 5% CO_2 for the duration of the assay.

In the SSGIA two methods are used to measure parasite growth inhibition: (i) flow cytometric measurement of parasitaemia and parasite DNA content and (ii) microscopically determined measurements of intraerythrocytic growth stage. At each sampling time point, cells were resuspended and 10 µL of culture from each assay well was dispensed into 300 µL RPMI 1640 containing 0.31 µg mL^{-1} Hoechst 33342 (Invitrogen, H3570). Cells were stained for 30 mins at 37 °C in a FACs tube. The data from these samples were then acquired on a BD LSR II flow cytometer. Data from 150,000 cells were acquired for each sample.

In addition, at each sampling time point 3 µL of culture from duplicate wells containing the highest concentration (6 mg mL^{-1}) of each Ab treatment were placed onto a microscope slide, spread thinly with a clean microscope slide, allowed to air dry and stained for 20 minutes with 10% Giemsa solution. These smears were examined by light microscopy and 100 parasites per smear scored into four classes: ring stage, trophozoite stage (haemozoin evident, single nucleus unless a multiple invasion event), schizont (multiple nuclei, with or without segmentation) and pynotic (condensed nuclei, parasite rounded in shape and densely stained).

Time point	Assay	Hours post (initial) invasion	Stage of negatve control culture
Assay set up	SSGIA(R)	12-16	Mid ring
Time point 1	SSGIA(R)	30-34	Mid trophozoite
Time point 2	SSGIA(R)	40-44	Mid schizont
Time point 3	SSGIA(R)	60-64	Mid ring
Assay set up	SSGIA(T)	30-34	Mid trophozoite
Time point 1	SSGIA(T)	40-44	Mid schizont
Time point 2	SSGIA(T)	60-64	Mid ring
Time point 3	SSGIA(T)	78-82	Mid trophozoite
Assay set up	SSGIA(S)	40-44	Mid schizont
Time point 1	SSGIA(S)	60-64	Mid ring
Time point 2	SSGIA(S)	78-82	Mid trophozoite
Time point 3	SSGIA(S)	88-92	Mid schizont

Table 5.1 Table 5.1 Assay set up and sampling time points of the SSGIA.

5.2.4. Immunofluorescence assay

Immunofluorescence assay (IFA) is a technique used to visualise parasite antigens using an antigen-specific primary antibody followed by a secondary antibody conjugated to a fluorochrome. Parasite cultures were washed with RPMI 1640 and resuspended at 20% haematocrit in RPMI 1640. Approximately 3 µL of this culture was placed onto a microscope slide, spread thinly with a clean microscope slide and allowed to air dry. Smears were fixed with 2% paraformaldehyde/PBS for 2 minutes at 4 °C and then with 90% acetone/10% methanol for 2 minutes at 4 °C. Smears were air-dried, blocked with 1% BSA/PBS for 1 h at RT and then reacted with 5 µg mL^{-1} of anti-EXP-2 mouse mAb 7.7 and 31.5 µg mL^{-1} of MSP3.3C-specific, affinity purified IgG for 1 h at RT in 1% BSA/PBS. Slides were washed 3 times in PBS and incubated with FITC-conjugated goat anti-mouse IgG (DakoCytomation) and 12.5 µg mL^{-1} Alexa Fluor 568 goat anti-rabbit IgG (Invitrogen, A-11036) in 1% BSA/PBS for 1 h at RT. Slides were washed a further 3 times in PBS, stained with 0.5 µg mL^{-1} DAPI/PBS and mounted in Citifluor (Citifluor Ltd). Single stained slides of each primary and each secondary Ab were prepared as controls. Parasites were viewed using on an Olympus BX50 fluorescence microscope with a 100 x oil-immersion objective lens.

5.2.5 IgG uptake

Parasites were synchronised by 3 rounds of sorbitol treatment in order to obtain a 0-4 h post invasion culture as detailed for the SSGIA assay. Treatments included MSP3.3C-specific, affinity purified IgG from rabbit 6066, anti-AMA1 IgG, NR IgG and RPMI 1640 alone (see section 5.3 for details of exact treatments used in each experiment). 50 µL of each antibody treatment at a concentration of 1 mg mL^{-1} or RPMI alone was dispensed in duplicate into the wells of a flat-bottomed microtitre plate. 50 µL of a 12 h post invasion parasite culture at 0.5% parasitaemia and 4% haematocrit, in twofold-concentration complete medium, was dispensed into each well. Therefore, at the start of the assay parasites were present at 0.5% parasitaemia in complete medium at 2% haematocrit. Plates were incubated at 37 °C, 5% CO_2 for the duration of the assay.

At sampling time points (30 h, 40 h and 60 h post initial invasion) 3 µL of resuspended culture was placed onto a microscope slide, spread thinly with a clean microscope slide and allowed to air dry. Smears were fixed with 2% paraformaldehyde/PBS for 2 minutes at 4°C and then with 90% acetone/10% methanol for 2 minutes at 4°C. Smears were air-dried, blocked with 1% BSA/PBS for 1 h at RT and then reacted with 5 µg mL^{-1} of the anti-EXP-2 mouse mAb 7.7 for 1 h at RT in 1% BSA/PBS. Slides were washed three times in PBS, and incubated with FITC-conjugated goat anti-mouse IgG and 12.5 µg mL^{-1} AlexaFluor 568 goat anti-rabbit IgG (Invitrogen, A-11036) in 1% BSA/PBS for 1 h at RT. Slides were washed a further 3 times in PBS, stained with 0.5 µg mL^{-1} DAPI/PBS and mounted in Citifluor (Citifluor Ltd.). Single stained slides for mAb 7.7 and each secondary Ab were prepared as controls. In order to determine whether IgG could be detected inside iRBCs, parasites were viewed using a Olympus BX50 fluorescence microscope with a 100 x oil-immersion objective lens.

5.2.6 Confocal microscopy

For confocal microscopy experiments looking at MSP3.3 expression, slides were prepared as detailed under the IFA section above with the following modification; sampling time points were at 30 h and 40 h post invasion and not 60 h post invasion. For confocal microscopy experiments looking at IgG uptake, slides were prepared as detailed in the IgG uptake section above with the following modifications; anti-AMA1 IgG was included as a treatment and sampling time points were 30h and 40h post invasion. In both experiments, slides were viewed on a Leica SP5II confocal microscope (Leica Microsystems) with the 63 x objective using LAS AP software (Leica). Dianne Murray assisted with data acquisition. Data were analysed using Volocity software (Improvision).

5.2.7 JC-1 assays

Parasites were synchronised by three rounds of sorbitol treatment in order to obtain a 0-4 h post invasion culture as detailed for the SSGIA assay. Ab treatments included MSP3.3C-specific, affinity purified IgG from rabbit 6066 and NR IgG. Each IgG

treatment was serially diluted across four concentrations; 12mg mL^{-1}, 6mg mL^{-1}, 3mg mL^{-1} and 1.5 mg mL^{-1}. Then, 50 µL of each antibody dilution in RPMI 1640 was dispensed in duplicate into the wells of a flat-bottomed microtitre plate. Additionally, 50 µL of the following treatments were dispensed in duplicate into wells; 60 µM chloroquine, 0.2% sodium azide and RPMI 1640. Following this, 50 µL of a 10 h parasite culture at 0.5% parasitaemia and 4% haematocrit, in twofold-concentration complete medium, was dispensed into each well. Therefore, at the start of the assay parasites were present at 0.5% parasitaemia in complete culture medium at 2% haematocrit. Plates were incubated at 37 °C, 5% CO_2 for the duration of the assay.

Sampling time points, unless stated otherwise, were 10 h (immediately after assay set up), 22 h, 30 h and 36 h post invasion. At each time-point 10 µL of resuspended cells were taken from each assay well and dispensed into 300 µL of 6 µM JC-1/0.5 µM Hoechst 33342, and stained in the dark at 37 °C for 30 minutes. Subsequently, all samples were washed once with RPMI 1640, resuspended in 300 µL RPMI 1640 and 150,000 cells from each sample acquired on a BD LSR II flow cytometer.

Flow cytometry data acquried from JC-1 assays were analysed using FlowJo software (Tree Star Inc) to determine the co-ordinates of a gate, which on an FSC versus Hoescht axis, would only include iRBCs. This gate was applied to JC-1 assay flow cytometry data in R(R, 2005). A ratio was derived for each gated fluorescence event (i.e. each iRBC acquired by flow cytometry) by dividing JC-1 red fluorescence by JC-green fluorescence. The R code used to carry out this computation was written by Graeme Cowan.

5.2.8 DHCF-DA assays

Parasites were synchronised by 3 rounds of sorbitol treatment in order to obtain a 0-4 h post invasion culture as detailed for the SSGIA assay. Ab treatments included MSP3.3C-specific, affinity purified IgG from rabbit 6066 and NR IgG. Each IgG treatment was serially diluted across four concentrations; 12 mg mL^{-1}, 6 mg mL^{-1}, 3

mg mL^{-1} and 1.5 mg mL^{-1}. Then, 50 µL of each antibody dilution in RPMI 1640 was dispensed in duplicate into the wells of a flat-bottomed microtitre plate. Following this, 50 µL of a 10 h parasite culture at 0.5% parasitaemia and 4% haematocrit, in twofold-concentration complete medium, was dispensed into each well. Therefore, at the start of the assay parasites were present at 0.5% parasitaemia in complete culture medium at 2% haematocrit. Plates were incubated at 37 °C, 5% CO_2 for the duration of the assay.

Sampling time points, unless stated otherwise, were 10 h (immediately after assay set up), 22 h, 30 h and 36 h post invasion. At each time point 10 µL of resuspended cells were taken from each assay well and dispensed into 300 µL of 5 µM DCFH-DA (Invitrogen, C2938)/0.5 µM Hoechst 33342 and stained in the dark at 37 °C for 30 minutes. Subsequently, all samples were washed once with RPMI 1640, resuspended in 300 µL RPMI 1640 and 150,000 cells from each sample acquired on a BD LSR II flow cytometer.

5.2.9 Statistical anlayses: SSGIA data

For each of the 3 types of SSGIA, namely SSGIA(R), SSGIA(T) and SSGIA(S), data from 3 independent experiments were analysed together. For each of these 3 sets of data, one analysis was carried out to explain variation in the outcome parasitaemia and another carried out to explain variation in the outcome DNA content. Therefore, a total of 6 statistical analyses were carried out.

"Well" was the independent statistical unit and as repeated sampling from wells had taken place, data were treated as repeated measures data. A covariance mixed model analysis was carried out by Margo Chase-Topping in SAS version 9.3. 'Well' was treated as a random effect. The advantage of using a covariance pattern mixed model instead of a regular mixed model with a random effect is that it does not assume there is a constant correlation between all time points(Brown and Prescott, 2006). A variety of covariance patterns were tested prior to each analysis and the one that provided the best fit was used in the final model . Analysis was performed

on all data and then on each treatment (antibody) separately. To examine the nature of any statistically significant effects within each treatment (antibody), the differences in least square means were examined, after carrying out a Bonferroni adjustment for the number of comparisons made. Analyses were carried out on log transformed raw parasitaemias and median fluorescence intensities of the Hoescht channel, for parasitaemia and DNA content analyses, respectively.

5.2.10 Statistical analyses: JC-1 data

Statistical analyses of JC-1 red to green ratios were carried out by Liam Herbert in R. Preliminary analysis showed that the range of ratios obtained in each of the 3 experimental replicates were statistically significantly different from one another. Therefore, analysing the data from all 3 replicates in 1 statistical analysis was not possible. Therefore, one experimental replicate was taken to be representative used for statistical analysis. Linear mixed models were fitted separately for each of the 4 sampling time points. Treatment and concentration were treated as fixed effects and well as a random effect.

5.3 Results

5.3.1 Stage-specific growth inhibition assay: method development

Dhanasarnsombut *et al.* (Dhanasarnsombut) observed numerous parasites with abnormal morphology during GIAs carried out in the presence of anti-MSP3.3C IgG, which were reminiscent of unhealthy parasites that had been observed in cultures treated with anti-MSP1-19 IgG (Arnot et al., 2008; Bergmann-Leitner et al., 2009) and indicated that the development of post invasion intraerythrocytic forms might be inhibited or disrupted.

In a standard GIA, Abs are added to synchronous late stage cultures (trophozoites and schizonts) and growth inhibition is measured 42 hours later, by comparing the

parasitaemia of the experimental culture to that of a control culture. In order to investigate whether abnormal development of intraerythrocytic parasites was occurring in anti-MSP3.3C IgG treated cultures, and in particular to determine at which morphological stage of parasite development these abnormalities might become apparent, the temporal resolution of the GIA was increased by sampling from treatment wells at multiple time points over the course of the GIA.

MSP3.3C specific IgG was added to a synchronous schizont stage culture, and parasitaemia and parasite DNA content measured at three time points post invasion (16, 27 and 44 hours after assay set up), corresponding to the ring, trophozoite and schizont stages of healthy NR IgG treated control cultures. The level of growth inhibition observed at the highest concentration of anti-MSP3.3C IgG at each of these time points was 41%, 43%, and 40%, respectively (Figure 5.2e). This was approximately half the level of growth inhibition exhibited by the positive control, anti-AMA1 IgG and differed from the results of GIAs carried out by Dhanasarnsombut *et al.* (Dhanasarnsombut) where the strong inhibitory activity of anti-MSP3.3C IgG and anti-AMA1 IgG had been comparable.

In this experiment parasitaemia and DNA content were determined using the acridine derivative Coriphosphine O, a dual colour stain that emits red fluorescence when bound to RNA and green fluorescence when bound to DNA and subcellular vesicles. Based on these dual fluorescence properties, coriphosphine O staining can distinguish between ring, trophozoite and schizont stages. Figure 5.2b displays red (FL3 channel) versus green (FL1 channel) fluorescence of iRBCs from healthy control cultures 16, 27 and 44 hours after assay set up. The progression of the culture through the IDC is reflected by the predominance of rings, rings and trophozoites, and schizonts, respectively, at each of these time points.

Surprisingly, comparison of plots of red (FL3 channel) versus green (FL1 channel) fluorescence of iRBCs treated with the highest concentration (6 mg mL^{-1}) of anti-MSP3.3C IgG to iRBCs treated with the same concentration of NR IgG revealed that a whole population of cells, namely schizonts, were completely absent from

MSP3.3C IgG treated cultures (Figure 5.2c). This inhibitory effect was dose-dependent, with the proportion of schizonts detected increasing as the concentration of MSP3.3C IgG decreased. This striking effect was quantified by determining the median fluorescence intensity (MFI) of the FL1 channel, as a measure of parasite DNA content, for each sample (Figure 5.2e). At the 16 and 27 h time points, parasite DNA replication has not occurred yet and there is no difference between parasite DNA content in MSP3.3C IgG and NR IgG treated cultures. However, at the 44 h time point, it is clear that the ability of MSP3.3C IgG cultures to develop to schizonts and undergo DNA replication is severely inhibited.

This stage-specific growth inhibition by anti-MSP3.3C IgG may explain the surprisingly lower level of growth inhibitory activity seen in this GIA compared to those of Dhanasarnsombut *et al.* in our laboratory (Dhanasarnsombut). In the GIA carried out by Dhanasarnsombut *et al.*, Ab treatments were added to synchronous trophozoite stage cultures, as is standard practice in GIA, whereas in this experiment Ab treatments had been applied to schizont stage cultures. I therefore reasoned that the parasite stage at which Ab is added might be critical to the level and nature of growth inhibition observed.

In order to determine if this was the case, a GIA was carried out, adding Ab treatments to a trophozoite stage culture and measuring parasitaemia and DNA content at four time points post-invasion. The temporal resolution of the GIA was further from the one described above by (i) using a highly synchronous 4 hour post invasion culture of parasites and (ii) monitoring when merozoite invasion was complete so that time points were measured as hours post merozoite invasion instead of hours since assay set up.

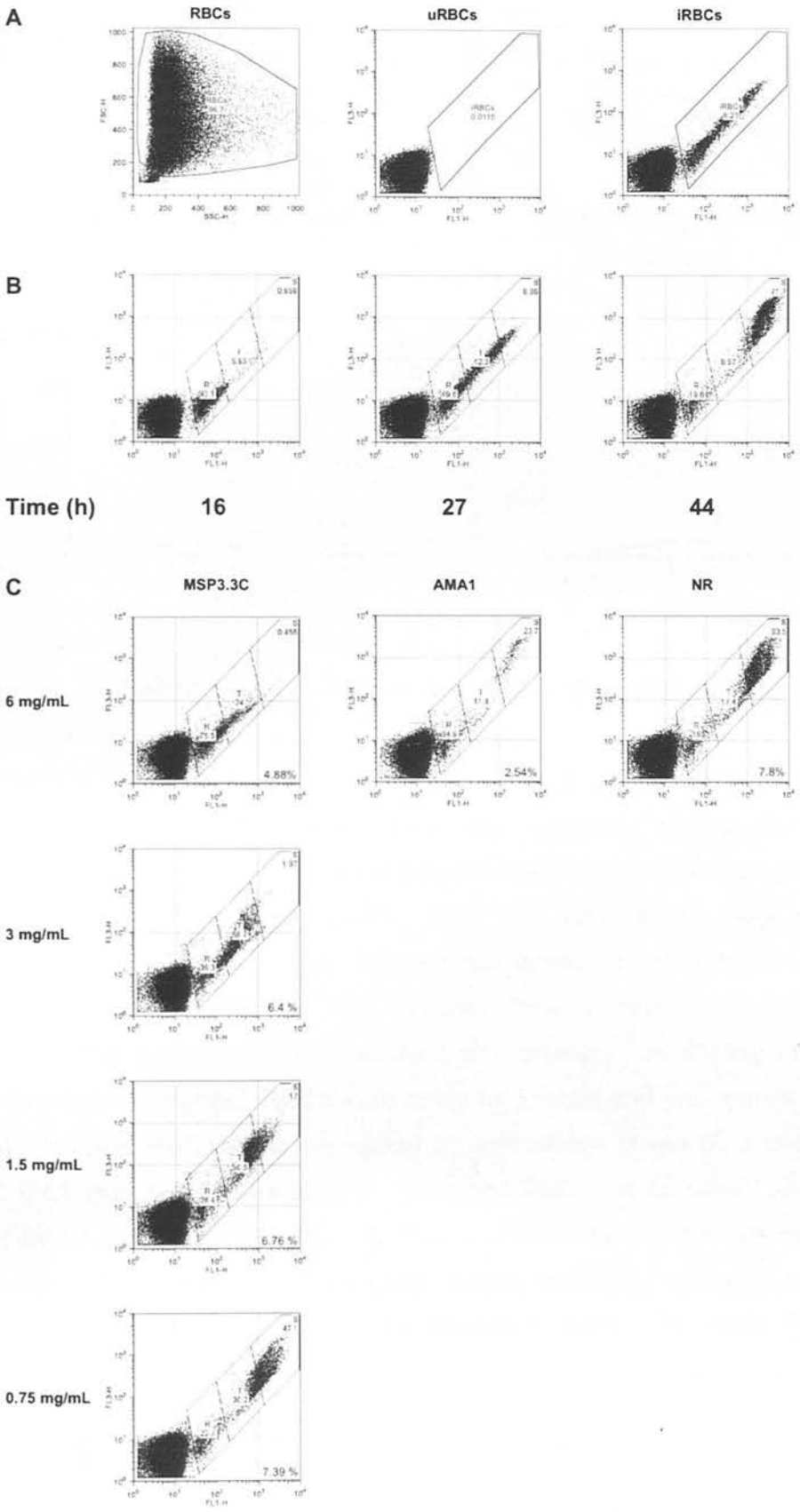
A
RBCs
uRBCs
iRBCs
B
Time (h)
16
27
44
C
MSP3.3C
AMA1
NR
6 mg/mL
3 mg/mL
1.5 mg/mL
0.75 mg/mL
4.88%
2.54%
7.8%
6.4 %
6.76 %
7.39 %

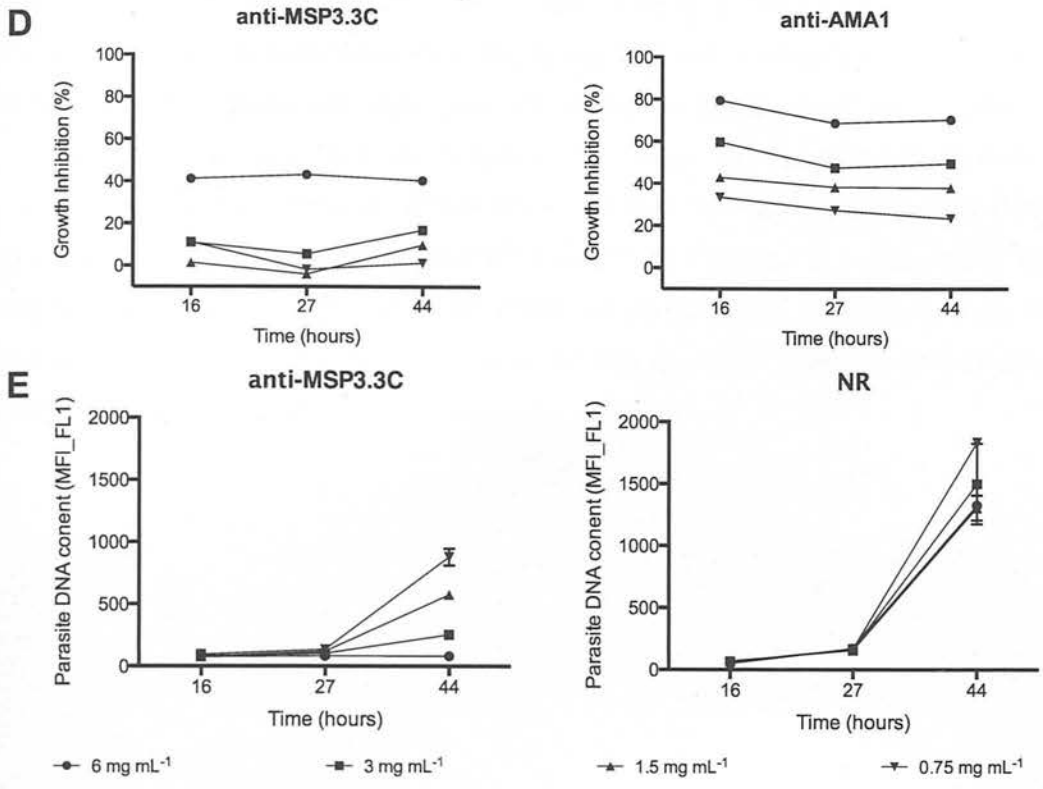

Figure 5.2 Anti-MSP3.3C IgG inhibits the intraerythrocytic development of *P. falciparum*

Anti-MSP3.3 IgG, anti-AMA1 IgG or NR IgG were serially diluted across four concentrations; 6 mg mL^{-1} (circle), 3 mg mL^{-1} (square), 1.5 mg mL^{-1} (upward triangle) and 0.75 mg mL^{-1} (downward triangle) and added to synchronous schizont stage cultures. At three time points, 16h , 27h and 44h after assay set up, corresponding to ring, trophozoite and schizont stages of development in NR IgG control cultures, parasitaemia and parasite DNA content measured by flow cytometry after Coriphosphine O staining of parasites. **A,** Gating strategy for determining parasitaemia. RBCs were gated by forward and side scatter (left hand panel). Infected RBCs were then gated by comparison of red (FL3 channel) and green (FL1 channel) fluorescence in uninfected RBC (middle panel) and infected RBC (right hand panel) samples. **B,** Representative bivariate scatterplots of red fluorescence (FL3 channel) versus green fluorescence (FL1 channel) of iRBCs in the absence of antibody 16, 27 and 44 h after assay set up. The gates R, T and S, define areas of FL3 and FL1 fluorescence of rings, trophozoite and schizonts, respectively. The percentage of iRBCs in R, T and S gates are displayed. **C,** Representative bivariate scatter plots of red (FL3 channel) versus green (FL1 channel) fluorescence of anti-MSP3.3C IgG treated samples 44 h after the addition

of Ab. For comparison, representative plots of samples treated with 6 mg mL^{-1} of the positive control, anti-AMA1 IgG, and 6 mg mL^{-1} of the negative control, NR IgG, at the same time point, are displayed. Parasitaemia (bottom right hand corner) and percentage of iRBCs in R, T and S gates are shown. **D,** Parasite growth inhibition (percentage) in the presence of anti-MSP3.3C IgG (left hand panel) or anti-AMA1 IgG (right hand panel). **E,** Parasite DNA content (MFI of the FL-1 channel) of iRBCs treated with anti-MSP3.3C IgG (left hand panel) or naive rabbit IgG (right hand panel). Data points represent the mean of two duplicate samples and error bars indicate the standard error of the mean.

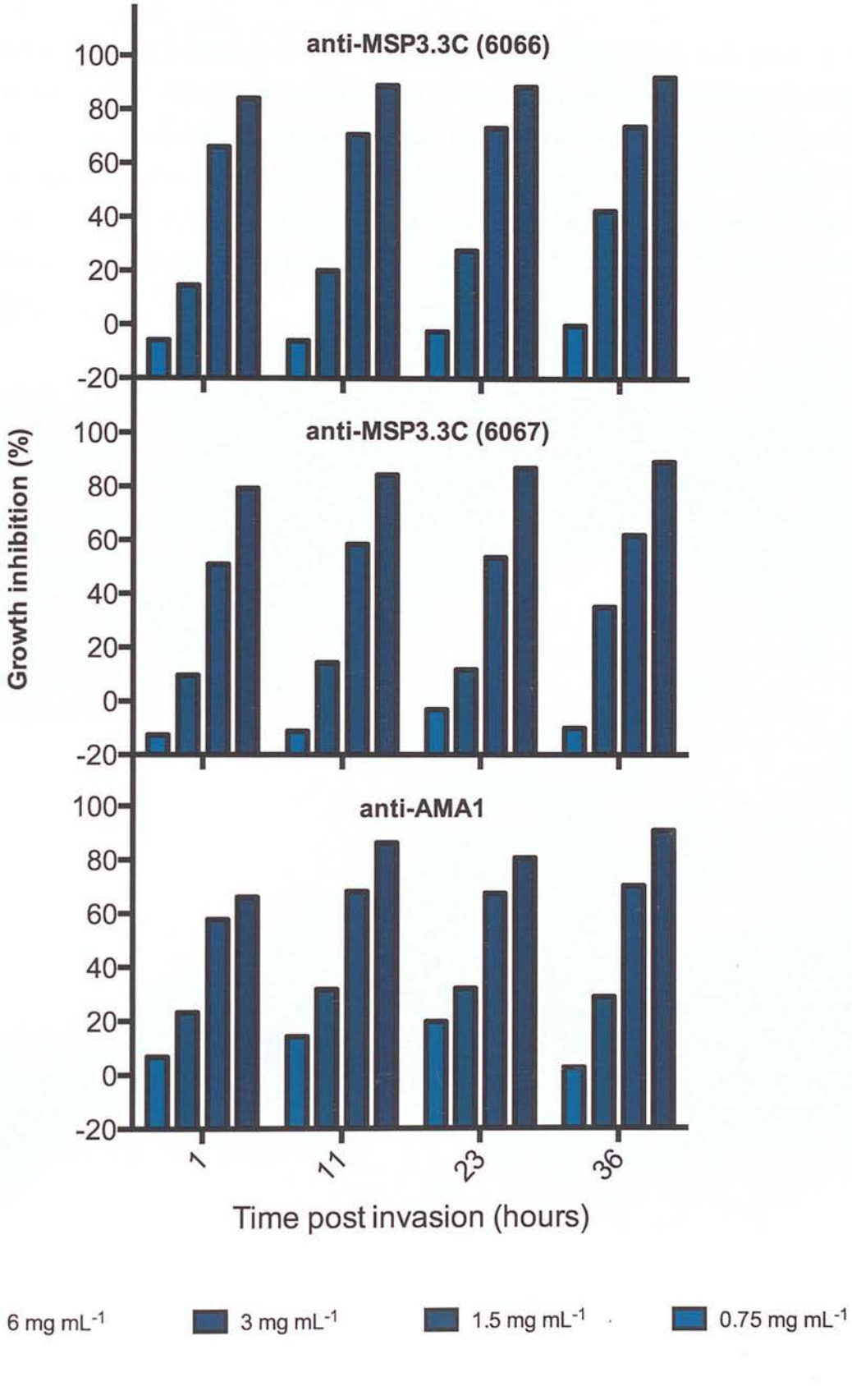
anti-MSP3.3C (6066)
anti-MSP3.3C (6067)
anti-AMA1
Growth inhibition (%)
100
80
60
40
20
0
-20
1
11
23
36
Time post invasion (hours)
6 mg mL-1
3 mg mL-1
1.5 mg mL-1
0.75 mg mL-1

Figure 5.3 Growth inhibition by anti-MSP3.3C IgG added to trophozoite stage cultures.

Percentage growth inhibition of cultures treated with anti-MSP3.3C IgG (total IgG from rabbit 6066 or rabbit 6067) or anti-AMA1 IgG relative to control cultures treated with the same concentration of naive rabbit IgG. Treatment IgG, serially diluted across four concentrations (6 mg mL^{-1}, 3 mg mL^{-1}, 1.5 mg mL^{-1} and 0.75 mg mL^{-1}), was added to trophozoite stage cultures and parasitaemia measured by flow cytometry of Hoechst 33342-stained samples at 1, 11, 23 and 36 hours post invasion.

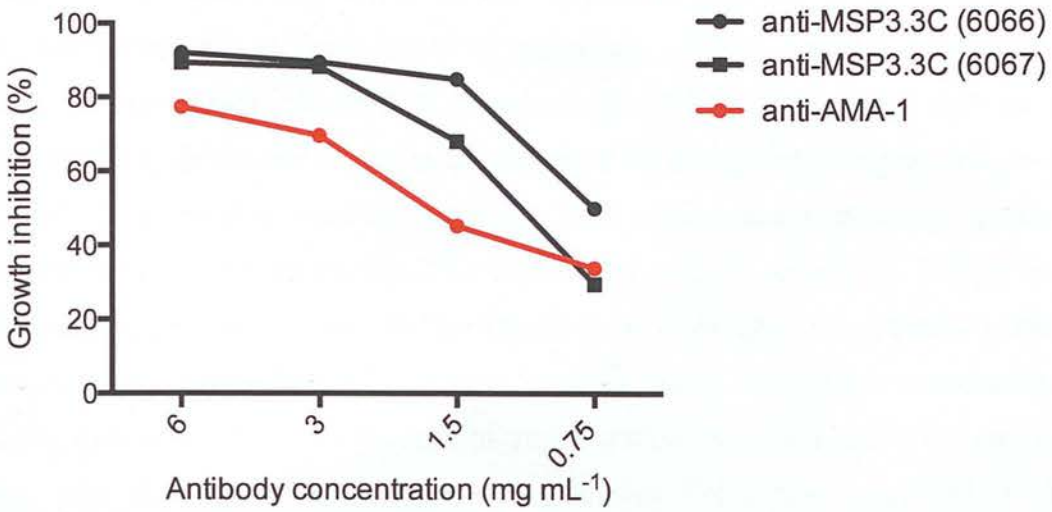

Figure 5.4 Growth inhibition by anti-MSP3.3C IgG added to ring stage stage cultures.

Percentage growth inhibition of cultures treated with anti-MSP3.3C IgG (total IgG from rabbit 6066 or rabbit 6067) or anti-AMA1 IgG relative to control cultures treated with the same concentration of NR IgG. Treatment IgG, serially diluted across four concentrations (6 mg mL^{-1}, 3 mg mL^{-1}, 1.5 mg mL^{-1} and 0.75 mg mL^{-1}), was added to ring stage cultures and parasitaemia measured by flow cytometry of Hoechst 33342 stained samples 48 hours later.

In the first GIA with multiple time points, carried out using anti-MSP3.3C IgG, the dye Coriphosphine O was used to enumerate iRBCs by flow cytometry. Discrimination of ring infected RBCs from uninfected RBCs had proved difficult in some samples. This could be due to quenching of the dye upon binding nucleic acids or staining of parasite vesicles interfering with measurements of DNA content. Hoechst 33342 is a minor groove DNA-binding dye with AT selectivity (Müller and Gautier, 1975) and thus lends itself well to studying *P. falciparum*, a parasite whose genome is greater than 80% AT rich (Gardner et al., 2002). Given that reproducible, precise measurements of DNA content and merozoite invasion inhibition can be made with this dye (Dent et al., 2008), Hoechst 33342 was employed in all subsequent experiments investigating the functional activity of anti-MSP3.3C IgG.

The advantages of measuring GIA outcomes via flow cytometry, as opposed to the standard method employed, parasite specific enzyme lactate dehydrogenase, which is generated by active parasite metabolism (Malkin et al., 2005), are twofold. Firstly, given that levels of PfLDH mRNA and enzymatic activity vary significantly throughout the intraerythrocytic cycle of the parasite (Vivas et al., 2005), this detection method does not allow comparative measures of growth inhibition when stage-specific effects are involved, whereas flow cytometry does. Secondly, analysis of the flow cytometric data from each parasite infected can accurately determine DNA content, providing information about the stage of intraerythrocytic development of the parasite, whereas pLDH assays do not.

When anti-MSP3.3C IgG was added to trophozoite stage cultures, the level of growth inhibition detected was comparable to that of Dhanasarnsombut *et al.*(K. Dhanasarnsombut, PhD thesis, University of Edinburgh; Dhanasarnsombut *et al.*, manuscript in preparation); i.e. ~ 80% at the highest concentration of anti-MSP3.3C IgG, and of a comparable magnitude to that seen with the positive anti-AMA1 control (Figure 5.3). Light microscopic examination of Giemsa-stained smears taken at the first time point (1 h post invasion) revealed that anti-MSP3.3C IgG treated cultures contained a high proportion of schizonts relative to NR IgG treated cultures,

indicating that these cultures had developed into schizonts, but having had their development blocked during this stage, had not been able to undergo invasion.

Finally, I investigated the effect of adding anti-MSP3.3C IgG to ring stage cultures. Ab treatments were added to mid-ring stage cultures and parasitaemia, DNA content and parasite morphology examined at 3 time points corresponding to subsequent trophozoite, schizont and ring stages of control cultures. The level of growth inhibition observed in anti-MSP3.3C IgG treated cultures 48 hours after the addition of antibody was ~ 90%, higher than the level of inhibition observed with the anti-AMA1 positive control (Figure 5.4). Furthermore, using 6 mg mL^{-1} IgG, at the timepoint when corresponding negative control cultures were predominantly schizonts, cultures treated with anti-MSP3.3C IgG had not developed beyond the trophozoite stage, and this inhibitory effect was dose-dependent (Figure 5.5).

Data from the preliminary experiments described above were put together to develop the stage specific growth inhibition assay (SSGIA) in order to dissect in finer detail the mechanism of action of MSP3.3C specific Abs in GIAs. This assay, depicted schematically in Figure 5.6, involves the addition of immune IgG to highly synchronous mid-ring, mid-trophozoite and mid-schizont stage cultures. In each case, at the following three stages of intraerythrocytic development, parasitaemia and parasite DNA content are measured by flow cytometry, and parasite morphology examined by light microscopy of Giemsa stained smears. For example, after the addition of immune IgG to a mid-ring stage culture, samples are taken at two pre-invasion time points, corresponding to when healthy control cultures are at the trophozoite and schizont stage of development, respectively, and at one post-invasion time point, when control cultures have undergone merozoite invasion and are at ring stage. All SSGIA time points are given relative to hours since the initial merozoite invasion event, as shown in Figure 5.6. In the SSGIA, anti-AMA1 IgG is used as a positive GIA control, and also as an example of an Ab whose functional activity is to block the ability of merozoites to invade erythrocytes. NR IgG was used to control for any non-specific growth inhibitory or growth promoting effects of rabbit IgG. Thus, this assay is able to differentiate between intra-erythrocytic growth inhibition

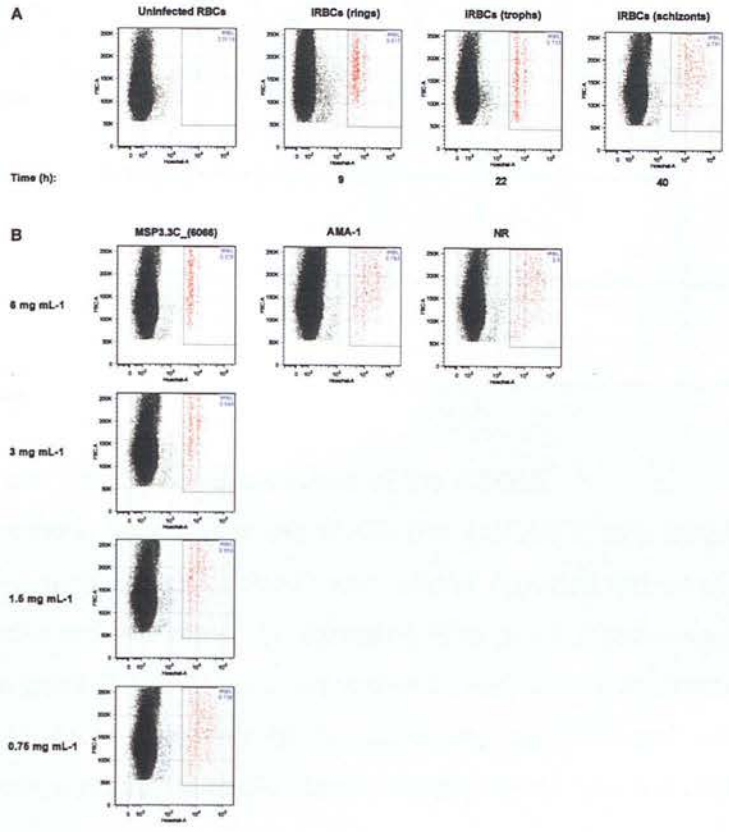

Figure 5.5 Intraerythrocytic growth inhibition by anti-MSP3.3C IgG added to ring stage stage cultures.

Treatment IgG was added to synchronous ring stage cultures 9 hours post invasion and the DNA content of Hoechst 33342-stained parasites measured by flow cytometry 22 and 40 hours after invasion, in addition to 9 hours into the next invasion cycle. **A,** Bivariate scatter plots of forward scatter (FSC-A) versus Hoechst fluorescence (Hoechst-A) of uRBC (left) and iRBC samples were compared in order to gate iRBCs. Hoescht staining of iRBCs in the absence of antibody 9 h (middle, left), 22 h (middle, right) and 40 h (right) post invasion, when parasites are predominantly, rings, trophozoites and schizonts, respectively, are displayed. Note the shift along Hoescht-A axis between trophozoite and schizont samples. **B,** Bivariate scatter plots of FSC-A versus Hoechst-A staining of RBCs at 40 hours post invasion, when control cultures (NR IgG treated) were schizonts. For comparison, representative plots of samples treated with the highest concentration of anti-AMA1 IgG and NR IgG are displayed. Uninfected RBCs are shown in black and gated iRBCs in red. The iRBC gate and percentage of total RBCs within this gate are displayed.

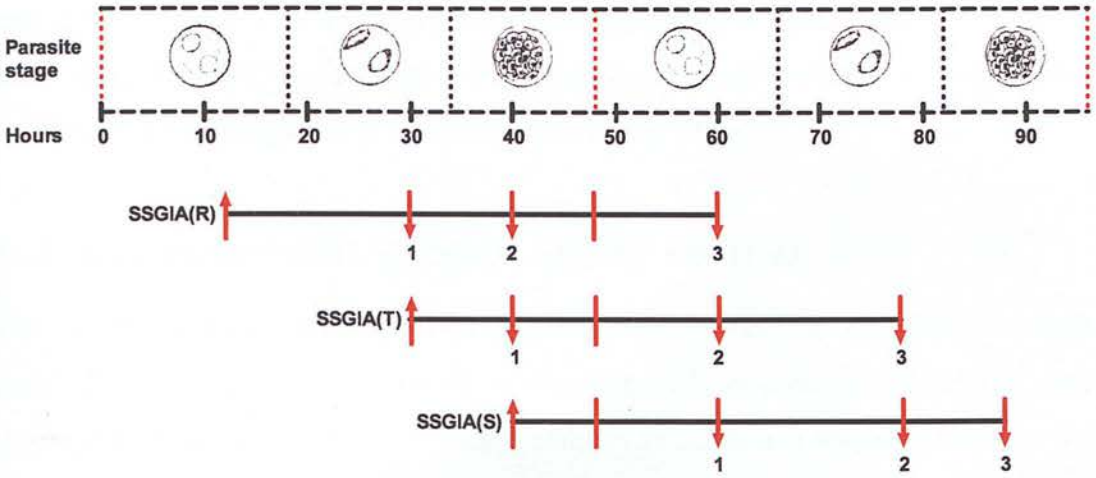

Figure 5.6 Schematic outline of the SSGIA

Schematic timelines of the SSGIA(R), SSGIA(T) and SSGIA(S). On each time line, the time at which antibody was added (upward red arrow), sampline time point 1 (downward red arrow 1), sampling time point 2 (downward red arrow 2), sampling time point 3 (downward red arrow 3) and merozoite invasion events (red line) are depicted. The time in hours since the first merozoite invasion event and intraerythrocytic parasite stages are depicted at the top of the figure.

and merozoite invasion inhibitory effects, to delineate at which stages of parasite development inhibitory effects become apparent, and to account for any effects due to the stage of development at which immune IgG is added.

5.3. Stage-specific growth assay results

The results of three independent SSGIA experiments carried out with total IgG, purified from each of two rabbits immunised with recombinant MSP3.3C, are displayed in Figures 5.7-5.10. For each sample, parasitaemia was calculated as the percentage of total RBC gated events in the iRBC gate and mean parasitaemia computed for each set of duplicate wells. Relative parasitaemia was calculated according to the equation RP = Pt/Pc where RP = relative parasitaemia, Pt = mean parasitaemia in the presence of test antibody and Pc = mean parasitaemia in the presence of naive rabbit IgG at the same concentration as the test antibody. Therefore, an RP value of 1 indicates no difference from the negative control, RP values > 1 denote increased parasitaemia relative to the negative control and RP values < 1 indicate parasitaemias lower than the negative control. Calculating relative parasitaemia in this way controls for any non-specific growth promoting or growth-inhibitory effects of rabbit IgG, however significant differences between parasitaemias in the presence or absence of NR IgG were not observed (data not shown). This data normalisation was carried out in order to allow comparison between the three independent experiments carried out.

For each sample, the Hoechst median fluorescence intensity (MFI) of iRBC gated events was calculated as a measure of DNA content. Relative DNA content was calculated according to the equation RDC = RDCt/RDCc where RDC = relative DNA content, RDCt = mean DNA content of two independent wells in the presence of test antibody and RDCc = mean DNA content of two independent wells in the presence of naive rabbit IgG at the same concentration as the test antibody. RDC values greater than or less than 1, signify a higher and lower DNA content than controls, respectively.

At all time points in the SSGIA assays, Giemsa-stained blood smears were prepared from duplicate wells of the highest concentration of each IgG treatment. These smears were scored by light microscopy to determine the proportion of each intraerythrocytic parasite stage present in each sample. In addition, pycnotic parasites were scored, defined as those parasites with condensed nuclei that were rounded in shape and densely stained.

5.3.2. SSGIA(R)

The statistical models fitted to explain variation in parasitaemia and DNA content in the SSGIA(R) are displayed in Tables 5.2 and 5.7, respectively. For parasitaemia the effects of Ab concentration and time point within each treatment are displayed in Tables 5.3-5.6 and for DNA content in Tables 5.8-5.11. For the outcome parasitaemia the concentration of anti-AMA1 IgG ($p<0.001$), anti-MSP3.3C (6066) IgG ($p<0.001$) and anti-MSP3.3C (6067) IgG ($p<0.001$) significantly affected parasitaemia. The concentration of NR IgG had no affect on parasitaemia ($p=0.9292$). For the outcome DNA content the concentration of anti-MSP3.3C (6066) IgG ($p<0.001$) and anti-MSP3.3C (6067) IgG ($p=0.0007$) significantly affected DNA content. The concentration of anti-AMA1 IgG ($p=0.9727$) and NR IgG ($p=0.7740$) did not affect DNA content.

At 30 h post invasion RPs and RDCs are ~ 1 in anti-AMA1 IgG and both anti-MSP3.3C IgG treated cultures (Figure 5.7, panels A and B). At 40 h post invasion, two effects are noticeable in anti-MSP3.3C IgG treated cultures: (i) RP values start to fall below 1 at higher concentrations of the Ab (Figure 5.7, panel A) and (ii) RDC values are strikingly reduced at higher concentrations of the Ab (Figure 5.7, panel B). Effect (i) is due to a drop in DNA content of iRBCs such that they no longer sit within the confines of the iRBC gate. At 30 h post invasion, a proportion of pycnotic, densely stained trophozoites were observed and these forms persisted for the duration of the assay (Figure 5.7, panel C and Figure 5.10, contrast plates A and B with plates C and D). Between 30 h and 40 h post invasion control cultures have developed from the trophozoite stage to the schizont stage. This is exemplified by a

statistically significant increase in DNA content between these two time points at all concentrations of anti-AMA1 IgG and NR IgG. This statistically significant increase is not seen in anti-MSP3.3C IgG (6066) at 6, 3 and 1.5 mg mL^{-1} and anti-MSP3.3C IgG (6067) at 6 and 3 mg mL^{-1}. This could be explained by anti-MSP3.3C IgG treated parasites being inhibited during either the ring stage or the trophozoite stage. Examination of Giemsa-stained smears reveals that these parasites stall at the trophozoite stage of development and that development from the ring to trophozoite stage is not inhibited (Figure 5.7, panel C).

Merozoite invasion occurs between the 40 h and 60 h time points and consequently there is a statistically significant increase in parasitaemia in NR IgG treated cultures between these two time points. As anti-MSP3.3C IgG treated parasites have at this stage not developed beyond the trophozoite stage of the previous cycle (Figure 5.7, panel C), their ability to undergo invasion is severely inhibited and this is reflected in the low RP values at 60h in Figure 5.7, panel A. At 6, 3 and 1.5 mg mL^{-1} of both anti-MSP3.3C IgG treatments, there is no statistically significant increase in parasitaemia between 40 h and 60 h.

Between 40 h and 60 h the DNA content of anti-AMA1 IgG and NR IgG treated cultures decreases statistically significantly as parasites undergo invasion and move from the schizont stage to the ring stage. In anti-MSP3.3C (6066) IgG at 6, 3 and 1.5 mg mL^{-1} there is no statistically significant decrease in DNA content (at 0.75 mg mL^{-1} there is) and the same is true for anti-MSP3.3C (6067) at 6 and 3 mg mL^{-1}. This explains the shape of the titration seen at 60 h in Figure 5.7, panel B. It also exemplifies an effect seen in all the SSGIAs, namely that the inhibitory activity of anti-MSP3.3C IgG from rabbits 6066 and 6067 is very similar, with the effect of IgG from rabbit 6067 tending to titrate out slightly quicker than that of IgG from rabbit 6066.

5.3.2. SSGIA(T)

The statistical models fitted to explain variation in parasitaemia and DNA content in the SSGIA(T) are displayed in Tables 5.12 and 5.17, respectively. For parasitaemia the effects of Ab concentration and time point within each treatment are displayed in Tables 5.13-5.16 and for DNA content in Tables 5.18-5.21. For the outcome parasitaemia the concentration of anti-AMA1 IgG ($p<0.001$), anti-MSP3.3C (6066) IgG ($p<0.001$) and anti-MSP3.3C (6067) IgG ($p<0.001$) significantly affected parasitaemia. The concentration of NR IgG had no affect on parasitaemia ($p=0.9147$). For the outcome DNA content the concentration of anti-MSP3.3C (6066) IgG ($p<0.001$) and anti-MSP3.3C (6067) IgG ($p<0.001$) significantly affected DNA content. The concentration of anti-AMA1 IgG ($p=0.1547$) and NR IgG ($p=0.1702$) did not affect DNA content.

At 40 h post invasion RP (Figure 5.8, panel A) and RDA (Figure 5.8, panel B) values in anti-MSP3.3C IgG treated cultures are ~ 1 with the exception of 6 mg mL^{-1} of Ab, where they fall slightly below 1. Hence, progression into S phase is not inhibited and the majority of parasites develop into schizonts by 40 h post invasion (Figure 5.8, panel C). Following merozoite invasion, at the 60 h and 78 h time points, RPs are substantially reduced in anti-MSP3.3C IgG treated cultures, to a similar extent as that seen with the positive anti-AMA1 control (Figure 5.8 panel A). At 6 mg mL^{-1} there is no statistically significant difference between parasitaemias at the 40 h and 60 h time points in anti-AMA1 and anti-MSP3.3C treatments, despite merozoite invasion having occurred between these two time points. This is in contrast to all other concentrations of anti-AMA1 and anti-MSP3.3C treatments, in addition to all concentrations of NR IgG, where statistically significant differences between parasitaemias detected at 40 h and 60 h were detected.

This inhibition of increase in parasitaemia between 40 h and 60 h in anti-MSP3.3C IgG treated cultures could be due to inhibition of merozoite invasion or it could be due to inhibition of intraerythrocytic schizont development. The latter is the case as exemplified by the persistence of schizonts in anti-MSP3.3C IgG treated cultures at 60 h and 78 h (Figure 5.8, panel C). At 6 mg mL-1 of either anti-MSP3.3C IgG

treatment there was no statistically significant decrease in DNA content between 40 h (where control cultures are schizonts) and 60 h (where control cultures are rings). This is in contrast to anti-AMA1 and NR IgG where there was a statistically significant decrease in DNA content between these two time points. Graphically, this effect is exemplified by RDC values substantially above 1 at the highest concentration of MSP3.3C specific IgG (Figure 5.8b). At 60 h many of these schizonts had disintegrated to the point that it was no longer possible to distinguish whether they were trophozoites or schizonts without prior knowledge of their developmental stage at the previous time point (Figure 5.10, contrast plates E and F with plates G and H). By 78 h a very high proportion of the parasites scored lacked their RBC and appeared to be extracellular (Figure 5.10, plates M and N).

It is not possible to discern from this data whether or not these stalled schizonts have undergone fewer mitotic divisions than control cultures prior to schizont rupture. RDC values fall slightly below 1 at the 40 h time point for the highest concentration of anti-MSP3.3C IgG, when control cultures were at mid-schizont stage, thus a greater difference in DNA content may have been detected if sampling had occurred just prior to schizont rupture (Figure 5.8b).

5.3.2. SSGIA(S)

The statistical models fitted to explain variation in parasitaemia and DNA content in the SSGIA(T) are displayed in Tables 5.22 and 5.26, respectively. For parasitaemia the effects of Ab concentration and timepoint within each treatment are displayed in Tables 5.23-5.55 and for DNA content in Tables 5.27-5.30. For the outcome parasitaemia the concentration of anti-AMA1 IgG ($p<0.001$), anti-MSP3.3C (6066) IgG ($p=0.0003$) and NR IgG ($p=0.0286$) significantly affected parasitaemia. The significant affect of the concentration of NR IgG, although only weakly statistically significant, is likely to be due to a slight inhibition of parasitaemia following merozoite invasion at 6 mg mL^{-1}. For the outcome DNA content the concentration of anti-MSP3.3C (6066) IgG ($p<0.001$), anti-MSP3.3C (6067) IgG ($p<0.001$) and

anti-AMA1 IgG ($p<0.001$) significantly affected DNA content. The concentration of NR IgG ($p=0.1702$) did not affect DNA content ($p=0.70781$).

The addition of anti-MSP3.3C IgG to mid-schizont stage cultures results in noticeably reduced RPs at all sampling time points (Figure 5.9a). This reduction in RP is less than that seen when anti-MSP3.3C IgG is added to mid-ring (Figure 5.7a) or mid-schizont (Figure 5.8a) stage cultures. This inhibitory effect of anti-MSP3.3C IgG is due to partial inhibition of parasite development during the schizont stage preceding the 60 h time point, as evidenced by the persistence of schizonts in anti-MSP3.3C treated cultures at this time point, which is not seen in anti-AMA1 or NR treated control cultures (Figure 5.9, panel C).

At the 88 h time points, two effects are noticeable: (i) the drop in RP values in anti-MSP3.3C IgG treated cultures becomes more substantial and effects a wider range of concentrations of the Ab (Figure 5.9, panel A) and (ii) RDC values are substantially reduced. In NR IgG and anti-AMA1 treated cultures there is a statistically significant increase in DNA content between 78 h and 88 h as parasites develop from the trophozoite stage to the schizont stage. At 6, 3 and 1.5 mg mL^{-1} of both anti-MSP3.3C IgG treatments there was no statistically significant increase in DNA content from 78 h to 88 h. Analysis of Giemsa-stained smears revealed that this was due to the inhibitory action of these antibodies blocking development beyond the trophozoite stage. Trophozoites in 78h post invasion cultures treated with anti-MSP3.3C IgG appeared to have not formed properly; they were lightly stained, wispy in appearance and frequently lacking a cytoplasm. By the final assay time point the majority of parasites scored were deformed or visible only as small, densely stained dots (Figure 5.10, contrast plates I and J with plates K and L). As for SSGIA(T), apparently extracellular parasites were observed, which may explain the drop in forward scatter of iRBCs observed by flow cytometry in cultures treated with anti-MSP3.3C IgG. Overall, the developmental stage at which anti-MSP3.3C IgG is added significantly affects relative parasitaemia at post invasion time points, with much lower relative parasitaemias observed when Ab addition occurs at ring or

trophozoite stages than at stages. The stage of Ab addition has no effect on RP values in anti-AMA1 IgG treated samples.

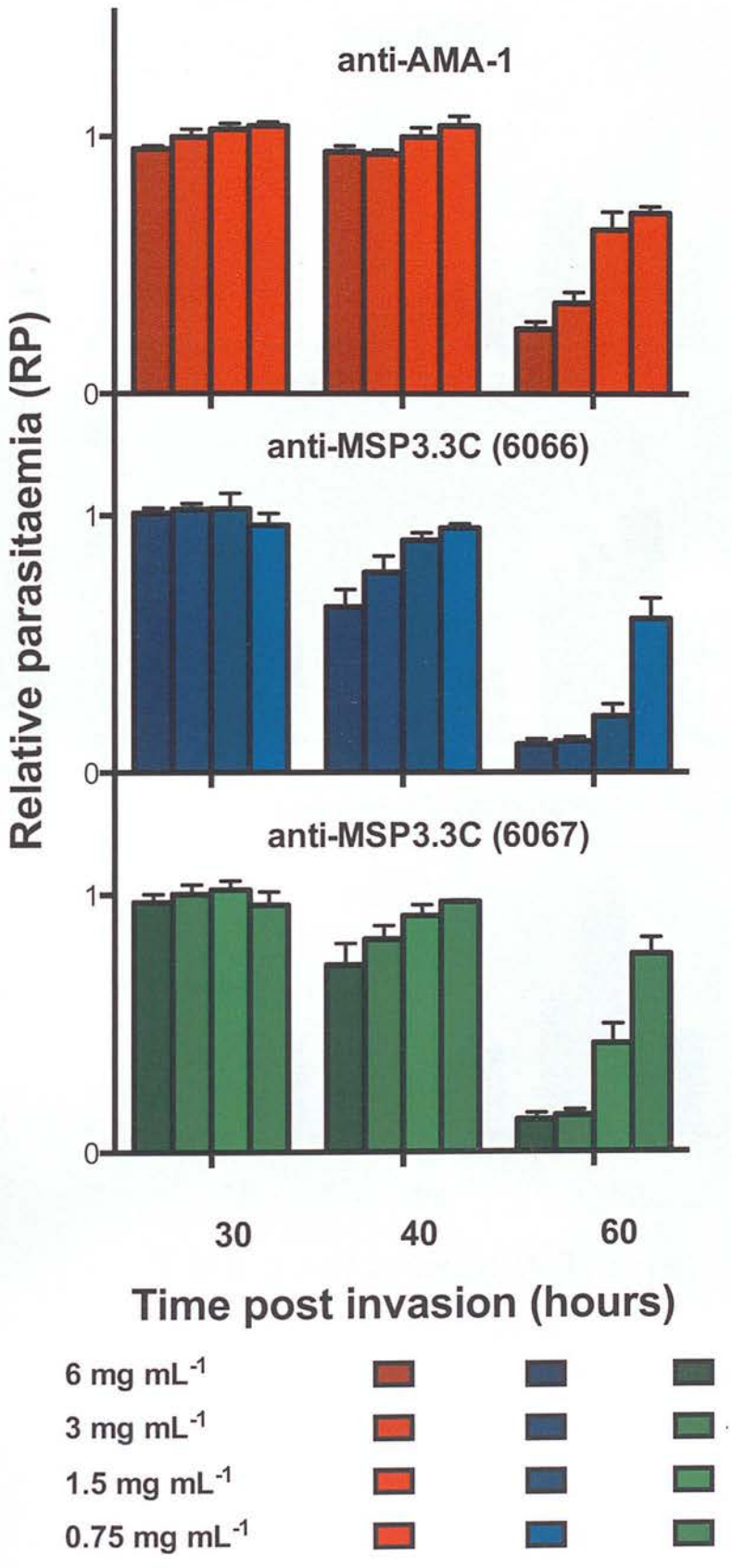
A
SSGIA(R)
anti-AMA-1
anti-MSP3.3C (6066)
anti-MSP3.3C (6067)
Relative parasitaemia (RP)
1
0
30
40
60
Time post invasion (hours)
6 mg mL-1
3 mg mL-1
1.5 mg mL-1
0.75 mg mL-1

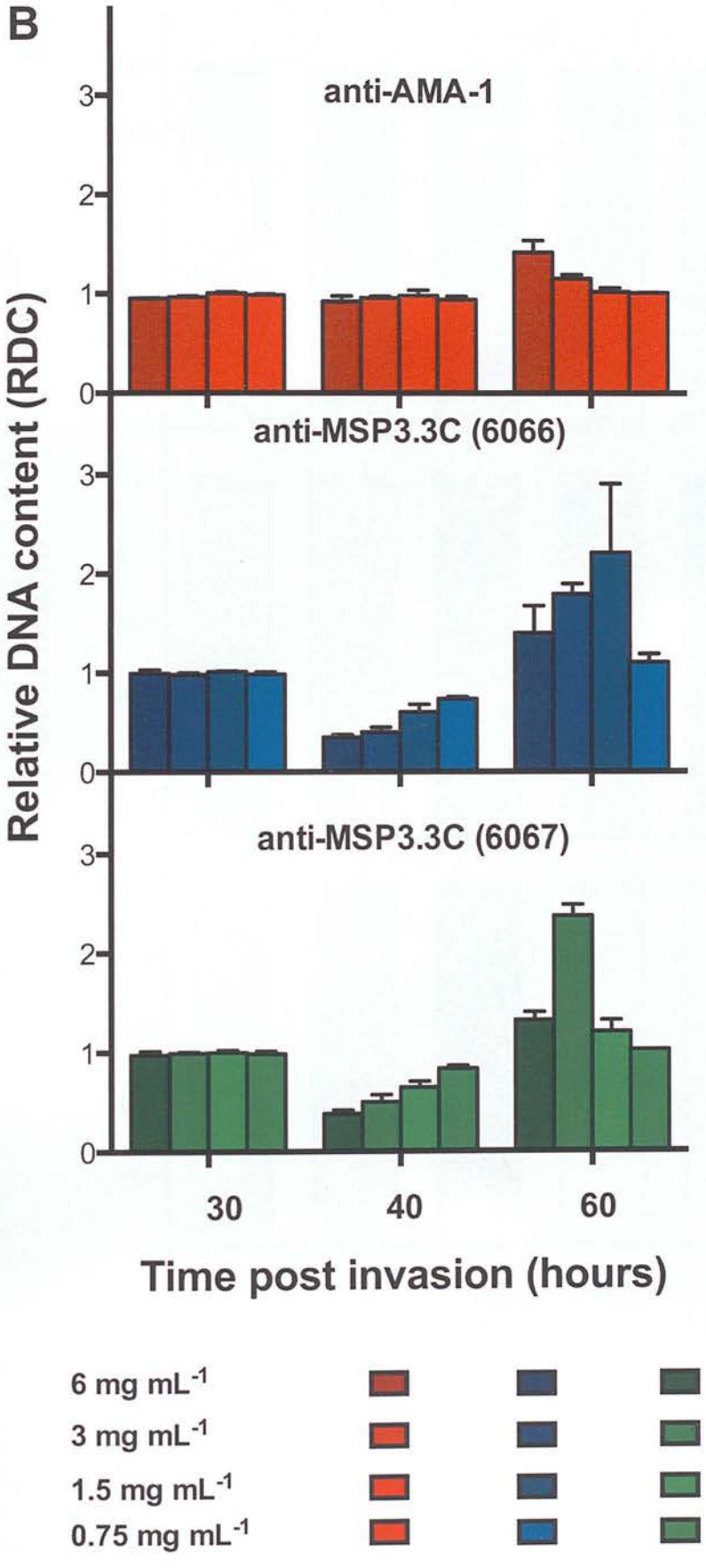
B
anti-AMA-1
anti-MSP3.3C (6066)
anti-MSP3.3C (6067)
Relative DNA content (RDC)
0
1
2
3
30
40
60
Time post invasion (hours)
6 mg mL-1
3 mg mL-1
1.5 mg mL-1
0.75 mg mL-1

schizont

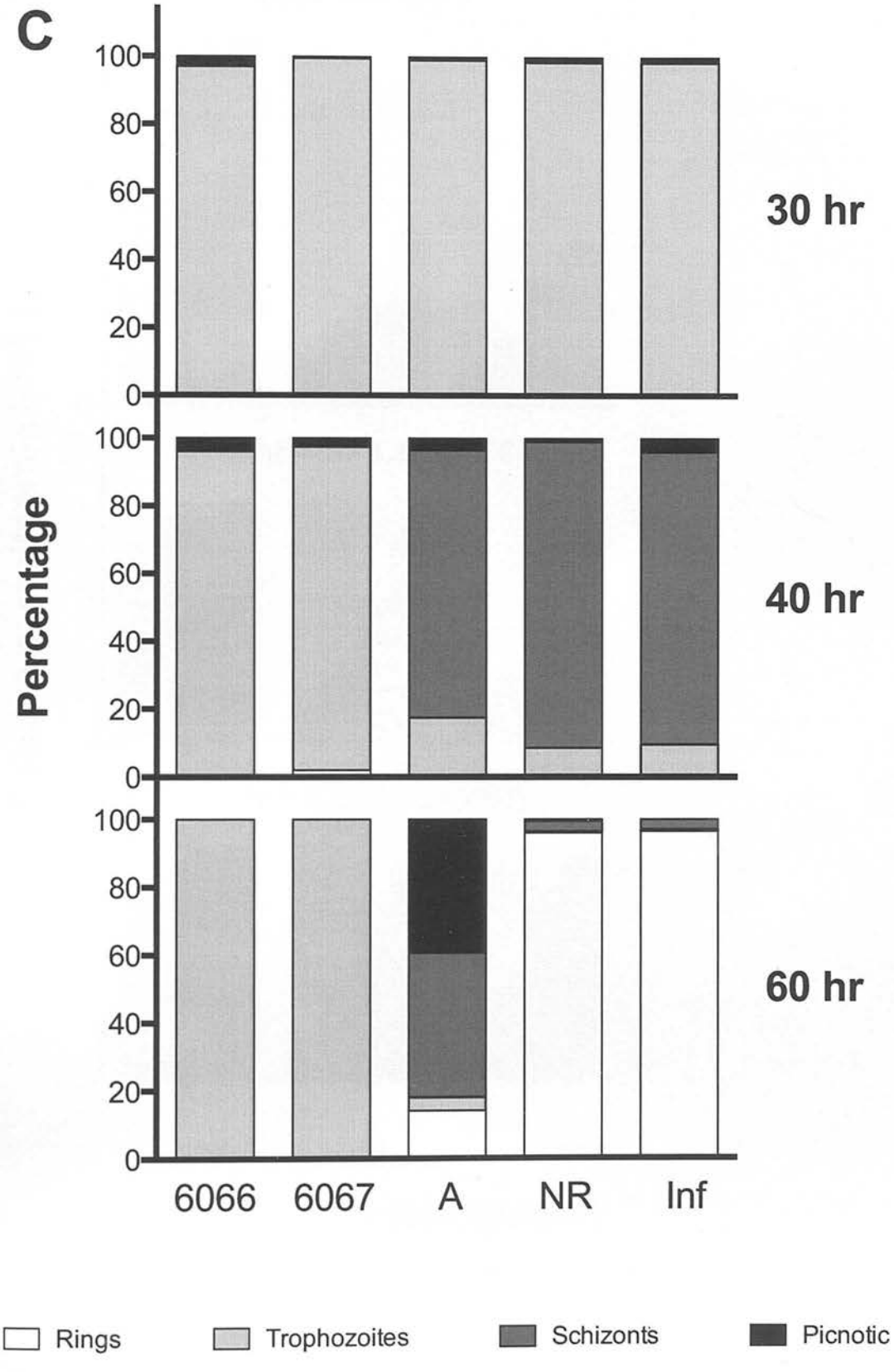
C
Percentage
100
80
60
40
20
0
30 hr
40 hr
60 hr
6066
6067
A
NR
Inf
Rings
Trophozoites
Schizonts
Picnotic

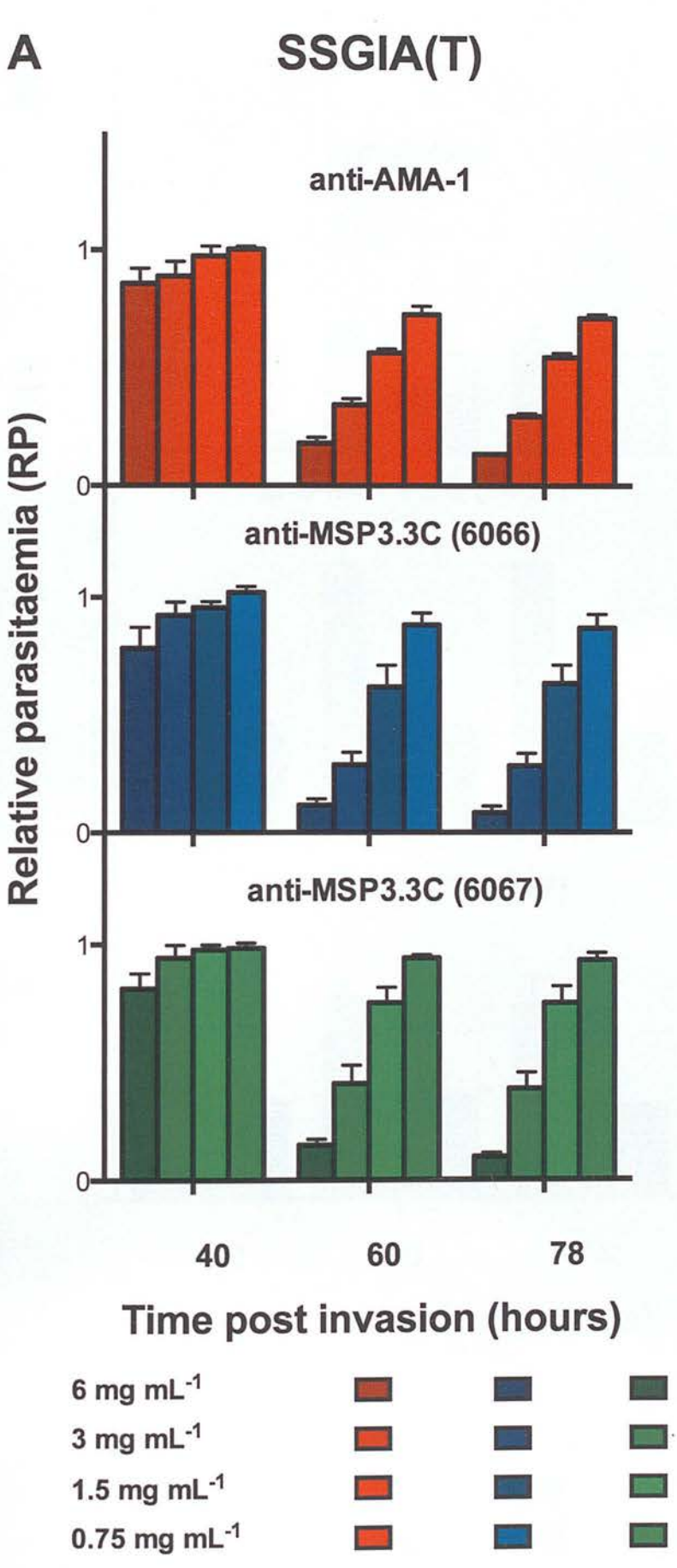
A
SSGIA(T)
anti-AMA-1
anti-MSP3.3C (6066)
anti-MSP3.3C (6067)
Relative parasitaemia (RP)
1
0
40
60
78
Time post invasion (hours)
6 mg mL-1
3 mg mL-1
1.5 mg mL-1
0.75 mg mL-1

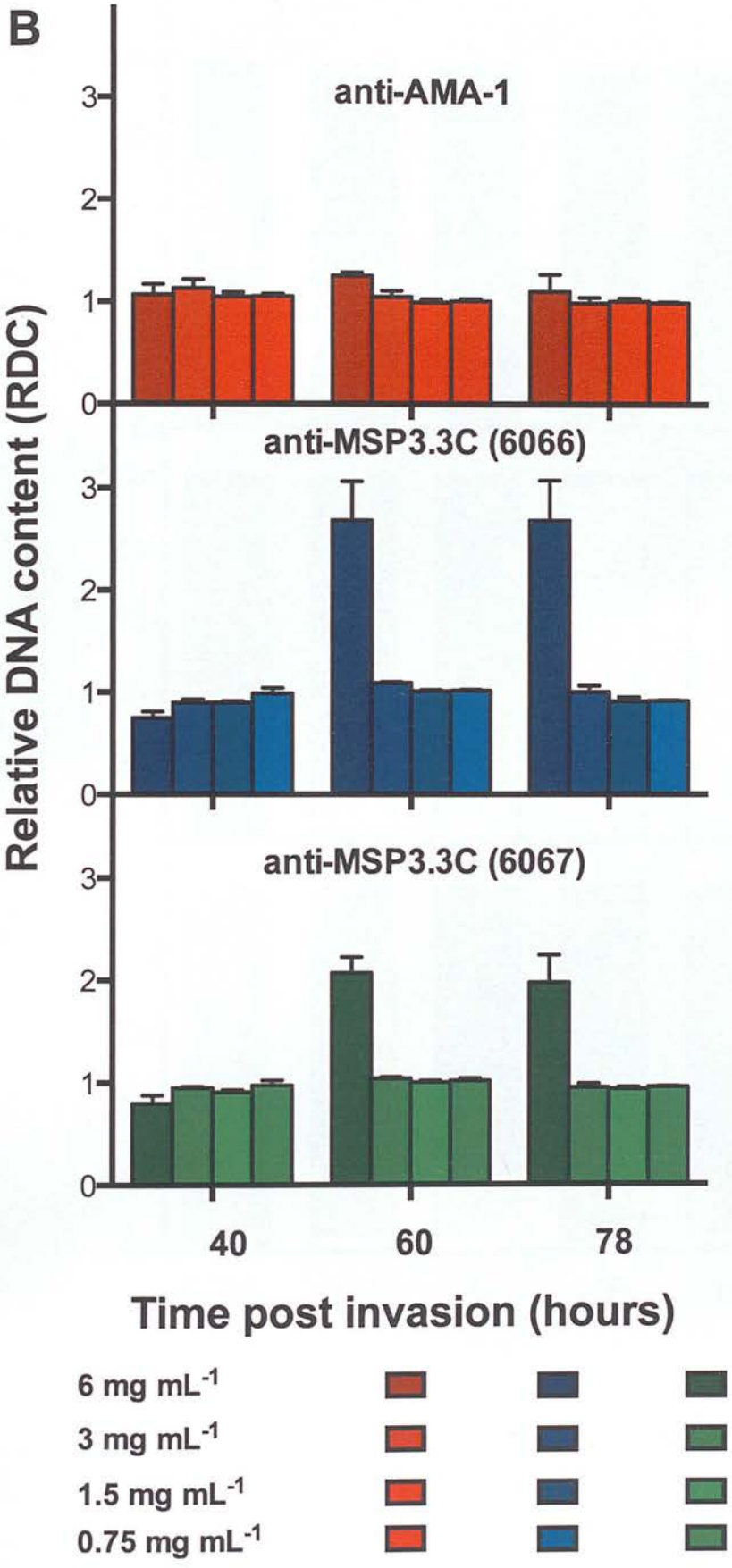
B
anti-AMA-1
anti-MSP3.3C (6066)
anti-MSP3.3C (6067)
Relative DNA content (RDC)
0
1
2
3
40
60
78
Time post invasion (hours)
6 mg mL-1
3 mg mL-1
1.5 mg mL-1
0.75 mg mL-1

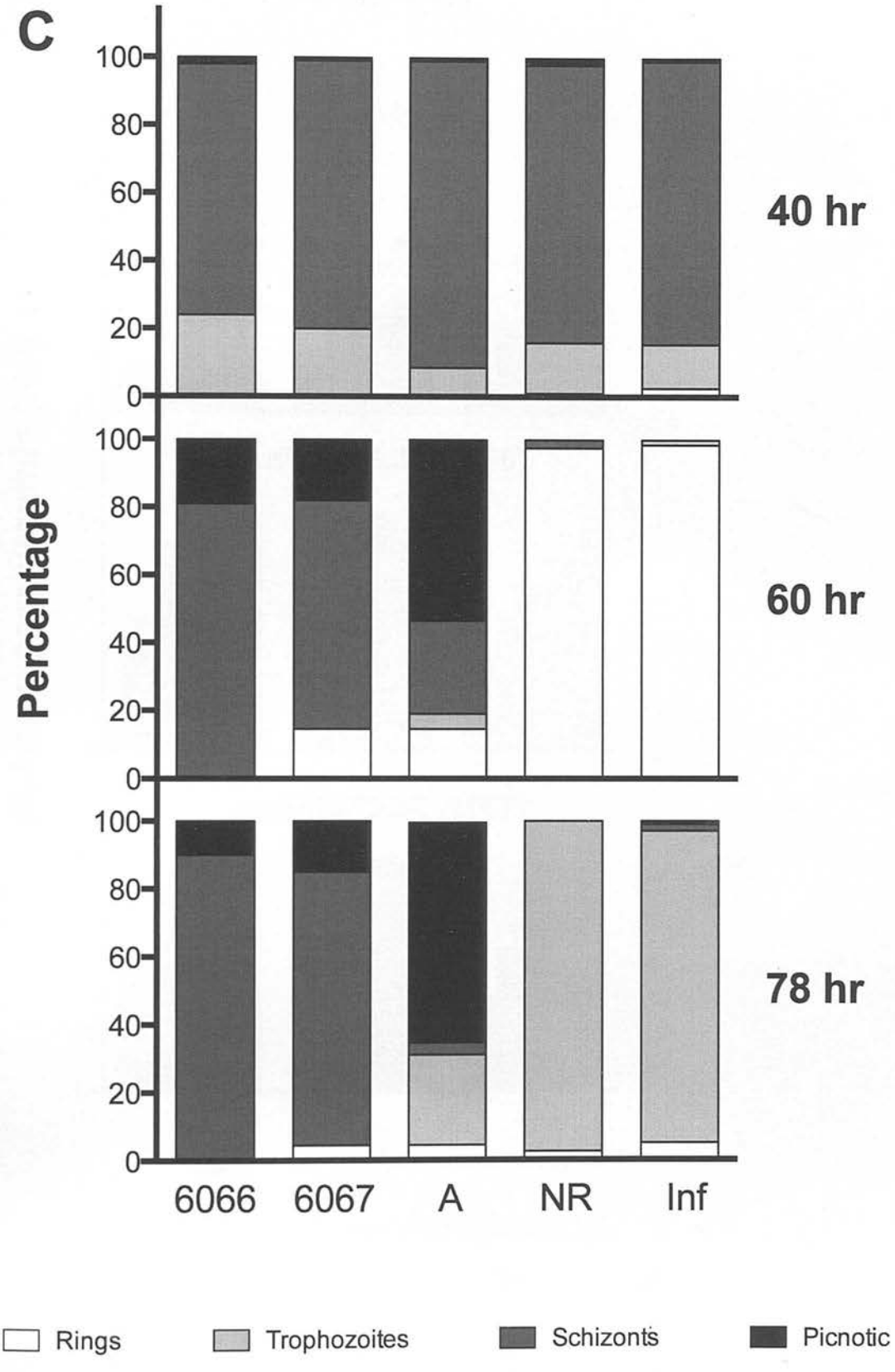
C
Percentage
100
80
60
40
20
0
40 hr
60 hr
78 hr
6066
6067
A
NR
Inf
Rings
Trophozoites
Schizonts
Picnotic

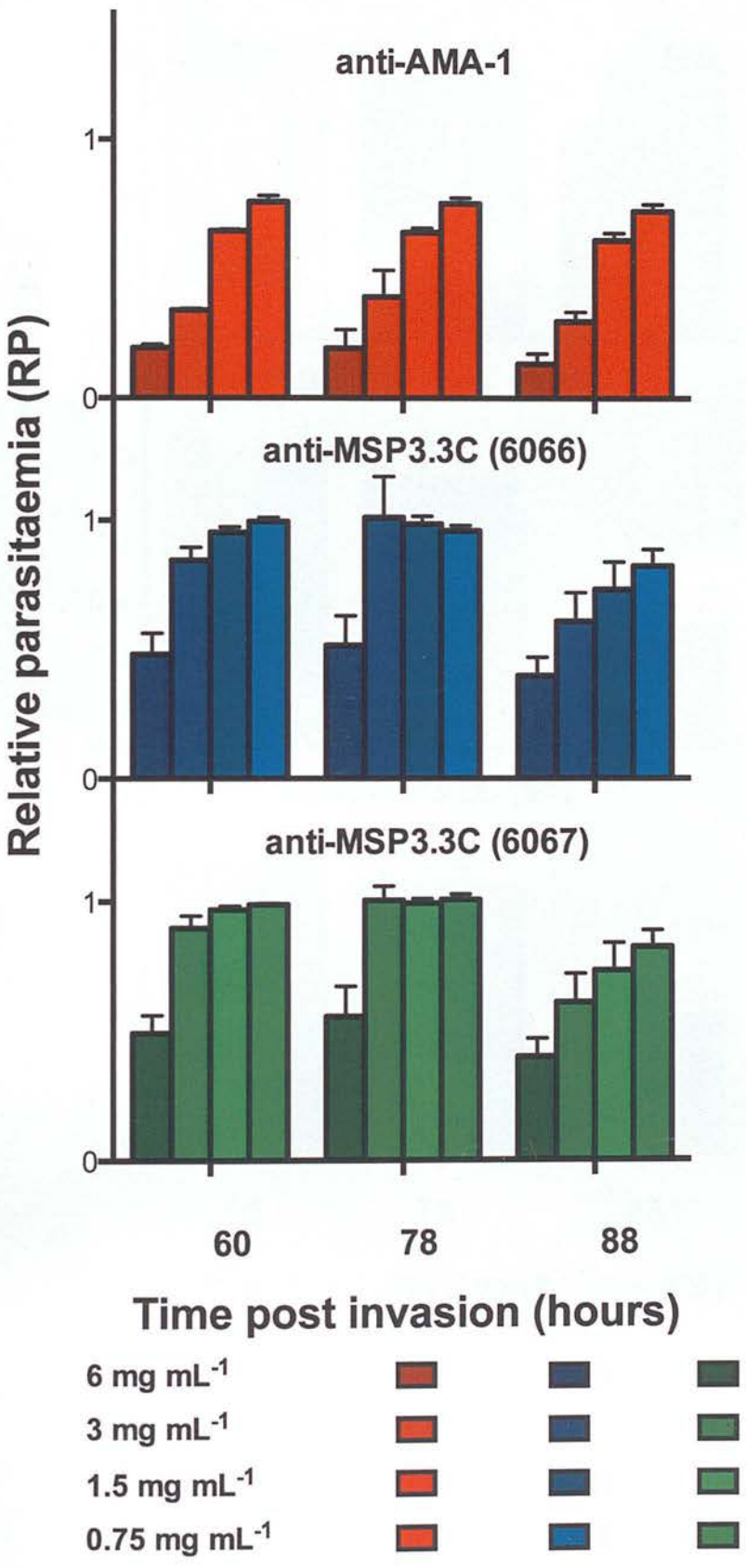
A
SSGIA(S)
anti-AMA-1
anti-MSP3.3C (6066)
anti-MSP3.3C (6067)
Relative parasitaemia (RP)
1
0
60
78
88
Time post invasion (hours)
6 mg mL-1
3 mg mL-1
1.5 mg mL-1
0.75 mg mL-1

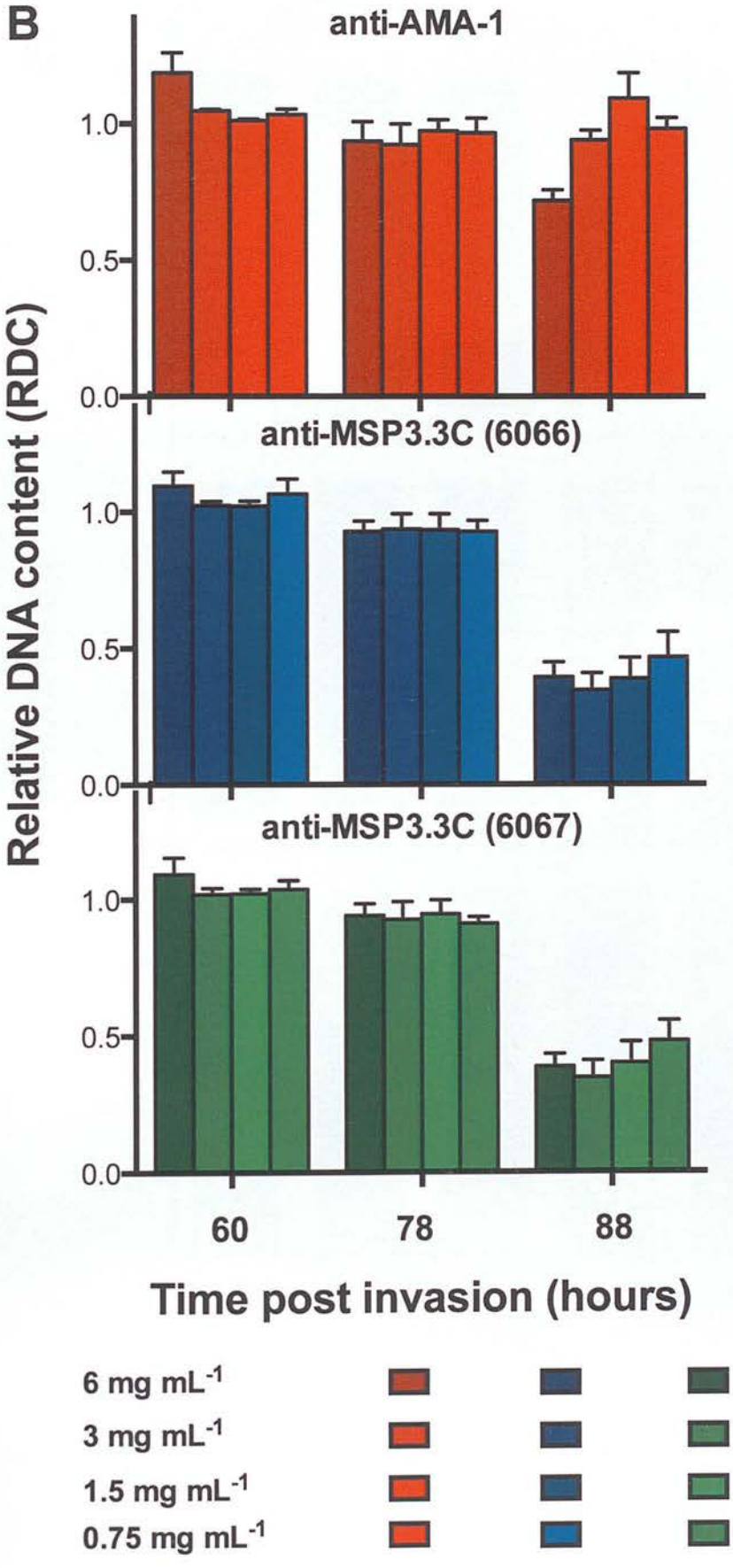
B
anti-AMA-1
anti-MSP3.3C (6066)
anti-MSP3.3C (6067)
Relative DNA content (RDC)
1.0
0.5
0.0
60
78
88
Time post invasion (hours)
6 mg mL-1
3 mg mL-1
1.5 mg mL-1
0.75 mg mL-1

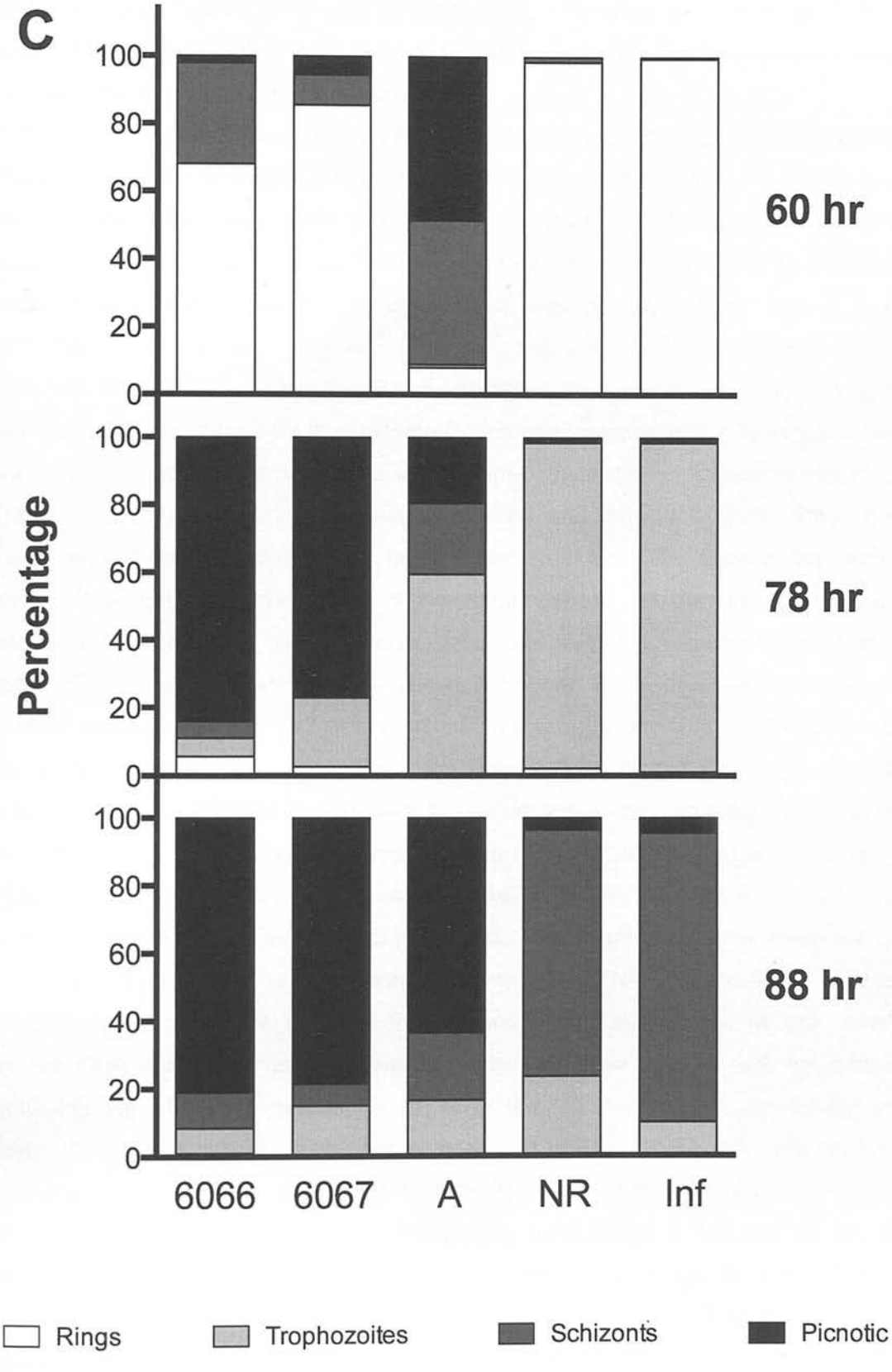
C
Percentage
100
80
60
40
20
0
60 hr
78 hr
88 hr
6066
6067
A
NR
Inf
Rings
Trophozoites
Schizonts
Picnotic

Figures 5.7-5.9 Anti-MSP3.3C IgG inhibits the *in vitro* growth of *P. falciparum* by blocking its intraerythrocytic development. The degree of this inhibition and the stage at which it occurs is dependent upon the developmental stage at which the inhibitory IgG is added.

A panels, Changes in relative parasitaemia of parasites cultured in the presence anti-MSP3.3C IgG (total IgG purified from each of two rabbits, 6066 and 6067) or a standard pool of purified rabbit α-AMA1 IgG added at different stages of parasite development; ring stage (Figure 5.7a), trophozoite stage (Figure 5.8a) or schizont stage (Figure 5.9a). Each IgG preparation was serially diluted across four concentrations; 6mg mL^{-1}, 3mg mL^{-1}, 1.5 mL^{-1} and 0.75 mL^{-1}. At the time points indicated on the graphs parasitaemia of anti-MSP3.3C IgG/anti-AMA1 IgG treated samples was determined by flow cytometry and compared to RBCs cultured in the presence of control naive rabbit IgG of the same concentration (parasitaemia = 1). Three independent experiments were performed and individual bars display the mean relative parasitaemia for IgG preparations from the three assays, with error bars indicating the standard error of the mean (SEM). **B panels,** Changes in relative DNA content of parasites cultured in the presence of anti-MSP3.3C IgG (total IgG purified from each of two rabbits, 6066 and 6067) or a standard pool of purified rabbit anti-AMA1 IgG added at different stages of parasite development; ring stage (Figure 5.7b), trophozoite stage (Figure 5.8b) or schizont stage (Figure 5.9b). Each IgG preparation was serially diluted across four concentrations; 6mg mL^{-1}, 3mg mL^{-1}, 1.5 mL^{-1} and 0.75 mL^{-1}. At the time points indicated on the graphs infected RBCs were stained with Hoechst 33342 and their DNA content measured by flow cytometry and compared to parasitised RBCs cultured in the presence of control naive rabbit IgG of the same concentration (DNA content = 1). Three independent experiments were performed and individual bars show the mean relative DNA content for IgG preparations from the three assays, with error bars indicating the SEM. **C panels,** Changes in the intraerythrocytic developmental stage of parasites cultured in the presence of anti-MSP3.3C IgG (total IgG purified from each of two rabbits, 6066 and 6067), NR IgG, a standard pool of purified rabbit anti-AMA1 IgG (A) or no IgG (Inf). Treatments were added at different stages of parasite development; ring stage (Figure 5.7c), trophozoite stage (Figure 5.8c) or schizont stage (Figure 5.9c). At the time points indicated on the graph, giemsa-stained smears were prepared and the proportion of ring (white), trophozoite (light grey), schizont (dark grey) and pycnotic (black) parasites enumerated by light

microscopy. Percentages shown are the mean of two independent wells from one of the three independent experiments shown in panels A and B above.

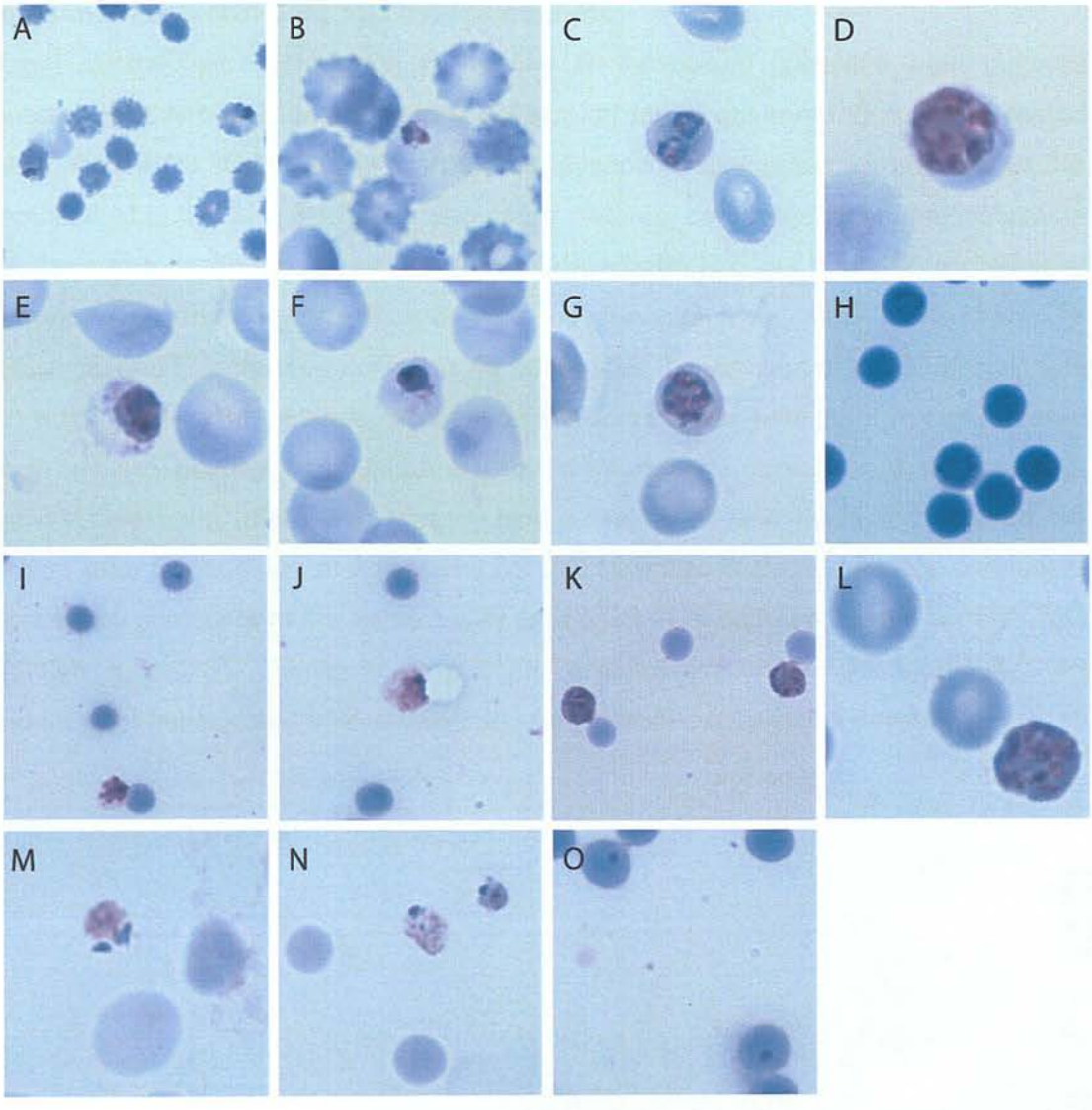
A
B
C
D
E
F
G
H
I
J
K
L
M
N
O

Figure 5.10 An abundance of pycnotic and abnormally developing forms is present in anti-MSP3.3C IgG treated cultures.

Light microscopic comparison of healthy *P. falciparum* parasites from cultures treated with NR IgG, or abnormally developing forms observed in cultures treated with anti-MSP3.3C IgG. Plates A and B: pycnotic trophozoites 28 hours after the addition of anti-MSP3.3C IgG to ring stage cultures, compared to healthy schizonts at the same assay time point in cultures treated with NR IgG (plate D) and healthy trophozoites treated with NR IgG from the previous assay time point (plate C). Plates E and F, deformed schizonts 40 hours after the addition of anti-MSP3.3C IgG to trophozoite stage cultures, whereas at the same assay time point NR IgG treated cultures are healthy rings (plate H) and were healthy schizonts at the previous assay time point (plate G). Plates I and J, deformed and pycnotic parasites, 48 hours after the addition of anti-MSP3.3C IgG to schizont stage cultures, contrasted to healthy schizonts at the same assay time point from cultures treated with NR IgG (plates K and L). Plates M-O, pycnotic and extracellular/collapsedparasites 48 hours after the addition of anti-MSP3.3C Abs to trophozoite stage cultures.

Effect	DF	f	p
Treatment	3,106	128.44	<0.001
Concentration	3,106	75.32	<0.001
Time	2,134	269.68	<0.001
Treatment*concentration	9,106	11.25	<0.001
Treatment*time	6,148	62.43	<0.001
Concentration*time	6,148	46.16	<0.001
Treatment*concentration*time	18,153	5.75	<0.001

Table 5.2 Statistical model fitted to explain variation in parasitaemia for all treatments in the SSGIA(R).

Effect	DF	f	p
Concentration	3,25	30.81	<0.001
Time	2,32.6	164.64	<0.001
Concentration*time	6,35.3	18.38	<0.001

Table 5.3 Statistical model fitted to explain variation in parasitaemia for the anti-AMA1 IgG treatment in the SSGIA(R)

Effect	DF	f	p
Concentration	3,16.6	0.17	0.9292
Time	2,36.1	2777.40	<0.001

Table 5.4 Statistical model fitted to explain variation in parasitaemia for the NR IgG treatment in the SSGIA(R)

Effect	DF	f	p
Concentration	3,25.8	35.78	<0.001
Time	2,34	3.11	0.0574
Concentration*time	6,36.6	19.33	<0.001

Table 5.5 Statistical model fitted to explain variation in parasitaemia for the anti-MSP3.3C IgG (6066) treatment in the SSGIA(R)

.

Effect	DF	f	p
Concentration	3,23.3	39.57	<0.001
Time	2,33.5	14.36	<0.001
Concentration*time	6,36	21.86	<0.001

Table 5.6 Statistical model fitted to explain variation in parasitaemia for the anti-MSP3.3C IgG (6067) treatment in the SSGIA(R).

Effect	DF	f	p
Treatment	3,153	5.55	0.0012
Concentration	3,153	9.06	<0.001
Time	2,139	122.53	<0.001
Treatment*concentration	9,153	3.01	0.0025
Treatment*time	6,154	16.55	<0.001
Concentration*time	6,154	7.52	<0.001
Treatment*concentration*time	18,161	1.99	0.0127

Table 5.7 Statistical model fitted to explain variation in parasite DNA content for all treatments in the SSGIA(R).

Effect	DF	f	p
Concentration	3,21.3	0.08	0.9727
Time	2,37.9	86.66	<0.001
Concentration*time			NS

Table 5.8 Statistical model fitted to explain variation in parasite DNA content for the anti-AMA1 IgG treatment in the SSGIA(R).

Effect	DF	f	p
Concentration	3,17.8	0.37	0.7740
Time	2,36.8	163.91	<0.001
Concentration*time			NS

Table 5.9 Statistical model fitted to explain variation in parasite DNA content for the NR IgG treatment in the SSGIA(R).

Effect	DF	f	p
Concentration	3,51.4	9.61	<0.001
Time	2,34.6	1.34	0.2758
Concentration*time	6,38	3.95	0.0037

Table 5.10 Statistical model fitted to explain variation in parasite DNA content for the anti-MSP3.3C IgG (6066) treatment in the SSGIA(R).

Effect	DF	f	p
Concentration	3,38.1	7.03	0.0007
Time	2,34.4	7.08	0.0027
Concentration*time	6,37.5	6.20	<0.001

Table 5.11 Statistical model fitted to explain variation in parasite DNA content for the anti-MSP3.3C IgG (6067) treatment in the SSGIA(R).

Effect	DF	f	p
Treatment	3,89.4	262.69	<0.001
Concentration	3,89.4	465.43	<0.001
Time	2,163	2791.44	<0.001
Treatment*concentration	9,89.4	57.87	<0.001
Treatment*time	6,167	106.26	<0.001
Concentration*time	6,167	220.95	<0.001

Table 5.12 Statistical model fitted to explain variation in parasitaemia for all treatments in the SSGIA(T).

Effect	DF	f	p
Concentration	3,28	336.06	<0.001
Time	2,43.2	16.49	<0.001
Concentration*time	6,44.5	75.15	<0.001

Table 5.13 Statistical model fitted to explain variation in parasitaemia for the anti-AMA1 IgG treatment in the SSGIA(T).

Effect	DF	f	p
Concentration	3,24.4	0.17	<0.9147
Time	2,39.9	2777.40	<0.001

Table 5.14 Statistical model fitted to explain variation in parasitaemia for the NR IgG treatment in the SSGIA(T).

Effect	DF	f	p
Concentration	3,16.8	189.26	<0.001
Time	2,36.7	306.63	<0.001
Concentration*time	6,37.3	94.80	<0.001

Table 5.15 Statistical model fitted to explain variation in parasitaemia for the anti-MSP3.3C IgG (6066) treatment in the SSGIA(T).

Effect	DF	f	p
Concentration	3,22.4	308.84	<0.001
Time	2,41.7	651.50	<0.001
Concentration*time	6,42.4	123.64	<0.001

Table 5.16 Statistical model fitted to explain variation in parasitaemia for the anti-MSP3.3C IgG (6067) treatment in the SSGIA(T).

Effect	DF	f	p
Treatment	3,88	9.96	<0.001
Concentration	3,88	59.79	<0.001
Time	2,149	2130.81	<0.001
Treatment*concentration	9,88	21.27	<0.001
Treatment*time	6,158	20.33	<0.001
Concentration*time	6,158	45.85	<0.001
Treatment*concentration*time	18,160	11.38	<0.001

Table 5.17 Statistical model fitted to explain variation in parasite DNA content for all treatments in the SSGIA(T).

Effect	DF	f	p
Concentration	3,22.9	1.92	0.1547
Time	2,38.5	703.84	<0.001
Concentration*time			NS

Table 5.18 Statistical model fitted to explain variation in parasite DNA content for the anti-AMA1 IgG treatment in the SSGIA(T).

Effect	DF	f	p
Concentration	3,25	1.81	0.1702
Time	2,39.1	1114.82	<0.001
Concentration*time			NS

Table 5.19 Statistical model fitted to explain variation in parasite DNA content for the NR IgG treatment in the SSGIA(T).

Effect	DF	f	p
Concentration	3,20.2	43.9	<0.001
Time	2,39.5	301.42	<0.001
Concentration*time	6,40.3	46.19	<0.001

Table 5.20 Statistical model fitted to explain variation in parasite DNA content for the anti-MSP3.3C IgG (6066) treatment in the SSGIA(T).

Effect	DF	f	p
Concentration	3,21.6	46.21	<0.001
Time	2,36.4	419.01	<0.001
Concentration*time	6,38.3	27.38	<0.001

Table 5.21 Statistical model fitted to explain variation in parasite DNA content for the anti-MSP3.3C IgG (6067) treatment in the SSGIA(T).

Effect	DF	f	p
Treatment	3,78	33.35	<0.001
Concentration	3,78	25.80	<0.001
Time	2,122	71.37	<0.001
Treatment*concentration	9,78	3.27	0.0020
Treatment*time	6,145	15.38	<0.001

Table 5.22 Statistical model fitted to explain variation in parasitaemia for all treatments in the SSGIA(S).

Effect	DF	f	p
Concentration	3,18	17.12	<0.001
Time	2,29.6	20.85	<0.001

Table 5.23 Statistical model fitted to explain variation in parasitaemia for the anti-AMA1 IgG treatment in the SSGIA(S).

Effect	DF	f	p
Concentration	3,15.9	3.92	0.0286
Time	2,34.6	36.74	<0.001

Table 5.24 Statistical model fitted to explain variation in parasitaemia for the NR IgG treatment in the SSGIA(S).

Effect	DF	f	p
Concentration	3,18	10.77	0.0003
Time	2,29.8	76.72	<0.001

Table 5.25 Statistical model fitted to explain variation in parasitaemia for the anti-MSP3.3C IgG (6066) treatment in the SSGIA(S).

Effect	DF	f	p
Treatment	3,78	303.84	<0.001
Concentration	3,78	17.46	<0.001
Time	2,178	374.78	<0.001
Treatment*concentration	9,78	2.75	0.0076
Treatment*time	6,178	86.12	<0.001
Concentration*time	6,178	8.45	<0.001
Treatment*concentration*time			NS

Table 5.26 Statistical model fitted to explain variation in parasite DNA content for all treatments in the SSGIA(S).

Effect	DF	f	p
Concentration	3,18	13.11	<0.001
Time	2,40	139.10	<0.001
Concentration*time	6,40	3.08	0.0141

Table 5.26 Statistical model fitted to explain variation in parasite DNA content for the anti-AMA1 IgG treatment in the SSGIA(S).

Effect	DF	f	p
Concentration	3,18	2.68	0.70781
Time	2,46	249.34	<0.001
Concentration*time			NS

Table 5.27 Statistical model fitted to explain variation in parasite DNA content for the NR IgG treatment in the SSGIA(S).

Effect	DF	f	p
Concentration	3,18	14.55	<0.001
Time	2,40	16.69	<0.001
Concentration*time	6,40	15.20	<0.001

Table 5.28 Statistical model fitted to explain variation in parasite DNA content for the anti-MSP3.3C IgG (6066) treatment in the SSGIA(S).

Effect	DF	f	p
Concentration	3,18	27.66	<0.001
Time	2,40	19.99	<0.001
Concentration*time	6,40	17.30	<0.001

Table 5.29 Statistical model fitted to explain variation in parasite DNA content for the anti-MSP3.3C IgG (6067) treatment in the SSGIA(S).

5.3.3 MSP3.3 expression

The SSGIA results demonstrated that *P. falciparum* is only susceptible to growth inhibition by anti-MSP3.3C Abs over a specific time window of its development within the host erythrocyte. Thus ascertaining where MSP3.3 is located at the different stages of the erythrocytic cycle may provide some insight into how anti-MSP3.3C Abs inhibit parasite development.

The subcellular localisation of MSP3.3 at each stage of the erythrocytic cycle was determined by IFA; parasites were probed with MSP3.3C-specific, affinity purified IgG and the mouse mAb 7.7, which recognises the PVM antigen EXP-2. MSP3.3 is expressed in the intraerythrocytic ring, trophozoite and schizont stages, and on free merozoites (Figure 5.11). IFAs of young trophozoite stages revealed that MSP3.3 is located outside of the PV, in the erythrocyte cytoplasm (Figure 5.11, 2nd column of rows 3 and 4). This was highly surprising given that up until this point MSP3.3 was thought to only localise to the merozoite surface. The identification of this novel MSP3.3 location was made possible by the examination of young trophozoite stages, which occupy a small area of the RBC and thus MSP3.3 export is visible. By the schizont stage, the parasite occupies the majority of the RBC cytoplasm and the exported MSP3.3 is no longer visible (Figure 5.11, 3rd column of rows 3 and 4). A short peptide sequence, known as the *Plasmodium* export element (PEXEL), is frequently found in parasite proteins that are exported outside of the PV (Haase and de Koning-Ward, 2010). A search of the MSP3.3 protein sequence revealed a PEXEL motif from amino acid positions 19-23 (Figure 5.1) and this may explain the staining pattern observed in IFAs with trophozoite stage cultures.

In order to investigate the subcellular location of MSP3.3 at a higher resolution, IFAs were repeated on trophozoite and schizont stage cultures and examined via confocal microscopy. These IFAs confirmed the localisation patterns observed in the first experiment. In young trophozoites anti-MSP3.3 staining occurs in a particulate pattern outside of the PVM, in the RBC cytoplasm (Figure 5.12a). In mature schizonts, the anti-MSP3.3 staining pattern is consistent with a merozoite surface

location and appears to co-localise with anti-EXP2 staining at some areas of the merozoite surface, as indicated by the partial overlap of red and green (yellow staining, Figure 5.12b, panels in the 6th column). This partial co-localisation may result from the punctate staining pattern of EXP-2 (Figure 5.12 panels A and B, 2nd column).

For all IFAs the following controls were carried out: (i) single stain slides to check that EXP-2 and MSP3.3 single stain patterns were the same as that on double stain slides and (ii) parasites were probed with secondary Abs alone in order to confirm their specificity.

5.3.4 IgG uptake

The observation that MSP3.3C specific Abs can inhibit intraerythrocytic parasite development in the absence of merozoite invasion, for example as seen during the SSGIA(R) assay, indicates that these Abs may be able to access the intraerythrocytic parasite post invasion. To test this hypothesis ring stage parasites were incubated with MSP3.3C specific, affinity purified rabbit IgG or NR IgG and evaluated by fluorescence microscopy for the presence of internalised IgG. At 30h (Figure 5.13, panels in column 1, rows 3 and 4) 40h (Figure 5.13, panels in column 2, rows 3 and 4) and 60h post invasion (Figure 5.13, panels in column 3, rows 3 and 4), MSP3.3 specific IgG was detected within trophozoite, schizont and ring infected RBCs, respectively. The panels in the 5th row of Figure 5.13 display merged images of DAPI, anti-EXP-2 and anti-NR IgG staining in NR IgG treated samples. NR IgG was not dected within trophozoite, schizont or ring infected RBCs.

In order to investigate this IgG uptake at higher resolution, a similar experiment was performed using confocal microscopy. In this experiment anti-AMA1 IgG was included as an experimental treatment to determine whether Abs recognising other target antigens are also able to access the intraerythrocytic parasite post invasion. Anti-AMA1 IgG was detected in schizont iRBCs 40h post invasion (Figure 5.14b, panels in the 2nd row of columns 3 and 4) and MSP3.3C-specific IgG was detected in

trophozoite and schizont iRBCs 30h (Figure 5.14a, 1st row of columns 3 and 4) and 40h post invasion (Figure 5.14b, 1st row of columns 3 and 4), respectively. High background staining in some NR IgG treated samples (Figure 5.14b, 4th row, columns 3 and 4) meant that it was not possible to define whether or not NR IgG was located inside iRBCs in this experiment, however, no staining colocalising with iRBCs was above background and no specific staining pattern was observed in these samples.

5.3.5 JC-1 assays

The ability of Abs to disrupt the intraerythrocytic development of *P. falciparum* and cause deterioration of the parasite was first noted by Jensen (Jensen et al., 1982). These "crisis forms" have since been observed in cultures treated with Abs specific to MSP-1 (Arnot et al., 2008; Woehlbier et al., 2006), Pf332 (Ahlborg et al., 1996) and MSP3.3 (Dhanasarnsombut). To date, the fate of these Ig-induced crisis forms has not been investigated. Similar "crisis forms", observed in cultures exposed to antimalarial drugs (Ch'ng et al., 2010; Meslin et al., 2007), febrile temperatures (Oakley et al., 2007) and steroids (López et al., 2010), have been shown to be undergoing parasite death. It therefore follows that the unhealthy forms observed in response to anti-MSP3.3C IgG treatment may similarly be undergoing parasite death.

To explore this hypothesis, the lipophilic dye JC-1 was used to determine if any loss of mitochondrial membrane potential (MMP), a marker of parasite death, was occurring in cultures treated with anti-MSP3.3C IgG. In healthy cells, JC-1 exists in two different forms; the negative charge across the mitochondrial membrane enables the dye to accumulate as aggregates in the mitochondrial matrix, which emit a red fluorescence, whereas in the cell cytoplasm JC-1 exists as a monomer, which emits a green fluorescence. During parasite death, pores form in the mitochondrion, leading

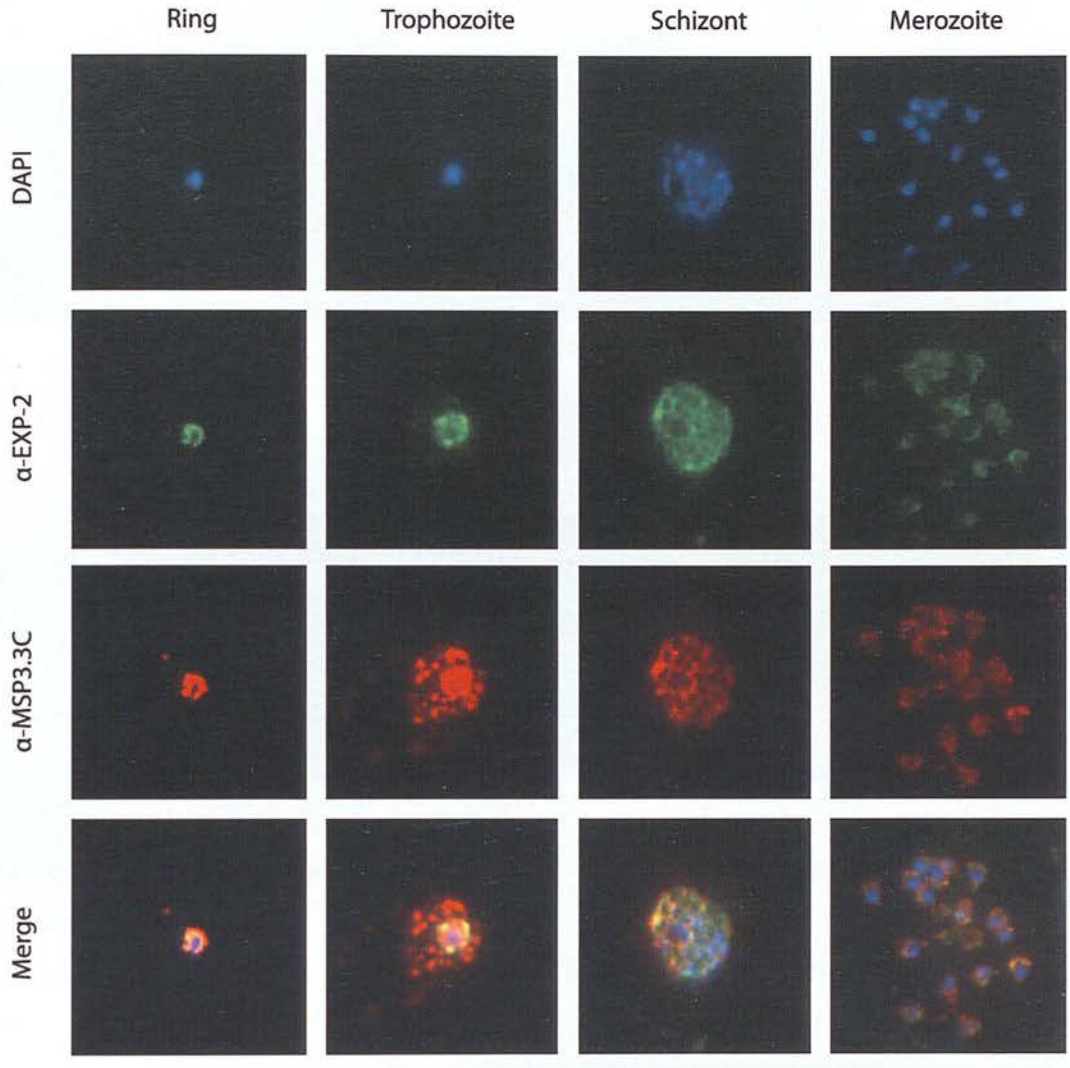

Figure 5.11 MSP3.3 is expressed in blood stage parasites and exported outside of the parasitophorous vacuole.

Representative IFA photomicrographs of rings (1st column), trophozoites (2nd column), schizonts (3rd column) and free merozoites (4th column) probed with MSP3.3C specific, affinity purified rabbit IgG (red) and the anti-EXP-2 mouse mAb 7.7 (green), which served as a marker for the PVM of the intracellular parasite. Nuclear staining (DAPI) is whosn in blue. Single channels and a merged image are shown for each stage.

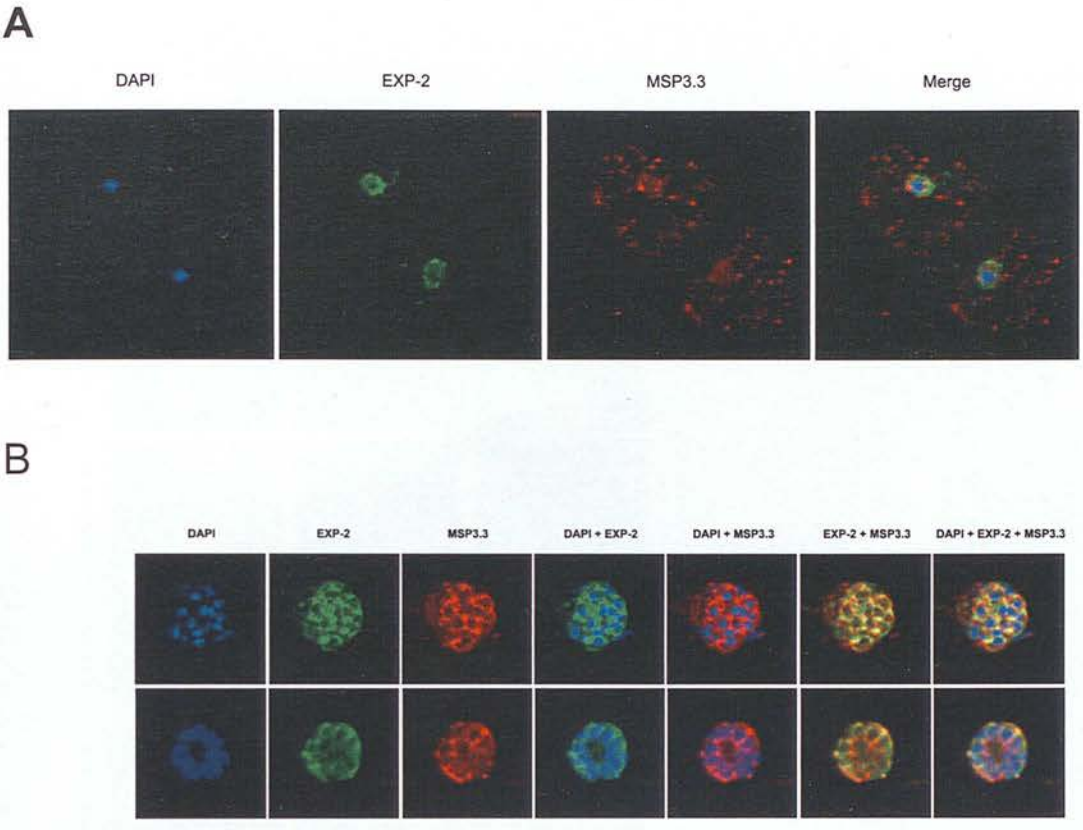

Figure 5.12 Confocal microscopy images of MSP3.3C staining in trophozoites and schizonts.

Representative confocal microscopy images of trophozoites (panel A) and schizonts (panel B) probed with MSP3.3C specific, affinity purified IgG (red) and the anti-EXP-2 mouse mAb 7.7 (green), which marks the PVM of the intraerythrocytic parasite. Parasite nuclei were visualised with DAPI (blue). Single channels and merged images are displayed.

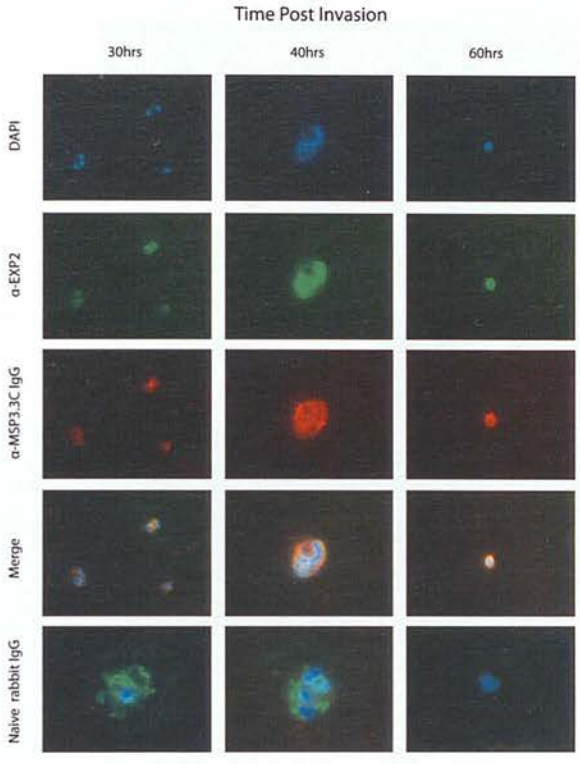

Figure 5.13 MSP3.3C specific IgG enters the iRBC post invasion.

MSP3.3C specific, affinity purified rabbit IgG or NR IgG was added to synchronous ring stage cultures 12 hours post invasion. At 30h, 40h and 60h post invasion IFA slides were prepared from treatment wells. Parasites were probed with the anti-EXP-2 mouse mAb 7.7 and DAPI and visualised by fluorescence microscopy. Representative images from anti-MSP3.3C IgG treated cultures of single channel DAPI (first row), FITC (anti-EXP2, second row), Alexa 568 (anti-MSP3.3, third row) fluorescence, in addition to merged images from all three channels (fourth row) at 30h (1st column), 40h (2nd column) and 60h (3rd column) post invasion. In the fifth row a representative merged image of DAPI, FITC (anti-EXP2) and Alexa 568 (anti-MSP3.3C) at 30h (1st column), 40h (2nd column) and 60h (3rd column) is displayed. Anti-MSP3.3 IgG but not NR IgG could be detected inside iRBCs 30 h, 40 h and 60 h post invasion.

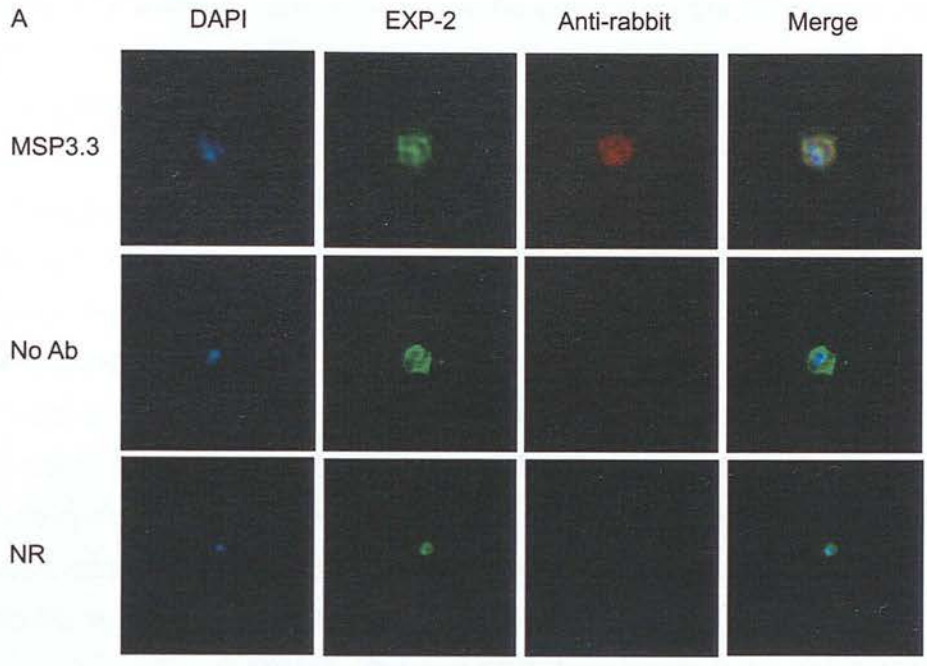
A
DAPI
EXP-2
Anti-rabbit
Merge
MSP3.3
No Ab
NR

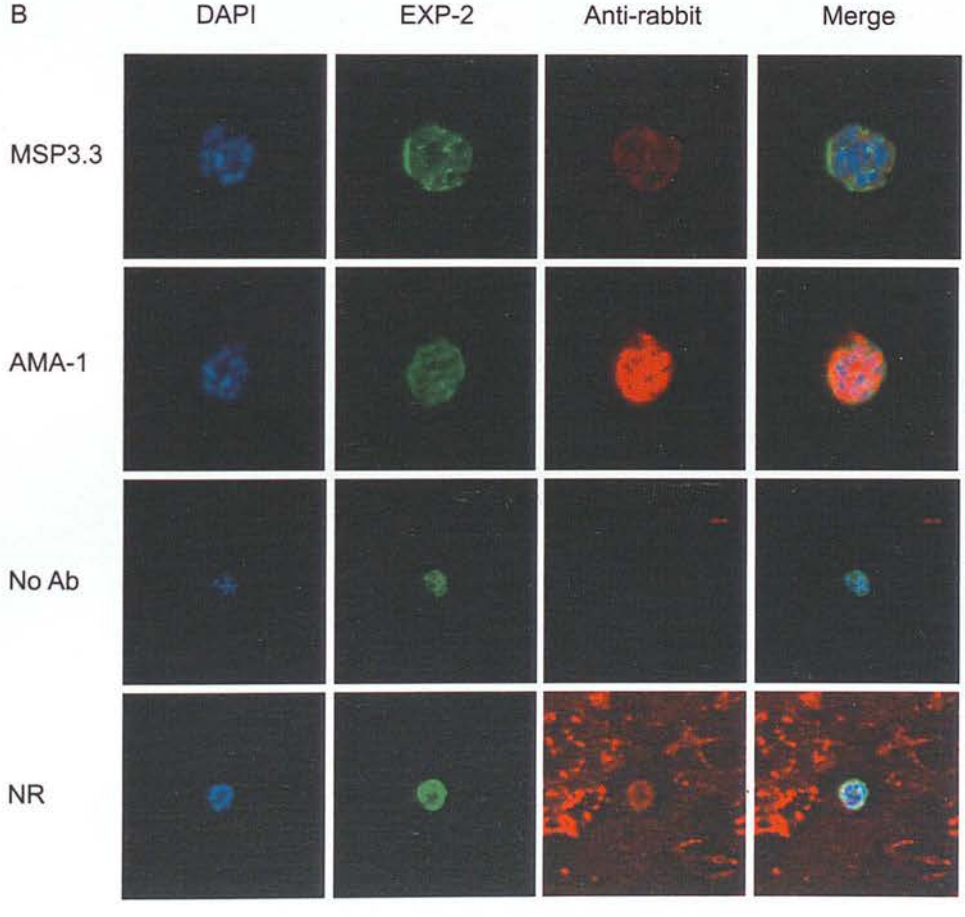
B
DAPI
EXP-2
Anti-rabbit
Merge
MSP3.3
AMA-1
No Ab
NR

Figure 5.14 MSP3.3C and AMA1 specific IgG enters the iRBC post invasion.
Confocal microscopy of *P. falciparum* treated with MSP3.3C-specific, affinity purified rabbit IgG or anti-AMA1 IgG or NR IgG added to synchronous ring stage cultures 12 h post invasion. At 30 h post invasion, MSP3.3C-specific IgG, but not NR IgG could be detected by confocal microscopy inside trophozoite iRBCs (panel A). Single channel DAPI (column 1), FITC (anti-EXP-2, column 2) and Alexa 568 (anti-mouse, column 3) fluorescence or a merged image from all 3 channels (column 4) for cultures treated with anti-MSP3.3C IgG (1st row), no antibody (2^{nd} row) or NR IgG (3^{rd} row) is displayed. 40 h post invasion MSP3.3C-specific IgG and AMA1 specific IgG could be detected by confocal microscopy inside schizont iRBCs (panel B). Single channel DAPI (column 1), FITC (anti-EXP-2, column 2) and Alexa 568 (anti-mouse, column 3) fluorescence or a merged image from all 3 channels (column 4) for cultures treated with anti-MSP3.3C IgG (1st row), anti-AMA1 (2^{nd} row), no Ab (3^{rd} row) or NR IgG is displayed. The anti-EXP-2 mouse mAb 7.7 and DAPI were used to demarcate the PVM and parasite nuclei, respectively.

to the collapse of the electrochemical gradient across the mitochondrial membrane, resulting in a loss of JC1-red fluorescence but not JC1-green fluorescence.

An initial experiment was carried out to determine: (i) that JC-1 could be used to detect MMP loss under the conditions tested, (ii) whether there was any indication that loss of parasite MMP was occurring in response to anti-MSP3.3C IgG treatment and (iii) the time of onset and duration of any such loss detected. NR IgG served as a negative control and the antimalarial drug chloroquine (CQ) as a positive control, as loss of MMP has been shown to occur when parasites undergo programmed cell death in response to CQ treatment (Ch'ng et al., 2010). The standard method used by researchers to analyse JC-1 flow data is to define JC-1 red and JC-1 green - positive gates based on an arbitrarily defined level of fluorescence intensity. In order to circumvent the subjectivity required by this method of analysis, in the analyses presented below I have calculated the ratio of JC-1 red fluorescence to JC-1 Green fluorescence for each individual infected RBC. The data are presented as the distribution of these ratios for the entire iRBC population of each sample.

In the preliminary experiment, treatments were added to highly synchronous ring stage cultures and MMP measured at three time points over the following 48h replication cycle. Eight hours after treatments had been applied (20h post invasion), loss of MMP could be detected at the highest concentration of anti-MSP3.3C IgG and in the CQ-treated positive control (Figure 5.15). By 32 h post invasion anti-MSP3.3C IgG treated parasites displayed a highly significant loss of MMP relative to controls, and this effect was dose-dependent.

Interpretation of the results at the next time point (60h post invasion), which occurs after control cultures have undergone merozoite invasion, becomes more difficult. This is because the JC1 red fluorescence to JC1 green fluorescence ratio (R:G) increases throughout the intraerythrocytic cycle of the parasite, with ring stage parasites having a significantly lower R:G that trophozoites, which in turn have a lower R:G than schizonts. Hence, at this time point "parasite stage" becomes a confounding factor making any meaningful interpretation of the results extremely

difficult. Due to this, the JC-1 assay was adapted so that sampling occurred at shorter intervals and only covered the developmental period over which parasite stage is the same in both experimental and control cultures. In this assay MSP3.3C specific IgG or NR IgG were added to highly synchronous ring stage cultures 10 h post invasion and sampling time points were immediately after assay set up (10h), 22h, 30h and 36h post invasion.

Three independent replicates of this experiment were carried out. The range of JC-1 R:G ratios were statistically significantly different between these experiments, possibly due to the fact that different voltage settings were used on the flow cytometer for each experiment. Therefore, all three experiments were not combined for statistical analysis. The general trends were the same in all three experiments and representative results from one of them are displayed in Figure 5.16.

For the 10 h post invasion time point, samples were taken immediately after treatments were applied and as expected there is no statistical significant difference between treatments ($p=0.18$). At 22 h and 36 h JC-1 R:G ratios obtained with anti-MSP3.3C IgG and NR IgG treated samples were statistically significantly different from one another ($p<0.05$ and $p<0.001$, respectively). At 30 h post invasion treatment was not a significant risk factor in the statistical model fitted to explain the data ($p=0.93$). The loss of statistical significance at this time point is likely due to the higher R:G ratios observed in the second set of anti-MSP3.3C IgG treated wells (Figure 5.16, bottom left-hand graph, box plots 5-8). MMP loss was detected for CQ and sodium azide positive control treatments, as expected.

5.3.6 DCFH-DA assays

Chapter 4 of this thesis explored the hypothesis that Abs to MSP-1_{19} are able to inhibit the intraerythrocytic growth of *P. falciparum* by carrying out ACWO inside the RBC. Given that Abs to MSP3.3C can access the intraerythrocytic parasite and inhibit the development of the parasite inside the RBC, it seemed logical to examine whether this could be occurring through activation of the ACWO pathway.

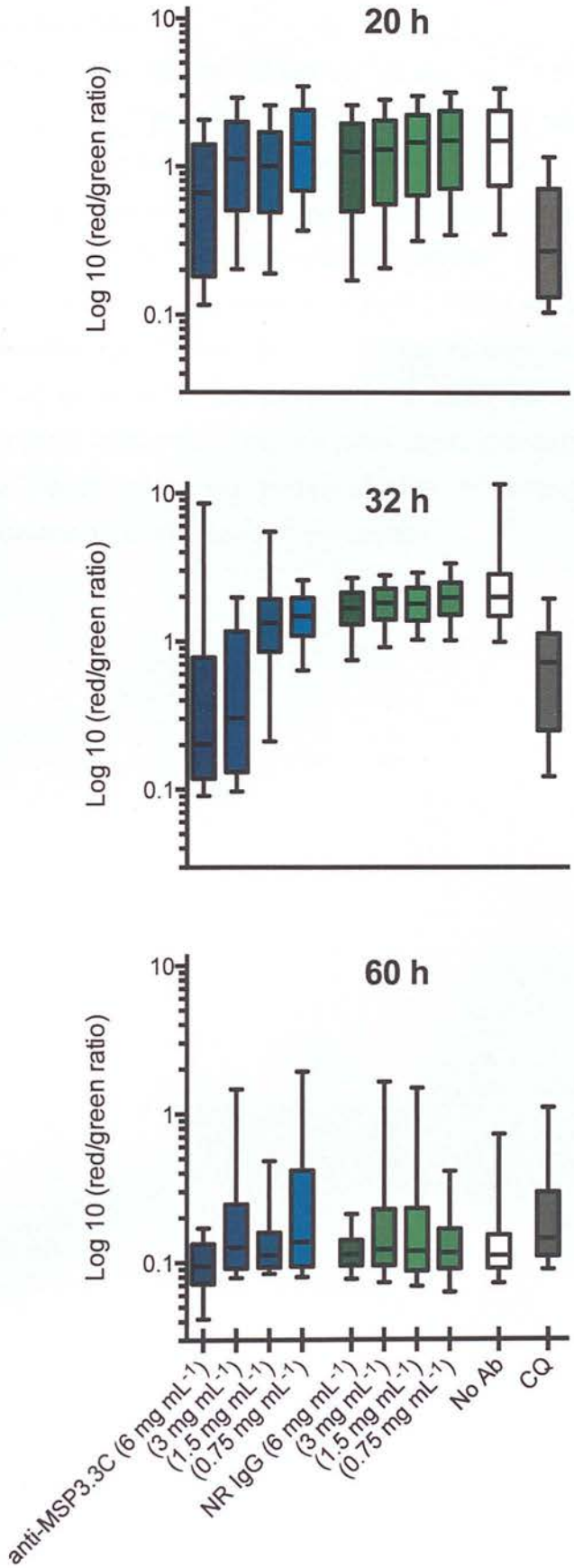
20 h
32 h
60 h
Log 10 (red/green ratio)
10
1
0.1
anti-MSP3.3C (6 mg mL-1)
(3 mg mL-1)
(1.5 mg mL-1)
(0.75 mg mL-1)
NR IgG (6 mg mL-1)
(3 mg mL-1)
(1.5 mg mL-1)
(0.75 mg mL-1)
No Ab
CQ

Figure 5.15 JC-1 red:gree ratios of iRBCs after treatment with MSP3.3C-specific IgG.

MSP3.3C specific IgG (6 mg mL^{-1}, 3 mg mL^{-1}, 1.5 mg mL^{-1}, 0.75 mg mL^{-1}), NR IgG (6 mg mL^{-1}, 3 mg mL^{-1}, 1.5 mg mL^{-1}, 0.75 mg mL^{-1}), no Ab or 30 µM chloroquine (CQ) was added to highly synchronous ring stage cultures 12 hours post invasion. 20h, 32h and 60h post invasion, samples were taken from each treatment well, stained with JC-1 and Hoechst, and Hoechst, JC-1 green and JC-1 red fluorescence measured by flow cytometry. Infected RBCs were gated on hoecsht fluorescence. Following this, the ratio of JC-1 red fluorescence to JC-1 green fluorescence of each individual infected red blood cell in each sample was calculated using the R statistical language. The box plots depict the distribution of ratios for each sample with the 25^{th} percentile, median and the 75^{th} percentile displayed. The whisker range is between the 10^{th} and 90^{th} percentiles.

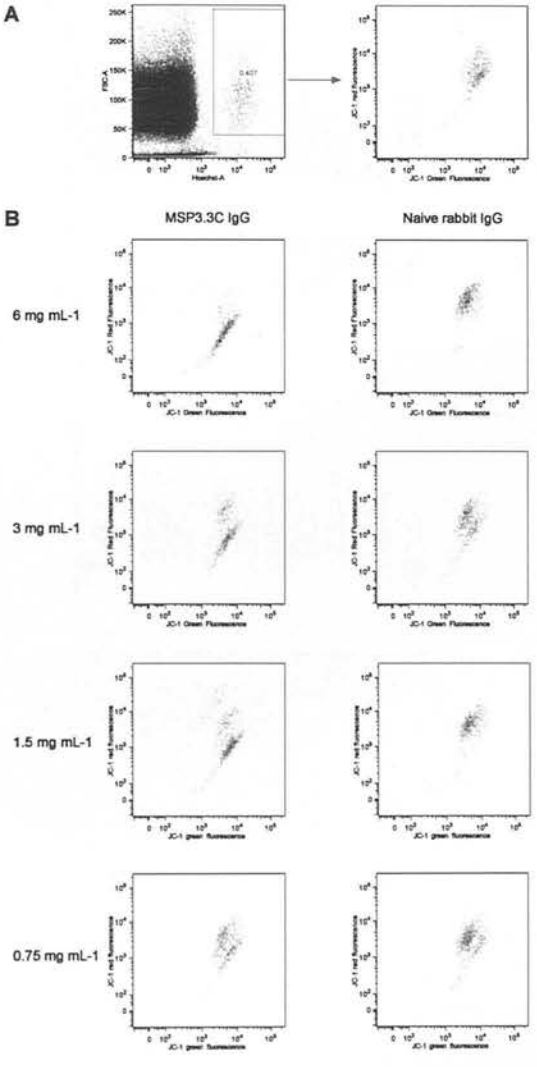
A
B
MSP3.3C IgG
Naive rabbit IgG
6 mg mL-1
3 mg mL-1
1.5 mg mL-1
0.75 mg mL-1

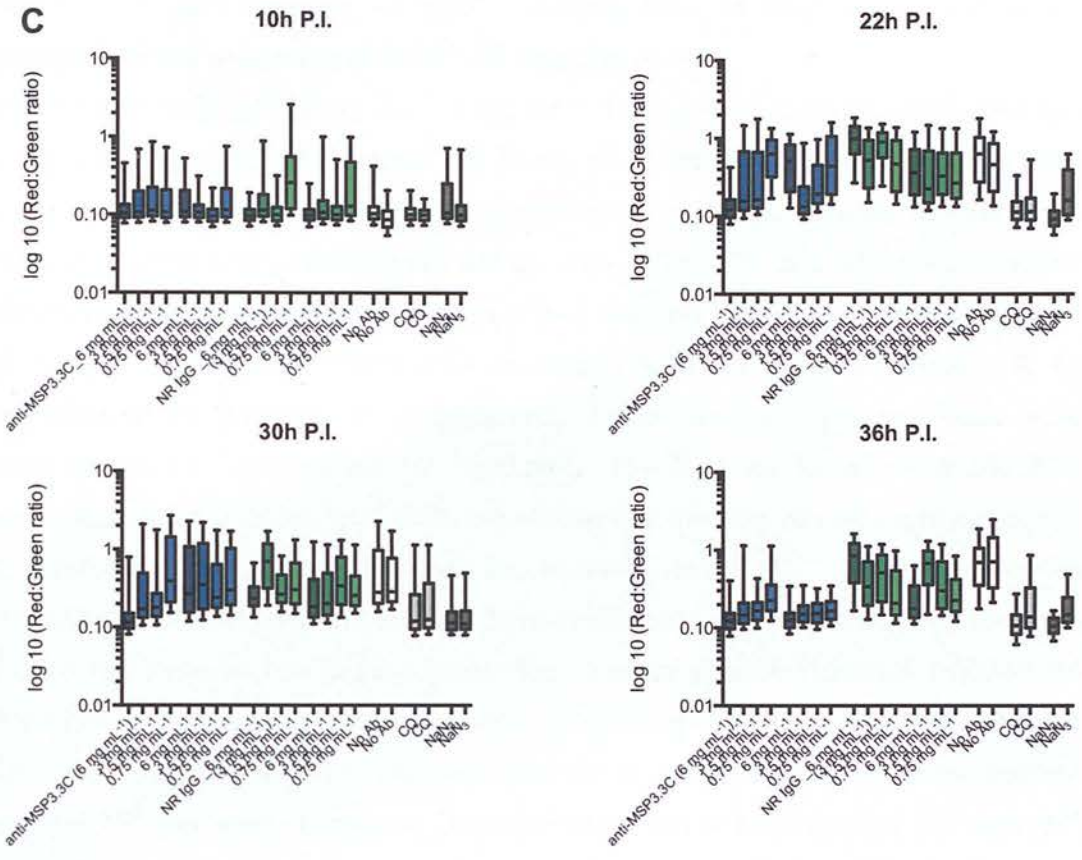
C
10h P.I.
22h P.I.
30h P.I.
36h P.I.
log 10 (Red:Green ratio)
10
1
0.10
0.01
anti-MSP3.3C_6 mg mL-1
3 mg mL-1
1.5 mg mL-1
0.75 mg mL-1
NR IgG
No Ab
CC
NaN3

Figure 5.16 JC-1 staining of iRBCs reveals loss of MMP in *P. falciparum* parasites in the presence of MSP3.3C specific Abs.

MSP3.3C specific IgG (6 mg mL^{-1}, 3 mg mL^{-1}, 1.5 mg mL^{-1}, 0.75 mg mL^{-1}), NR IgG (6 mg mL^{-1}, 3 mg mL^{-1}, 1.5 mg mL^{-1}, 0.75 mg mL^{-1}), no Ab, 30 µM chloroquine (CQ) or sodium azide was added to highly synchronous ring stage cultures 10 hours post invasion. Immediately after assay set up (10h), 22h, 30h and 36h post invasion, samples were taken from each treatment well, stained with JC-1 and Hoechst, and JC-1 green, JC-1 red and Hoechst fluorescence measured by flow cytometry. **A,** An illustration of the gating strategy employed. For all samples, infected RBCs were gated on hoecsht fluorescence (left hand plot). The JC-1 red fluorescence and JC-1 green fluorescence of the total iRBC population can then be viewed (right hand plot) **B,** Bivariate scatter plots of JC-1 red fluorescence versus JC-1 green fluorescence of iRBCs from MSP3.3C and NR IgG treated samples at time point 2. **C,** The ratio of JC-1 red fluorescence to JC-1 green fluorescence of each individual infected red blood cell in each sample was calculated using the R statistical language. The box plots depict the distribution of ratios for each sample with the 25^{th} percentile, median and the 75^{th} percentile displayed. The whisker range is between the 10^{th} and 90^{th} percentiles. Data from two duplicate wells of each sample is shown, from one of three independent experiments.

Variable	P value	Relative Risk	95% CI
Treatment	0.18	1.07	0.97 – 1.17
Concentration 2	0.11	1.12	0.97- 1.28
Concentration 3	0.49	1.05	0.91 – 1.2
Concentration 4	<0.001	1.27	1.11 – 1.45

Table 5.30 The results of the statistical model fitted to explain variation in JC-1 R:G 10 h post invasion.

Variable	P value	Relative Risk	95% CI
Treatment	0.038	1.21	1.01 – 1.45
Concentration 2	0.43	0.90	0.7 – 1.16
Concentration 3	0.92	1.01	0.78 – 1.31
Concentration 4	0.57	1.08	0.83 – 1.39

Table 5.31 The results of the statistical model fitted to explain variation in JC-1 R:G 22 h post invasion.

Variable	P value	Relative Risk	95% CI
Treatment	.93	0.99	0.87-1.14
Concentration 2	0.1	1.18	0.97-1.43
Concentration 3	0.35	1.1	0.9-1.33
Concentration 4	0.05	1.21	1.00 – 1.48

Table 5.32 The results of the statistical model fitted to explain variation in JC-1 R:G 30 h post invasion.

Variable	P value	Relative Risk	95% CI
Treatment	<0.001	1.34	1.16-1.54
Concentration 2	0.41	1.09	0.89-1.32
Concentration 3	0.52	1.07	0.88-1.30
Concentration 4	0.81	1.03	0.84 – 1.25

Table 5.33 The results of the statistical model fitted to explain variation in JC-1 R:G 36 h post invasion.

To this end, a preliminary experiment was carried out to determine whether an increased level of ROS could be detected in iRBCs cultured in the presence of MSP3.3C specific IgG relative to those cultured in the presence of NR IgG. Two different assays were carried out in parallel, in the first assay Ab treatments were applied to a parasite culture pre-loaded with DCFH-DA, where as in the second assay, Ab treatments were applied to a standard parasite culture and at each sampling time point parasites were stained with DCFH-DA in order to measure the DCF signal at the particular time point. In both assays, anti-MSP3.3C IgG or NR IgG was added to highly synchronous ring stage cultures 10h post invasion and sampling time points were immediately after the addition of treatments to the assay culture (10 h time point), 22h and 30h post invasion.

Figure 5.17 displays the DCF fluorescence of iRBCs, expressed as the median fluorescence intensity in the FITC channel, in the assay where the cumulative DCF signal over time was measured i.e. Ab treatments had been applied to a culture pre-loaded with DCFH-DA. At 22 h and 30 h post invasion, at the higher concentrations of anti-MSP3.3C IgG, there is some indication that the ROS level inside the iRBC up until these time points is slightly higher than in untreated samples. This is, however, unlikely to be a specific effect of anti-MSP3.3C Abs, as a similar effect can be seen in NR IgG treated samples.

Figure 5.18 displays the normalised DCF fluorescence when the DCF signal is measured at specific time-points during the assay i.e. parasites stained with DHCF-DA at sampling time points. For each sample, iRBCs were gated on the basis of Hoechst fluorescence. The DCF signal of the total iRBC population was determined, expressed as the median fluorescence intensity of the FITC channel. The arithmetic mean DCF signal was computed for each set of duplicate wells and normalised by dividing it by the mean DCF signal of duplicate wells treated with the same concentration of NR IgG at the same time point. Therefore, a normalised DCF fluorescence of 1 indicates no difference from the negative control, normalised DCF fluorescence values > 1 denote increased DCF signal relative to the negative control

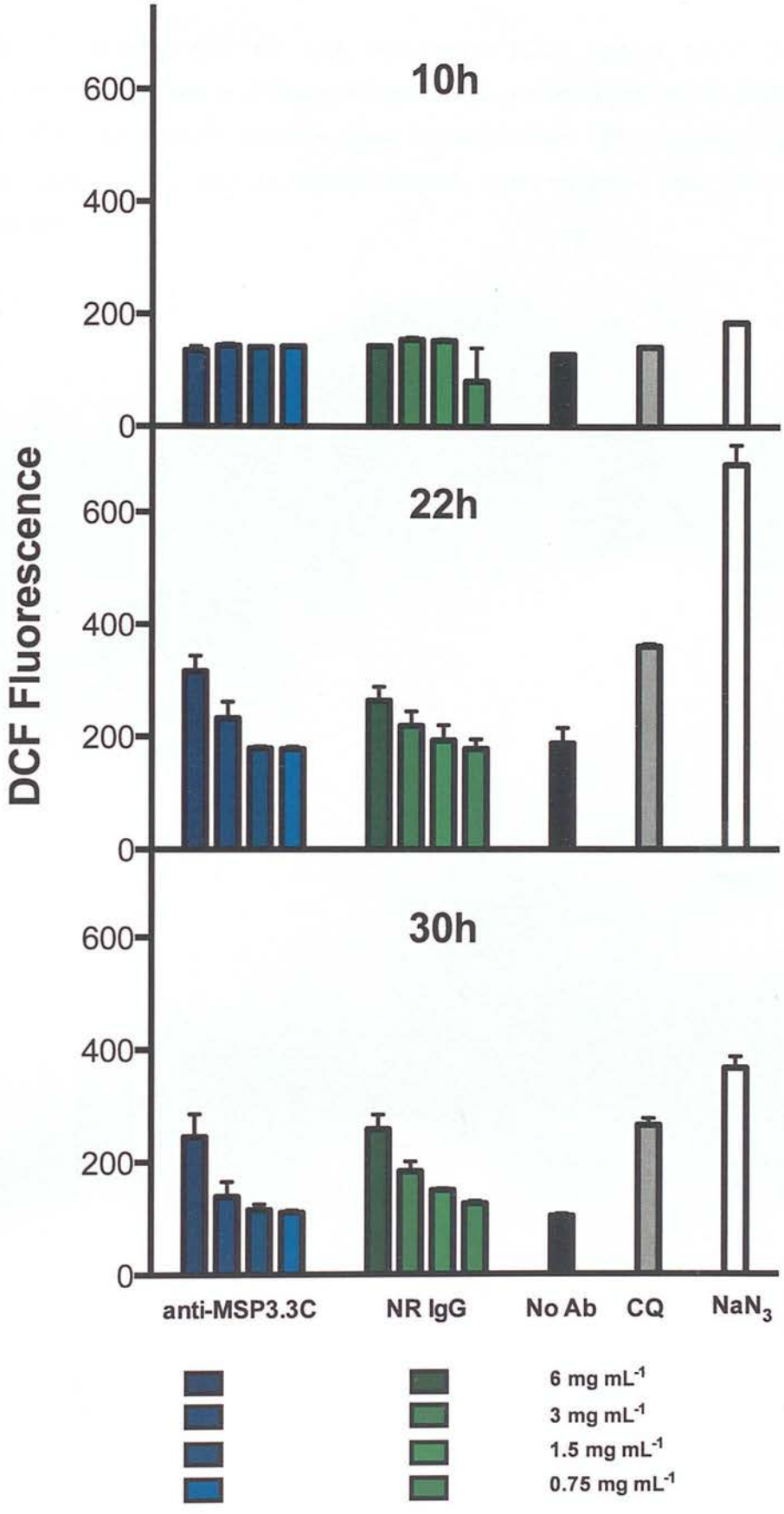
10h
22h
30h
DCF Fluorescence
600
400
200
0
anti-MSP3.3C
NR IgG
No Ab
CQ
NaN3
6 mg mL-1
3 mg mL-1
1.5 mg mL-1
0.75 mg mL-1

Figure 5.17 Cumulative DCF signals in cultures treated with MSP3.3C specific IgG.

MSP3.3C specific IgG, NR IgG, chloroquine (CQ), sodium azide (NaN3) or no treatment was added to iRBCs pre-loaded with the ROS probe DHCF-DA. 10h, 22h and 30h post invasion samples were taken, stained with Hoechst 33342 and the DCF signal (expressed as median fluorescence intensity) was detected by flow cytometry.

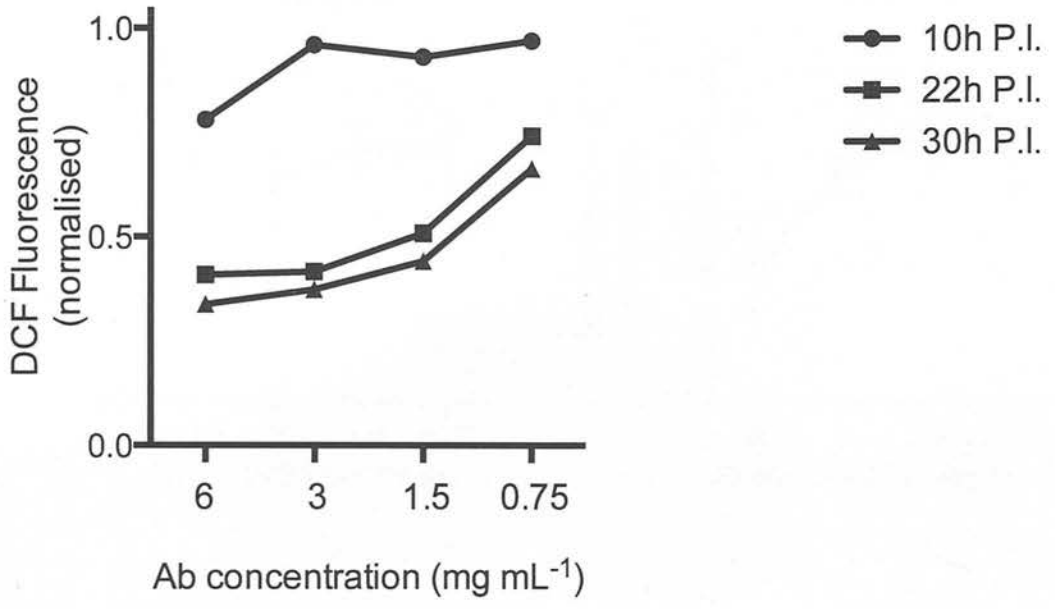

Figure 5.18 DCF signals detected at specific time points in the presence of MSP3.3C specific IgG.

MSP3.3C specific IgG or naive rabbit IgG was added to highly synchronous ring stage cultures 10 h after invasion and the ROS level of iRBCs measured at 10 h (circles), 22 h (squares) and 30 h (triangles) post invasion with the intracellular ROS probe DCFH-DA. The DCF signal (median fluorescence intensity) of the total iRBC population was determined prior to normalising the data to the DCF signal (median fluorescence intensity) detected at that time time point at the same concentration of NR IgG.

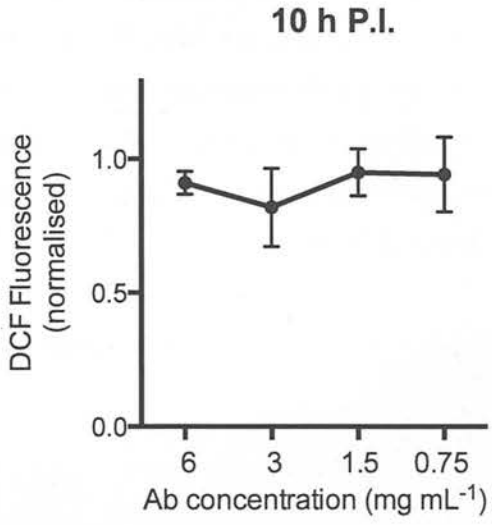
10 h P.I.
DCF Fluorescence (normalised)
1.0
0.5
0.0
6
3
1.5
0.75
Ab concentration (mg mL-1)

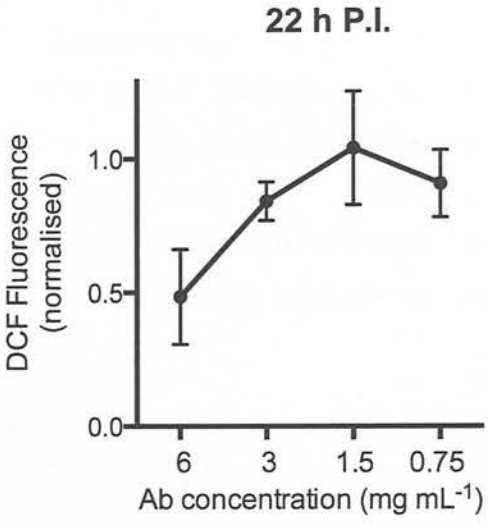
22 h P.I.
DCF Fluorescence (normalised)
1.0
0.5
0.0
6
3
1.5
0.75
Ab concentration (mg mL-1)

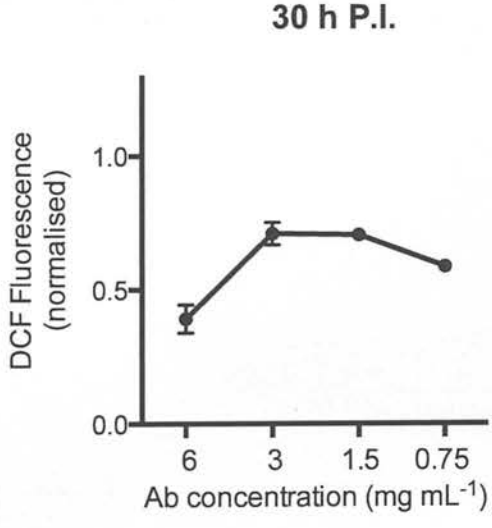
30 h P.I.
DCF Fluorescence (normalised)
1.0
0.5
0.0
6
3
1.5
0.75
Ab concentration (mg mL-1)

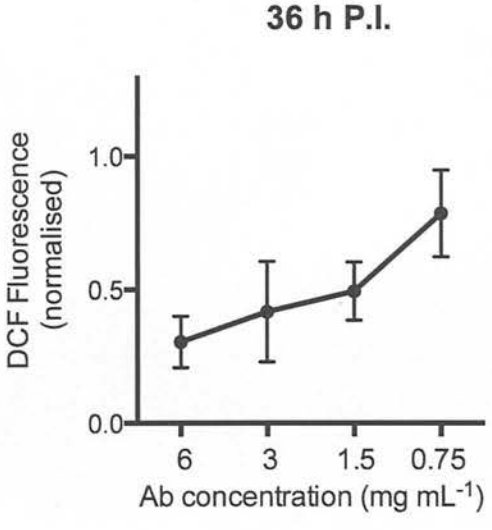
36 h P.I.
DCF Fluorescence (normalised)
1.0
0.5
0.0
6
3
1.5
0.75
Ab concentration (mg mL-1)

Figure 5.19 The effect of MSP3.3C specific Abs on parasite ROS levels.

MSP3.3C specific IgG or NR IgG was added to highly synchronous ring stage cultures 10h post invasion and the ROS level of iRBCs measured at 10h, 22h, 30h and 36h post invasion using the intracellular ROS probe, DCFH-DA. The DCF signal (median fluorescence intensity) of the total iRBC population was determined prior to normalising the data to the DCF signal detected at the same concentration of NR IgG. Two independent experiments were performed and individual bars display the mean normalised DCF fluorescence from these two experiments, with error bard indicating the standard error of the mean.

and normalised DCF fluorescence values < 1 indicate DCF signals lower than the negative control.

In contrast to the higher level of ROS in the presence of anti-MSP3.3C IgG that one would expect to see if ACWO were occurring, at 22h and 30h post invasion, iRBCs treated with anti-MSP3.3C IgG exhibited normalised DCF fluorescence significantly below this level and this effect was dose-dependent (Figure 5.18). It appears that this effect may occur within minutes of Ab addition as, at the highest concentration of anti-MSP3.3C IgG, a reduced DCF signal is detected at the 10 h post invasion time point i.e. immediately after antibodies had been added to the assay culture (Figure 5.18).

In order to confirm the reduced level of ROS detected in MSP3.3C IgG treated cultures, two further independent experiments were carried out, adding MSP3.3C specific IgG or NR IgG 10 h post-invasion and measuring the ROS level of iRBCs, immediately after treatments had been added to the assay culture (i.e at 10h), and at 22h, 30h and 36h post invasion. Samples taken immediately after treatments were added to wells did not display a normalised DCF fluorescence ratio significantly different from 1. At all later sampling time points, at 6 and 3 mg mL^{-1} of anti-MSP3.3C IgG the normalised DCF fluorescence falls far below 1. This effect appears to decline at 1.5 and 0.75 mg mL^{-1} anti-MSP3.3C IgG at 30 and 36 h post invasion (Figure 5.19).

5.4 Discussion

The activity of Abs in parasite GIAs can result from inhibition of merozoite invasion or inhibition of the intraerythrocytic development of the parasite. The terminology used is confusing; the word "growth" in GIA refers to the increase in parasitaemia that occurs over successive invasion cycles, yet "growth" is also used in reference to the physiological and biochemical development of the parasite inside the RBC. For the purpose of clarity, I will refer to the latter as parasite development and the former as parasite growth. A common misconception by some authors (Bergmann-Leitner et al., 2009; Duncan and Hill, 2012) is that functional GIA readouts which detect

both live and dead parasites, measure inhibition of merozoite invasion, where as read outs detecting only live parasites measure both inhibition of merozoite invasion and parasite development. While the latter statement is correct, the former is not; inhibition of merozoite invasion can result from development inhibition earlier in the erythrocytic cycle. For example, if Abs block development of the parasite at the schizont stage, merozoite invasion will not occur, yet this does not directly result from Abs interfering with merozoite invasion.

By using a modified GIA, the stage-specific GIA (SSGIA), which measures the effect of adding Ab to each intraerythrocytic parasite stage, and then monitors the intraerythrocytic development of the parasite over one invasion cycle, I have shown that the GIA activity of MSP3.3C specific Abs is due to developmental inhibition of the parasite. *P. falciparum* is only susceptible to this inhibition over a limited time period of its development inside the RBC; the formation of ring forms and their maturation into trophozoite forms was not inhibited in the SSGIA, whereas the further development of trophozoite and schizont stages was. It took some hours from the time of Ab addition until development of the parasite was retarded or halted. This is seen most clearly during the SSGIA(T), where MSP3.3C specific Abs are added to a synchronous culture 30-34 h P.I. We know from the SSGIA(R) data that trophozoites are vulnerable to growth retardation by MSP3.3C specific Abs, however in the SSGIA(T), the intraerythrocytic development of the parasite is not halted until the schizont stage.

I cannot rule out the possibility that MSP3.3C specific Abs are able to carry out a small level of merozoite invasion inhibition, as inhibition assays were not carried out using purified merozoites, which would be the only way to definitively rule out this possibility. However, the data presented here supports the proposal that the predominant mode of action of MSP3.3C specific Abs is to block the development of the intraerythrocytic trophozoite and schizont stages. This is in contrast to Abs to well-characterised antigens such as AMA-1 and Rh5, which work by preventing the ability of extracellular merozoite to invade the RBC (Douglas et al., 2011; Kocken et al., 1998).

The ability of Abs to disrupt the intraerythrocytic development of *P. falciparum in vitro* has been recognised for many years (Jensen et al., 1982; Jensen et al., 1984). Abs to antigenically distinct regions of MSP-1 display development inhibitory activity in GIAs (Arnot et al., 2008; Bergmann-Leitner et al., 2009; Woehlbier et al., 2006), and in the case of anti-MSP-1_{19} Abs this may be due to interference of the Ab with food vacuole formation (Moss et al., 2012). Additionally, in GIAs Abs to Pf332 can inhibit the development of mature asexual blood stages (Balogun et al., 2011). These cases of development inhibition occur in the absence of immune effector cells, however, Abs can also act in cooperation with monocytes to inhibit the growth of *P. falciparum in vitro*. This process is called antibody-dependent cellular inhibition (ADCI) and results in intraerythrocytic inhibition of the parasite at the trophozoite stage (Bouharoun-Tayoun et al., 1995; Jafarshad et al., 2007). In all of the aforementioned cases of development inhibition, and in the SSGIA assays carried out in the presence of anti-MSP3.3C IgG, parasites displaying abnormal morphology and resembling "crisis forms" were observed. However, to date no one has investigated the phenotype of these unhealthy forms.

Here, I have demonstrated that in response to treatment with MSP3.3C specific Abs, *P. falciparum* undergoes parasite death, as demonstrated by loss of parasite MMP. Recently, a CQ induced programmed cell death (PCD) pathway has been described in *P. falciparum* (Ch'ng et al., 2010; Ch'ng et al., 2011). In these studies MMP loss was used as a marker for parasite PCD and distinguished from unregulated necrotic death seen in response to heat or sodium azide treatment. I included CQ and sodium azide treatments, at the same concentration as these researchers, in my JC-1 experiments and also observed loss of MMP in response to CQ treatment. However, contrary to the Tan group, I also observed a similar magnitude of MMP loss in response to sodium azide treatment. This is not surprising as sodium azide blocks the mitochondrial electron transport chain and decreases MMP in rat cells (Sato et al., 2008). Jogdand *et al.* (Jogdand et al., 2012) demonstrated loss of MMP in dying parasites treated with hyperimmune IgG and anti-GLURP Abs during ADCI assays. These researchers also detected loss of parasite MMP in response to medium starvation and temperature fluctuation, further indicating that loss of MMP may be a

general indicator of parasite death, not just PCD. It is therefore not possible to determine from my data whether α-MSP3.3C IgG treated parasites are undergoing parasite PCD or necrotic death. The measurement of other PCD markers during SSGIAs might prove useful in this regard. However, measurement of *P. falciparum* PCD has been inconsistent among different research groups (Meslin et al., 2007; Nyakeriga et al., 2006; Totino et al., 2008). It would be interesting to investigate whether MMP loss, and parasite death occur in response to treatment with Abs of different specificities, such as those to MSP-1 and Pf332, where unhealthy parasites have been observed microscopically in response to Ab treatment. RBCs undergo eryptosis in response to a variety of treatments (Lang and Qadri, 2012) and it is possible that parasites are dying in response to α-MSP3.3C IgG treatment because the RBCs they inhabit are undergoing eryptosis. This hypothesis is consistent with the large number of extracellular intraerythrocytic forms observed in MSP3.3C treated cultures. A high proportion of extracellular intraerythrocytic forms have also been observed in α-Pf332 Ab treated cultures.

GIAs fulfil two primary roles in malaria research. Firstly, they are used to comparatively test between different asexual vaccine candidate antigens and platforms (Arnot et al., 2008; Douglas et al., 2011; Reed et al., 2009). Secondly, they are used to assess the functional activities of antimalarial Abs and thereby provide insight into what effector mechanisms might govern human immunity to *P. falciparum* infection. There are several limitations to both of these approaches; *in vitro* mechanisms of antibody action may not operate *in vivo* and it has yet to be demonstrated that GIAs are of any value in predicting vaccine efficacy (Duncan and Hill, 2012).

The research presented here highlights the importance of ensuring that the assay techniques used in GIAs are relevant to the mode of action of the Abs in question. For example the National Institute of Health GIA reference centre uses biochemical measurement of pLDH as its functional readout in GIAs. However, the enzymatic activity of pLDH is higher in more mature intraerythrocytic parasite stages (Vivas et al., 2005), therefore comparing the comparative efficiency of two different Abs via

this readout, if one Ab were to block intraerythrocytic development at the ring stage, and the other were to block development at the schizont stage, would not be an accurate comparison.

It is paramount that where functional GIA readouts vary naturally according to parasite stage, this must be taken into account as a potentially confounding factor when interpreting results. For example, both I and Jogdand *et al.* (Jogdand et al., 2012) have shown that parasite MMP varies naturally over the intraerythrocytic developmental cycle. Where Abs work by blocking parasite intraerythrocytic development, as is possibly the case during ADCI (Bouharoun-Tayoun et al., 1995), this could easily lead one to erroneously conclude that parasites are undergoing parasite death, where the effect is in fact simply due to a difference in parasite stage. The JC-1 assay presented in this chapter was developed so that parasite stage was not a confounding factor.

I also investigated the hypothesis that anti-MSP3.3C Ab treated parasites were exposed to oxidative stress. Contrary to this, I found that MSP3.3C specific Ab treated cultures had a lower ROS level than controls treated with NR IgG. Parasite ROS levels increase in mature intraerythrocytic parasite stages (see Chapter 4) and Fu *et al.* (Fu et al., 2010) have suggested that this is consistent with the increased metabolic activity of the parasite that occurs at this time. It is possible that the lower parasite ROS levels I observed are due to a decreased metabolic activity in parasites that are undergoing parasite death.

Singh *et al.* (Singh et al., 2009) reported a merozoite surface location for MSP3.3 in mature schizonts and free merozoites. The IFA data presented here are in agreement with a merozoite surface location of MSP3.3 in schizonts but further colocalisation studies would be needed in order to confirm whether MSP3.3 is located on the surface of free merozoites. I detected expression of MSP3.3 in ring stage parasites, contrary to Pearce *et al.* 2005 (Pearce et al., 2005) who did not detect MSP3.3 in parasite protein extracts prepared from ring stage cultures. This discrepancy could be due to differing sensitivities of the techniques used, or due to differences in the

antibody epitope specificities induced by immunisation with the respective constructs used.

Given that inhibition by MSP3.3C-specific Abs occurs in the absence of merozoite invasion, it follows that these Abs must be accessing their cognate antigen at some time other than during merozoite invasion. Initial IFA data indicated that MSP3.3C-specific, affinity purified IgG could access the intraerythrocytic parasite when added to ring stage cultures i.e. after merozoite invasion had occurred. The MSP3.3 specific IgG could be detected in trophozoite, schizont and following an invasion, ring stage parasites. The IgG could have accessed the ring stage iRBC following invasion, or the IgG could have bound to free merozoites and been carried into the iRBC during invasion. In the initial IFA, I could not detect NR IgG inside the iRBC, however, a further experiment using confocal microscopy identified a non-specific pattern in the iRBC, although this was no higher than background staining. In the latter experiment I found that anti-AMA1 IgG is also able to access intraerythrocytic schizonts. This raises the possibility that any Ig can access the intraerythrocytic parasite but that only those binding their epitopes remain specifically within the iRBC. This notion is supported by Bergmann-Leitner *et al.* (Bergmann-Leitner et al., 2009) who found that fluorescent beads could access the iRBC but showed only a non-specific staining pattern.

Initially, the ability of Ig to access the intraerythrocytic parasite post invasion may seem surprising given the relatively large size of the Ab molecule, and the selective uptake pathways that exist in the malaria parasite (Desai et al., 2000; Staines et al., 2007). This is, however, not a new phenomenon; Pouvelle *et al.* (Pouvelle et al., 1991) demonstrated that intraerythrocytic *P. falciparum* can endocytose protein A, dextran and IgG Ab without these macromolecules passing through the erythrocytic and PV membranes. This lead these authors to propose the 'parasitophorous duct' hypothesis, postulating that the TVN extends to the RBC membrane, thereby forming an aqueous channel that enables direct access of macromolecules to the intraerythrocytic parasite. Although the presence of such a duct remains a bone of contention (Sherman and Zidovetzki, 1992; Taraschi et al., 1992), it has been

demonstrated that labelled polypeptides ranging up to 206 kDa in size can gain direct access to the intraerythrocytic parasite through a membrane network. Furthermore, MSP-1_{42}-specific Abs are able to access late trophozoite/early schizont stage parasites post invasion (Bergmann-Leitner et al., 2009). A number of human RBC proteins are imported into the parasite cytoplasm (Foth et al., 2011; Koncarevic et al., 2009), possibly through the same mechanisms that IgG uses to access the intraerythrocytic parasite.

The possibility exists, although it is unlikely, that the intraerythrocytic access of MSP3.3C-specific IgG post invasion is an artefact of the fixation and permeabilisation steps used in the IFA. Carrying out a live IFA, 4D-imaging experiments tracking labelled-Ab in individual live parasites and detection of the intraerythrocytic IgG via biochemical means would help to address this concern.

MSP3.3, lacking either a transmembrane domain or a consensus sequence for the attachment of a GPI membrane anchor, is presumed to locate to the merozoite surface through protein-protein interactions with neighbouring ligands. Microarray analysis has identified two low-level peaks of transcription at 14 and 36 hours post invasion in the parasite strain HB3 (Bozdech et al., 2003a), with similar transcription profiles also observed in the Dd2 and 3D7 strains (Bozdech et al., 2003b; Le Roch et al., 2003). However, how this correlates with the actual MSP3.3 protein abundance levels over the intraerythrocytic cycle is not known. A large scale proteomic study recently found that many *P. falciparum* protein abundance profiles over the erythrocytic cycle exhibited a significant time delay relative to their mRNA transcript abundance profiles (Foth et al., 2011), challenging the "just in time" induction of gene expression hypothesis and the assumption that transcription profiles can be read as protein expression profiles.

The IFA data presented here indicates that MSP3.3 is exported outside of the PV into the erythrocyte cytosol and this proposition is supported by the presence of a PEXEL motif in the MSP3.3 protein sequence. However, MSP3.3 does not occur in 3 predicted *P. falciparum* secretomes (Hiller et al., 2004; Sargeant et al., 2006; van Ooij et al., 2008). It is tempting to speculate that MSP3.3 is a bifunctional protein,

one function occurring after its first expression peak and involving its spatial location in the erythrocyte cytosol, the second occurring during its second expression peak and involving its merozoite surface location. Alternatively, MSP3.3 bifunctionality may result from engagement with multiple interaction partners; IUPs employ a template-induced folding process, which can result in the protein adopting different conformations, and thereby potentially different functions, when binding to different interaction partners(Jeffery, 2009; Tompa et al., 2005).

MSP3.3C specific Abs may prevent the export of MSP3.3, thereby disrupting a critical function of the protein or may disturb a metabolic pathway that is essential to the development of the intraerythrocytic parasite. Consistent with this first hypothesis, I did not detect export of MSP3.3 in the IgG uptake experiments. However, partial disruption of the *PF10_0347* locus does not significantly affect parasite survival *in vitro* (Pearce et al., 2005), suggesting that one would not expect disruption of MSP3.3 protein function by Abs to result in the drastic inhibition levels seen during SSGIAs. Alternatively, an evident phenotype upon gene disruption may only become apparent *in vivo* through host-parasite interactions. MSP3.3 has also been identified as a target of ADCI (Singh et al., 2009), although this inhibition occurs via a different mechanism than the developmental inhibition presented here.

The *P. falciparum* MSP3.3 family of proteins contains shared or cross-reactive C-terminal epitopes (Singh et al., 2009). MSP3.3C specific Abs do not cross react with MSP3 or MSP6 in Western blots of parasite extracts, suggesting that MSP3.3C contains unique epitopes (Dhanasarnsombut), as does MSP3.4 (Sakamoto et al., 2012). However, a ~100 kDa protein was also detected in these Western blots, raising the possibility that these Abs may cross-react with another antigen. Sakamoto *et al.* similarly detected a ~100 kDa band when probing schizont extracts with Abs raised against recombinant MSP3.4 but found that this was not due to cross-reactivity with other MSP3 family members.

As MSAs are directly exposed to the immune system whilst the merozoite is extracellular, research investigating the *modus operandi* of these Abs, has, to a large

extent, focused on growth inhibition that results from Abs binding to free merozoites (Bouharoun-Tayoun et al., 1995; Jafarshad et al., 2007; Moss et al., 2012). Here, I have shown that Abs to MSP3.3C are able to access the intraerythrocytic parasite after merozoite invasion has occurred and induce parasite death. To my knowledge this is the first demonstration that MSA-specific Abs can induce parasite death *in vitro*. This challenges the prevailing view that once the parasite is under the protective cover of the RBC, intracellular Ags such as MSAs are physically separated from, and therefore no longer vulnerable to, immune attack by serum Abs. This may have implications for both our understanding of naturally acquired Ab-mediated immunity to asexual *P. falciparum* stages and for effective vaccine design against this deadly pathogen. Further dissection of the mechanism by which MSP3.3C specific Abs kill intraerythrocytic *P. falciparum*, in addition to investigation of whether Abs to other antigenic targets known to induce development inhibition operate in this manner, will be informative to both of these research avenues.

6 General discussion

The overall aim of this thesis was to further the understanding of how merozoite surface antigen-specific antibodies inhibit the *in vitro* growth of *P. falciparum*. This aim has been successfully achieved. Specifically, in this thesis, I have: i) generated polyclonal B cell lines producing MSP-1 Block 2 RO33-specific mAbs and determined the light chain isotype, IgG subclass and epitope specificity of these mAbs, ii) developed an *in vitro* functional assay to detect oxidative stress levels during the intraerythrocytic cycle and presented data which suggests that internalised MSP-1-$_{19}$ specific Abs may carry out ACWO *in vitro* and iii) developed novel functional *in vitro* inhibition assays, which I have utilised to dissect the mechanism by which Abs to hte novel merozoite surface antigen MSP3.3C kill *P. falciparum* parasites *in vitro*. A detailed discussion of these findings with respect to the relevant literature is presented at the end of each chapter. Instead of repeating these here, the potential significance and relevance of these findings will be discussed, in the broader context of understanding the mechanisms of antibody mediated immunity to blood stage *P. falciparum* infection, and the development of therapeutic interventions against this parasite stage. In addition, I pinpoint areas where there are still significant gaps in understanding and suggest avenues for future research.

When this project was conceived, it was intended that in the first instance human mAbs to MSAs would be generated, which would then be utilised in both existing and novel *in vitro* inhibition assays, such as the GIA and the *in vitro* ACWO assays. Although I was not able to generate sufficient quantities of human mAbs for use in *in vitro* functional assays, the arguments presented in Chapter 3 for the generation of MSA-specific human mAbs as useful tools with which to investigate mechanisms of antibody action *in vitro* still apply. This is illustrated by the fact that a human mAb specific to MSP-2 has recently proved a highly informative reagent with which to investigate strain-transcending Ab responses in Fc-dependent *in vitro* functional assays such as ADCI (Stubbs et al., 2011).

The limitations of using polyclonal non-human Abs as reagents in functional *in vitro* assays, which formed part of the rationale for the development of MSA-specific

human mAbs in the first place, are applicable to the research detailed in Chapters 4 and 5 of this thesis. For example, mAbs specific to MSP3.3C would allow investigation of the epitopes recognised by growth inhibitory anti-MSP3.3C Abs. The region of MSP3.3 identified as a target of ADCI (amino acids 228-424) (Singh et al., 2009) almost entirely covers the MSP3.3C antigen (amino acids 229-360 of MSP3.3). It would be therefore be interesting to investigate whether the epitopes recognised by Abs active in ADCI overlapped with, or were entirely different from the inhibitory MSP3.3 Abs described in Chapter 5. Such an analysis would require MSP3.3-specific human mAbs, as the Fc-dependent effects necessary for ADCI might not be replicated with murine mAbs. However, given that MSP3.3 appears to be only weakly and infrequently recognised by Abs elicited in response to *P. falciparum* infection (Pearce et al., 2005), isolating low-frequency anti-MSP3.3 human mAbs from human PBMC samples may prove difficult.

It has been argued that there is a need for the development of high throughput standardised *in vitro* Ab inhibition assays to act as surrogate endpoints with which to assess the efficacy of blood stage vaccines in clinical trials (Ockenhouse et al., 2006; Polhemus et al., 2007; Withers et al., 2006). Given that we have a limited understanding of the different mechanisms by which Abs can inhibit *P. falciparum* growth *in vitro*, such assays may ignore the significance of Abs whose function have not yet been fully characterised *in vitro*. Additionally, whilst the scalability of *in vitro* assays is an important consideration, it is worth noting that full interpretation of the flow cytometry data from the SSGIA required relatively time-intensive gathering of semi-quantitative and arguably subjective data by examination of stained blood smears using light microscopy. It is hoped that the *in vitro* functional assays presented in this thesis, such as the SSGIA and JC-1 assay, may prove useful in uncovering some of the mechanisms by which other inhibitory Abs act. For example it would be interesting to investigate whether intraerythrocytic growth inhibition by anti-MSP-1_{19} and Pf332 antibodies results in parasite death.

Understanding the mechanisms of Ab-mediated *in vitro* growth inhibition may provide insight into how antibody mediated immunity is brought about in natural

P. falciparum infections. However, it is important to note that any mechanisms of Ab action identified in an *in vitro* assay are a model of what may be functional mechanisms of immunity that operate *in vivo*. In particular, the large quantities of Ab required to observe GIA effects calls into question its relevance as a functional correlate of immunity. Furthermore, GIAs are frequently carried out using well-characterised laboratory strains of *P. falciparum*, which may not represent the characteristics of parasite strains circulating in endemic populations. Studies which have identified correlations between *in vitro* functional assays and clinical immunity (Crompton et al., 2010; Dent et al., 2008; Druilhe and Khusmith, 1987; Jensen et al., 1983; John et al., 2004; Joos et al., 2010) offer some encouragement that these *in vitro* assays may have some relevance to what occurs *in vivo*. It is important to recognise that both innate and cell-mediated immunity are thought to contribute to acquired protective immunity to blood stage *P. falciparum* infection (McCall and Sauerwein, 2010; McMorran et al., 2009; Spence and Langhorne, 2012), and potential mechanisms of Ab-mediated immunity identified *in vitro* should be considered in light of their potential interactions with these processes. For example, MSP-1_{19}-specific Abs can inhibit SUB2-mediated processing of MSP-1_{42} (Blackman et al., 1994; Harris et al., 2005). It would be interesting to explore whether this inhibition of proteolytic processing blocks the recently identified interaction between MSP-1_{33} and the human pro-inflammatory protein S100P (Waisberg et al., 2012).

Data in chapter 4 of this thesis suggest that MSP-1_{19}-specific Abs may carry out ACWO inside the parasite, which could harm the intraerythrocytic development of the parasite. Although this research was not able to determine whether this is a realistic mechanism by which *in vitro* growth inhibition operates. Given that Abs can function directly as bactericidal, fungicidal and parasiticidal agents (Brena et al., 2011; Connolly et al., 2004; Vouldoukis et al., 2011) the investigation of other mechanisms by which MSA-specific Abs may directly kill *P. falciparum* parasites is worthy of further investigation.

The research presented in Chapter 5 of this thesis describes a novel mechanism of antibody mediated *in vitro* growth inhibition, and would not have been possible

without the research carried out in Chapter 4. During the development of the *in vitro* ACWO assay it was not known at what stage of the intraerythrocytic developmental cycle ACWO might occur. Therefore, repeated sampling across the intraerythrocytic developmental cycle using a highly synchronous parasite culture was employed to increase the likelihood of detecting any such effects. Within this context, the idea of carrying out a GIA with multiple time points was first formed. When data that intraerythrocytic parasite development might be compromised during anti-MSP3.3C IgG GIAs arose in earlier studies by other lab members, it was the fortuitous addition of anti-MSP3.3C IgG to GIA assays using multiple time-point sampling as part of the ACWO assays that lead to the first evidence of the mechanism by which anti-MSP3.3C Abs might exert their effect.

One of the assumptions of this project was that understanding the mechanisms by which MSA-specific Abs act is significant because MSAs are thought to be targets of protective immunity. However, sero-epidemiological studies linking Ab responses to particular antigens with prospective protection to *P. falciparum* infection only demonstrate associative correlations, which may disappear once confounding factors such as age or exposure are controlled for. A parasite-specific Ab response, predictive of protection against malaria in a diverse range of transmission settings remains elusive.

One of the arguments that has been used in support of MSAs as targets of protective immunity is that they are directly accessible to anibodies whilst the merozoite is extracellular. The research presented here and by others (Bergmann-Leitner et al., 2009; Pouvelle et al., 1991) suggests that antibodies can access the intraerythrocytic parasite, and raises the possibility that other antigens hidden under the "protective cover of the RBC" may also be vulnerable to antibody-mediated immune attack and there worthy of consideration as vaccine candidate antigens.

Whilst efforts have been made to dissect which components of the inhibitory response to MSAs are due to inhibition of merozoite invasion and which are due to intraerythrocytic development inhibition, there is little information regarding the

molecular mechanisms of this inhibition. It is known that some Abs to MSP-1 and AMA-1 inhibit merozoite invasion by blocking proteolytic processing by SUB-2 (Woehlbier et al., 2010). In the case of the mechanism of action of MSP3.3C Abs, and Abs of other antigen specificities that inhibit intraerythrocytic development of the parasite, an analysis of how the addition of immune IgG to asexual *P. falciparum* cultures effects stage-specific mRNA transcript and protein abundance levels over the course of the IDC may prove informative. However, the interpretation of such information against a background in which the functions of MSP3.3, in addition to other MSAs are unknown remains challenging. To quote "we may not know enough about malaria to make an effective vaccine" (Pierce and Miller, 2009).

7 References

Adisa, A., Rug, M., Klonis, N., Foley, M., Cowman, A. F. and Tilley, L. (2003). The signal sequence of exported protein-1 directs the green fluorescent protein to the parasitophorous vacuole of transfected malaria parasites. *J Biol Chem* **278**, 6532–6542.

Ahlborg, N., Iqbal, J., Björk, L., Ståhl, S., Perlmann, P. and Berzins, K. (1996). *Plasmodium falciparum*: differential parasite growth inhibition mediated by antibodies to the antigens Pf332 and Pf155/RESA. *Exp Parasitol* **82**, 155–163.

Ahlborg, N., Ling, I. T., Howard, W., Holder, A. A. and Riley, E. M. (2002). Protective immune responses to the 42-kilodalton (kDa) region of *Plasmodium yoelii* merozoite surface protein 1 are induced by the C-terminal 19-kDa region but not by the adjacent 33-kDa region. *Infect Immun* **70**, 820–825.

Aikawa, M., Hepler, P. K., Huff, C. G. and Sprinz, H. (1966). The feeding mechanism of avian malarial parasites. *J. Cell Biol* **28**, 355–373.

Akpogheneta, O. J., Duah, N. O., Tetteh, K. K. A., Dunyo, S., Lanar, D. E., Pinder, M. and Conway, D. J. (2008). Duration of naturally acquired antibody responses to blood-stage *Plasmodium falciparum* is age dependent and antigen specific. *Infect Immun* **76**, 1748–1755.

al-Yaman, F., Genton, B., Anders, R., Taraika, J., Ginny, M., Mellor, S. and Alpers, M. P. (1995). Assessment of the role of the humoral response to *Plasmodium falciparum* MSP2 compared to RESA and SPf66 in protecting Papua New Guinean children from clinical malaria. *Parasite Immunol* **17**, 493–501.

al-Yaman, F., Genton, B., Kramer, K. J., Chang, S. P., Hui, G. S., Baisor, M. and Alpers, M. P. (1996). Assessment of the role of naturally acquired antibody levels to Plasmodium falciparum merozoite surface protein-1 in protecting Papua New Guinean children from malaria morbidity. *Am J Trop Med Hyg* **54**, 443–448.

Allison, A. C. and Eugui, E. M. (1983). The role of cell-mediated immune responses in resistance to malaria, with special reference to oxidant stress. *Annu Rev Immunol* **1**, 361–392.

Amaratunga, C., Lopera-Mesa, T. M., Brittain, N. J., Cholera, R., Arie, T., Fujioka, H., Keefer, J. R. and Fairhurst, R. M. (2011). A role for fetal hemoglobin and maternal immune IgG in infant resistance to *Plasmodium falciparum* malaria. *PLoS ONE* **6**, e14798.

Amer, J., Goldfarb, A. and Fibach, E. (2003). Flow cytometric measurement of reactive oxygen species production by normal and thalassaemic red blood cells. *Eur . Haematol* **70**, 84–90.

Anders, R. F., Adda, C. G., Foley, M. and Norton, R. S. (2010). Recombinant protein vaccines against the asexual blood stages of *Plasmodium falciparum*. *Hum Vaccin* **6**, 39–53.

Arnot, D. E., Cavanagh, D. R., Remarque, E. J., Creasey, A. M., Sowa, M. P. K., Morgan, W. D., Holder, A. A., Longacre, S. and Thomas, A. W. (2008). Comparative testing of six antigen-based malaria vaccine candidates directed toward merozoite-stage *Plasmodium falciparum*. *Clin Vaccine Immunol* **15**, 1345–1355.

Babior, B. M., Takeuchi, C., Ruedi, J., Gutierrez, A. and Wentworth, P. (2003). Investigating antibody-catalyzed ozone generation by human neutrophils. *Proc Natl Acad Sci USA* **100**, 3031–3034.

Baird, J. K. (1995). Host age as a determinant of naturally acquired immunity to *Plasmodium falciparum*. *Parasitol Today* **11**, 105–111.

Baird, J. K., Jones, T. R., Danudirgo, E. W., Annis, B. A., Bangs, M. J., Basri, H., Purnomo and Masbar, S. (1991). Age-dependent acquired protection against *Plasmodium falciparum* in people having two years exposure to hyperendemic malaria. *Am J Trop Med Hyg* **45**, 65–76.

Balogun, H. A., Awah, N. W., Farouk, S. E. and Berzins, K. (2011). Pf332-C231-reactive antibodies affect growth and development of intra-erythrocytic *Plasmodium falciparum* parasites. *Vaccine* **30**, 21–28.

Bannister, L. H. and Mitchell, G. H. (1995). The role of the cytoskeleton in *Plasmodium falciparum* merozoite biology: an electron-microscopic view. *Ann Trop Med Parasitol* **89**, 105–111.

Bannister, L. H., Hopkins, J. M., Dluzewski, A. R., Margos, G., Williams, I. T., Blackman, M. J., Kocken, C. H., Thomas, A. W. and Mitchell, G. H. (2003). *Plasmodium falciparum* apical membrane antigen 1 (PfAMA-1) is translocated within micronemes along subpellicular microtubules during merozoite development. *J Cell Sci* **116**, 3825–3834.

Bannister, L. H., Hopkins, J. M., Fowler, R. E., Krishna, S. and Mitchell, G. H. (2000a). Ultrastructure of rhoptry development in *Plasmodium falciparum* erythrocytic schizonts. *Parasitology* **121**, 273–287.

Bannister, L. H., Hopkins, J. M., Fowler, R. E., Krishna, S. and Mitchell, G. H. (2000b). A brief illustrated guide to the ultrastructure of *Plasmodium falciparum* asexual blood stages. *Parasitol. Today* **16**, 427–433.

Bannister, L. H., Hopkins, J. M., Margos, G., Dluzewski, A. R. and Mitchell, G. H. (2004). Three-dimensional ultrastructure of the ring stage of *Plasmodium falciparum*: evidence for export pathways. *Microsc Microanal* **10**, 551–562.

Barfod, L., Bernasconi, N. L., Dahlbäck, M., Jarrossay, D., Andersen, P. H., Salanti, A., Ofori, M. F., Turner, L., Resende, M., Nielsen, M. A., et al. (2007). Human pregnancy-associated malaria-specific B cells target polymorphic, conformational epitopes in VAR2CSA. *Mol Microbiol* **63**, 335–347.

Barfod, L., Dobrilovic, T., Magistrado, P., Khunrae, P., Viwami, F., Bruun, J., Dahlbäck, M., Bernasconi, N. L., Fried, M., John, D., et al. (2010). Chondroitin sulfate A-adhering *Plasmodium falciparum*-infected erythrocytes express functionally important antibody epitopes shared by multiple variants. *The Journal of Immunology* **185**, 7553–7561.

Baruch, D. I., Pasloske, B. L., Singh, H. B., Bi, X., Ma, X. C., Feldman, M., Taraschi, T. F. and Howard, R. J. (1995). Cloning the *P. falciparum* gene encoding PfEMP1, a malarial variant antigen and adherence receptor on the surface of parasitized human erythrocytes. *Cell* **82**, 77–87.

Baum, J., Papenfuss, A. T., Baum, B., Speed, T. P. and Cowman, A. F. (2006). Regulation of apicomplexan actin-based motility. *Nat Rev Microbiol* **4**, 621–628.

Becker, K., Rahlfs, S., Nickel, C. and Schirmer, R. H. (2003). Glutathione – functions and metabolism in the malarial parasite *Plasmodium falciparum. Biol Chem* **384**, 551–566.

Becker, K., Tilley, L., Vennerstrom, J. L., Roberts, D., Rogerson, S. and Ginsburg, H. (2004). Oxidative stress in malaria parasite-infected erythrocytes: host-parasite interactions. *Int J Parasitol* **34**, 163–189.

Bergmann-Leitner, E. S., Duncan, E. H. and Angov, E. (2009). MSP-1p42-specific antibodies affect growth and development of intra-erythrocytic parasites of *Plasmodium falciparum. Malar J* **8**, 183-195.

Bergmann-Leitner, E. S., Duncan, E. H., Mullen, G. E., Burge, J. R., Khan, F., Long, C. A., Angov, E. and Lyon, J. A. (2006). Critical evaluation of different methods for measuring the functional activity of antibodies against malaria blood stage antigens. *Am J Trop Med Hyg* **75**, 437–442.

Blackman, M. J. and Holder, A. A. (1992). Secondary processing of the *Plasmodium falciparum* merozoite surface protein-1 (MSP1) by a calcium-dependent membrane-bound serine protease: shedding of MSP133 as a noncovalently associated complex with other fragments of the MSP1. *Mol Biochem Parasitol* **50**, 307–315.

Blackman, M. J., Heidrich, H. G., Donachie, S., McBride, J. S. and Holder, A. A. (1990). A single fragment of a malaria merozoite surface protein remains on the parasite during red cell invasion and is the target of invasion-inhibiting antibodies. *J Exp Med* **172**, 379–382.

Blackman, M. J., Ling, I. T., Nicholls, S. C. and Holder, A. A. (1991). Proteolytic processing of the *Plasmodium falciparum* merozoite surface protein-1 produces a membrane-bound fragment containing two epidermal growth factor-like domains. *Mol Biochem Parasitol* **49**, 29–33.

Blackman, M. J., Scott-Finnigan, T. J., Shai, S. and Holder, A. A. (1994). Antibodies inhibit the protease-mediated processing of a malaria merozoite surface protein. *J Exp Med* **180**, 389–393.

Blisnick, T., Morales Betoulle, M. E., Barale, J. C., Uzureau, P., Berry, L., Desroses, S., Fujioka, H., Mattei, D. and Braun Breton, C. (2000). Pfsbp1, a Maurer's cleft *Plasmodium falciparum* protein, is associated with the erythrocyte skeleton. *Mol Biochem Parasitol* **111**, 107–121.

Boddey, J. A., Hodder, A. N., Günther, S., Gilson, P. R., Patsiouras, H., Kapp, E. A., Pearce, J. A., de Koning-Ward, T. F., Simpson, R. J., Crabb, B. S., et al. (2010). An aspartyl protease directs malaria effector proteins to the host cell. *Nature* **463**, 627–631.

Bonini, M. G., Rota, C., Tomasi, A. and Mason, R. P. (2006). The oxidation of 2",7-"dichlorofluorescin to reactive oxygen species: a self-fulfilling prophesy? *Free Radic Biol Med* **40**, 968–975.

Bouharoun-Tayoun, H. and Druilhe, P. (1992). *Plasmodium falciparum* malaria: evidence for an isotype imbalance which may be responsible for delayed acquisition of protective immunity. *Infect Immun* **60**, 1473–1481.

Bouharoun-Tayoun, H., Attanath, P., Sabchareon, A., Chongsuphajaisiddhi, T. and Druilhe, P. (1990). Antibodies that protect humans against *Plasmodium falciparum* blood stages do not on their own inhibit parasite growth and invasion in vitro, but act in cooperation with monocytes. *J Exp Med* **172**, 1633–1641.

Bouharoun-Tayoun, H., Oeuvray, C., Lunel, F. and Druilhe, P. (1995). Mechanisms underlying the monocyte-mediated antibody-dependent killing of *Plasmodium falciparum* asexual blood stages. *J Exp Med* **182**, 409–418.

Bozdech, Z., Llinás, M., Pulliam, B. L., Wong, E. D., Zhu, J. and DeRisi, J. L. (2003a). The transcriptome of the intraerythrocytic developmental cycle of *Plasmodium falciparum*. *PLoS Biol* **1**, E5.

Bozdech, Z., Zhu, J., Joachimiak, M. P., Cohen, F. E., Pulliam, B. and DeRisi, J. L. (2003b). Expression profiling of the schizont and trophozoite stages of *Plasmodium falciparum* with a long-oligonucleotide microarray. *Genome Biol* **4**, R9.

Brena, S., Cabezas-Olcoz, J., Moragues, M. D., Fernández de Larrinoa, I., Domínguez, A., Quindós, G. and Pontón, J. (2011). Fungicidal monoclonal antibody C7 interferes with iron acquisition in *Candida albicans*. *Antimicrob Agents Chemother* **55**, 3156–3163.

Brown, H. and Prescott, R. (2006). *Applied Mixed Models in Medicine*. Wiley.

Bryce, J., Boschi-Pinto, C., Shibuya, K., Black, R. E.WHO Child Health Epidemiology Reference Group (2005). WHO estimates of the causes of death in children. *Lancet* **365**, 1147–1152.

Bullen, H. E., Charnaud, S. C., Kalanon, M., Riglar, D. T., Dekiwadia, C., Kangwanrangsan, N., Torii, M., Tsuboi, T., Baum, J., Ralph, S. A., et al. (2012). Biosynthesis, localisation and macromolecular arrangement of the *Plasmodium falciparum* translocon of exported proteins; PTEX. *J Biol Chem* **287**, 7871-7884.

Cao, J., Kaneko, O., Thongkukiatkul, A., Tachibana, M., Otsuki, H., Gao, Q., Tsuboi, T. and Torii, M. (2009). Rhoptry neck protein RON2 forms a complex with microneme protein AMA1 in *Plasmodium falciparum* merozoites. *Parasitol Int* **58**, 29–35.

Cavanagh, D. R. and McBride, J. S. (1997). Antigenicity of recombinant proteins derived from Plasmodium falciparum merozoite surface protein 1. *Mol Biochem Parasitol* **85**, 197–211.

Cavanagh, D. R., Dobaño, C., Elhassan, I. M., Marsh, K., Elhassan, A., Hviid, L., Khalil, E. A., Theander, T. G., Arnot, D. E. and McBride, J. S. (2001). Differential patterns of human immunoglobulin G subclass responses to distinct regions of a single protein, the merozoite surface protein 1 of *Plasmodium falciparum*. *Infect Immun* **69**, 1207–1211.

Cavanagh, D. R., Dodoo, D., Hviid, L., Kurtzhals, J. A. L., Theander, T. G., Akanmori, B. D., Polley, S., Conway, D. J., Koram, K. and McBride, J. S. (2004). Antibodies to the N-terminal block 2 of *Plasmodium falciparum* merozoite surface protein 1 are associated with protection against clinical malaria. *Infect Immun* **72**, 6492–6502.

Cavanagh, D. R., Elhassan, I. M., Roper, C., Robinson, V. J., Giha, H., Holder, A. A., Hviid, L., Theander, T. G., Arnot, D. E. and McBride, J. S. (1998). A longitudinal study of type-specific antibody responses to *Plasmodium falciparum* merozoite surface protein-1 in an area of unstable malaria in Sudan. *J Immunol* **161**, 347–359.

Ch'ng, J.-H., Kotturi, S. R., Chong, A. G.-L., Lear, M. J. and Tan, K. S.-W. (2010). A programmed cell death pathway in the malaria parasite *Plasmodium falciparum* has general features of mammalian apoptosis but is mediated by clan CA cysteine proteases. *Cell Death and Disease* **1**, e26–13.

Ch'ng, J.-H., Liew, K., Goh, A. S.-P., Sidhartha, E. and Tan, K. S.-W. (2011). Drug-induced permeabilization of parasite's digestive vacuole is a key trigger of programmed cell death in *Plasmodium falciparum*. *Cell Death and Disease* **2**, e216.

Chang, H. H., Falick, A. M., Carlton, P. M., Sedat, J. W., DeRisi, J. L. and Marletta, M. A. (2008). N-terminal processing of proteins exported by malaria parasites. *Mol Biochem Parasitol* **160**, 107–115.

Chang, S. P., Case, S. E., Gosnell, W. L., Hashimoto, A., Kramer, K. J., Tam, L. Q., Hashiro, C. Q., Nikaido, C. M., Gibson, H. L., Lee-Ng, C. T., et al. (1996). A recombinant baculovirus 42-kilodalton C-terminal fragment of *Plasmodium falciparum* merozoite surface protein 1 protects Aotus monkeys against malaria. *Infect Immun* **64**, 253–261.

Chasis, J. A., Prenant, M., Leung, A. and Mohandas, N. (1989). Membrane assembly and remodeling during reticulocyte maturation. *Blood* **74**, 1112–1120.

Chauhan, V. S., Yazdani, S. S. and Gaur, D. (2010). Malaria vaccine development based on merozoite surface proteins of *Plasmodium falciparum*. *Hum Vaccin* **6**, 757-762.

Chen, Q., Fernandez, V., Sundström, A., Schlichtherle, M., Datta, S., Hagblom, P. and Wahlgren, M. (1998). Developmental selection of var gene expression in *Plasmodium falciparum*. *Nature* **394**, 392–395.

Cheng, Q., Cloonan, N., Fischer, K., Thompson, J., Waine, G., Lanzer, M. and Saul, A. (1998). stevor and rif are *Plasmodium falciparum* multicopy gene families which potentially encode variant antigens. *Mol Biochem Parasitol* **97**, 161–176.

Cheresh, P., Harrison, T., Fujioka, H. and Haldar, K. (2002). Targeting the malarial plastid via the parasitophorous vacuole. *J Biol Chem* **277**, 16265–16277.

Child, M. A., Epp, C., Bujard, H. and Blackman, M. J. (2010). Regulated maturation of malaria merozoite surface protein-1 is essential for parasite growth. *Mol Microbiol* **78**, 187–202.

Chizzolini, C., Dupont, A., Akue, J. P., Kaufmann, M. H., Verdini, A. S., Pessi, A. and Del Giudice, G. (1988). Natural antibodies against three distinct and defined antigens of *Plasmodium falciparum* in residents of a mesoendemic area in Gabon. *Am J Trop Med Hyg* **39**, 150–156.

Clark, I. A. and Hunt, N. H. (1983). Evidence for reactive oxygen intermediates causing hemolysis and parasite death in malaria. *Infect Immun* **39**, 1–6.

Clark, J. T., Donachie, S., Anand, R., Wilson, C. F., Heidrich, H. G. and McBride, J. S. (1989). 46-53 kilodalton glycoprotein from the surface of *Plasmodium falciparum* merozoites. *Mol Biochem Parasitol* **32**, 15–24.

Cohen, S., McGregor, I. A. and Carrington, S. (1961). Gamma-globulin and acquired immunity to human malaria. *Nature* **192**, 733–737.

Collins, C. R., Withers-Martinez, C., Hackett, F. and Blackman, M. J. (2009). An inhibitory antibody blocks interactions between components of the malarial invasion machinery. *PLoS Pathog* **5**, e1000273.

Connolly, S. E., Thanassi, D. G. and Benach, J. L. (2004). Generation of a complement-independent bactericidal IgM against a relapsing fever Borrelia. *J Immunol* **172**, 1191–1197.

Conway, D. J. (1997). Natural selection on polymorphic malaria antigens and the search for a vaccine. *Parasitol. Today* **13**, 26–29.

Conway, D. J., Cavanagh, D. R., Tanabe, K., Roper, C., Mikes, Z. S., Sakihama, N., Bojang, K. A., Oduola, A. M., Kremsner, P. G., Arnot, D. E., et al. (2000). A principal target of human immunity to malaria identified by molecular population genetic and immunological analyses. *Nat Med* **6**, 689–692.

Conway, D. J., Greenwood, B. M. and McBride, J. S. (1992). Longitudinal study of *Plasmodium falciparum* polymorphic antigens in a malaria-endemic population. *Infect Immun* **60**, 1122–1127.

Cooke, B. M., Lingelbach, K., Bannister, L. H. and Tilley, L. (2004). Protein trafficking in *Plasmodium falciparum*-infected red blood cells. *Trends Parasitol* **20**, 581–589.

Cooke, B. M., Mohandas, N. and Coppel, R. L. (2001). The malaria-infected red blood cell: structural and functional changes. *Adv Parasitol* **50**, 1–86.

Cooper, J. A. (1993). Merozoite surface antigen-I of Plasmodium. *Parasitol Today* **9**, 50–54.

Corti, D., Langedijk, J. P. M., Hinz, A., Seaman, M. S., Vanzetta, F., Fernandez-Rodriguez, B. M., Silacci, C., Pinna, D., Jarrossay, D., Balla-Jhagjhoorsingh, S., et al. (2010). Analysis of memory B cell responses and isolation of novel monoclonal antibodies with neutralizing breadth from HIV-1-infected individuals. *PLoS ONE* **5**, e8805.

Counter, C. M., Botelho, F. M., Wang, P., Harley, C. B. and Bacchetti, S. (1994). Stabilization of short telomeres and telomerase activity accompany immortalization of Epstein-Barr virus-transformed human B lymphocytes. *J. Virol.* **68**, 3410–3414.

Cowan, G. J. M., Creasey, A. M., Dhanasarnsombut, K., Thomas, A. W., Remarque, E. J. and Cavanagh, D. R. (2011). A malaria vaccine based on the polymorphic block 2 region of MSP-1 that elicits a broad serotype-spanning immune response. *PLoS ONE* **6**, e26616.

Cox-Singh, J. (2012). Zoonotic malaria: *Plasmodium knowlesi*, an emerging pathogen. *Curr Opin Infect Dis* **25**, 530–536.

Crompton, P. D., Miura, K., Traore, B., Kayentao, K., Ongoiba, A., Weiss, G., Doumbo, S., Doumtabe, D., Kone, Y., Huang, C.-Y., et al. (2010). In vitro growth-inhibitory activity and malaria risk in a cohort study in mali. *Infect Immun* **78**, 737–745.

Daly, T. M. and Long, C. A. (1995). Humoral response to a carboxyl-terminal region of the merozoite surface protein-1 plays a predominant role in controlling blood-stage infection in rodent malaria. *J Immunol* **155**, 236–243.

Datta, D., Vaidehi, N., Xu, X. and Goddard, W. A. (2002). Mechanism for antibody catalysis of the oxidation of water by singlet dioxygen. *Proc Natl Acad Sci USA* **99**, 2636–2641.

de Koning-Ward, T. F., Gilson, P. R., Boddey, J. A., Rug, M., Smith, B. J., Papenfuss, A. T., Sanders, P. R., Lundie, R. J., Maier, A. G., Cowman, A. F., et al. (2009). A newly discovered protein export machine in malaria parasites. *Nature* **459**, 945–949.

del Portillo, H. A., Nussenzweig, R. S. and Enea, V. (1987). Circumsporozoite gene of a *Plasmodium falciparum* strain from Thailand. *Mol Biochem Parasitol* **24**, 289–294.

Dent, A. E., Bergmann-Leitner, E. S., Wilson, D. W., Tisch, D. J., Kimmel, R., Vulule, J., Sumba, P. O., Beeson, J. G., Angov, E., Moormann, A. M., et al. (2008). Antibody-mediated growth inhibition of *Plasmodium falciparum*: relationship to age and protection from parasitemia in Kenyan children and adults. *PLoS ONE* **3**, e3557.

Desai, S. A., Bezrukov, S. M. and Zimmerberg, J. (2000). A voltage-dependent channel involved in nutrient uptake by red blood cells infected with the malaria parasite. *Nature* **406**, 1001–1005.

Dickinson, B. C. and Chang, C. J. (2008). A targetable fluorescent probe for imaging hydrogen peroxide in the mitochondria of living cells. *J Am Chem Soc* **130**, 9638–9639.

Dluzewski, A. R., Ling, I. T., Hopkins, J. M., Grainger, M., Margos, G., Mitchell, G. H., Holder, A. A. and Bannister, L. H. (2008). Formation of the food vacuole in *Plasmodium falciparum*: a potential role for the 19 kDa fragment of merozoite surface protein 1 (MSP1(19)). *PLoS ONE* **3**, e3085.

Douglas, A. D., Williams, A. R., Illingworth, J. J., Kamuyu, G., Biswas, S., Goodman, A. L., Wyllie, D. H., Crosnier, C. E. C., Miura, K., Wright, G. J., et al. (2011). The blood-stage malaria antigen PfRH5 is susceptible to vaccine-inducible cross-strain neutralizing antibody. *Nature Communications* **3**, 601–8.

Drakeley, C. J., Carneiro, I., Reyburn, H., Malima, R., Lusingu, J. P. A., Cox, J., Theander, T. G., Nkya, W. M. M. M., Lemnge, M. M. and Riley, E. M. (2005). Altitude-dependent and -independent variations in *Plasmodium falciparum* prevalence in northeastern Tanzania. *J Infect Dis* **191**, 1589–1598.

Druilhe, P. and Khusmith, S. (1987). Epidemiological correlation between levels of antibodies promoting merozoite phagocytosis of *Plasmodium falciparum* and malaria-immune status. *Infect Immun* **55**, 888–891.

Duah, N. O., Miles, D. J. C., Whittle, H. C. and Conway, D. J. (2010). Acquisition of antibody isotypes against *Plasmodium falciparum* blood stage antigens in a birth cohort. *Parasite Immunol* **32**, 125–134.

Duncan, C. J. A. and Hill, A. V. S. (2012). Can growth inhibition assays (GIA) predict blood-stage malaria vaccine efficacy? *Hum Vaccin Immunother* **8**, 706-714.

Dvorak, J. A., Miller, L. H., Whitehouse, W. C. and Shiroishi, T. (1975). Invasion of erythrocytes by malaria merozoites. *Science* **187**, 748–750.

Egan, A. F., Morris, J., Barnish, G., Allen, S., Greenwood, B. M., Kaslow, D. C., Holder, A. A. and Riley, E. M. (1996). Clinical immunity to *Plasmodium falciparum* malaria is associated with serum antibodies to the 19-kDa C-terminal fragment of the merozoite surface antigen, PfMSP-1. *J Infect Dis* **173**, 765–769.

Eisen, D. P., Saul, A., Fryauff, D. J., Reeder, J. C. and Coppel, R. L. (2002). Alterations in *Plasmodium falciparum* genotypes during sequential infections suggest the presence of strain specific immunity. *Am J Trop Med Hyg* **67**, 8–16.

Eisen, D., Billman-Jacobe, H., Marshall, V. F., Fryauff, D. and Coppel, R. L. (1998). Temporal variation of the merozoite surface protein-2 gene of *Plasmodium falciparum*. *Infect Immun* **66**, 239–246.

Fenton, B., Clark, J. T., Khan, C. M., Robinson, J. V., Walliker, D., Ridley, R., Scaife, J. G. and McBride, J. S. (1991). Structural and antigenic polymorphism of the 35- to 48-kilodalton merozoite surface antigen (MSA-2) of the malaria parasite *Plasmodium falciparum*. *Mol Cell Biol* **11**, 963–971.

Ferreira, M. U., Kimura, E. A., Katzin, A. M., Santos-Neto, L. L., Ferrari, J. O., Villalobos, J. M. and de Carvalho, M. E. (1998). The IgG-subclass distribution of naturally acquired antibodies to *Plasmodium falciparum*, in relation to malaria exposure and severity. *Ann Trop Med Parasitol* **92**, 245–256.

Fischer, K., Marti, T., Rick, B., Johnson, D., Benting, J., Baumeister, S., Helmbrecht, C., Lanzer, M. and Lingelbach, K. (1998). Characterization and cloning of the gene encoding the vacuolar membrane protein EXP-2 from *Plasmodium falciparum*. *Mol Biochem Parasitol* **92**, 47–57.

Flint, J., Harding, R. M., Boyce, A. J. and Clegg, J. B. (1998). The population genetics of the haemoglobinopathies. *Baillieres Clin. Haematol* **11**, 1–51.

Flint, J., Hill, A. V., Bowden, D. K., Oppenheimer, S. J., Sill, P. R., Serjeantson, S. W., Bana-Koiri, J., Bhatia, K., Alpers, M. P. and Boyce, A. J. (1986). High frequencies of alpha-thalassaemia are the result of natural selection by malaria. *Nature* **321**, 744–750.

Flueck, C., Frank, G., Smith, T., Jafarshad, A., Nebie, I., Sirima, S. B., Olugbile, S., Alonso, P., Tanner, M., Druilhe, P., et al. (2009). Evaluation of two long synthetic merozoite surface protein 2 peptides as malaria vaccine candidates. *Vaccine* **27**, 2653–2661.

Foth, B. J., Zhang, N., Chaal, B. K., Sze, S. K., Preiser, P. R. and Bozdech, Z. (2011). Quantitative time-course profiling of parasite and host cell proteins in the human malaria parasite *Plasmodium falciparum*. *Mol Cell Proteomics* **10**, M110.006411.

Francis, S. E., Sullivan, D. J. and Goldberg, D. E. (1997). Hemoglobin metabolism in the malaria parasite *Plasmodium falciparum*. *Annu Rev Microbiol* **51**, 97–123.

Fu, Y., Tilley, L., Kenny, S. and Klonis, N. (2010). Dual labeling with a far red probe permits analysis of growth and oxidative stress in *P. falciparum*-infected erythrocytes. *Cytometry A* **77**, 253–263.

Galamo, C. D., Jafarshad, A., Blanc, C. and Druilhe, P. (2009). Anti-MSP1 block 2 antibodies are effective at parasite killing in an allele-specific manner by monocyte-mediated antibody-dependent cellular inhibition. *J Infect Dis* **199**, 1151–1154.

Galinski, M. R., Corredor-Medina, C., Povoa, M., Crosby, J., Ingravallo, P. and Barnwell, J. W. (1999). *Plasmodium vivax* merozoite surface protein-3 contains coiled-coil motifs in an alanine-rich central domain. *Mol Biochem Parasitol* **101**, 131–147.

Galinski, M. R., Ingravallo, P., Corredor-Medina, C., Al-Khedery, B., Povoa, M. and Barnwell, J. W. (2001). *Plasmodium vivax* merozoite surface proteins-3beta and-3gamma share structural similarities with *P. vivax* merozoite surface protein-3alpha and define a new gene family. *Mol Biochem Parasitol* **115**, 41–53.

Gardner, M. J., Hall, N., Fung, E., White, O., Berriman, M., Hyman, R. W., Carlton, J. M., Pain, A., Nelson, K. E., Bowman, S., et al. (2002). Genome sequence of the human malaria parasite *Plasmodium falciparum*. *Nature* **419**, 498–511.

Garner, A. L., St Croix, C. M., Pitt, B. R., Leikauf, G. D., Ando, S. and Koide, K. (2009). Specific fluorogenic probes for ozone in biological and atmospheric samples. *Nat Chem* **1**, 316–321.

Gilson, P. R. and Crabb, B. S. (2009a). Do apicomplexan parasite-encoded proteins act as both ligands and receptors during host cell invasion? *F1000 Biol Rep* **1**, 64.

Gilson, P. R. and Crabb, B. S. (2009b). Morphology and kinetics of the three distinct phases of red blood cell invasion by *Plasmodium falciparum* merozoites. *Int J Parasitol* **39**, 91–96.

Gilson, P. R., O'Donnell, R. A., Nebl, T., Sanders, P. R., Wickham, M. E., McElwain, T. F., de Koning-Ward, T. F. and Crabb, B. S. (2008). MSP1(19) miniproteins can serve as targets for invasion inhibitory antibodies in *Plasmodium falciparum* provided they contain the correct domains for cell surface trafficking. *Mol Microbiol* **68**, 124–138.

Greve, B., Lehman, L. G., Lell, B., Luckner, D., Schmidt-Ott, R. and Kremsner, P. G. (1999). High oxygen radical production is associated with fast parasite clearance in children with *Plasmodium falciparum* malaria. *J Infect Dis* **179**, 1584–1586.

Grüring, C., Heiber, A., Kruse, F., Ungefehr, J., Gilberger, T.-W. and Spielmann, T. (2011). Development and host cell modifications of *Plasmodium falciparum* blood stages in four dimensions. *Nature Communications* **2**, 165.

Guevara Patiño, J. A., Holder, A. A., McBride, J. S. and Blackman, M. J. (1997). Antibodies that inhibit malaria merozoite surface protein-1 processing and erythrocyte invasion are blocked by naturally acquired human antibodies. *J Exp Med* **186**, 1689–1699.

Gupta, S., Snow, R. W., Donnelly, C. A., Marsh, K. and Newbold, C. (1999). Immunity to non-cerebral severe malaria is acquired after one or two infections. *Nat Med* **5**, 340–343.

Gysin, J., Moisson, P., Pereira da Silva, L. and Druilhe, P. (1996). Antibodies from immune African donors with a protective effect in *Plasmodium falciparum* human infection are also able to control asexual blood forms of the parasite in Saimiri monkeys. *Res Immunol* **147**, 397–401.

Haase, S. and de Koning-Ward, T. F. (2010). New insights into protein export in malaria parasites. *Cell Microbiol* **12**, 580–587.

Haldar, K., Samuel, B. U., Mohandas, N., Harrison, T. and Hiller, N. L. (2001). Transport mechanisms in *Plasmodium*-infected erythrocytes: lipid rafts and a tubovesicular network. *Int J Parasitol* **31**, 1393–1401.

Hall, N., Karras, M., Raine, J. D., Carlton, J. M., Kooij, T. W. A., Berriman, M., Florens, L., Janssen, C. S., Pain, A., Christophides, G. K., et al. (2005). A comprehensive survey of the *Plasmodium* life cycle by genomic, transcriptomic, and proteomic analyses. *Science* **307**, 82–86.

Harris, P. K., Yeoh, S., Dluzewski, A. R., O'Donnell, R. A., Withers-Martinez, C., Hackett, F., Bannister, L. H., Mitchell, G. H. and Blackman, M. J. (2005). Molecular identification of a malaria merozoite surface sheddase. *PLoS Pathog* **1**, 241–251.

Hartmann, G. and Krieg, A. M. (2000). Mechanism and function of a newly identified CpG DNA motif in human primary B cells. *J Immunol* **164**, 944–953.

Healer, J., Crawford, S., Ralph, S., McFadden, G. and Cowman, A. F. (2002). Independent translocation of two micronemal proteins in developing *Plasmodium falciparum* merozoites. *Infect Immun* **70**, 5751–5758.

Henderson, K. A., Streltsov, V. A., Coley, A. M., Dolezal, O., Hudson, P. J., Batchelor, A. H., Gupta, A., Bai, T., Murphy, V. J., Anders, R. F., et al. (2007). Structure of an IgNAR-AMA1 complex: targeting a conserved hydrophobic cleft broadens malarial strain recognition. *Structure* **15**, 1452–1466.

Hill, A. V., Allsopp, C. E., Kwiatkowski, D., Anstey, N. M., Twumasi, P., Rowe, P. A., Bennett, S., Brewster, D., McMichael, A. J. and Greenwood, B. M. (1991). Common west African HLA antigens are associated with protection from severe malaria. *Nature* **352**, 595–600.

Hiller, N. L., Bhattacharjee, S., van Ooij, C., Liolios, K., Harrison, T., Lopez-Estraño, C. and Haldar, K. (2004). A host-targeting signal in virulence proteins reveals a secretome in malarial infection. *Science* **306**, 1934–1937.

Hinterberg, K., Scherf, A., Gysin, J., Toyoshima, T., Aikawa, M., Mazie, J. C., da Silva, L. P. and Mattei, D. (1994). *Plasmodium falciparum*: the Pf332 antigen is secreted from the parasite by a brefeldin A-dependent pathway and is translocated to the erythrocyte membrane via the Maurer's clefts. *Exp Parasitol* **79**, 279–291.

Hirunpetcharat, C., Tian, J. H., Kaslow, D. C., van Rooijen, N., Kumar, S., Berzofsky, J. A., Miller, L. H. and Good, M. F. (1997). Complete protective immunity induced in mice by immunization with the 19-kilodalton carboxyl-terminal fragment of the merozoite surface protein-1 (MSP1[19]) of *Plasmodium yoelii* expressed in *Saccharomyces cerevisiae*: correlation of protection with antigen-specific antibody titer, but not with effector CD4+ T cells. *J Immunol* **159**, 3400–3411.

Hogh, B., Petersen, E., Dziegiel, M., David, K., Hanson, A., Borre, M., Holm, A., Vuust, J. and Jepsen, S. (1992). Antibodies to a recombinant glutamate-rich

Plasmodium falciparum protein: evidence for protection of individuals living in a holoendemic area of Liberia. *Am J Trop Med Hyg* **46**, 307–313.

Holder, A. A. and Freeman, R. R. (1982). Biosynthesis and processing of a *Plasmodium falciparum* schizont antigen recognized by immune serum and a monoclonal antibody. *J Exp Med* **156**, 1528–1538.

Holder, A. A. and Freeman, R. R. (1984). The three major antigens on the surface of *Plasmodium falciparum* merozoites are derived from a single high molecular weight precursor. *J Exp Med* **160**, 624–629.

Holder, A. A., Lockyer, M. J., Odink, K. G., Sandhu, J. S., Riveros-Moreno, V., Nicholls, S. C., Hillman, Y., Davey, L. S., Tizard, M. L. and Schwarz, R. T. (1985). Primary structure of the precursor to the three major surface antigens of *Plasmodium falciparum* merozoites. *Nature* **317**, 270–273.

Holder, A. A., Sandhu, J. S., Hillman, Y., Davey, L. S., Nicholls, S. C., Cooper, H. and Lockyer, M. J. (1987). Processing of the precursor to the major merozoite surface antigens of *Plasmodium falciparum*. *Parasitology* **94**, 199–208.

Hopkins, J., Fowler, R., Krishna, S., Wilson, I., Mitchell, G. and Bannister, L. (1999). The plastid in *Plasmodium falciparum* asexual blood stages: a three-dimensional ultrastructural analysis. *Protist* **150**, 283–295.

Howell, S. A., Hackett, F., Jongco, A. M., Withers-Martinez, C., Kim, K., Carruthers, V. B. and Blackman, M. J. (2005). Distinct mechanisms govern proteolytic shedding of a key invasion protein in apicomplexan pathogens. *Mol Microbiol* **57**, 1342–1356.

Howell, S. A., Well, I., Fleck, S. L., Kettleborough, C., Collins, C. R. and Blackman, M. J. (2003). A single malaria merozoite serine protease mediates shedding of multiple surface proteins by juxtamembrane cleavage. *J Biol Chem* **278**, 23890–23898.

Hui-Yuen, J., McAllister, S., Koganti, S., Hill, E. and Bhaduri-McIntosh, S. (2011). Establishment of Epstein-Barr virus growth-transformed lymphoblastoid cell lines. *J Vis Exp* **57**, e3321.

Jafarshad, A., Dziegiel, M. H., Lundquist, R., Nielsen, L. K., Singh, S. and Druilhe, P. L. (2007). A novel antibody-dependent cellular cytotoxicity mechanism involved in defense against malaria requires costimulation of monocytes FcgammaRII and FcgammaRIII. *J. Immunol.* **178**, 3099–3106.

Janda, K. D., Shevlin, C. G. and Lerner, R. A. (1993). Antibody catalysis of a disfavored chemical transformation. *Science* **259**, 490–493.

Jeffery, C. J. (2009). Moonlighting proteins – an update. *Mol Biosyst* **5**, 345–350.

Jeffery, G. M. (1966). Epidemiological significance of repeated infections with

homologous and heterologous strains and species of *Plasmodium Bull World Health Organ* **35**, 873–882.

Jensen, J. B., Boland, M. T., Allan, J. S., Carlin, J. M., Vande Waa, J. A., Divo, A. A. and Akood, M. A. (1983). Association between human serum-induced crisis forms in cultured *Plasmodium falciparum* and clinical immunity to malaria in Sudan. *Infect Immun* **41**, 1302–1311.

Jensen, J. B., Boland, M. T. and Akood, M. (1982). Induction of crisis forms in cultured *Plasmodium falciparum* with human immune serum from Sudan. *Science* **216**, 1230–1233.

Jensen, J. B., Hoffman, S. L., Boland, M. T., Akood, M. A., Laughlin, L. W., Kurniawan, L. and Marwoto, H. A. (1984). Comparison of immunity to malaria in Sudan and Indonesia: crisis-form versus merozoite-invasion inhibition. *Proc Natl Acad Sci USA* **81**, 922–925.

Jiang, G., Daubenberger, C., Huber, W., Matile, H., Tanner, M. and Pluschke, G. (2000). Sequence diversity of the merozoite surface protein 1 of *Plasmodium falciparum* in clinical isolates from the Kilombero District, Tanzania. *Acta Trop* **74**, 51–61.

Jogdand, P. S., Singh, S. K., Christiansen, M., Dziegiel, M. H., Singh, S. and Theisen, M. (2012). Flow cytometric readout based on Mitotracker Red CMXRos staining of live asexual blood stage malarial parasites reliably assesses antibody dependent cellular inhibition. *Malar J* **11**, 235.

John, C. C., O'Donnell, R. A., Sumba, P. O., Moormann, A. M., de Koning-Ward, T. F., King, C. L., Kazura, J. W. and Crabb, B. S. (2004). Evidence that invasion-inhibitory antibodies specific for the 19-kDa fragment of merozoite surface protein-1 (MSP-1 19) can play a protective role against blood-stage *Plasmodium falciparum* infection in individuals in a malaria endemic area of Africa. *J Immunol* **173**, 666–672.

Jones, L. H., Harwig, C. W., Wentworth, P., Simeonov, A., Wentworth, A. D., Py, S., Ashley, J. A., Lerner, R. A. and Janda, K. D. (2001). Conversion of enediynes into quinones by antibody catalysis and in aqueous buffers: implications for an alternative enediyne therapeutic mechanism. *J Am Chem Soc* **123**, 3607–3608.

Joos, C., Marrama, L., Polson, H. E. J., Corre, S., Diatta, A.-M., Diouf, B., Trape, J.-F., Tall, A., Longacre, S. and Perraut, R. (2010). Clinical protection from *falciparum* malaria correlates with neutrophil respiratory bursts induced by merozoites opsonized with human serum antibodies. *PLoS ONE* **5**, e9871.

Jouin, H., Garraud, O., Longacre, S., Baleux, F., Mercereau-Puijalon, O. and Milon, G. (2005). Human antibodies to the polymorphic block 2 domain of the *Plasmodium falciparum* merozoite surface protein 1 (MSP-1) exhibit a highly skewed, peptide-specific light chain distribution. *Immunol Cell Biol* **83**, 392–

395.

Jouin, H., Rogier, C., Trape, J. F. and Mercereau-Puijalon, O. (2001). Fixed, epitope-specific, cytophilic antibody response to the polymorphic block 2 domain of the *Plasmodium falciparum* merozoite surface antigen MSP-1 in humans living in a malaria-endemic area. *Eur J Immunol* **31**, 539–550.

Kadekoppala, M., O'Donnell, R. A., Grainger, M., Crabb, B. S. and Holder, A. A. (2008). Deletion of the *Plasmodium falciparum* merozoite surface protein 7 gene impairs parasite invasion of erythrocytes. *Eukaryotic Cell* **7**, 2123–2132.

Kara, U. A., Stenzel, D. J., Ingram, L. T., Bushell, G. R., Lopez, J. A. and Kidson, C. (1988). Inhibitory monoclonal antibody against a (myristylated) small-molecular-weight antigen from *Plasmodium falciparum* associated with the parasitophorous vacuole membrane. *Infect Immun* **56**, 903–909.

Karpas, A., Dremucheva, A. and Czepulkowski, B. H. (2001). A human myeloma cell line suitable for the generation of human monoclonal antibodies. *Proc Natl Acad Sci USA* **98**, 1799–1804.

Kauth, C. W., Woehlbier, U., Kern, M., Mekonnen, Z., Lutz, R., Mücke, N., Langowski, J. and Bujard, H. (2006). Interactions between merozoite surface proteins 1, 6, and 7 of the malaria parasite *Plasmodium falciparum*. *J Biol Chem* **281**, 31517–31527.

Keeley, A. and Soldati, D. (2004). The glideosome: a molecular machine powering motility and host-cell invasion by Apicomplexa. *Trends Cell Biol.* **14**, 528–532.

Kinyanjui, S. M., Conway, D. J., Lanar, D. E. and Marsh, K. (2007). IgG antibody responses to *Plasmodium falciparum* merozoite antigens in Kenyan children have a short half-life. *Malar J* **6**, 82.

Klonis, N., Tan, O., Jackson, K., Goldberg, D., Klemba, M. and Tilley, L. (2007). Evaluation of pH during cytostomal endocytosis and vacuolar catabolism of haemoglobin in *Plasmodium falciparum*. *Biochem J* **407**, 343–354.

Kocken, C. H., van der Wel, A. M., Dubbeld, M. A., Narum, D. L., van de Rijke, F. M., van Gemert, G. J., van der Linde, X., Bannister, L. H., Janse, C., Waters, A. P., et al. (1998). Precise timing of expression of a *Plasmodium falciparum*-derived transgene in *Plasmodium berghei* is a critical determinant of subsequent subcellular localization. *J Biol Chem* **273**, 15119–15124.

Koncarevic, S., Rohrbach, P., Deponte, M., Krohne, G., Prieto, J. H., Yates, J., Rahlfs, S. and Becker, K. (2009). The malarial parasite *Plasmodium falciparum* imports the human protein peroxiredoxin 2 for peroxide detoxification. *Proc Natl Acad Sci USA* **106**, 13323–13328.

Koussis, K., Withers-Martinez, C., Yeoh, S., Child, M., Hackett, F., Knuepfer,

E., Juliano, L., Woehlbier, U., Bujard, H. and Blackman, M. J. (2009). A multifunctional serine protease primes the malaria parasite for red blood cell invasion. *EMBO J* **28**, 725–735.

Kozbor, D. and Roder, J. C. (1981). Requirements for the establishment of high-titered human monoclonal antibodies against tetanus toxoid using the Epstein-Barr virus technique. *J Immunol* **127**, 1275–1280.

Kozbor, D., Roder, J. C., Chang, T. H., Steplewski, Z. and Koprowski, H. (1982). Human anti-tetanus toxoid monoclonal antibody secreted by EBV-transformed human B cells fused with murine myeloma. *Hybridoma* **1**, 323–328.

Köhler, S., Delwiche, C. F., Denny, P. W., Tilney, L. G., Webster, P., Wilson, R. J., Palmer, J. D. and Roos, D. S. (1997). A plastid of probable green algal origin in Apicomplexan parasites. *Science* **275**, 1485–1489.

Kriek, N., Tilley, L., Horrocks, P., Pinches, R., Elford, B. C., Ferguson, D. J. P., Lingelbach, K. and Newbold, C. I. (2003). Characterization of the pathway for transport of the cytoadherence-mediating protein, PfEMP1, to the host cell surface in malaria parasite-infected erythrocytes. *Mol Microbiol* **50**, 1215–1227.

Krugliak, M., Zhang, J. and Ginsburg, H. (2002). Intraerythrocytic *Plasmodium falciparum* utilizes only a fraction of the amino acids derived from the digestion of host cell cytosol for the biosynthesis of its proteins. *Mol Biochem Parasitol* **119**, 249–256.

Kumaratilake, L. M., Ferrante, A. and Rzepczyk, C. (1991). The role of T lymphocytes in immunity to *Plasmodium falciparum*. Enhancement of neutrophil-mediated parasite killing by lymphotoxin and IFN-gamma: comparisons with tumor necrosis factor effects. *J Immuno.* **146**, 762–767.

Kumaratilake, L. M., Ferrante, A. and Rzepczyk, C. M. (1990). Tumor necrosis factor enhances neutrophil-mediated killing of *Plasmodium falciparum*. *Infect Immun* **58**, 788–793.

Kumaratilake, L. M., Ferrante, A., Robinson, B. S., Jaeger, T. and Poulos, A. (1997). Enhancement of neutrophil-mediated killing of *Plasmodium falciparum* asexual blood forms by fatty acids: importance of fatty acid structure. *Infect Immun* **65**, 4152–4157.

Kyes, S. A., Rowe, J. A., Kriek, N. and Newbold, C. I. (1999). Rifins: a second family of clonally variant proteins expressed on the surface of red cells infected with *Plasmodium falciparum*. *Proc Natl Acad Sci USA* **96**, 9333–9338.

Kyes, S., Horrocks, P. and Newbold, C. (2001). Antigenic variation at the infected red cell surface in malaria. *Annu Rev Microbiol* **55**, 673–707.

Lamarque, M., Besteiro, S., Papoin, J., Roques, M., Vulliez-Le Normand, B., Morlon-Guyot, J., Dubremetz, J.-F., Fauquenoy, S., Tomavo, S., Faber, B. W., et al. (2011). The RON2-AMA1 interaction is a critical step in moving

junction-dependent invasion by apicomplexan parasites. *PLoS Pathog* **7**, e1001276.

Lambros, C. and Vanderberg, J. P. (1979). Synchronization of *Plasmodium falciparum* erythrocytic stages in culture. *J. Parasitol* **65**, 418–420.

Lane, R. D., Renno, W., Nepomuceno, V., Schafer, C. and Mellgren, R. L. (1988). The influence of stimulated peritoneal feeder cells and mitogens upon antibody secreting hybridomas. *Hybridoma* **7**, 289–299.

Lang, F. and Qadri, S. M. (2012). Mechanisms and significance of eryptosis, the suicidal death of erythrocytes. *Blood Purif* **33**, 125–130.

Langhorne, J., Cross, C., Seixas, E., Li, C. and Weid, von der, T. (1998). A role for B cells in the development of T cell helper function in a malaria infection in mice. *Proc Natl Acad Sci USA* **95**, 1730–1734.

Le Roch, K. G., Johnson, J. R., Florens, L., Zhou, Y., Santrosyan, A., Grainger, M., Yan, S. F., Williamson, K. C., Holder, A. A., Carucci, D. J., et al. (2004). Global analysis of transcript and protein levels across the *Plasmodium falciparum* life cycle. *Genome Res* **14**, 2308–2318.

Le Roch, K. G., Zhou, Y., Blair, P. L., Grainger, M., Moch, J. K., Haynes, J. D., La Vega, De, P., Holder, A. A., Batalov, S., Carucci, D. J., et al. (2003). Discovery of gene function by expression profiling of the malaria parasite life cycle. *Science* **301**, 1503–1508.

Leonhardt, H., Gordon, L. and Livingston, R. (1971). Acid-base equilibriums of fluorescein and 2", 7-"dichlorofluorescein in their ground and fluorescent states. *The Journal of Physical Chemistry* **75**, 245–249.

Lew, V. L., Macdonald, L., Ginsburg, H., Krugliak, M. and Tiffert, T. (2004). Excess haemoglobin digestion by malaria parasites: a strategy to prevent premature host cell lysis. *Blood Cells Mol Dis* **32**, 353–359.

Lew, V. L., Tiffert, T. and Ginsburg, H. (2003). Excess hemoglobin digestion and the osmotic stability of *Plasmodium falciparum*-infected red blood cells. *Blood* **101**, 4189–4194.

Li, T., Janda, K. D., Ashley, J. A. and Lerner, R. A. (1994). Antibody catalyzed cationic cyclization. *Science* **264**, 1289–1293.

Lindesmith, L. C., Beltramello, M., Donaldson, E. F., Corti, D., Swanstrom, J., Debbink, K., Lanzavecchia, A. and Baric, R. S. (2012). Immunogenetic mechanisms driving norovirus GII.4 antigenic variation. *PLoS Pathog* **8**, e1002705.

Ling, I. T., Ogun, S. A. and Holder, A. A. (1995). The combined epidermal growth factor-like modules of Plasmodium yoelii Merozoite Surface Protein-1 are required for a protective immune response to the parasite. *Parasite Immunol* **17**,

425–433.

Lobo, C.-A., Rodriguez, M., Reid, M. and Lustigman, S. (2003). Glycophorin C is the receptor for the *Plasmodium falciparum* erythrocyte binding ligand PfEBP-2 (baebl). *Blood* **101**, 4628–4631.

Locher, C. P., Tam, L. Q., Chang, S. P., McBride, J. S. and Siddiqui, W. A. (1996). *Plasmodium falciparum*: gp195 tripeptide repeat-specific monoclonal antibody inhibits parasite growth in vitro. *Exp Parasitol* **84**, 74–83.

Logie, D. E., McGREGOR, I. A., Rowe, D. S. and Billewicz, W. Z. (1973). Plasma immunoglobulin concentrations in mothers and newborn children with special reference to placental malaria: Studies in the Gambia, Nigeria, and Switzerland. *Bull. World Health Organ* **49**, 547–554.

Lougovskoi, A. A., Okoyeh, N. J. and Chauhan, V. S. (1999). Mice immunised with synthetic peptide from N-terminal conserved region of merozoite surface antigen-2 of human malaria parasite *Plasmodium falciparum* can control infection induced by *Plasmodium yoelii yoelii* 265BY strain. *Vaccine* **18**, 920–930.

López, M. L., Vommaro, R., Zalis, M., de Souza, W., Blair, S. and Segura, C. (2010). Induction of cell death on *Plasmodium falciparum* asexual blood stages by Solanum nudum steroids. *Parasitol Int* **59**, 217–225.

Lyon, J. A., Carter, J. M., Thomas, A. W. and Chulay, J. D. (1997). Merozoite surface protein-1 epitopes recognized by antibodies that inhibit *Plasmodium falciparum* merozoite dispersal. *Mol Biochem Parasitol* **90**, 223–234.

Lyon, J. A., Geller, R. H., Haynes, J. D., Chulay, J. D. and Weber, J. L. (1986a). Epitope map and processing scheme for the 195,000-dalton surface glycoprotein of *Plasmodium falciparum* merozoites deduced from cloned overlapping segments of the gene. *Proc Natl Acad Sci USA* **83**, 2989–2993.

Lyon, J. A., Haynes, J. D., Diggs, C. L., Chulay, J. D. and Pratt-Rossiter, J. M. (1986b). *Plasmodium falciparum* antigens synthesized by schizonts and stabilized at the merozoite surface by antibodies when schizonts mature in the presence of growth inhibitory immune serum. *J Immunol* **136**, 2252–2258.

Lyon, J. A., Haynes, J. D., Diggs, C. L., Chulay, J. D., Haidaris, C. G. and Pratt-Rossiter, J. (1987). Monoclonal antibody characterization of the 195-kilodalton major surface glycoprotein of *Plasmodium falciparum* malaria schizonts and merozoites: identification of additional processed products and a serotype-restricted repetitive epitope. *J Immunol* **138**, 895–901.

Macagno, A., Bernasconi, N. L., Vanzetta, F., Dander, E., Sarasini, A., Revello, M. G., Gerna, G., Sallusto, F. and Lanzavecchia, A. (2010). Isolation of human monoclonal antibodies that potently neutralize human cytomegalovirus

infection by targeting different epitopes on the gH/gL/UL128-131A complex. *J. Virol.* **84**, 1005–1013.

Malkin, E. M., Diemert, D. J., McArthur, J. H., Perreault, J. R., Miles, A. P., Giersing, B. K., Mullen, G. E., Orcutt, A., Muratova, O., Awkal, M., et al. (2005). Phase 1 clinical trial of apical membrane antigen 1: an asexual blood-stage vaccine for *Plasmodium falciparum* malaria. *Infect Immun* **73**, 3677–3685.

Mandal, D., Mazumder, A., Das, P., Kundu, M. and Basu, J. (2005). Fas-, caspase 8-, and caspase 3-dependent signaling regulates the activity of the aminophospholipid translocase and phosphatidylserine externalization in human erythrocytes. *J Biol Chem* **280**, 39460–39467.

Margos, G., Bannister, L. H., Dluzewski, A. R., Hopkins, J., Williams, I. T. and Mitchell, G. H. (2004). Correlation of structural development and differential expression of invasion-related molecules in schizonts of *Plasmodium falciparum*. *Parasitology* **129**, 273–287.

Marti, M., Good, R. T., Rug, M., Knuepfer, E. and Cowman, A. F. (2004). Targeting malaria virulence and remodeling proteins to the host erythrocyte. *Science* **306**, 1930–1933.

Mawili-Mboumba, D. P., Borrmann, S., Cavanagh, D. R., McBride, J. S., Matsiegui, P.-B., Missinou, M. A., Kremsner, P. G. and Ntoumi, F. (2003). Antibody responses to *Plasmodium falciparum* merozoite surface protein-1 and efficacy of amodiaquine in Gabonese children with *P. falciparum* malaria. *J Infect Dis* **187**, 1137–1141.

McBride, J. S. and Heidrich, H. G. (1987). Fragments of the polymorphic Mr 185,000 glycoprotein from the surface of isolated *Plasmodium falciparum* merozoites form an antigenic complex. *Mol Biochem Parasitol* **23**, 71–84.

McCall, M. B. B. and Sauerwein, R. W. (2010). Interferon-γ--central mediator of protective immune responses against the pre-erythrocytic and blood stage of malaria. *J. Leukoc. Biol.* **88**, 1131–1143.

McCarthy, J. S., Marjason, J., Elliott, S., Fahey, P., Bang, G., Malkin, E., Tierney, E., Aked-Hurditch, H., Adda, C., Cross, N., et al. (2011). A phase 1 trial of MSP2-C1, a blood-stage malaria vaccine containing 2 isoforms of MSP2 formulated with Montanide® ISA 720. *PLoS ONE* **6**, e24413.

McColl, D. J., Silva, A., Foley, M., Kun, J. F., Favaloro, J. M., Thompson, J. K., Marshall, V. M., Coppel, R. L., Kemp, D. J. and Anders, R. F. (1994). Molecular variation in a novel polymorphic antigen associated with *Plasmodium falciparum* merozoites. *Mol Biochem Parasitol* **68**, 53–67.

McGregor, I. A. and Carrington, S. P. (1963). Treatment of East African *P. falciparum* Malaria With West African Human y-Globulin. *Trans R Soc Trop Med Hyg* **57**, 170-175.

McKerrow, J. H., Sun, E., Rosenthal, P. J. and Bouvier, J. (1993). The proteases and pathogenicity of parasitic protozoa. *Annu Rev Microbiol* **47**, 821–853.

McLean, G. R., Nakouzi, A., Casadevall, A. and Green, N. S. (2000). Human and murine immunoglobulin expression vector cassettes. *Mol Immunol* **37**, 837–845.

McMorran, B. J., Marshall, V. M., de Graaf, C., Drysdale, K. E., Shabbar, M., Smyth, G. K., Corbin, J. E., Alexander, W. S. and Foote, S. J. (2009). Platelets kill intraerythrocytic malarial parasites and mediate survival to infection. *Science* **323**, 797–800.

Mendis, K. N., David, P. H. and Carter, R. (1991). Antigenic polymorphism in malaria: is it an important mechanism for immune evasion? *Immunol Today* **12**, A34–7.

Meraldi, V., Nebie, I., Tiono, A. B., Diallo, D., Sanogo, E., Theisen, M., Druilhe, P., Corradin, G., Moret, R. and Sirima, B. S. (2004). Natural antibody response to *Plasmodium falciparum* Exp-1, MSP-3 and GLURP long synthetic peptides and association with protection. *Parasite Immunol* **26**, 265–272.

Meslin, B., Barnadas, C., Boni, V., Latour, C., de Monbrison, F., Kaiser, K. and Picot, S. (2007). Features of apoptosis in *Plasmodium falciparum* erythrocytic stage through a putative role of PfMCA1 metacaspase-like protein. *J Infect Dis* **195**, 1852–1859.

Metzger, W. G., Okenu, D. M. N., Cavanagh, D. R., Robinson, J. V., Bojang, K. A., Weiss, H. A., McBride, J. S., Greenwood, B. M. and Conway, D. J. (2003). Serum IgG3 to the *Plasmodium falciparum* merozoite surface protein 2 is strongly associated with a reduced prospective risk of malaria. *Parasite Immunol* **25**, 307–312.

Mharakurwa, S., Mutambu, S. L., Mudyiradima, R., Chimbadzwa, T., Chandiwana, S. K. and Day, K. P. (2004). Association of house spraying with suppressed levels of drug resistance in Zimbabwe. *Malar J* **3**, 35.

Miller, G., Shope, T., Lisco, H., Stitt, D. and Lipman, M. (1972). Epstein-Barr virus: transformation, cytopathic changes, and viral antigens in squirrel monkey and marmoset leukocytes. *Proc Natl Acad Sci USA* **69**, 383–387.

Miller, L. H., Roberts, T., Shahabuddin, M. and McCutchan, T. F. (1993). Analysis of sequence diversity in the *Plasmodium falciparum* merozoite surface protein-1 (MSP-1). *Mol Biochem Parasitol* **59**, 1–14.

Monge-Maillo, B. and López-Vélez, R. (2012). Migration and malaria in europe. *Mediterr J Hematol Infect Dis* **4**, e2012014.

Morgan, W. D., Birdsall, B., Frenkiel, T. A., Gradwell, M. G., Burghaus, P. A., Syed, S. E., Uthaipibull, C., Holder, A. A. and Feeney, J. (1999). Solution

structure of an EGF module pair from the *Plasmodium falciparum* merozoite surface protein 1. *J Mol Biol* **289**, 113–122.

Moss, D. K., Remarque, E. J., Faber, B. W., Cavanagh, D. R., Arnot, D. E., Thomas, A. W. and Holder, A. A. (2012). *Plasmodium falciparum* 19-kilodalton merozoite surface protein 1 (MSP1)-specific antibodies that interfere with parasite growth in vitro can inhibit MSP1 processing, merozoite invasion, and intracellular parasite development. *Infect Immun* **80**, 1280–1287.

Mulhern, T. D., Howlett, G. J., Reid, G. E., Simpson, R. J., McColl, D. J., Anders, R. F. and Norton, R. S. (1995). Solution structure of a polypeptide containing four heptad repeat units from a merozoite surface antigen of *Plasmodium falciparum*. *Biochemistry* **34**, 3479–3491.

Murray, C. J. L., Rosenfeld, L. C., Lim, S. S., Andrews, K. G., Foreman, K. J., Haring, D., Fullman, N., Naghavi, M., Lozano, R. and Lopez, A. D. (2012). Global malaria mortality between 1980 and 2010: a systematic analysis. *Lancet* **379**, 413–431.

Müller, W. and Gautier, F. (1975). Interactions of heteroaromatic compounds with nucleic acids. A - T-specific non-intercalating DNA ligands. *Eur J Biochem* **54**, 385–394.

Nardi, M., Tomlinson, S., Greco, M. A. and Karpatkin, S. (2001). Complement-independent, peroxide-induced antibody lysis of platelets in HIV-1-related immune thrombocytopenia. *Cell* **106**, 551–561.

Narum, D. L. and Thomas, A. W. (1994). Differential localization of full-length and processed forms of PF83/AMA-1 an apical membrane antigen of *Plasmodium falciparum* merozoites. *Mol Biochem Parasitol* **67**, 59–68.

Narum, D. L., Ogun, S. A., Thomas, A. W. and Holder, A. A. (2000). Immunization with parasite-derived apical membrane antigen 1 or passive immunization with a specific monoclonal antibody protects BALB/c mice against lethal *Plasmodium yoelii yoelii* YM blood-stage infection. *Infect Immun* **68**, 2899–2906.

Nwuba, R. I., Sodeinde, O., Anumudu, C. I., Omosun, Y. O., Odaibo, A. B., Holder, A. A. and Nwagwu, M. (2002). The human immune response to *Plasmodium falciparum* includes both antibodies that inhibit merozoite surface protein 1 secondary processing and blocking antibodies. *Infect Immun* **70**, 5328–5331.

Nyakeriga, A. M., Perlmann, H., Hagstedt, M., Berzins, K., Troye-Blomberg, M., Zhivotovsky, B., Perlmann, P. and Grandien, A. (2006). Drug-induced death of the asexual blood stages of *Plasmodium falciparum* occurs without typical signs of apoptosis. *Microbes Infect* **8**, 1560–1568.

Oakley, M. S. M., Kumar, S., Anantharaman, V., Zheng, H., Mahajan, B., Haynes, J. D., Moch, J. K., Fairhurst, R., McCutchan, T. F. and Aravind, L. (2007). Molecular factors and biochemical pathways induced by febrile temperature in intraerythrocytic *Plasmodium falciparum* parasites. *Infect Immun* **75**, 2012–2025.

Obando-Martinez, A. Z., Curtidor, H., Vanegas, M., Arévalo-Pinzón, G., Patarroyo, M. A. and Patarroyo, M. E. (2010). Conserved regions from *Plasmodium falciparum* MSP11 specifically interact with host cells and have a potential role during merozoite invasion of red blood cells. *J Cell Biochem* **110**, 882–892.

Ockenhouse, C. F., Angov, E., Kester, K. E., Diggs, C., Soisson, L., Cummings, J. F., Stewart, A. V., Palmer, D. R., Mahajan, B., Krzych, U., et al. (2006). Phase I safety and immunogenicity trial of FMP1/AS02A, a *Plasmodium falciparum* MSP-1 asexual blood stage vaccine. *Vaccine* **24**, 3009–3017.

Oeuvray, C., Bouharoun-Tayoun, H., Gras-Masse, H., Bottius, E., Kaidoh, T., Aikawa, M., Filgueira, M. C., Tartar, A. and Druilhe, P. (1994). Merozoite surface protein-3: a malaria protein inducing antibodies that promote *Plasmodium falciparum* killing by cooperation with blood monocytes. *Blood* **84**, 1594–1602.

Okech, B. A., Corran, P. H., Todd, J., Joynson-Hicks, A., Uthaipibull, C., Egwang, T. G., Holder, A. A. and Riley, E. M. (2004). Fine specificity of serum antibodies to *Plasmodium falciparum* merozoite surface protein, PfMSP-1(19), predicts protection from malaria infection and high-density parasitemia. *Infect Immun* **72**, 1557–1567.

Olivieri, A., Collins, C. R., Hackett, F., Withers-Martinez, C., Marshall, J., Flynn, H. R., Skehel, J. M. and Blackman, M. J. (2011). Juxtamembrane shedding of *Plasmodium falciparum* AMA1 is sequence independent and essential, and helps evade invasion-inhibitory antibodies. *PLoS Pathog* **7**, e1002448.

Osier, F. H. A., Fegan, G., Polley, S. D., Murungi, L., Verra, F., Tetteh, K. K. A., Lowe, B., Mwangi, T., Bull, P. C., Thomas, A. W., et al. (2008). Breadth and magnitude of antibody responses to multiple *Plasmodium falciparum* merozoite antigens are associated with protection from clinical malaria. *Infect Immun* **76**, 2240–2248.

Pachebat, J. A., Ling, I. T., Grainger, M., Trucco, C., Howell, S., Fernandez-Reyes, D., Gunaratne, R. and Holder, A. A. (2001). The 22 kDa component of

the protein complex on the surface of *Plasmodium falciparum* merozoites is derived from a larger precursor, merozoite surface protein 7. *Mol Biochem Parasitol* **117**, 83–89.

Pal, A. K., Bello, D., Budhlall, B., Rogers, E. and Milton, D. K. (2012). Screening for Oxidative Stress Elicited by Engineered Nanomaterials: Evaluation of Acellular DCFH Assay. *Dose Response* **10**, 308–330.

Pearce, J. A., Mills, K., Triglia, T., Cowman, A. F. and Anders, R. F. (2005). Characterisation of two novel proteins from the asexual stage of *Plasmodium falciparum*, H101 and H103. *Mol Biochem Parasitol* **139**, 141–151.

Perkins, M. E. and Rocco, L. J. (1988). Sialic acid-dependent binding of *Plasmodium falciparum* merozoite surface antigen, Pf200, to human erythrocytes. *J Immunol* **141**, 3190–3196.

Pierce, S. K. and Miller, L. H. (2009). World Malaria Day 2009: what malaria knows about the immune system that immunologists still do not. *The Journal of Immunology* **182**, 5171–5177.

Pizarro, J. C., Chitarra, V., Verger, D., Holm, I., Pêtres, S., Dartevelle, S., Nato, F., Longacre, S. and Bentley, G. A. (2003). Crystal structure of a Fab complex formed with PfMSP1-19, the C-terminal fragment of merozoite surface protein 1 from *Plasmodium falciparum*: a malaria vaccine candidate. *J Mol Biol* **328**, 1091–1103.

Polhemus, M. E., Magill, A. J., Cummings, J. F., Kester, K. E., Ockenhouse, C. F., Lanar, D. E., Dutta, S., Barbosa, A., Soisson, L., Diggs, C. L., et al. (2007). Phase I dose escalation safety and immunogenicity trial of *Plasmodium falciparum* apical membrane protein (AMA-1) FMP2.1, adjuvanted with AS02A, in malaria-naïve adults at the Walter Reed Army Institute of Research. *Vaccine* **25**, 4203–4212.

Pollack, S. J., Jacobs, J. W. and Schultz, P. G. (1986). Selective chemical catalysis by an antibody. *Science* **234**, 1570–1573.

Polley, S. D., Conway, D. J., Cavanagh, D. R., McBride, J. S., Lowe, B. S., Williams, T. N., Mwangi, T. W. and Marsh, K. (2006). High levels of serum antibodies to merozoite surface protein 2 of *Plasmodium falciparum* are associated with reduced risk of clinical malaria in coastal Kenya. *Vaccine* **24**, 4233–4246.

Polley, S. D., Tetteh, K. K. A., Cavanagh, D. R., Pearce, R. J., Lloyd, J. M., Bojang, K. A., Okenu, D. M. N., Greenwood, B. M., McBride, J. S. and Conway, D. J. (2003). Repeat sequences in block 2 of *Plasmodium falciparum* merozoite surface protein 1 are targets of antibodies associated with protection from malaria. *Infect Immun* **71**, 1833–1842.

Pouvelle, B., Buffet, P. A., Lépolard, C., Scherf, A. and Gysin, J. (2000). Cytoadhesion of *Plasmodium falciparum* ring-stage-infected erythrocytes. *Nat Med* **6**, 1264–1268.

Pouvelle, B., Spiegel, R., Hsiao, L., Howard, R. J., Morris, R. L., Thomas, A. P. and Taraschi, T. F. (1991). Direct access to serum macromolecules by intraerythrocytic malaria parasites. *Nature* **353**, 73–75.

Przyborski, J. M., Wickert, H., Krohne, G. and Lanzer, M. (2003). Maurer's clefts – a novel secretory organelle? *Mol Biochem Parasitol* **132**, 17–26.

R (2005). *Development Core Team, R: A language and environment for statistical computing. R Foundation for Statistical Computing, Vienna, Austria. ISBN 3-900051-07-0.*

Rahlfs, S., Nickel, C., Deponte, M., Schirmer, R. H. and Becker, K. (2003). *Plasmodium falciparum* thioredoxins and glutaredoxins as central players in redox metabolism. *Redox Rep* **8**, 246–250.

Ravetch, J. V. and Lanier, L. L. (2000). Immune inhibitory receptors. *Science* **290**, 84–89.

Reddy, S. B., Anders, R. F., Beeson, J. G., Färnert, A., Kironde, F., Berenzon, S. K., Wahlgren, M., Linse, S. and Persson, K. E. M. (2012). High affinity antibodies to *Plasmodium falciparum* merozoite antigens are associated with protection from malaria. *PLoS ONE* **7**, e32242.

Reed, Z. H., Kieny, M. P., Engers, H., Friede, M., Chang, S., Longacre, S., Malhotra, P., Pan, W. and Long, C. (2009). Comparison of immunogenicity of five MSP1-based malaria vaccine candidate antigens in rabbits. *Vaccine* **27**, 1651–1660.

Reeder, J. C. and Brown, G. V. (1996). Antigenic variation and immune evasion in *Plasmodium falciparum* malaria. *Immunol Cell Biol* **74**, 546–554.

Richard, D., MacRaild, C. A., Riglar, D. T., Chan, J.-A., Foley, M., Baum, J., Ralph, S. A., Norton, R. S. and Cowman, A. F. (2010). Interaction between *Plasmodium falciparum* apical membrane antigen 1 and the rhoptry neck protein complex defines a key step in the erythrocyte invasion process of malaria parasites. *J Biol Chem* **285**, 14815–14822.

Riley, E. M., Allen, S. J., Wheeler, J. G., Blackman, M. J., Bennett, S., Takacs, B., Schönfeld, H. J., Holder, A. A. and Greenwood, B. M. (1992). Naturally acquired cellular and humoral immune responses to the major merozoite surface antigen (PfMSP1) of *Plasmodium falciparum* are associated with reduced malaria morbidity. *Parasite Immunol* **14**, 321–337.

Riley, E. M., Morris-Jones, S., Blackman, M. J., Greenwood, B. M. and Holder,

A. A. (1993). A longitudinal study of naturally acquired cellular and humoral immune responses to a merozoite surface protein (MSP1) of *Plasmodium falciparum* in an area of seasonal malaria transmission. *Parasite Immunol* **15**, 513–524.

Robinson, J., Halliwell, J. A., McWilliam, H., Lopez, R., Parham, P. and Marsh, S. G. E. (2012). The IMGT/HLA database. *Nucleic Acids Research* **41**, D1222–D1227.

Roussilhon, C., Oeuvray, C., Müller-Graf, C., Tall, A., Rogier, C., Trape, J.-F., Theisen, M., Balde, A., Pérignon, J. L. and Druilhe, P. (2007). Long-term clinical protection from *falciparum* malaria is strongly associated with IgG3 antibodies to merozoite surface protein 3. *PLoS Med* **4**, e320.

Ruwende, C., Khoo, S. C., Snow, R. W., Yates, S. N., Kwiatkowski, D., Gupta, S., Warn, P., Allsopp, C. E., Gilbert, S. C. and Peschu, N. (1995). Natural selection of hemi- and heterozygotes for G6PD deficiency in Africa by resistance to severe malaria. *Nature* **376**, 246–249.

Sabchareon, A., Burnouf, T., Ouattara, D., Attanath, P., Bouharoun-Tayoun, H., Chantavanich, P., Foucault, C., Chongsuphajaisiddhi, T. and Druilhe, P. (1991). Parasitologic and clinical human response to immunoglobulin administration in *falciparum* malaria. *Am J Trop Med Hyg* **45**, 297–308.

Sakamoto, H., Takeo, S., Maier, A. G., Sattabongkot, J., Cowman, A. F. and Tsuboi, T. (2012). Antibodies against a *Plasmodium falciparum* antigen PfMSPDBL1 inhibit merozoite invasion into human erythrocytes. *Vaccine* **30**, 1972-1980.

Salmon, B. L., Oksman, A. and Goldberg, D. E. (2001). Malaria parasite exit from the host erythrocyte: a two-step process requiring extraerythrocytic proteolysis. *Proc Natl Acad Sci USA* **98**, 271–276.

Sargeant, T. J., Marti, M., Caler, E., Carlton, J. M., Simpson, K., Speed, T. P. and Cowman, A. F. (2006). Lineage-specific expansion of proteins exported to erythrocytes in malaria parasites. *Genome Biol* **7**, R12.

Sato, E., Suzuki, T., Hoshi, N., Sugino, T. and Hasegawa, H. (2008). Sodium azide induces necrotic cell death in rat squamous cell carcinoma SCC131. *Med Mol Morphol* **41**, 211–220.

Saul, A., Lord, R., Jones, G. L. and Spencer, L. (1992). Protective immunization with invariant peptides of the *Plasmodium falciparum* antigen MSA2. *J. Immunol.* **148**, 208–211.

Scherf, A., Hernandez-Rivas, R., Buffet, P., Bottius, E., Benatar, C., Pouvelle, B., Gysin, J. and Lanzer, M. (1998). Antigenic variation in malaria: in situ switching, relaxed and mutually exclusive transcription of var genes during

intra-erythrocytic development in *Plasmodium falciparum*. *EMBO J* **17**, 5418–5426.

Schofield, L. and Mueller, I. (2006). Clinical immunity to malaria. *Curr Mol Med* **6**, 205–221.

Shay, J. W. and Wright, W. E. (2005). Senescence and immortalization: role of telomeres and telomerase. *Carcinogenesis* **26**, 867–874.

Sherman, I. W. and Zidovetzki, R. (1992). A parasitophorous duct in *Plasmodium*-infected red blood cells. *Parasitol Today* **8**, 2–3.

Siddiqui, W. A., Tam, L. Q., Kramer, K. J., Hui, G. S., Case, S. E., Yamaga, K. M., Chang, S. P., Chan, E. B. and Kan, S. C. (1987). Merozoite surface coat precursor protein completely protects Aotus monkeys against *Plasmodium falciparum* malaria. *Proc Natl Acad Sci USA* **84**, 3014–3018.

Sim, B. K., Chitnis, C. E., Wasniowska, K., Hadley, T. J. and Miller, L. H. (1994). Receptor and ligand domains for invasion of erythrocytes by *Plasmodium falciparum*. *Science* **264**, 1941–1944.

Singh, S., Soe, S., Weisman, S., Barnwell, J. W., Pérignon, J. L. and Druilhe, P. (2009). A conserved multi-gene family induces cross-reactive antibodies effective in defense against *Plasmodium falciparum*. *PLoS ONE* **4**, e5410.

Slomianny, C. (1990). Three-dimensional reconstruction of the feeding process of the malaria parasite. *Blood Cells* **16**, 369–378.

Slomianny, C. and Prensier, G. (1986). Application of the serial sectioning and tridimensional reconstruction techniques to the morphological study of the *Plasmodium falciparum* mitochondrion. *J. Parasitol* **72**, 595–598.

Smythe, J. A., Peterson, M. G., Coppel, R. L., Saul, A. J., Kemp, D. J. and Anders, R. F. (1990). Structural diversity in the 45-kilodalton merozoite surface antigen of *Plasmodium falciparum*. *Mol Biochem Parasitol* **39**, 227–234.

Snow, R. W., Nahlen, B., Palmer, A., Donnelly, C. A., Gupta, S. and Marsh, K. (1998). Risk of severe malaria among African infants: direct evidence of clinical protection during early infancy. *J Infect Dis* **177**, 819–822.

Spence, P. J. and Langhorne, J. (2012). T cell control of malaria pathogenesis. *Curr Opin Immunol* **24**, 1-5.

Spencer Valero, L. M., Ogun, S. A., Fleck, S. L., Ling, I. T., Scott-Finnigan, T. J., Blackman, M. J. and Holder, A. A. (1998). Passive immunization with antibodies against three distinct epitopes on *Plasmodium yoelii* merozoite surface protein 1 suppresses parasitemia. *Infect Immun* **66**, 3925–3930.

Spielmann, T., Fergusen, D. J. P. and Beck, H.-P. (2003). etramps, a new *Plasmodium falciparum* gene family coding for developmentally regulated and

highly charged membrane proteins located at the parasite-host cell interface. *Mol Biol Cell* **14**, 1529–1544.

Spielmann, T., Hawthorne, P. L., Dixon, M. W. A., Hannemann, M., Klotz, K., Kemp, D. J., Klonis, N., Tilley, L., Trenholme, K. R. and Gardiner, D. L. (2006). A cluster of ring stage-specific genes linked to a locus implicated in cytoadherence in *Plasmodium falciparum* codes for PEXEL-negative and PEXEL-positive proteins exported into the host cell. *Mol Biol Cell* **17**, 3613–3624.

Spycher, C., Klonis, N., Spielmann, T., Kump, E., Steiger, S., Tilley, L. and Beck, H.-P. (2003). MAHRP-1, a novel *Plasmodium falciparum* histidine-rich protein, binds ferriprotoporphyrin IX and localizes to the Maurer's clefts. *J Biol Chem* **278**, 35373–35383.

Staines, H. M., Alkhalil, A., Allen, R. J., De Jonge, H. R., Derbyshire, E., Egée, S., Ginsburg, H., Hill, D. A., Huber, S. M., Kirk, K., et al. (2007). Electrophysiological studies of malaria parasite-infected erythrocytes: current status. *Int J Parasitol* **37**, 475–482.

Steinitz, M., Klein, G., Koskimies, S. and Makel, O. (1977). EB virus-induced B lymphocyte cell lines producing specific antibody. *Nature* **269**, 420–422.

Steinitz, M., Koskimies, S., Klein, G. and Mäkelä, O. (1979). Establishment of specific antibody producing human lines by antigen preselection and Epstein-Barr virus (EBV)-transformation. *J Clin Lab Immunol* **2**, 1–7.

Stewart, S. A. and Weinberg, R. A. (2006). Telomeres: cancer to human aging. *Annu Rev Cell Dev Biol* **22**, 531–557.

Stubbs, J., Olugbile, S., Saidou, B., Simpore, J., Corradin, G. and Lanzavecchia, A. (2011). Strain-transcending Fc-dependent killing of *Plasmodium falciparum* by merozoite surface protein 2 allele-specific human antibodies. *Infect Immun* **79**, 1143–1152.

Sugimoto, M., Tahara, H., Ide, T. and Furuichi, Y. (2004). Steps involved in immortalization and tumorigenesis in human B-lymphoblastoid cell lines transformed by Epstein-Barr virus. *Cancer Res* **64**, 3361–3364.

Sztajer, H., Gamain, B., Aumann, K. D., Slomianny, C., Becker, K., Brigelius-Flohé, R. and Flohé, L. (2001). The putative glutathione peroxidase gene of *Plasmodium falciparum* codes for a thioredoxin peroxidase. *J Biol Chem* **276**, 7397–7403.

Tanabe, K., Mackay, M., Goman, M. and Scaife, J. G. (1987). Allelic dimorphism in a surface antigen gene of the malaria parasite *Plasmodium falciparum*. *J Mol Biol* **195**, 273–287.

Taraschi, T. F., Pouvelle, B. and Howard, R. J. (1992). A parasitophorous duct in *Plasmodium*-infected red blood cells - reply. *Parasitol Today* **8**, 17.

Taylor, R. R., Egan, A., McGuinness, D., Jepson, A., Adair, R., Drakely, C. and Riley, E. (1996). Selective recognition of malaria antigens by human serum antibodies is not genetically determined but demonstrates some features of clonal imprinting. *Int Immunol* **8**, 905–915.

Tebo, A. E., Kremsner, P. G. and Luty, A. J. (2001). *Plasmodium falciparum*: a major role for IgG3 in antibody-dependent monocyte-mediated cellular inhibition of parasite growth in vitro. *Exp Parasitol* **98**, 20–28.

Tetteh, K. K. A., Stewart, L. B., Ochola, L. I., Amambua-Ngwa, A., Thomas, A. W., Marsh, K., Weedall, G. D. and Conway, D. J. (2009). Prospective identification of malaria parasite genes under balancing selection. *PLoS ONE* **4**, e5568.

Tham, W.-H., Wilson, D. W., Lopaticki, S., Schmidt, C. Q., Tetteh-Quarcoo, P. B., Barlow, P. N., Richard, D., Corbin, J. E., Beeson, J. G. and Cowman, A. F. (2010). Complement receptor 1 is the host erythrocyte receptor for *Plasmodium falciparum* PfRh4 invasion ligand. *Proc Natl Acad Sci USA* **107**, 17327–17332.

Theisen, M., Soe, S., Jessing, S. G., Okkels, L. M., Danielsen, S., Oeuvray, C., Druilhe, P. and Jepsen, S. (2000). Identification of a major B-cell epitope of the *Plasmodium falciparum* glutamate-rich protein (GLURP), targeted by human antibodies mediating parasite killing. *Vaccine* **19**, 204–212.

Tompa, P., Szász, C. and Buday, L. (2005). Structural disorder throws new light on moonlighting. *Trends Biochem Sci* **30**, 484–489.

Totino, P. R. R., Daniel-Ribeiro, C. T., Corte-Real, S. and de Fátima Ferreira-da-Cruz, M. (2008). *Plasmodium falciparum*: erythrocytic stages die by autophagic-like cell death under drug pressure. *Exp Parasitol* **118**, 478–486.

Trager, W. (1993). FCR-3, chloroquine resistance and cross-contamination of culture lines of *Plasmodium falciparum*. *Parasitol Today* **9**, 127–author reply 127.

Traggiai, E., Becker, S., Subbarao, K., Kolesnikova, L., Uematsu, Y., Gismondo, M. R., Murphy, B. R., Rappuoli, R. and Lanzavecchia, A. (2004). An efficient method to make human monoclonal antibodies from memory B cells: potent neutralization of SARS coronavirus. *Nat Med* **10**, 871–875.

Tramontano, A., Janda, K. D. and Lerner, R. A. (1986). Catalytic antibodies. *Science* **234**, 1566–1570.

Trieu, A., Kayala, M. A., Burk, C., Molina, D. M., Freilich, D. A., Richie, T. L., Baldi, P., Felgner, P. L. and Doolan, D. L. (2011). Sterile protective immunity to malaria is associated with a panel of novel *P. falciparum* antigens. *Mol Cell Proteomics* **10**, M111.007948.

Trucco, C., Fernandez-Reyes, D., Howell, S., Stafford, W. H., Scott-Finnigan, T.

J., Grainger, M., Ogun, S. A., Taylor, W. R. and Holder, A. A. (2001). The merozoite surface protein 6 gene codes for a 36 kDa protein associated with the *Plasmodium falciparum* merozoite surface protein-1 complex. *Mol Biochem Parasitol* **112**, 91–101.

Tutterrow, Y. L., Salanti, A., Avril, M., Smith, J. D., Pagano, I. S., Ako, S., Fogako, J., Leke, R. G. F. and Taylor, D. W. (2012). High avidity antibodies to full-length VAR2CSA correlate with absence of placental malaria. *PLoS ONE* **7**, e40049.

van Ooij, C., Tamez, P., Bhattacharjee, S., Hiller, N. L., Harrison, T., Liolios, K., Kooij, T., Ramesar, J., Balu, B., Adams, J., et al. (2008). The malaria secretome: from algorithms to essential function in blood stage infection. *PLoS Pathog.* **4**, e1000084.

Vivas, L., Easton, A., Kendrick, H., Cameron, A., Lavandera, J.-L., Barros, D., las Heras, de, F. G., Brady, R. L. and Croft, S. L. (2005). *Plasmodium falciparum*: stage specific effects of a selective inhibitor of lactate dehydrogenase. *Exp Parasitol* **111**, 105–114.

Vouldoukis, I., Mazier, D., Moynet, D., Thiolat, D., Malvy, D. and Mossalayi, M. D. (2011). IgE mediates killing of intracellular *Toxoplasma gondii* by human macrophages through CD23-dependent, interleukin-10 sensitive pathway. *PLoS ONE* **6**, e18289.

Waisberg, M., Cerqueira, G. C., Yager, S. B., Francischetti, I. M. B., Lu, J., Gera, N., Srinivasan, P., Miura, K., Rada, B., Lukszo, J., et al. (2012). *Plasmodium falciparum* merozoite surface protein 1 blocks the proinflammatory protein S100P. *Proc Natl Acad Sci USA* **109**, 5429–5434.

Waller, R. F., Reed, M. B., Cowman, A. F. and McFadden, G. I. (2000). Protein trafficking to the plastid of *Plasmodium falciparum* is via the secretory pathway. *EMBO J* **19**, 1794–1802.

Warrell, D. A. and Gilles, H. M. (2003). *Essential Malariology*. Hodder Arnold.

Weatherall, D. J. and Clegg, J. B. (2001). Inherited haemoglobin disorders: an increasing global health problem. *Bull World Health Organ* **79**, 704–712.

Weid, von der, T., Honarvar, N. and Langhorne, J. (1996). Gene-targeted mice lacking B cells are unable to eliminate a blood stage malaria infection. *J Immunol* **156**, 2510–2516.

Wentworth, A. D., Jones, L. H., Wentworth, P., Janda, K. D. and Lerner, R. A. (2000). Antibodies have the intrinsic capacity to destroy antigens. *Proc Natl Acad Sci USA* **97**, 10930–10935.

Wentworth, P., Jones, L. H., Wentworth, A. D., Zhu, X., Larsen, N. A., Wilson, I. A., Xu, X., Goddard, W. A., Janda, K. D., Eschenmoser, A., et al. (2001). Antibody catalysis of the oxidation of water. *Science* **293**, 1806–1811.

Wentworth, P., McDunn, J. E., Wentworth, A. D., Takeuchi, C., Nieva, J., Jones, T., Bautista, C., Ruedi, J. M., Gutierrez, A., Janda, K. D., et al. (2002). Evidence for antibody-catalyzed ozone formation in bacterial killing and inflammation. *Science* **298**, 2195–2199.

Wickham, M. E., Culvenor, J. G. and Cowman, A. F. (2003). Selective inhibition of a two-step egress of malaria parasites from the host erythrocyte. *J Biol Chem* **278**, 37658–37663.

Wickham, M. E., Rug, M., Ralph, S. A., Klonis, N., McFadden, G. I., Tilley, L. and Cowman, A. F. (2001). Trafficking and assembly of the cytoadherence complex in *Plasmodium falciparum*-infected human erythrocytes. *EMBO J* **20**, 5636–5649.

Wilson, C. F., Anand, R., Clark, J. T. and McBride, J. S. (1987). Topography of epitopes on a polymorphic schizont antigen of *Plasmodium falciparum* determined by the binding of monoclonal antibodies in a two-site radioimmunoassay. *Parasite Immunol* **9**, 737–746.

Wipasa, J., Xu, H., Makobongo, M., Gatton, M., Stowers, A. and Good, M. F. (2002). Nature and specificity of the required protective immune response that develops postchallenge in mice vaccinated with the 19-kilodalton fragment of *Plasmodium yoelii* merozoite surface protein 1. *Infect Immun* **70**, 6013–6020.

Withers, M. R., McKinney, D., Ogutu, B. R., Waitumbi, J. N., Milman, J. B., Apollo, O. J., Allen, O. G., Tucker, K., Soisson, L. A., Diggs, C., et al. (2006). Safety and reactogenicity of an MSP-1 malaria vaccine candidate: a randomized phase Ib dose-escalation trial in Kenyan children. *PLoS Clin Trials* **1**, e32.

Woehlbier, U., Epp, C., Hackett, F., Blackman, M. J. and Bujard, H. (2010). Antibodies against multiple merozoite surface antigens of the human malaria parasite *Plasmodium falciparum* inhibit parasite maturation and red blood cell invasion. *Malar J* **9**, 77.

Woehlbier, U., Epp, C., Kauth, C. and Lutz, R. (2006). Analysis of antibodies directed against merozoite surface protein 1 of the human malaria parasite *Plasmodium falciparum*. *Infect Immun* **74**, 1313-1322.

World Malaria Report 2011 (2011). *World Malaria Report 2011*. World Health Organization.

Yu, X., McGraw, P. A., House, F. S. and Crowe, J. E. (2008a). An optimized

electrofusion-based protocol for generating virus-specific human monoclonal antibodies. *Journal of Immunological Methods* **336**, 142–151.

Yu, X., Tsibane, T., McGraw, P. A., House, F. S., Keefer, C. J., Hicar, M. D., Tumpey, T.M., Pappas, C., Perrone, L.A., Martinez, O., et al. (2008b). Neutralizing antibodies derived from the B cells of 1918 influenza pandemic survivors. *Nature* **455**, 532-536.